Patterning by cell-to-cell communication

Michael Cohen

Thesis submitted for the
Degree of Doctor of Philosophy

CoMPLEX
University College London

January 2010

Disclaimer

The work in this thesis is that of the candidate alone, except where other people's work is cited in the text, and as described below.

Chapters 4 and 5 are a modified version of the paper:
'Measuring the robustness of a developmental system based on sequential growth rules', M. Cohen, M. Miodownik, and B. Baum, Artificial Life, Vol 11, Page 118, 2008.

Chapters 7 and 9 are a modified version of the paper:
'Ordered tissue patterning via dynamic protrusion-mediated lateral inhibition' M.Cohen, M. Georgiou, M. Miodownik and B. Baum. Submitted for publication 2009.

The co-authors contributed to the text of the above papers.

The biological experiments described in chapter 7 were designed and performed by Marios Georgiou in the Baum Lab at the Laboratory for Molecular Cell Biology, University College London.

The quantitative analysis of the biological data was carried out by the candidate who also participated in some of the confocal microscopy experiments.

Michael Cohen
January 2010

Abstract

This thesis addresses the question of how patterning may arise through cell-to-cell communication. It combines quantitative data analysis with computational techniques to understand biological patterning processes. The first section describes an investigation into the robustness of an evolved artificial patterning system. Cellular automata rules were implemented sequentially according to the instructions in a simple 'genome'. In this way, a set of target patterns could be evolved using a genetic algorithm. The patterning systems were tested for robustness by perturbing cell states during their development. This exposed how certain types of patterning rule had very different levels of robustness to perturbations. Rules that generated patterns with complex divergent patterns were more likely to amplify the effect of a perturbation. When smaller genomes, comprising less individual rules, were evolved to match certain target patterns, these were shown to be more likely to select complex patterning rules. As a result, the developmental systems based on smaller genomes were less robust than those with larger genome sizes.

Section two provides an analysis of the patterning of microchaetes in the epithelial layer of the notum of Drosophila flies. It is shown that the pattern spacing is not sufficiently described by a model of lateral inhibition through Delta-Notch signalling between adjacent cells. A computational model is used to demonstrate the viability of long range signalling through a dynamic network of filopodia, observed in the basal layer of the epithelium. In-vivo experiments confirm that when filopodia lengths are effected by mutations the pattern spacing reduces in accordance with the model.

In the final section the behaviour of simple asynchronous cellular automata are analysed. It is shown how these differ to the synchronous cellular automata used in the first section. A set of rules are identified whose emergent behaviour is similar to the lateral inhibition patterning process established by the Delta-Notch signalling system. Among these rules a particular subset are found to produce patterns that adjust their spacing, over the course of their development, towards a more ordered and densely packed state. A re-examination of the Delta-Notch signalling model reveals that this type of packing optimisation could take place with either dynamic filopodial signalling, or as an alternative, transient Delta signalling at each cell. Under certain parameter regimes the patterns become more densely packed over time, whilst maintaining a minimum zone of inhibition around each Delta expressing cell. The asynchronous CA are also used to demonstrate how stripes can be formed by cell-to-cell signalling and optimised, under certain conditions, so that they align in a single direction. This is presented as a possible novel alternative to the reaction-diffusion mechanism that is commonly used to model the patterning of spots and stripes.

Acknowledgements

Above all I would like to thank Buzz Baum [1] who as my principle PhD supervisor has mentored me throughout this work. He has consistently been available to offer his time, support and expert knowledge. His keen scientific instinct has continually driven this project forward and motivated my overall development as a scientist.

Likewise, my secondary supervisor, Mark Miodownik, [2] has provided guidance and support over the course of my PhD. Our regular meetings, which often transcended into fascinating philosophical debates, have simultaneously been a source of creative inspiration and scientific rigour throughout this project.

Marios Georgiou [1] is an experimental biologist in the Baum Lab who collaborated on an extensive part of this project. I am hugely grateful for his willingness to participate in this work and his skilful provision of so much of the biological data that underpins this thesis.

I would also like to thank: K. VanHegan and S. Myerson for help in initiating the biological aspects of this project; Antonio Jacinto, Soren Prag and the whole Jacinto Lab [3] for their help with laser ablation experiments; and T. Duke and A. Mehonic [4] for advice on aspects of the computational modelling.

This work was funded and supported by the Centre for Mathematics and Physics in the Life Sciences and Experimental Biology (CoMPLEX), University College London. It was undertaken as part of the 4 year training program that they provide.

CoMPLEX are funded by the Engineering and Physical Sciences Research Council (EPSRC).

The biological aspects of this work were carried out at the LMCB, UCL. The work was funded by Cancer Research UK, UCL-Wellcome VIP funding and The Royal Society.

[1] Laboratory for Molecular Cell Biology (LMCB), University College London
[2] Materials Research Group, Kings College London
[3] Instituto de Medicina Molecular, University of Lisbon
[4] London Centre for Nanotechnology, University College London

Contents

List of Figures

Chapter 1

Introduction

This chapter provides an introduction to the main themes of the thesis, the scientific background and the aims and objectives of the work. Also included is a summary of the overall thesis structure.

Modern science has been remarkably successful at identifying the building blocks of nature. These can now be measured and manipulated in a spectacular variety of ways. The challenge now facing scientists and engineers is to determine how to better understand, predict and control the outcome of the self-organising processes which occur ubiquitously in natural systems. This thesis describes an investigation into patterning during animal development and demonstrates how studying abstract computational systems can aid our understanding of nature.

The universality of self-organising systems

Scientific references to terms such as 'self-organisation', 'self-assembly', 'self-ordering' and 'emergence' are increasingly common. In many ways these terms collectively encompass the basic paradigm underlying any modern scientific text; that the fundamental particles of the universe, manipulated by just a handful of fundamental forces, arrange themselves into atoms and molecules, stars, galaxies and planets. On Earth, highly complex molecules self-assemble in such a way that they can subsequently self-replicate. This enables the forces of evolution to drive the formation of vastly intricate networks of interacting chemical components capable of assembling and maintaining structures as complex as cells and higher organisms.

In a strong sense then all of science is an attempt to qualify these kinds of processes; however often the associated terminology is remarkably difficult to specify. A common interpretation based on thermodynamic principles describes a self-organising system as one in which there is an increase in order, or entropy, which is not imposed by an external agent [Prigogine: 1978]. However, it has been noted that different specifications of a particular system may reveal both organisation or disorganisation depending on how boundary conditions and measures of entropy are applied [Gershenson and Heylighen: 2003]. In [Halley and Winkler: 2008] 'self-assembly' is distinguished from 'self-organisation' by the tendency of self-assembling systems to move towards thermodynamic equilibrium; as apposed to self-organising processes which may occur at non-equilibrium. In [Abel and Trevors: 2006] they further distinguish between self-organisation and self-ordering, making the distinction that most naturally occurring processes (pre-biotic evolution) are self-ordering and only algorithmically functional systems (including biological systems) can be declared as self-organising. Furthermore, a closely related phenomenon, 'emergence' is defined in [Coming: 2002] as 'the arising of novel and coherent structures, patterns and properties during the process of self-organisation in complex systems'. These examples highlight just a few of a vast number of definitions that

can be found on this subject matter. In fact, one commentator suggests that 'defining structure and detecting the emergence of complexity in nature are inherently subjective, though essential, scientific activities' [Crutchfield: 1994]. With this in mind, it is not the purpose of this thesis to attempt to clarify these terms. Here, self-organisation and emergence will be used in reference to any phenomena in which some observable type of order arises from the interaction of a system's component parts.

In many ways our ability to interpret and manipulate self-organising systems is only just developing. Mathematics has, to date, been remarkably successful in providing the tools by which to interrogate our environment. Engineering, guided by mathematics, has enabled us to design and build complex structures. We can collect and identify materials, measure their mechanical or electrical properties and then, using the required tools, reassemble them into forms that we can understand and whose properties we can predict. And similarly we can now map out entire genomes and identify many of the proteins and other chemicals that make up cells. But rarely, given a quantity of those constituent parts, can we accurately predict the form or function into which they will arrange themselves. However, the endeavour to understand self-organising systems is clearly not new to modern science. As has been argued our entire understanding of the natural world hinges on this paradigm. We have long interpreted the orbits of the planets not as a predetermined set of paths mapped out in the sky, but as a harmonious self sustained system that emerges from the gravitational forces acting between bodies in space. What is new, however, is the recognition that traditional mathematics is not perfectly suited to interrogating systems of this kind. Mathematics has proven to be a very useful tool for making deterministic predictions about deliberately simplified systems comprising a relatively small set of interactions. Likewise statistics and probability theory provide the tools for making predictions about the distribution of outcomes of large numbers of events. However, making predictions about more specific emergent properties of systems comprising many interacting elements is a distinct type of challenge. The emergent outcomes of these types of systems are often far from intuitive and new techniques are required to study them. In addition to analytical mathematics, high powered computers now provide a new way of interrogating systems. By using simulation, the fundamental properties of complex interactions can be recreated. This allows emergent behaviours to be identified and related back to a system's components. To a large part the study of complex systems has been made viable by these new technologies.

Nowhere is the challenge of understanding complex self-organising systems greater than in biology. Though biological systems are ultimately governed by the fundamental forces of chemistry and physics, at every level of development, complex molecules interact to form increasingly complex structures and behaviours. The production of these molecules can be switched on and off according to the blue print laid down in DNA. The result is a vastly complex evolved network of interactions which determine a set of rules for the command and control of the emergent system.

Developmental patterning by cell-to-cell communication

The development of a biological organism may therefore be regarded as a chain of self-organising processes governed by control rules [Wolpert: 2002, Carroll: 2005]. It results in the transformation of a single fertilised egg into a complex arrangement of cells with many different forms and functions. Throughout development, cells differentiate into distinct states of gene expression and cells and tissues grow and move in order to generate structure; in a process known as morphogenesis.

This thesis is concerned with the concept of patterning during biological development. The word pattern stems from the latin *patronus* which means a model or template, and in this context it refers to a regularly-repeating sequence of shapes, objects or states in time or space. However, the term is often used more loosely to mean any characteristic variation of shape, structure or

form [Othmer et al.: 2009]. A problem arises in applying this definition in that one cannot easily identify unique stages of development that are specifically patterning processes as distinct from cell differentiation, growth or morphogenesis. As Turing put it, 'Most of an organism, most of the time, is developing from one pattern into another, rather than from homogeneity into a pattern' [Turing: 1952]. Development and, indeed, self-organisation are in a sense synonymous with patterning; but there is room for a distinction to be made. Consistent with Turing's statement, one may interpret developmental patterning as a departure from homogeneity. For example, when regarded in isolation, the uniform growth of a group of cells would not qualify as a patterning process (although ultimately it may contribute to the overall form of an organism). However, if that growth were, in some way, to alter the relative shape (or some other property) of a sub-set of those cells, then this would qualify as patterning. The establishment of any new variation within a biological structure is, by this working definition, a patterning process. Whilst it may be more common for texts to refer to a superficial two-dimensional *pattern* of epithelial spots or stripes [Meinhardt: 2007, Maini: 2004], it is equally valid to refer to the branching of lungs or skeletal formation as a developmental pattern [Hentschel et al.: 2004, Cardoso: 1995]. Both of these types of system are considered in this thesis.

In order to generate variation in structure or gene expression during development there must be underlying physical processes that give rise to some kind of non-uniformity or asymmetry either within cells themselves or among a group of cells. During development cells respond to chemical signalling and physical forces to initiate actions [Wolpert: 2002]. This may include altering their internal chemistry or external signals, or performing some kind of physical action such as to move, die, grow or divide. The range of a particular signal, whether it is chemical or physical in nature may vary considerably. Long range forces or chemical signals may propagate the length of an entire organism or short range signals may only extend to neighbouring cells. In either case, differences in the signal must cause different responses among otherwise homogenous cells in order to generate a pattern. For example the different tensile forces experienced by cells located at different sites in a growing tissue may cause differences in their gene expression or morphogenetic behaviour. Likewise different chemical concentrations arising from a diffusing signal located at a particular source (or multiple sources) may produce similar differences in cellular response [Wolpert: 2002]. It is easy to envisage in these examples how a pattern may arise over the full extent of a tissue, but what if the signals are restricted to the range of direct cellular contact? Is it possible to generate patterns with short range communication and if so what are the limitations of this type of patterning? Can a homogenous group of cells signal to one another in such a way that complex patterns emerge? And can a single cell divide and grow to form a complex structure without evoking long range signalling in order to control growth?

The use of cellular automata as an exploratory tool

To explore how patterning can be achieved by cell-to-cell communication this report employs a type of model system known as a *cellular automaton*. Cellular automata are a computational device that were developed in the 1950s and have since been used extensively to study the properties of self-organising systems [Wolfram: 2002]. They represent a particular sub-set of agent based models in which a collection of cells, typically arranged in some kind of regular topology, act as autonomous agents, reacting to each other according to a set of rules. The complexity of cellular automata may vary considerably in regard to the topology of a system, the rules that each cell may follow, the type and number of states that a cell may occupy and the way in which cells are selected to act. A very complex model based on many physical parameters may qualify as a cellular automaton; however, the nomenclature is more commonly applied to more simple abstracted systems. Whereas

a complex, parameter-rich computational model allows one to investigate specific behaviours that are pertinent to a particular system, a simple cellular automaton can provide a reasoning tool by which more fundamental behaviours can be elucidated. They are particularly useful for looking at emergent phenomena as they offer a framework in which local interactions can be processed a large number of times by a large number of units, and the resultant behaviour of the whole system can be easily visualised. They therefore provide an alternative analytical tool to traditional mathematical modelling. By identifying emergent behaviours that are fundamental to simple abstract systems, heuristic principles can be extrapolated to explain the behaviour of more complex systems that may otherwise be mathematically intractable.

Cellular automata can be used to model different types of physical systems in which some kind of state transition occurs at locally identifiable sites. For example a cell state may be used to represent to the presence or absence of some physical material, the expression of a particular gene in a biological cell or the spin state of an atom in a ferrous substance [Wolfram: 2002]. In the context of this thesis, cellular automata are particularly suited to investigating biological patterning systems where a very straightforward correspondence may be drawn between a cell state and for example the gene expression of a biological cell. Furthermore, the most simple cellular automata function using transition rules that are based on the states of directly neighbouring cells. Hence, they provide an ideal tool for analysing fundamental questions relevant to biological patterning by cell-to-cell signalling.

Developmental robustness and evolvability

Development has been described here as a sequence of self-organising patterning events governed by control rules defined in DNA code. The end result of development is a fully functional organism that must be able to survive and reproduce in a competitive environment [Dawkins: 2006]. Therefore, there is a fundamental requirement for developmental processes to be sufficiently robust to ensure that ultimately they gives rise to a viable phenotype. Development occurs in a noisy environment that is subject to variation in temperature, food supply and stochastic chemical fluctuations [Keller: 2002]. Remarkably there are processes in place that ensure the relative position and size of different cells, tissues and organs are accurately maintained. The self-organising events that drive these processes must not only be sufficient to generate a particular pattern at a particular time, but must be robust enough to respond and adapt to perturbations across the whole system.

In biology there is no single quantifiable measurement of robustness; it is a relative concept used to describe an organisms response to a wide variety of things such things as genetic mutation, environmental changes or developmental noise [Hammerstein et al.: 2005]. Robustness may therefore be analysed from many alternative perspectives. At the phenotypic level, a developed adult organism could be described as being robust towards its environment if it can survive factors such as temperature changes, food shortages or changes in the numbers or types of potential predators. At the genotypic level, mutational robustness, considers perturbations at the level of DNA, and provides a relative measure of the phenotypic response to changes in genotype. The evolved ability of a phenotype to maintain its form and function irrespective of genetic mutations is known as canalization [Huerta-Sanchez and Durrett: 2007, Hornstein and Shomron: 2006]. Moreover, genetic mutations are fundamental to evolution and successful organisms must find a balance between the ability to produce a consistent functional phenotype, with the ability to explore new phenotypes in response to environmental selection pressures [Lenski et al.: 2006, Jen: 2005]. Mutational robustness is, in this sense, intimately related to evolvability which in itself constitutes a form of biological robustness to environmental change in the long term. Development represents an intermediate stage where each individual process must be sufficiently robust to ensure the viability of the phenotype.

Furthermore, developmental processes must have evolved via an ancestry in which mutational adaptations were equally viable. Therefore to truly understand development both of these aspects of robustness must be considered.

1.1 Thesis Structure

This thesis addresses the question of how self-organised patterning may arise through cellular contact in developing organisms. It uses the methodology of cellular automata modelling to analyse the fundamental properties of this type of system.

The report is divided into three sections. The first section details an experiment that was carried out in order to investigate the robustness of an abstract artificial developmental system comprising a set of evolved developmental rules. The section begins with an introductory chapter on cellular automata systems and other computational models of development. The following chapters then provide a description of the experimental procedure and an analysis and discussion of the results.

The second section begins with a review of patterning in biological systems. Particular emphasis is placed on Notch signalling and the generation of lateral inhibition patterns via the Delta-Notch pathway. The section continues with a description of a set of experiments that were carried out to investigate the role of Notch signalling in the patterning of microchaetes on the notum of Drosophila flies. Here, it is demonstrated that filopodial protrusions may have an effect on the spacing of the microchaete bristles. Following this empirical analysis is a description of a model that was used to describe the lateral inhibition process. The model is expanded and used to demonstrate the viability of dynamic filopodial Delta-Notch signalling as a mechanism for generating the observed patterns in the real system.

In the third section the cellular automata are revisited; this time using asynchronous cell updates. These elucidate a rule based mechanism by which lateral inhibition type patterns are able to dynamically optimise. It is shown that patterns of stripes can also be generated and refined by a corresponding type of patterning rule. The Delta-Notch signalling model is used to demonstrate that a similar patterning dynamic can be achieved using fillopodia based signalling.

Finally a discussion is provided of the overall thesis findings. This is followed by a concluding summary.

Chapter 2

Methods

This chapter details the computational algorithms and biological data analysis techniques that were used in this thesis.

2.1 Computational methods

All the computer experiments contained in this report were performed using software developed in C++ on a Macintosh 2.33 GHz Powerbook computer. Model output was visualised using the C++ library, OpenGL. The graphical analysis of the model data was performed using Microsoft Excel and MATLAB.

The computer algorithms used for the main experiments are described in this section using pseudo code. This was constructed to represent the key functions of each of the algorithms in such a way that they could be reconstructed elsewhere. Accompanying each of the algorithms is an indication of the runtime for the software.

2.1.1 Cellular automata robustness experiments: Chapters 4-5

Developmental programs based on cellular automata were evolved and tested for their robustness to perturbations. The details of the algorithms implemented are contained in Figures 2.1 and 2.2.

2.1.2 Delta-Notch signalling models: Chapters 8, 9, 11 and 12

To help analyse data collected from Drosophila flies a set of models were constructed in which protein signalling between cells was mediated by dynamic filopodial protrusions. Rate equations were used simulate gene activation and inhibition, and the filopodia dynamics were simulated according to a mechanistic algorithm which constantly updated cell-to-cell signalling connectivity.

Figure 2.3 describes the 1D model which was used to compare parameters taken from real data and establish the range of filopodial signalling.

Figure 2.4 describes a 2D model of signalling in a perfect hexagonal array which was used to analyse the pattern optimisation which took place through intermittent signalling.

Finally, Figure 2.5 describes the 2D model that was constructed in which cells were arranged in a pattern that was derived directly from real images of taken the epithelial cells. The real images were traced using Image-J. Each cell was filled with a different grey scale tone and was thus represented by a single number. By this method the image file could be directly read in C++ and converted to represent an array of signalling cells.

Model simulations of each these systems without filopodial signalling (nearest neighbour only) were also performed using equivalent algorithms to the ones provided, however signalling occurred more simply between adjacent cells. In these cases the run-times were slightly faster than those quoted.

A summary of the parameters that were used in each of the Delta-Notch simulations is included in Figure 2.6. A full discussion of how to interpret the model units is contained in the text in Chapter 8.

2.1.3 Asynchronous cellular automata experiments: Chapter 10

Asynchronous cellular automata were investigated and their behaviour was contrasted with the synchronous system outlined above. In these simulations the CA rules were simply implemented using C++ and the graphical visualisations which are displayed in Chapter 10 were constructed using OpenGL. The runtime for a single CA rule, implemented over 10000 time steps was approximately 1 minute.

```
Algorithm for CA developmental robustness experiments – evolving developmental programs

1. Establish set of N (500 in expts) genomes (G) of size n (3,11,23) genes (g) containing CA rules and transition times
for genomes G=1:N  {
      for genes g=1:(n+1)/2 { gene(g) = rand (0:128) x 2 }
     "rule genes 'g' assigned random even integer in the interval  0 : 256"
      for genes g=(n+1)/2+1:n { gene(g) = rand ( (g-(n+1)/2) *100/(n-1)  :  (g+1-(n+1)/2) *100/(n-1) }
     "transition time genes assigned as random integer situated within regular increments over 50 time steps"
                        }

2. Run each genome for 50 timesteps (t) updating the binary  'cell_state' of 100 cells according to CA rules
for genomes G=1:N {
      if (t=1) then (for cells c=1:100 { cell_state(c)=0 } ; cell_state(50)=1 )    "at timestep 1 set centre cell (#50) to
                                                                                    state 1, all other cells to 0"
      set CA_RULE = gene(1))  "all cells initially run genome rule 1"
      count=1    "sets a counter to the position of first time gene"
      for t=2:50 {
                  if (t=gene(count+(n+1)/2)) then (count=count+1; set CA_RULE = gene(count))
                  "if timestep matches transition time gene, then change to next rule gene and increment counter"

                  for cells c=1:100 {run CA_RULE}   "each cells state is updated according to the CA rule which analyse
                   }                                 the state of its nearest neighbours  – CA algorithm detailed in main text"
                     }

3. At time step 50 compare the pattern with the target pattern to obtain 'fitness' score
for genomes G=1:N {
     if (t=50) then ( for cells c=1:100 {
                                          if (cell_state(c) ≠ target_state(c)) then ( fitness (G) = fitness (G) + 1 )
                                        }
                   ) "compares the state of cells in CA array with cells in target pattern (target_state) of 100 cells.
                      "sums total difference (Hamming distance) between patterns. "
                      }

4. Apply tournament selection to establish next generation
for trials T=1:N {
   randSelection1 = rand(1:500)    "picks two random genomes"
   randSelection2 = rand(1:500)    "picks a random genome"
     if (fitness (randSelection1) < fitness (randSelection2) ) then (genome(T) = genome (randSelection1))
                                                                 else  (genome(T) = genome (randSelection2))
                  }

5. Apply random mutation to next generation
for genomes G=1:N  {
if (rand(1:100 < mutation_rate x 100) then(      "uses a random generator to simulate probability of mutation"
randMutation = rand(1:n)    "picks a random gene to mutate"
 if (randMutation <= n+1/2) then (
       gene(randMutation) = rand (0:128) x 2 } )
     "rule genes 'g' assigned random even integer in the interval  0 : 256"
 if (randMutation > n+1/2) then (
       gene(randMutation) = rand ( (randMutation) -(n+1)/2) *100/(n-1)  :  (randMutation) +1-(n+1)/2) *100/(n-1) })
     "transition time genes assigned as random integer situated within regular increments over 50 time steps"
                                        )
                        }

6. Repeat stages 2-5 for 1000 generations
```

Figure 2.1: Algorithm for evolving cellular automata (CA) in robustness experiments. This algorithm was used to evolve developmental programs using tournament selection and mutation. NB: This algorithm does not describe the implementation of the individual CA rules which are detailed in the thesis text and in other references. The CA programs could be visualised in realtime using the OpenGL library which was embedded in the functional code. The total computational runtime (with no graphical output) for evolving 500 genomes, of size n=11, for 1000 generations was approximately 15 minutes.

```
Algorithm for CA developmental robustness experiments – testing robustness to cell perturbations

Algorithm is initially implemented with a set of N, evolved genomes (G) of size n (3,11,23) genes (g) containing CA
rules and transition times. (Also compared with un-evolved genomes)

Run each genome for 50 timesteps (t) updating the binary 'cell_state' of 100 cells according to CA rules
for genomes G=1:N {
    if (t=1) then (for cells c=1:100 { cell_state(c)=0 } ; cell_state(50)=1 )   "at timestep 1 set centre cell (#50) to
                                                                                state 1, all other cells to 0"
    set CA_RULE = gene(1))  "all cells initially run genome rule 1"
    count=1   "sets a counter to the position of first time gene"
    for t=2:50 {
            if (t=gene(count+(n+1)/2)) then (count=count+1; set CA_RULE = gene(count))
            "if timestep matches transition time gene, then change to next rule gene and increment counter"

            for cells c=1:100 {run CA_RULE}   "each cells state is updated according to the CA rule which analyse
            }                                  the state of its nearest neighbours – CA algorithm detailed in main text"
        }

At time step 50 save the final pattern as new target pattern
for genomes G=1:N {
    if (t=50) then ( for cells c=1:100 {
                        (target_pattern(c) = cell_state(c))
                    }
            )
        }

Derive robustness measure. Develop genomes and compare old pattern with perturbed patterns.
for genomes G=1:N {
  cycle=0   "a counter that increases each time a new perturbation is made"
    for T=2:50
     for cells C=1:100  {{
      "repeats run stage this time perturbing each cell in the developing pattern"
      if (t=1) then (for cells c=1:100 { cell_state(c)=0 } ; cell_state(50)=1 )   "at timestep 1 set centre cell (#50) to
                                                                                  state 1, all other cells to 0"
       set CA_RULE = gene(1))  "all cells initially run genome rule 1"
       count=1   "sets a counter to the position of first time gene"
       for t=2:50 {
            if (t=gene(count+(n+1)/2)) then (count=count+1; set CA_RULE = gene(count))
            "if timestep matches transition time gene, then change to next rule gene and increment counter"

            for cells c=1:100 {
                    if (t=T AND c=C AND cell_state(c) = 1) then (cell_state (c) = 0, cycle++)
                    "perturbs each cell and registers as new cycle"
                    run CA_RULE   "each cells state is updated according to the CA rule which analyse
                    }              the state of its nearest neighbours – CA algorithm detailed in main text"
            }
    "repeats fitness measure with target pattern implemented as the original final pattern"
     if (t=50) then ( for cells c=1:100 { if (cell_state(c) ≠ target_state(c)) then ( fitness(cycle)++ ) } )
            "compares the state of cells in CA array with cells in original pattern (target_state) of 100 cells.
            }
                }}

Robustness=mean(fitness(cycle)) "robustness defined as the mean fitness measure after each perturbation"

            }
```

Figure 2.2: Algorithm for testing robustness of cellular automata (CA). This algorithm was used to test the evolved developmental programs for robustness to cell state perturbations. Open GL was used to visualise the experiment in real time. The total computational runtime (with no graphical output) to test 500 genomes of size n=11 was approximately 1 hour.

Algorithm for 1D filopodial signalling

Establish line of L cells (100 in model expts.) with apical radial sizes (A) based on measured data (mean = A_μ, sd = A_σ)
for *cells n=1:L* { A(n) = rand N(A_μ,A_σ) } "a random float sampled from a Normal distribution – algorithm derived from Central Limit Theorem"
x(1) = 0 "position first cell on 1D line at x=0"
for *cells n=2:L* { x(n) = x(n-1) + A(n-1) + A(n)} "all other cells are subsequently positioned relative to previous cell"

Assign each cell start values of Notch and Delta (mean = Base_μ, sd= Base_σ)
for *cells n=1:L* { Notch(n) = rand N(Base_μ, Base_σ), Delta(n) = rand N(Base_μ, Base_σ)} "samples from Normal dist"

Assign each cell filopodia (F) (also lamellipodia for models [2] & [3]) based on measured distribution (mean = F_μ, sd = F_σ)
for *cells n=1:L* { F_left(n) = rand N(F_μ,F_σ), F_right(n) = rand N(F_μ,F_σ) } "independently assign 'left' and 'right' extension from cell centre"

At each time step update Notch, Delta and filopodia distribution
for *each time step* {
"get Delta input (D_in) signal from contacting cells where filopodia 'overlap' (NB: same principle is applied for other models [1],[2],[3])"
for *cells n=1:L*
for *immediate neighbour cells m=n+1, m=n-1*
{ D_in(n) = D_in(n) + α_apical.Delta(m) } *"sum and scale (by α_apical) Delta in apically contacting cells*
for *all other cells p=1:L , p≠m≠n*
{ **if (** x(n) **>** x(p) **AND** x(n) – F_left(n) **<=** x(p) + F_right(p) **)** "establish if contact on left"
OR **if (** x(n) **<** x(p) **AND** x(n) + F_right(n) **>=** x(p) - F_left(p) **)** "establish if contact on right"
then (D_in(n) = D_in(n) + α_basal.Delta(p) **)** *"sum and scale (by α) Delta in contacting cells according to equation 1"*
}
"update Notch and Delta values for all cells according to numerical solution of equation 1 – assuming unity time step for δt in Euler method."
"includes random noise term with default scaling factor, e = 0.01"
for *cells n=1:L* { Notch(n) = Notch(n) – μ.Notch(n) + R_N.$D\_in(n)^k$ /(a+$D\_in(n)^k$) + rand N(0,Notch(n)*e)
Delta(n) = Delta(n) – ρ.Notch(n) + 1 /(1 + b*$Notch(n)^h$) +) + rand N(0, Delta(n)*e)
}
"simulate filopodia dynamics by updating over random intervals set by F_rate (0.01 in model expts. giving an effective mean 'lifetime' of 100 steps)"
for *cells n=1:L* { **if (** rand(1:1000) < F_rate*1000)**) then** F_left(n) = rand N(F_μ,F_σ) "generate rand int to determine if filopodia are resampled"
if (rand(1:1000) < F_rate*1000)**) then** F_right(n) = rand N(F_μ,F_σ)
}
}

Every t_test timesteps (100 in model expts.) compare cells with t_stableInt timesteps earlier (1000 in model expts.). If <stableMin % change in pattern of Delta expression (1% in expts.) measure spacing and end algorithm
for every t_test timesteps {
for *cells n=1:L* { **if (** Delta(n)>D_Threshold*)* *"decide if Delta is higher than threshold (set at 1 in expts.) and if so label cellstate=1"*
then (cellstate(n,t)=1 **else** cellstate(n,t)=0**)** *"save cellstate as function of time"*
}
if (sum (|cellstate(n,t)-cellstate(n,t-t_stableInt)**|) / L <=** stableMin**)** *"if less than stableMin % of pattern has changed in t_stableInt steps"*
then (for *cells n=1:L* {**if (**cellstate=1**) then (for** *cells m=n:L* {**if (**cellstate=1**) then (**spacing (n) = x(m)-x(n), breakloop **))** } *"measures spacing between centre of consecutive Delta expressing cells"*
exit) }
NB: Algorithm was repeated 30 times for each parameter set to obtain mean data

Figure 2.3: 1D model of filopodial signalling. The algorithm summarises the implementation of a model in which a line of cells signal via overlapping dynamic protrusions. The runtime for 30 simulations with typical parameters was approximately 5 minutes (this varied depending on the protein decay rates implemented which set the total stable patterning time). The model was visualised in real time using OpenGL.

Algorithm for 2D filopodial signalling in hexagonal array

Model is implemented on a 2D hexagonally packed array with total number of T uniform cells arranged in a square grid (T=30x30=900 in 2D packing expts.) Different communication ranges are defined by neighbourhood of hexagonal shells. This algorithm limits communication to apical contact via the nearest neighbour shell, R1, comprising 6 cells, and through filopodia at the second neighbour shell, R2, comprising 12 cells.

Assign each cell start values of Notch and Delta (mean = Base_μ, sd= Base_σ)
for *cells n=1:T* { Notch(n) = rand N(Base_μ, Base_σ), Delta(n) = rand N(Base_μ, Base_σ)} *"samples from Normal dist"*

At each time step update Notch, Delta and filopodia distribution
for *each time step* {
"get Delta input (D_in) signal from contacting cells"
for *cells n=1:T*
for all *cells at R1 m=1:6*
{ D_in(n) = D_in(n) + α_apical.Delta(m) } *"sum and scale (by α_apical) Delta in apically contacting cells"*
for all *cells at R2 p=1:12* *"sum and scale((by α_basal) Delta from any cells at R2 connected via filopodia link denoted F(n;p) – see below"*
{**if (**F(n;p)=1**) then** D_in(n) = D_in(n) + α_basal.Delta(p) }

"update Notch and Delta values for all cells according to numerical solution of equation 1 – assuming unity time step for δt in Euler method."
"includes random noise term with default scaling factor, e = 0.01"
for *cells n=1:T* { Notch(n) = Notch(n) – μ.Notch(n) + R_N.$D\_in(n)^k$ /(a+$D\_in(n)^k$) + rand N(0,Notch(n)*e)
Delta(n) = Delta(n) – ρ.Notch(n) + 1 /(1 + b*$Notch(n)^h$) +) + rand N(0, Delta(n)*e)
}

"simulate filopodia dynamics by updating over random intervals set by F_birthrate and F_deathrate (i.e. when equal this would lead to a steady state density of 0.5. The lifetime is set by changing F_deathrate only). – NB Filopodia connections are initially absent but are rapidly established in early time steps. *Static filopodial networks are established by excluding the following lines of code when a steady state density is reached"*
for *cells n=1:T*
for all *cells at R2 p=1:12*
{ **if (** rand(1:1000) < F_birthrate*1000)) **then** F (n;p) = 1 *"generate random int to see if filopodial connection is switched (or stays) on"*
if (rand(1:1000) < F_deathrate*1000)) **then** F (n;p) = 0 *"generate random int to see if filopodial connection is switched (or stays) off"*
}
}

At t_max time steps (40000 in expts.) measure spacing to 6 nearest neighbours
if (time step = t_max**) then**
for *cells n=1:T* { **if (** Delta(n)>D_Threshold**)** *"decide if Delta is higher than threshold (set to 1 in expts.)"*
then for *cells m=1:S* {**if (** Delta(n)>D_Threshold**)**
then get spacing (n,m)
}
sort spacing
store spacing (1:6)
} *"save the dist (in terms of hexagonal spacing between delta expressing cells and sort to find nearest 6 neighbours"*
"Coefficient of variation in the spacing is determined as the ratio of the standard deviation and mean in the spacing to the 6 nearest neighbours"
NB: Algorithm was repeated 30 times for each parameter set to obtain mean data

Figure 2.4: 2D model of filopodial signalling in a hexagonal array. In this model signalling occurred over a fixed range of cells defined by the hexagonal shells. The runtime for 30 simulations with typical parameters was approximately 10 minutes (this varied depending on the protein decay rates). The model was visualised in real time using OpenGL.

Algorithm for filopodial signalling with realistic cell packing

A simulated array of cells (total number T) with realistic packing was established by digitally tracing a real image of the epithelia from the Drosophila Notum using Cadherin GFP to determine cell boundaries. The images were traced onto a grid of pixels of size 200x200. Where two cells shared a common pixel boundary they were considered to be touching and would signal apically. The coordinate for the centre of mass of each cell was derived from an average of its component pixels.

Assign each cell start values of Notch and Delta (mean = Base_μ, sd= Base_σ)
for *cells n=1:T* { Notch(n) = rand N(Base_μ, Base_σ), Delta(n) = rand N(Base_μ, Base_σ)} *"samples from Normal dist"*

At each time step update Notch, Delta and filopodia
for *each time step* {
"get Delta input (D_in) signal from contacting cells"
for *cells n=1:T*
for *all cells in direct contact, m*
{ D_in(n) = D_in(n) + α_apical.Delta(m) } *"sum and scale (by α_apical) Delta in apically contacting cells"*
for *all other cells p=1:T, p≠m≠n* *"determine if other cells are connected via filopodia"*
{**if (**R(n;p) **<** (F_range(n) + F_range(p) **AND** | r(n)- r(p)| **<** P/R(n;p)^2 **)** "R(n;p) denotes distance between cell centres, F_range denotes filpodia max range for each cell, r denotes a directional term and P a fixed contact probability as described in text"
then D_in(n) = D_in(n) + α_basal.Delta(p) *"sum and scale Delta (by α_basal) from any cells at R2 connected via filopodia"*
}
"update Notch and Delta values for all cells according to numerical solution of equation 1 – assuming unity time step for δt in Euler method."
"includes random noise term with default scaling factor, e = 0.01"
for *cells n=1:T* { Notch(n) = Notch(n) – μ.Notch(n) + R_N.D_in(n)^k /(a+D_in(n)^k) + rand N(0,Notch(n)*e)
Delta(n) = Delta(n) – ρ.Notch(n) + 1 /(1 + b*Notch(n)^h) +) + rand N(0, Delta(n)*e)
}
"simulate filopodia dynamics by updating over random intervals set by F_rate. Static filopodial networks are established by executing the following code at the first time step only. Filopodia mean range and sd are derived from measured data as used in 1D model."
for *cells n=1:T*
{ **if (** rand(1:1000) < F_rate*1000)**) then** F_range(n) = rand N(F_μ,F_σ), r(n)=rand(1:100) }
"generate rand int to determine if filopodia range and direction term, r, are resampled"
}

At t_max time steps (5000 in expts.) measure density of Delta expressing cells
if (time step = t_max**) then**
for *cells n=1:T* { **if (** Delta(n)>D_Threshold**)** *"decide if Delta is higher than threshold (set to 1 in expts.) and count"*
then DeltaCount++
}
packing density=DeltaCount/T
"density is the ratio of cells expressing high levels of Delta to the total cell number"

NB: Algorithm was repeated 30 times for each parameter set to obtain mean data

Figure 2.5: Model of filopodial signalling implemented with realistic 2D cell topologies. Signalling occurred between overlapping dynamic filopodia extending outward from each cell. The runtime for 30 simulations with typical parameters was approximately 15 minutes (this varied depending on the protein decay rates). The model was visualised in real time using OpenGL.

Figure	Description	Simulation Parameters
8.1-8.3	Behaviour of single cell and two cell system with range of start condition	$\alpha = 1$, $k = h = 2$, $\mu = \rho = 0.01$, $R_N = R_D = 1$, $a = 0.01$, $b = 100$, $e = 0.0$. Start values N=D=10 with different variance implemented (see text) Size = 1 cell (8.1), 2 cell (8.2-3).
8.4	Two cell system with low feedback	$\alpha = 1$, $k = h = 2$, $\mu = \rho = 0.01$, $R_N = R_D = 1$, $a = 0.01$, $b = 0.01$, $e = 0.0$. Start values N=D=10 +/- 0.1. Size = 2 cells. *
8.5 a-c	Row of cells, varying length and variance	$\alpha = 1$, $k = h = 2$, $\mu = \rho = 0.01$, $R_N = R_D = 1$, $a = 0.01$, $b = 0.01$, $e = 0.0$. Start values N=D=10 (where specified +/- 0.1). Size = 20 or 21 cells.
8.6 a-b	Row of cells. Adjacent Delta expression	$\alpha = 0.01$, $k = h = 3$, $\mu = \rho = 0.01$, $R_N = R_D = 1$, $a = 1000$ & 10000, $b = 1000$, $e = 0.01$. Start values N=D=10 +/- 0.1). Row Size = 20 cells.
8.7	Patterning Dynamic In row with high a	$\alpha = 0.1$, $k = h = 3$, $\mu = \rho = 0.002$, $R_N = R_D = 0.1$, $a = 50$, $b = 100$, $e = 0.01$. Start values N=D=10 +/- 0.1). Size = 20 cells.
8.8	Patterning dynamics (variable a)	$\alpha = 0.1$, $k = h = 3$, $\mu = \rho = 0.002$, $R_N = R_D = 0.1$, $b = 100$, $e = 0.0$. Start values N=D=0.1 +/- 0.01). Size = 20 cells.
8.9	1D Parameter sensitivity analysis	Default parameters: $\alpha = 1$, $k = h = 3$, $\mu = \rho = 0.002$, $R_N = R_D = 0.1$, $a = 0.01$, $b = 100$, $e = 0.01$. Start values N=D=1 +/- 0.01. Size = 100 cells. NB: Test ranges are illustrated in figure.
8.10	Multi-parameter analysis of 1D system.	Sampled from ranges: $0.1 < \alpha < 1{,}1 < k < 10{,}1 < h < 10$, $0.001 < \mu < 0.9$, $0.001 < \rho < 0.9$, $0.001 < R_N < 100$, $0.001 < R_D < 100$, $0.001 < a < 10000$, $0.001 < b < 10000$, $0.0001 < N,D < 100$. Default size 100 cells
8.11	Patterning dynamics in 2D	$\alpha = 0.01$, $k = h = 3$, $\mu = \rho = 0.01$, $R_N = R_D = 1$, $b = 100$, $e = 0.01$. Start values N=D=0.1 +/- 0.01). Size = 34x34 cells.
8.13	Effect of hill function terms	$\alpha = 0.01$, k = variable, $\mu = \rho = 0.02$, $R_N = R_D = 1$, $a = 0.01$, $b = 100$, $e = 0.01$. Start values N=D=11. Size = 34x34 cells.
8.14	2D Parameter sensitivity analysis	Sampled from ranges: $0.1 < \alpha < 1{,}1 < k < 10{,}1 < h < 10$, $0.001 < \mu < 0.9$, $0.001 < \rho < 0.9$, $0.001 < R_N < 100$, $0.001 < R_D < 100$, $0.001 < a < 10000$, $0.001 < b < 10000$, $0.0001 < N,D < 100$. Default size 34x34 cells
8.15	Comparing data with real cell model	$\alpha = 0.01$, $k=h=3$, $\mu = \rho = 0.01$, $R_N = R_D = 1$, $a=0.01$, $b = 100$, $e = 0.01$. Start values N=D=10 +/- 0.1.
8.16	Cis-inhibtion	$\alpha = 1$, $\mu = \rho = 0.02$, $k=h=1$, $R_N = R_D = 1$, $a = 10$, $b = 1000$, $e = 0.01$. Start values N=D=10 +/- 0.1.
9.2	1D model with basal signalling with wild type parameters	$\alpha = 0.1$, $k = h = 3$, $\mu = \rho = 0.002$, $R_N = R_D = 0.1$, $a = 0.01$, $b = 100$, e=0.01, Start values N=D=1 +/- 0.01. Size = 100 cells. Algorithm variables** $A_\mu = 1.0$. $A_\sigma = 0.2$, $L_\mu = 0.9$, $L_\sigma = 0.1$, $F_\mu = 1.4$, $F_\sigma = 0.3$, F_rate= 0.01
9.3	1D model with basal signalling with mutant parameters	All parameters as for wild type model above except: Rac (for cells with Delta>1): $L_\mu = 0.8$, $L_\sigma = 0.1$, $F_\mu = 0.9$, $F_\sigma = 0.1$, static filopodia. Scar (for all cells): $L_\mu = 0.7$, $L_\sigma = 0.1$, $F_\mu = 0.7$, $F_\sigma = 0.1$, static filopodia
9.4-9.6	Patterning dynamics in 1D with filopodia	$\alpha = 0.01$, $k = h = 3$, $\mu = \rho = 0.002$, $R_N = R_D = 0.1$, $a = 50$, $b = 100$, e=0.01, Start values N=D=1 +/- 0.01. Size = 100 cells. **$A_\mu = 1.0$. $A_\sigma = 0.2$, $L_\mu = 0.9$, $L_\sigma = 0.1$, $F_\mu = 1.4$, $F_\sigma = 0.3$, F_rate= 0.01
9.7	Comparing basal/apical signal strength	$\alpha = 0.01$, $k = h = 3$, $\mu = \rho = 0.002$, $R_N = R_D = 0.1$, $a = 0.001$, $b = 100$, e=0.01, Start values N=D=1 +/- 0.01. Size = 100 cells. ** $A_\mu = 1.0$. $A_\sigma = 0.2$, $L_\mu = 0.9$, $L_\sigma = 0.1$, $F_\mu = 1.4$, $F_\sigma = 0.3$, F_rate= 0.01

Figure 2.6: Summary of Notch-Delta model parameters...

Figure	Description	Simulation Parameters
9.9-9.10	Example of 2D model with filopodial signalling	$\alpha = 1$, k = h = 6, $\mu = \rho = 0.02$, $R_N = R_D = 1$, a = 0.01, b = 100, e = 0.01. Start values N=D=10 +/- 0.01. Size = 24x24 cells. **: F_deathrate = 0.1, F_birthrate = 0.1.
9.11	Realistic cell packing model with varying contact probabilities.	$\alpha = 1$, k = h = 6, $\mu = \rho = 0.02$, $R_N = R_D = 1$, a = 0.01, b = 100, Start values N=D=1 +/- 0.01. e = 0.01. **: F_μ = 1.4 , F_σ = 0.3 F_rate = 0.5 (for dynamic filopodia): For high probability P=1000, low probability P=100.
11.2-11.4	2D model optimisation experiments	$\alpha = 1$, k = h = 6, $\mu = \rho = 0.02$, $R_N = R_D = 1$, a = 0.01, b = 100, e = 0.01. Start values N=D=10 +/- 0.01., Size = 24x24 cells. **: F_deathrate, F_birthrate were varied to changed connectivity and lifetime.
11.7	Large field filopodial signalling	As above. **: F_deathrate = F_birthrate=0.01
11.8	Large field filopodial signalling	As above. **: F_deathrate = F_birthrate=0.001
12.1	Transition to stripes	$\alpha = 1$, k = h = 6, $\mu = \rho = 0.02$, $R_N = R_D = 1$, a = variable, b = 1, e = 0.01. Start values N=D=10 +/- 0.1. e = 0.01. Size = 24x24.
12.2	Transition to stripes	As above. Signal range at 2 cells. Size = 50x50.
12.3	Stripes need non-linear system	$\alpha = 1$, k = h = 2, $\mu = \rho = 0.02$, $R_N = R_D = 1$, a = variable, b = 1, Start values N=D=10 +/- 0.1. e = 0.01. Size = 50x50
12.4	Stripes at other ranges	$\alpha = 1$, k = h = 6, $\mu = \rho = 0.02$, $R_N = R_D = 1$, a = variable, b = 1, Start values N=D=10 +/- 0.1. e = 0.01. Size variable.
12.5	Stripes refine	$\alpha = 1$, k = h = 6, $\mu = \rho = 0.02$, $R_N = R_D = 1$, a = (50x16)^k, b = 1, Start values N=D=10 +/- 0.1. e = 0.01. **: F_deathrate = F_birthrate = 0.01. Size = 30x30.
12.6	Stripes refine with other dynamics	$\alpha = 1$, k = h = 6, $\mu = \rho = 0.02$, $R_N = R_D = 1$, a = (50x16)^k, b = 1, Start values N=D=10 +/- 0.1. e = 0.01. **: F_deathrate = 0.001, F_birthrate = 0.005. Size = 30x30.
12.7	Stripes in irregular arrays	As for 12.5
12.8	Stripes in larger field	As for 12.5. Size = 50x50
12.9	Cis-inhibtion at range	$\alpha = 1$, k = h = 3, $\mu = \rho = 0.02$, $R_N = R_D = 1$, a = 10, b = 1, Start values N=D=10 +/- 0.1. e = 0.01. **: F_deathrate = F_birthrate = 0.1. Size=30x30
12.10	Cis-inhibtion at range	As above. **: F_deathrate = F_birthrate = 0.01.
12.11	Stripes with cis-inhibition	$\alpha = 1$, k = h = 6, $\mu = \rho = 0.02$, $R_N = R_D = 1$, a = 200, b = 1, Start values N=D=10 +/- 0.1. e = 0.01. **: F_deathrate = F_birthrate = 0.005. Size =30x30.

* +/- refers to standard deviation in the start values of N and D
** Variables relating to the filopodia dynamics are defined in the relevant model algorithms.

MODEL UNITS
Arbitrary units of protein concentration (referred to below as A.U.) are adopted for the purpose of modelling, as these were not explicitly quantified experimentally. Each simulation time step is used to represent a single arbitrary unit of time (referred to as τ) and the production and decay rates are correspondingly represented. The relation between these units and real data is discussed in the main text.

N, D are concentrations measured in A.U; decay rates μ and ρ are in τ^{-1}; production rates R_N and R_D are in A.U.τ^{-1} ; a is in A.U.^{k} ; b is in (A.U.)$^{-h}$; k and h are non-dimensional power terms.

Figure 2.6: Summary of Notch-Delta model parameters. The table lists the full set of model parameters that were implemented for each of the Figures occurring in the thesis. The model parameters relating to the protein dynamics are defined in the text in Chapter 8 where the signalling model is descibed. The remaining parameters are defined in the algorithms detailed in this section.

2.2 Biological Methods

This section summarises the techniques that were used to analyse biological data collected from Drosophila flies. The raw image data that is analysed in this thesis was supplied by the project's experimentalist collaborator, Marios Georgiou. The laboratory techniques used to generate this data have not been detailed here, but are presented in brief in the main text accompanying the relevant figures. All of the data was derived from the notum of developing Drosophila pupae. The pupae outer casing was removed and 3D stacked images of cells in the epithelial layer were obtained by confocal microscopy. A range of genetic fluorescence imaging techniques were employed to identify microchaete precursor cells, apical cell junctions and Notch and Delta protein localisation.

2.2.1 Measuring apical diameters

The thesis is largely concerned with pattern spacing. To obtain a consistent and comparable measure of the pattern spacing this was quantified in terms of the average apical cell diameter prior to the occurrence of any cell division in the developing system (which was observed to take place at 16h APF). Apical cell diameters were measured in 2 perpendicular, directions across randomly selected cells (Figure 2.7). Measurements were taken from 60 cells in 3 wild-type flies at 13-15hAPF (total pooled data size, n = 180). The cells were selected from regions within 3-20 cell diameters from the notum midline where the grid-like patterning of microchaetes took place. For the mutant flies the wild type cell diameter was assumed.

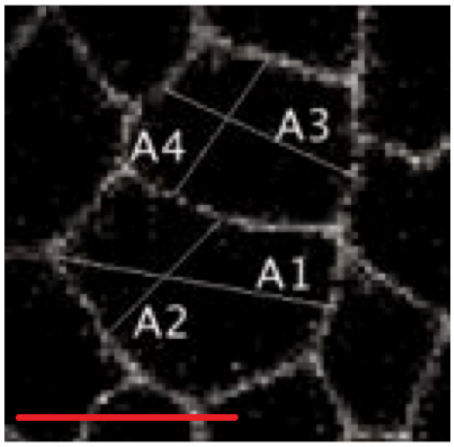

Figure 2.7: Measuring apical diameters. Apical cell diameters (A) were measured in two directions (selected to capture the longest and shortest axis) in 60 cells in 3 wild-type flies at 13-15hAPF. Cell boundaries in the epithelial layer are identified by Cadherin:GFP. Scale bar = 5μm

2.2.2 Measuring intra-row pattern spacing

The spacing between precursor (Neu-GFP expressing) cells was measured in the direction of their row (Figure 2.8) in flies in which the pattern had refined and the precursors were expected to form into microchaetes. For the wild type and Rac mutant these were measured in 3 flies at 23-26h APF, in 5 separate rows close to the fly mid-line, each comprising approximately 8 cells (total pooled data size, n = 87 for wildtype, n=73 for Rac). For the scar mutant, these distances were recorded in 2 flies at 19hAPF carrying large scar mutant clones (total pooled data size, n = 37). Later images of the scar mutants at $> 26h$ APF, in which bristles had begun to develop, were used to confirm the location of precursor cells in the earlier images where the pattern was not yet completely refined. The spacing was measured from one cell centre to the next.

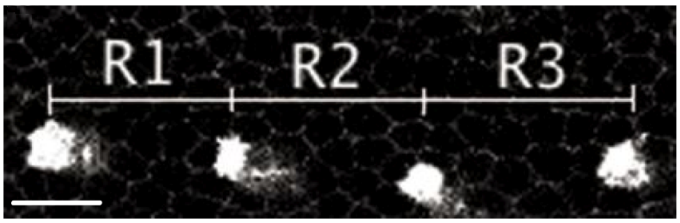

Figure 2.8: Measuring intra-row pattern spacing. The images show how pattern spacing was recorded in the apical section of epithelial cells in the fly notum. Precursor cells are identified by their expression of Neu-GFP. Scale bar = 10μm.

2.2.3 Measuring basal protrusion extension

The lamellipodia and filopodia were measured in the way depicted in Figure 2.9. Lamellipodial (L) and filopodial (F) extensions were measured from the cell centre to their maximum extension parallel to the direction of the microchaete rows. The lamellipodia were identified by the broad spreading of the basal area. Contrastingly the filopodia were identified by the longer thin protrusions. For the wild type, these were measured in three flies over 10 cells in two directions at two hourly intervals between 12h and 20h APF (total pooled data size at each time interval, n = 60) . For the Rac-N17 expressing flies and scar mutant animals these were recorded in 10 cells at 18h APF (total pooled data size, n = 20) . Scale bar = 10μm.

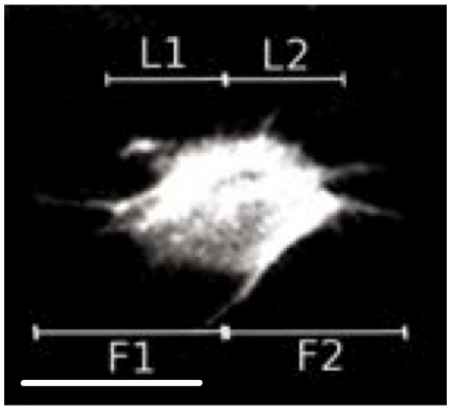

Figure 2.9: Measuring basal extensions. The image shows the basal section of an epithelial cell at 18h APF expressing Neu-GFP. Lamellipodial (L) and filopodial (F) extensions were measured from the cell centre in the direction of the microchaete rows. Scale bar = 10μm

2.2.4 Measuring basal protrusion dynamics

To measure the filopodia dynamics, 2-3 individual filopodia from 5 cells in a single fly pupae at 14hAPF were tracked over a 15 minute time course (total pooled data size, n = 12). The lifetime was defined as the time taken for a single filopodia to extend from a minimal range out to a maximal range and then fully retract .

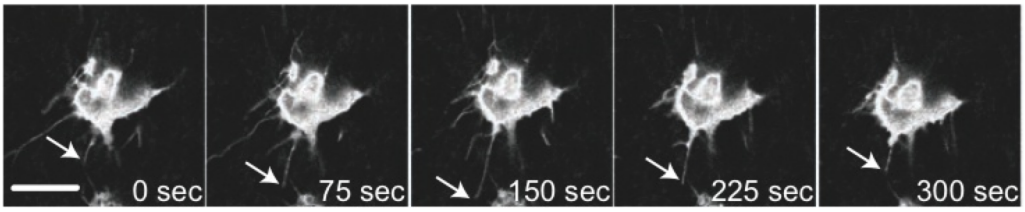

Figure 2.10: Basal filopodia extend and retract, in all directions, from the cell membrane over time. The basal section of a typical Neu-GFP expressing cell is shown. The arrows point to the ends of filopodia that can be observed extending and retracting over the time scale shown. Scale bar = 10μm

2.2.5 Quantifying mean data

The mean values for each of the measurements described were derived from the pooled data collected for the wild type and two mutant types. The standard deviations and errors (95% confidence in the mean) were also derived from the same pooled set of data. Distances are quoted in the thesis in proportions of the mean cell diameter for each fly type. For the Rac-N17 and scar flies, early in the patterning process, the average apical diameter was found to be approximately equal to that of the wildtype in negatively marked clones (data not shown). Therefore the wildtype apical cell diameter was used for calculations in all cases.

Part I

INVESTIGATING AN ARTIFICIAL DEVELOPMENTAL SYSTEM

Chapter 3

Modelling developmental patterning

This chapter provides an introduction to cellular automata as a tool for studying self-organising systems and reviews their application in the modelling of developmental patterning processes. Other model systems that are pertinent to this thesis are also presented here including developmental programs in which robustness has been measured.

3.1 Cellular Automata

Cellular automata are a computational device that were developed in the 1950s, largely by John von Neumann who was trying to create an abstract model of self-reproduction [Sarkar: 2000]. They have since been adopted as an analytical tool in areas as diverse as statistical physics, electronics, cryptography and ecology [Wolfram: 2002]. Perhaps most famously, in the 1970s they received much interest from computer scientists due to the popularity of the *Game of Life* developed by John Conway; wherein, a set of two dimensional cellular automata rules give rise to complex patterning behaviours [Wolfram: 2002, Sarkar: 2000].

Cellular automata represent a particular sub-set of agent based models in which a collection of cells, typically arranged in some kind of regular topology, act as autonomous agents, reacting to each other according to a set of rules. The complexity of cellular automata may vary considerably in regard to the topology of a system, the rules that each cell may follow, the type and number of states that a cell may occupy and the way in which cells are selected to act.

3.1.1 Simple 1D two-state cellular automata

One of the simplest kind of cellular automata that has been particularly well studied is illustrated in Figure 3.1. This shows an example of a one-dimensional (1D) two-state cellular automaton of the type numerically categorised by Wolfram with the rule numbers 0-255 [Wolfram: 2002]. This system consists of a line of *cells* in one of two states; black or white.

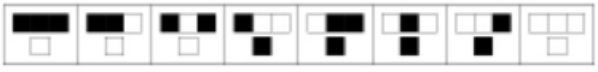

Figure 3.1: Rule 30 update rule set. The top line of each box represents the possible configurations of 3 adjacent squares in the cellular automaton. The square underneath represents the update rule for the cell in the middle based on each of the possible configurations.

When the system is seeded with a single cell it evolves in the way depicted in Figure 3.2.

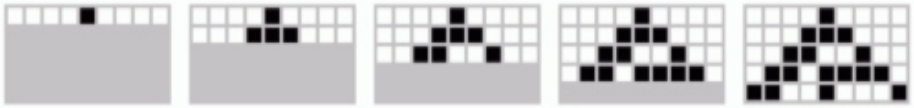

Figure 3.2: The evolution of Rule 30 from a single seed cell. The updated line of cells after each time-step is depicted moving down the page.

For this type of cellular automata, each square on the grid is updated simultaneously according to the set of rules. There are 256 possible configurations of the rules (based on the 8 conditions illustrated in Figure 3.1) which generate very different emergent patterns. Examples of four basic types of patterning persistent among the cellular automata are shown in Figure 3.3 alongside their corresponding rules. Here the cellular automata have been initiated with a single black cell.

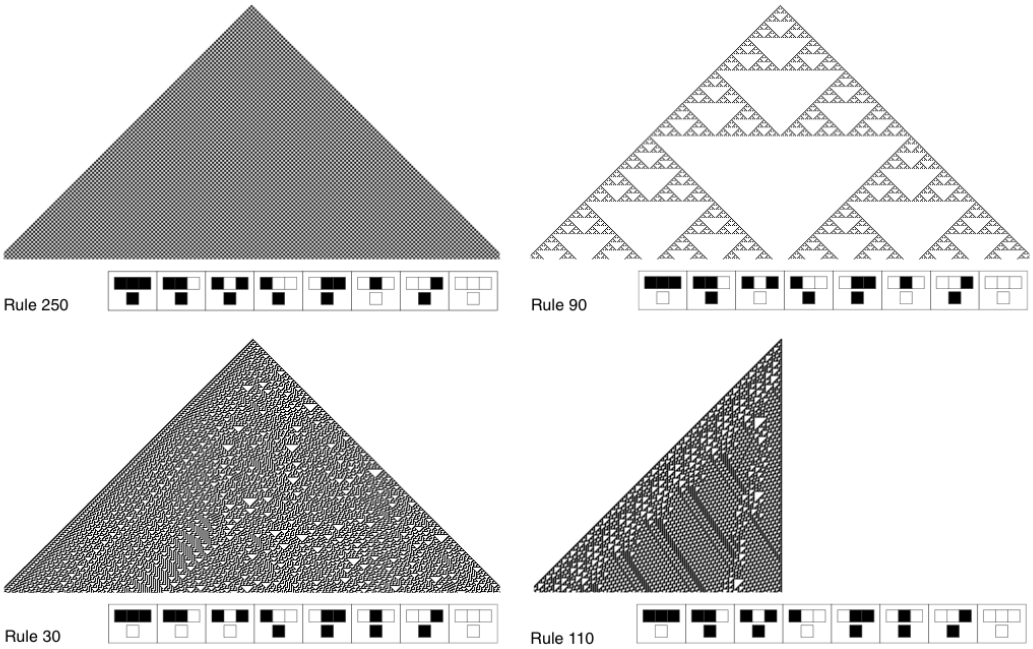

Figure 3.3: Examples of some of the patterning behaviour exhibited by the 256 simple 1D cellular automata. The development of the 1D systems after seeding with a single cell is visualised by showing their state at each time step as a discrete row, with each generation progressing down the page. The cellular automaton rule is shown below each pattern. Rule 250: Simple regular repetition, Rule 90: Nested patterning, Rule 30: Random patterning, Rule 110: Complex localised structures. Image taken from [Wolfram: 2002].

It is immediately apparent from these diagrams that simple rules are capable of generating very different types of rich behaviours. In the above examples the cellular automata were seeded from one black cell. Figure 3.4 shows four distinct classes of behaviour that have been identified when the cellular automata are randomly seeded.

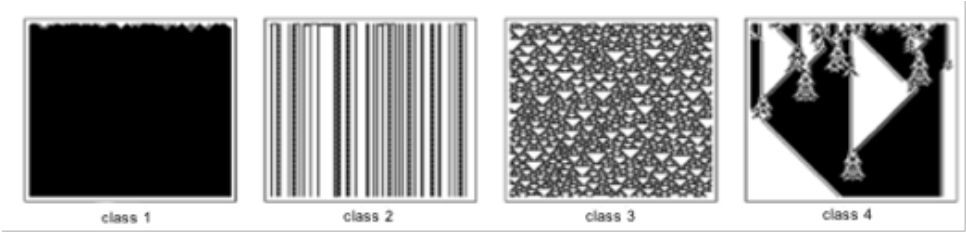

Figure 3.4: Four classes of cellular automata behaviour observed when they are randomly seeded. Image taken from [Wolfram: 2002].

It has been claimed that the behaviours observed among these 256 simple cellular automata are representative of many of the fundamental properties of other more complex dynamical systems with other types of intrinsic rules and emergent patterns [Wolfram: 1983, Wuensche and Lesser: 1992]. The four classes represented in Figure 3.4 have been shown to correspond, in many ways, to different types of *attractors* typically used in the mathematical analysis of dynamical systems [Milnor: 1985, Wuensche and Lesser: 1992]. In class 1 systems random initial conditions lead to a uniform final state. This may happen at differing rates depending on the underlying rules. This type of behaviour can be viewed as representing a simple fixed point or cyclic attractor system. Information contained in the initial conditions is rapidly lost. In class 2 systems simple structures remain indefinitely, sometimes repeating every few steps. This kind of behaviour is much like a system with many attractor states; analogous, in this case, to a ball placed on an uneven surface that falls to the nearest minima [Gray: 2003]. Some information about the initial conditions is maintained but it is always localised. These two classes of behaviour represent the majority of cellular automata; those in which single cell initiation leads to uniform states or regular patterns. In class 3 systems the behaviour is almost random, though small-scale structure such as triangles is always seen. Here information in the initial conditions rapidly spreads throughout the system. In class 4, a mixture of random and ordered behaviour creates localised structures that move around and interact with each other in complicated ways. Information in the initial conditions is spread through the system in a corresponding way. John Conways Game of Life is a famous example of a class 4 2D cellular automaton, in which after random seeding, localised structures can be very vividly seen to move around and interact.

These class definitions, though evidently useful, do not always accurately define the behaviour of all cellular automata rule-sets. Some rules demonstrate behaviours that are highly dependent on initial conditions and other more complex classifications have been proposed [Gray: 2003, Langton: 1990]. What this does provide however is compelling evidence that very different emergent patterns can be generated by very simple rule based interactions. The patterns develop with very different levels of complexity or regularity and correspondingly demonstrate different amounts of sensitivity to initial conditions. The set of 1D cellular automata identified here are explored further in the following chapter where they are used as a model system for generating developmental patterns.

3.1.2 More complex CA have similar emergent properties

Other cellular automata systems show very similar behaviours to the simple 1D patterning rules [Wolfram: 2002, Wuensche and Lesser: 1992]. In more complex cellular automata, cells can be assigned more than two discrete states (Figure 3.5) or cell states can assume a continuous variable (Figure 3.6). In either case the emergent patterns range from the highly regular or uniform to the seemingly chaotic. Characteristic nested triangle patterns can still be observed in the more complex patterns.

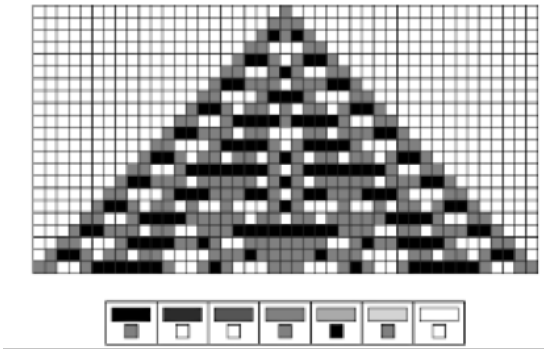

Figure 3.5: A 3-Colour Totalistic 1D cellular automaton (Rule 777). Image taken from [Wolfram: 2002].

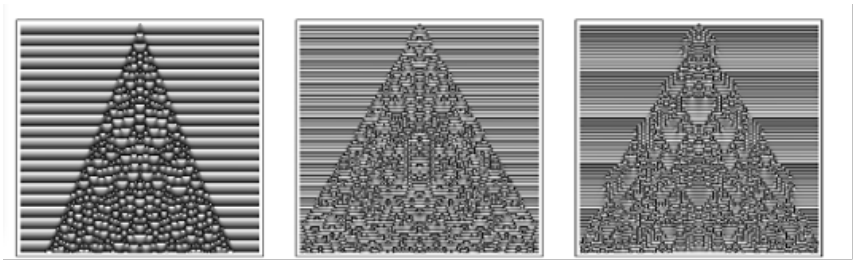

Figure 3.6: Examples of continuous cellular automata. Constants (0.1,0.3,0.325 from left to right) are added to an average of previous cell and neighbour values. The fractional remainder defines the new grey level. Image taken from [Wolfram: 2002].

Figure 3.7 shows examples of cellular automata operating in higher dimensional space. Interestingly when a 1D slice is taken from the higher dimensional systems they appear almost identical to the developmental profiles of the 1D cellular automata; indicating that there is a type of equivalence in these systems. The structures obtained from these cellular automata can be highly reminiscent of crystal structures observed in nature.

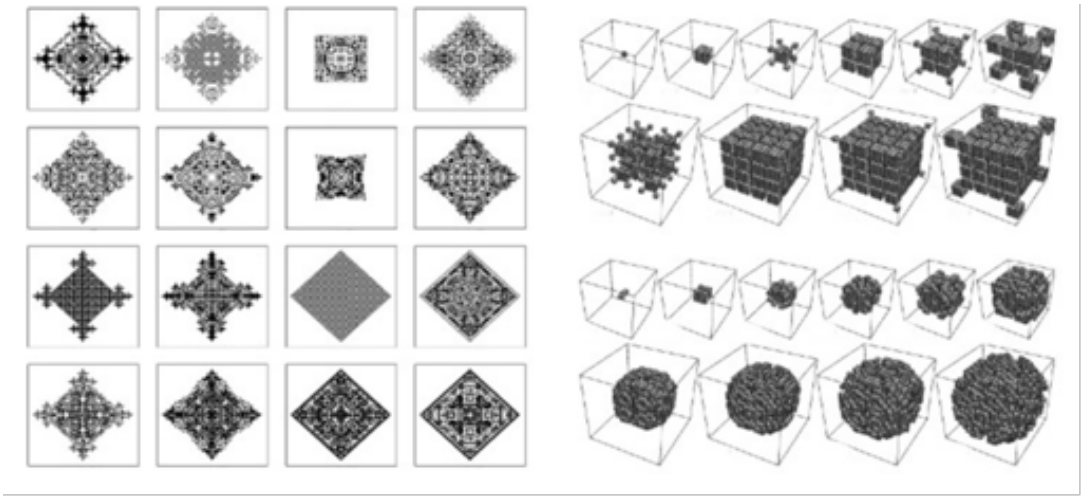

Figure 3.7: Examples of 2D and 3D cellular automata developed using growth rules based on the number of neighbours at each time step. Image taken from [Wolfram: 2002].

Other systems including Turing machines, and substitution systems have also shown to have equivalent behaviours to the simple 1D cellular automata [Wolfram: 2002].

3.1.3 Asynchronous cellular automata

The cellular automata thus far depicted are sometimes described as *parallel* processing systems [Wuensche and Lesser: 1992]. This is because rather than enacting rules in a sequence, as in more typical computer software, a collection of cells process the same rules at the same time (or *in parallel*). In asynchronous cellular automata this condition is broken and cells are allowed to update independently so that the new state of one cell effects the calculation of states in its neighbours. Different algorithms may be used to direct the order in which cells update. These range from completely random cell selection to cycling through cells in order [Cornforth et al.: 2005]. Whilst it has been shown that asynchronous cellular automata can reproduce some of the more abstract computational properties of the synchronous cellular automata (in particular the class 4 behaviour) [Nehaniv: 2004], much of the predictable patterning behaviour is lost. Rules that, in the synchronous system, produced complex nested patterns become chaotic and noisy [Bersini and Detours: 1994, Harvey and Bossomaier: 1997, Kanada: 1994]. These differences will be explored in more depth in chapter 10 of this thesis. It will be shown that although many of the more complex patterns are unattainable, with random cell updates a distinct dynamic is achievable which gives rise to the optimised packing of simple regular patterns.

3.1.4 Applied CA models

So far the cellular automata have been introduced as an abstract way of investigating the emergent behaviour of dynamical systems. Cellular automata have also been used to model the behaviour of more applied real world systems. For example, lattice gas cellular automata have been used to model fluid flow type systems where many particles interact locally to produce large scale patterns of movement [Nagel and Schreckenberg: 1992]. Examples of where this type of model has been applied in biology include rippling in myxobacteria, cell aggregation, swarming and limb bud formation [Alber et al.: 2002].

A common type of model that has been extensively used in physics to investigate the emergent behaviour of interactions on a molecular scale is the Potts model [Potts: 1952]. The Potts model was developed in the 1950s in order to model metallic grain formation. It is a generalisation of an even earlier model from the 1920s, known as the Ising model which was used to interpret ferromagnetism [Brush: 1967]. The Ising model describes the energy associated with spin alignments in neighbouring atoms. It shows that there are potential phase transitions in the global spin alignment associated with the input of external energy (in the form of heat). The Potts model has since been expanded to describe many other cases where local (and often external) energy constraints interact to induce some kind of order [Cipra: 1987]. For high dimensions the model becomes intractable and so simulations are often used which essentially take the form of cellular automata; whereby cells are selected and updated according to local rules [Domany: 1984]. Variants of the Ising/Potts model have been used to study biological phenomena including population dynamics [Baake and Wagner: 2001] and ion channel cooperativity [Liu and Dilger: 1993]. Later in this thesis a patterning process is revealed in which there is a balance between local and global order achieved by the inclusion of signal noise; a process that very closely mimics these types of model.

The *cellular Potts* model is an extension of the Potts model. This describes how local structures form and behave as a result of local interaction energies [Graner and Glazier: 1992, Anderson et al.: 2007]. The *cells* in this model represent small finite regions of space. Cells undergo state transition according to rules that reflect local interaction energies. A number of cells can be grouped together to represent a single unit (i.e. a biological cell). This type of model has been applied in biology to describe phenomena such as chemotaxis, cell sorting in aggregates of embryonic chicken cells, and avascular tumour growth [Alber et al.: 2002, Merks and Glazier: 2005, Chen et al.: 2007, Deutsch

and Dormann: 2005]. A model that incorporates cell adhesion and movement has been applied to stripe formation in salamanders [Deutsch and Dormann: 2005]. In some even more complex models of morphogenesis, other behaviours are introduced as an addition to the Potts model of cell interface energetics, including cell signalling, cell division, and apoptosis [Hogeweg: 2000, 2002].

There is no precise definition of a cellular automaton. For this thesis the term is generally applied to those models in which the local interaction is restricted to a simple rule in order to elucidate large scale emergent phenomena. Many other computational models may also fall within the definition of a cellular automaton although may not explicitly be referred to as such. For example in the cell-to-cell signalling models that will later be introduced and used extensively in this thesis (based on [Collier et al.: 1996]), cells are simulated as separate entities whose molecular components increase or decrease in a way that depends on the molecules expressed in neighbouring cells. Likewise in some models of diffusion cells are treated as separate entities through which chemicals are transferred in and out according to local concentration profiles [Reeves et al.: 2006].

3.1.5 Robustness in developmental cellular automata models

Both natural and artificial developmental systems are known to generate physical forms that are self-regulating and as such are highly robust to perturbations of many kinds including artificial wounding or cell removal [Wolpert: 2002, Kumar and Bentley: 2003]. Robustness to cell perturbation and self-regulation of developed patterns or 3D forms has previously been observed as an emergent property of evolved developmental cellular automata systems. A particular group of examples from computer science were inspired by a conceptual model, known as the French Flag Model which describes how patterns can be generated by morphogen gradients across a tissue [Wolpert: 1969]. In these artificial systems the implicit rules underlying cell state transitions were evolved so that a single seed cell would move, divide and signal in such a way as to generate the target pattern [Miller: 2004, Devert et al.: 2007, Federici and Downing: 2006, Grajdeanu and Kumar: 2006]. It was found that robustness to wounding was an emergent property of the evolved developmental process. Although robustness was not explicitly selected for, the systems were remarkably good at restoring the French flag pattern after a group of cells were removed. Likewise other similar types of cellular automata based models have also exhibited this property of robustness to cell perturbations [Andersen et al.: Fall 2006, Basanta et al.: 2008, Devert et al.: 2007, Federici and Downing: 2006, Grajdeanu and Kumar: 2006]. In all these examples, however, it is often unclear precisely how robustness has emerged, as the underlying rules of development are complex and cells may perform many types of actions. In the following chapter 1D cellular automata rules are employed to investigate the robustness of an artificial developmental system. Using such simple rules, the underlying causes of robustness can be more easily investigated.

3.2 A comparison with other model types

In the cellular Potts model, described above, each cell in the cellular automata represented a portion of a biological cell and local energy functions were applied in order to simulate intercellular forces and subsequent adhesion and motion. As an alternative, *network configuration* models have been used to simulate intercellular forces at cell boundaries and junctions to predict the resultant cellular topologies [Farhadifar et al.: 2007]. Likewise, finite element models may be used to model morphogenetic forces acting on tissues to predict the movements of cells, for example, during invagination [Conte et al.: 2008].

In other types of cellular automata, individual cells have underlying behavioural rules that can generate emergent developmental patterns [Miller: 2004]. In more complex models of plant

development, these two types of approach have been integrated in such a way that behavioural cell rules are implemented alongside a description of more realistic, intercellular physical forces [Rudge and Haseloff: 2005, Dupuy et al.: 2008].

Distinctive branching patterns are observed among plant life and also in the lungs, neurons and blood vessels of animals. It was evident that certain cellular automata rules can reproduce branching patterns (as in Figure 3.3) [Wolfram: 2002] but more typically these are represented by grammatical Lindenmayer (L) systems whereby iterative substitution rules govern cell division or regional tissue branching [Lindenmayer: 1971, Prusinkiewicz et al.: 2007]. In these systems there is no fixed topology as there is in the cellular automata. Figure 3.8 illustrates some of the compelling array of natural looking shapes that can be generated by simple intrinsic rule based systems of this kind.

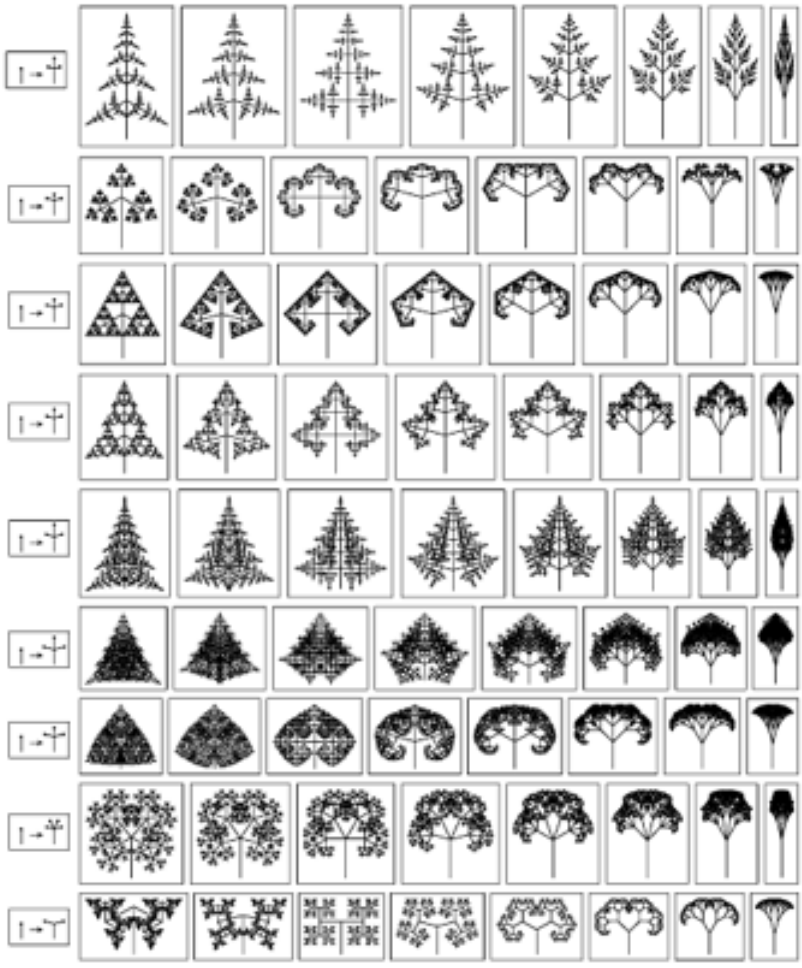

Figure 3.8: Substitution systems in which the rule on the left gives the substitution rule and relative lengths. The progressive images to the right increase the branching angle by 15 degrees. Many of the emergent shapes are recognisable in trees and leaves commonly found in nature. Image taken from [Wolfram: 2002].

3.2.1 Reaction-diffusion systems

In 1951 Alan Turing wrote "The Chemical Basis for Morphogenesis", which described how non-uniform patterns may arise from the reactions between diffusing chemicals [Turing: 1952]. These 'reaction-diffusion' systems have since formed the basis for numerous theoretical mathematical models of pattern formation in biology. It has been demonstrated analytically that for an inhomogeneous

stable pattern to form in a reaction-diffusion model, a minimum of two components are required to form what has been termed an 'activator-inhibtor' system [Gierer and Meinhardt: 1972, Britton: 2003, Murray: 2003]. In such a system one chemical must act as a self-promoting 'activator' with a short range of diffusion. This activator must also promote the production of a second chemical, the 'inhibitor', that, inhibits the production of the activator and must have a correspondingly longer range of diffusion. A simple example of an activator-inhibitor system can be represented by the following set of partial differential equations:

$$\frac{\partial u}{\partial t} = \frac{u^2}{v} - \mu_u u + D_u \nabla^2 u \tag{3.1}$$

$$\frac{\partial v}{\partial t} = u^2 - \mu_v v + D_v \nabla^2 v \tag{3.2}$$

where, u is the *activator* concentration, v the *inhibitor* concentration, μ_u and μ_v are their associated decay rates, and D_u and D_v their diffusion coefficients.

Under certain parameter regimes in which $D_u < D_v$ stable patterns can emerge with local regions high in activator concentration (see figure 3.9). When the range of the inhibitory substance is smaller than the field in which the reaction takes place periodic structures can emerge (in a 2D field these take the form of spots in a roughly hexagonally packed formation). When the field grows at the same time as the patterning these periodic structures can be shown to locate in a more regularly ordered locations [Koch and Meinhardt: 1994]. If the activating component saturates at high concentration then stripes and combinations of spots and stripes can emerge. In other types of reaction-diffusion system unstable patterns of spirals and other oscillating patterns have also been shown to form. Hence, this system has presented a compelling model for many patterns observed in biological organisms.

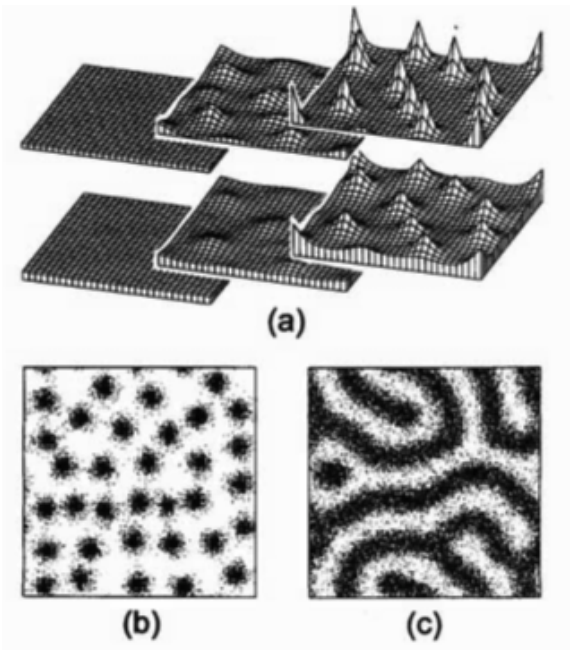

Figure 3.9: Patterning in a reaction-diffusion system. Copied from [Koch and Meinhardt: 1994]. (a) Top: The formation of peaks in activator concentration over time. Bottom: Equivalent collocated peaks in inhibitor concentration have a broader dispersal. (b) In a large field a pattern of roughly hexagonally packed spots (of high concentration) is formed. (c) When the activating component saturates at high concentration the system can form patterns of stripes.

Equivalent models can be derived by systems in which the inhibition or activation are indirect - i.e by the activation or inhibition of an inhibitor respectively. Another closely related set of models incorporate the depletion of a finite quantity of a substrate (with limited diffusive ranges) required for the production of some chemical component [Koch and Meinhardt: 1994]. This leads to regions of high and low concentration that closely resemble the activator-inhibitor model.

The reaction-diffusion system can be simulated by cellular automata [Wolfram: 2002]. This is achieved by having state transitions based on cells at range, whereby different weights are applied to different ranges. Essentially this is just a discrete simulation of diffusion. Later in this thesis, it is demonstrated that a model of cell-to-cell signalling can reproduce these patterns of spots and stripes typically associated with reaction-diffusion systems without the need for diffusion.

3.3 Summary

This chapter has provided a review of a number of different techniques by which patterning systems can be modelled. The simple cellular automata illustrated how seemingly simple rule based interactions can generate a huge range of complex patterns. Small adaptations to individual rules can cause massive changes in their emergent patterns. If such rules underly biological processes then this therefore poses the question; to what extent are developmental systems free to evolve and adapt? Are there rules with very fixed emergent properties acting in sequence and if so, is there some fundamental limit on what evolution can and cannot do? The following section addresses this question by asking what can be achieved by cellular automata rules acting in sequence. Can patterns that are otherwise unattainable by a single rule be achieved by using rules in series. Furthermore, robustness to cell perturbations was identified as a consequence of evolving target patterns using rule based systems with local interactions. The experiment that follows asks whether robustness is a consequence of evolving patterns in systems of this kind and whether genome size has any effect on the overall robustness.

Chapter 4

A model system to explore robust patterning by cell-to-cell communication.

This chapter describes the design and implementation of an in-silico, artificial development experiment in which evolved sequential cellular automata rules were tested for their robustness to cell perturbations.

4.1 Experimental aims

In biological systems there is a fundamental requirement that patterning process are evolvable. A particular developed phenotype must be free to change its form and function in response to environmental pressures. In the previous chapter it was shown how specific rules of interaction tend to generate highly specific patterns. If nature uses such processes then this might imply that small changes to developmental rules will create catastrophic phenotypic changes. Therefore, there must be some way in which nature is able to use different developmental processes in combination that allows for the exploration of different phenotypes.

Patterning processes must also be robust to the inherently noisy conditions that an organism faces during development [Hornstein and Shomron: 2006, Huerta-Sanchez and Durrett: 2007, Lenski et al.: 2006]. It has been suggested that there is a link between evolvability and robustness [Lenski et al.: 2006, Jen: 2005]. Evolutionary models can be used to determine the link between mutation rates, genome size and evolvability; however, it is less obvious how developmental robustness may be linked to these quantities. Robustness to cell perturbation (or 'wounding') and self-regulation of developed patterns or 3D forms has previously been observed as an emergent property of evolved developmental CA systems [Miller: 2004, Devert et al.: 2007, Federici and Downing: 2006, Grajdeanu and Kumar: 2006, Andersen et al.: Fall 2006, Basanta et al.: 2008, Devert et al.: 2007, Federici and Downing: 2006, Grajdeanu and Kumar: 2006]; however, it is unclear precisely how this has arisen in these relatively complex systems. This study investigates the robustness of a simple, evolved developmental system in which cellular automata rules are applied in sequence in order to generate a 1D pattern of cells.

4.2 The developmental system

In order to create a system in which the processes underlying the evolution of developmental robustness could be rapidly analysed in detail, a simple 1D model was developed, in which cellular automata rules are applied in series. Cellular automata rules are known to produce characteristic patterns relating to their dynamical properties and overall system stability [Wolfram: 2002] but it is not immediately apparent how such properties may contribute to the effect of cell perturbations during their development. In particular, no previous study has established how using cellular automata rules in temporal sequence may effect the overall system stability and hence the robustness of patterning. Using this very simple system, it was possible to explore the roles of evolution and genome complexity on developmental robustness.

The experiment uses a 1D two-state cellular automaton of the type defined by Wolfram [Wolfram: 2002] (see Figure 3.3). This system consists of a line of *cells* in one of two states; black or white. (The lines are effectively infinite to avoid edge effects.) For this experiment a black square is referred to as a cell a white square represents an empty space (The physical basis for the cellular automata will be addressed in the discussion of the experiment). At each time-step in the running of the cellular automata, each location is updated according to a set of conditions dependent only on its previous state and the state of its two adjacent neighbours. The complete set of conditions defines an update rule, which operates on all cells in the system at any one time step. Here, a sub-set of 128 rules are used which exclude those rules whereby a cell can emerge from an empty neighbourhood of cells. These are labelled according to Wolfram's numbering scheme and comprise the even numbers between 0 and 255.

The cellular automata are developed for 51 time-steps at which time the 1D pattern generated is referred to as the 'end-state pattern'. In this system the rules are allowed to vary over different time periods, as shown in Figure 4.1, where in this case 6 distinct rules are implemented in series.

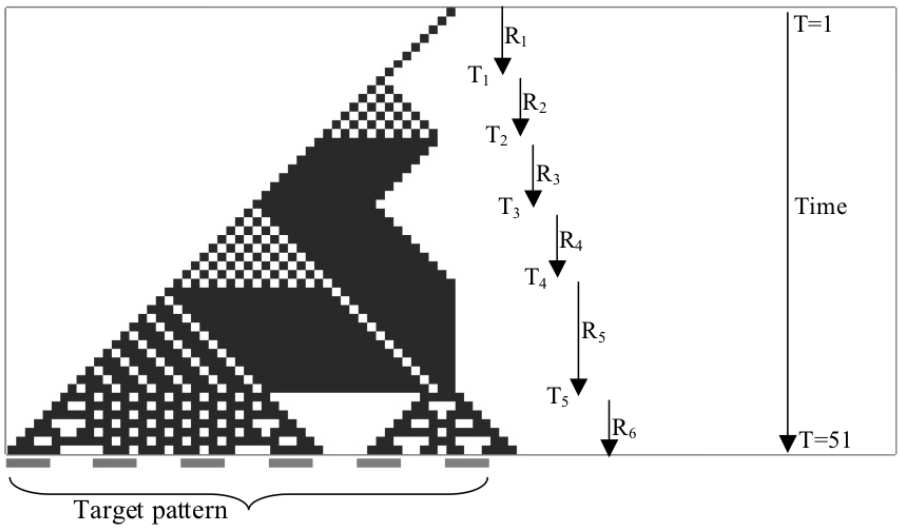

Figure 4.1: A screen shot of an individual experimental run. The end-state pattern at time-step 51 is developed according to the cell update rules. Six rules (R1 to R6) are applied to the system over six different time periods; the transition points of which are labelled T1-T5. The light grey pattern below the box shows the target pattern, P1, towards which the system may be evolved.

The particular rule applied to every cell at each time-step is contained in the 'genome' for each individual run of a cellular automaton. The whole population in any single experiment has the same genome length, or number of genes, n. The specific case illustrated by Figure 4.1 is represented by the n=11 genome: 10 50 174 242 230 122, 9 15 24 32 45. Here the first six numbers represent the

set of rules (R1-R6). The remaining five numbers represent the transitions times (T1-T5) at which the rules change. The transition times are constrained to occur in evenly distributed fractions of the total 51 time-steps. For example. in the n=11 case shown, the 5 transition times occur in bins of 10 time-steps. Where the cellular automata patterns are directed by artificial evolution, the fitness function (defined subsequently) is applied at time-step 51, where the end-state pattern of cells is compared to a pre-defined target pattern (shown in grey).

Genomes of length n=3, n=11 and n=23 were used throughout the experiment, representing 2, 6 and 12 distinct rules and 1, 5, and 11 time periods. The 101 cells in the target pattern can be arranged in 2.5 x 10^{30} different patterns. For n=3 there are 8.2 x 10^{5} possible combinations of rules and times, for n=11 there are 4.4 x 10^{17} and for n=23 there are 8.1 x 10^{31}. Thus for n=23 the number of possible solutions are significantly closer to the size of the target space than for the smaller genomes. However, it should be noted that not all combinations of rules and times will produce distinct patterns.

4.2.1 Evolving patterns

To test the behaviour of the system under specific types of directed patterning the cellular automata were evolved using a *genetic algorithm* [Davis: 1991, Mitchell: 1998]. This was implemented as follows:

A population of size, N, individual genomes was created and these were each developed in accordance with the cellular automata programs.

Genes were initially seeded by a random number generator. The rule defining genes were selected randomly from the complete set and the time values were randomised within the time period constraint as previously described. A fitness function scored each individual according to the similarity of their end-state pattern, at time-step 51, with a pre-defined target pattern.

The target patterns used are shown in Figure 4.2. These were selected to test the effects of varying pattern regularity, symmetry and breadth of distribution. The first six patterns, P1-P6, are the same size, 30 cells, to enable direct comparison, whilst patterns P7 and P8 are 60 cells in size to control for the effects of pattern size.

P1	30 cells, left sided pattern, 5 black, 5 white	
P2	30 cells, symmetrical centred pattern, 5 black, 5 white	
P3	30 cells, symmetrical wide pattern, 5 black, 5 white	
P4	30 cells, non-patterned, centred	
P5	30 cells, non-patterned, wide	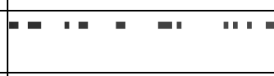
P6	30 cells, non-patterned, symmetrical, centred	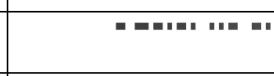
P7	60 cells, left sided, pattern, 6 black, 4 white	
P8	60 cells, non-patterned	

Figure 4.2: Target patterns selected to test for pattern regularity, symmetry, distribution and size.

The fitness function sums the number of cells that differ in their location between the target pattern and end-state pattern of the developed cellular automata. This is equivalent to the 'Hamming distance' between the two bitwise pattern encodings [Hamming: 1950]. Thus the most

'fit' individuals have the lowest 'fitness score' and a perfect correlation scores zero.

A selection process is used to determine which individuals pass to the next generation. During optimisation a number of genetic algorithms were tested that differed in the way they replicate individuals across generations. These comprised: 1) *roulette wheel* selection, where the probability of selection is proportional to fitness; 2) *position* based selection, where the probability of selection is directly proportional to the positional ranking of each individual; 3) *position-squared* selection, where selection pressure is increased by making the probability of selection proportional to the squared ranking of each individual; 4) *tournament selection* where two individuals are randomly chosen and the fitter individual selected [Davis: 1991, Mitchell: 1998]. In each of these cases individuals are randomly selected according to these probabilistic methods until enough individuals are supplied to fill the next generation.

The genomes of the next generation were mutated by randomly selecting either new cellular automaton rules from the complete set or transition times from within the constraints previously described.

Single point crossover was considered in the optimisation phase of the experiment. During crossover, two selected individuals were recombined. A random generator selected a location in the genome and the genes of the two individuals were mixed such that the offspring had the all the genes of one parent prior to the crossover point and the other parents genes after this point. (Crossover was not used for the bulk of the experiment.)

The process of selection and mutation leads to a new generation after which the whole process is repeated. Throughout the experiment a fixed population of N=500 was used and the system was evolved for 1000 generations for target patterns P1 to P8 as well as for an extended 5000 generations for pattern P1 (this set of data is referred to in the results as P1+). Ten evolutionary runs were carried out for every genome size and target pattern. These parameters were all optimised prior to the experiment and were found to be sufficient to achieve stable average fitness scores of low variance.

Optimising evolutionary parameters

The results of the parameter optimisation are shown in appendix Figures A.1 and A.2. The final champion (best individual) scores after 1000 generations were determined for each of the selection types at different mutation rates. It was found that the position-squared method marginally out-performs the tournament selection followed by the position method and finally the roulette method. The tournament selection method was selected for further use in the experiment over the position-squared method primarily as it is more commonly found to be optimal in other genetic algorithms and the differences between these methods were marginal [Oberoi and Rylander: 2004]. Adding crossover to the tournament selection appears to degrade overall performance and crossover was not used again in the experiment. The n=3 genomes showed less sensitivity to changes in mutation rate compared to n=11 and n=23 genomes, which suggests that the process is more dependent on a random search than an evolved transition through the fitness landscape. The mutation rate, per genome, used at each genome size, n=3, 11 and 23, were; 0.6, 0.8, and 1.0 respectively.

4.2.2 Robustness testing

Evolved solutions and unevolved, randomly generated genomes were tested for their robustness to cell perturbations. Each single (black) cell was systematically perturbed (cell state changed to white), one at a time, during the pattern development. The emergent end-state pattern after each cell perturbation was compared with that of the unperturbed cellular automata (see Figure 4.3).

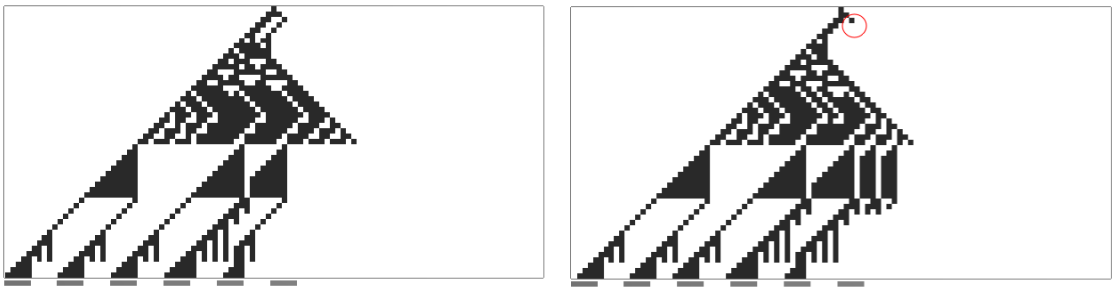

(a) Original n=23 solution consisting of 25 (black) cells.

(b) A single cell perturbation (from black to white) causes a shift in the end-state pattern such that 10 (black) cells are in a different location. Equivalent to a damage score of 40% of the final pattern size.

Figure 4.3: Measuring the effects of cell perturbations.

The damage caused by each cell perturbation was measured in terms of the Hamming distance between the perturbed pattern and the original end-state pattern. This difference was then expressed as a percentage of the original pattern size (the total number of black cells in the end-state pattern). The overall developmental robustness of a particular individual was regarded as being inversely proportional to the average percentage damage caused by all developmental cell perturbations. Mean data from 750 randomized genomes of each genome size was compared with mean data from the 10 evolutionary runs at each target pattern.

4.3 Summary

This chapter has outlined the design of an in silico experiment to investigate the robustness of simple patterning system. Evolved and unevolved developmental programs with genomes of different lengths are tested for their robustness to cell perturbations. Full details of how the model algorithm was implemented are contained in the methods section (Figures **??** and **??**). In the following chapter the results will be presented and discussed.

Chapter 5

Model results and interpretation

A set of cellular automata with genomes of different sizes were evolved under a genetic algorithm by selecting for their ability to match a set of pre-defined target patterns. The genomes contained instructions for the transient update of the cellular automata rules. In this chapter the evolved solutions are investigated with regard to their relative success in matching target patterns, the developmental methods adopted to try meet those target patterns and their robustness to developmental cell perturbations. A discussion is provided of the results and their wider relevance to understanding developmental patterning.

5.1 Pattern Characteristics

Examples of the evolved solutions are shown in Figure 5.1. There were variations in the 10 solutions obtained at each evolutionary run and the subset shown here are intended to illustrate some of the generic differences between the target pattern types and genome sizes. Most immediately striking is the difference in the developmental profiles (that is all the cells at each time-step leading up to the end-state pattern) among the different genome sizes. The n=3 solutions have very distinct profiles characterised by the two different rules applied to meet the target pattern. In contrast the n=23 developmental profiles share a common feature of branching or segmentation at the transition between the 12 rules comprising their genome. There is a complexity of patterning that arises as a result of these rule transitions. The n=11 solutions reflect an intermediate case. It is immediately apparent that the n=11 and n=23 genomes are good at matching the more regularly spaced target patterns but bad at matching a highly distributed random target pattern such as at P5. For the larger patterns, P7 and P8, all individuals of the 3 genome sizes rely on rules that cause an expansion or growth in the number of cells present, as might be expected.

Whilst the target patterns P1-P6 all consisted of 30 cells, the evolved end-state patterns varied in size between 8 and 35 cells. Among randomly generated genomes there was also a significant variation in pattern size. In data obtained from 750 random genomes of each genome size, the average end-state pattern size for n=3, 11 and 23 was 14, 7 and 3 cells respectively. Although the average size was seemingly, relatively low, significantly larger patterns of over 60 cells were also generated by the random samples. The size of the end-state patterns was found to have a significant effect on the robustness of the cellular automata, as is shown later in these results.

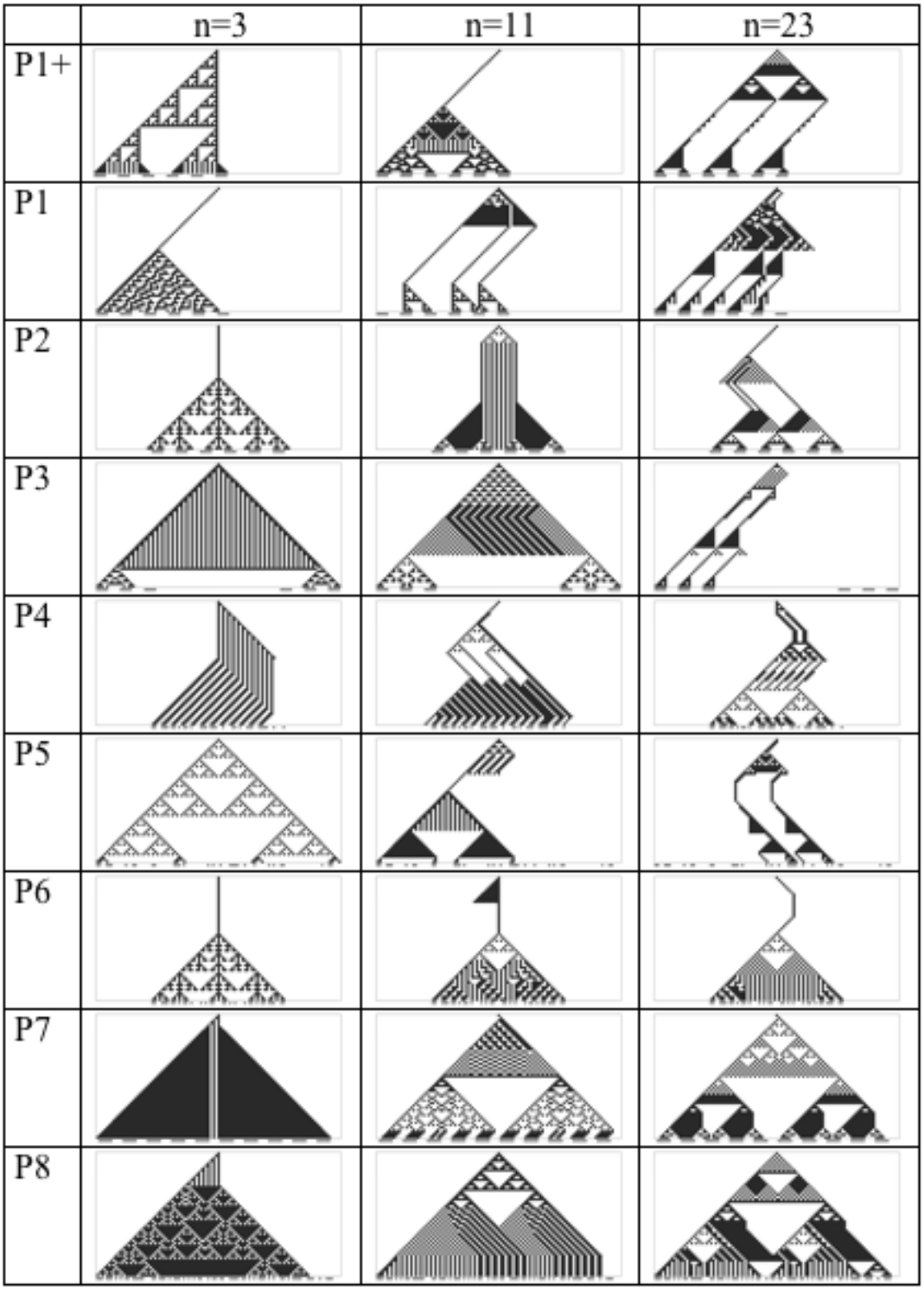

Figure 5.1: Examples of evolved champion solutions obtained at the last generation of evolutionary runs carried out for each genome size at each target pattern. The pattern at each time step is shown with developmental time represented in the vertical axis.

5.2 Fitness of Evolved Solutions

5.2.1 Evolutionary profiles

Figure 5.2 shows the evolution over 1000 generations of the champion individual scores in each of the 10 individual evolutionary runs at each genome size for pattern P1. It is immediately evident that individual runs show a variance in their outcome and are characterised by step changes in the champion score sometimes occurring in a less fit direction. In general the champion scores have become fairly stable after approximately 100 generations for the n=3 genome, 200 generations for the n=11 genome and 400 generations for the n=23 genomes. Smaller step changes in scores continue to occur later in evolution for all genome sizes. There is a range of approximately 5-10 in the final scores after 1000 generations. Similar variance in the individual runs was obtained for the other target patterns.

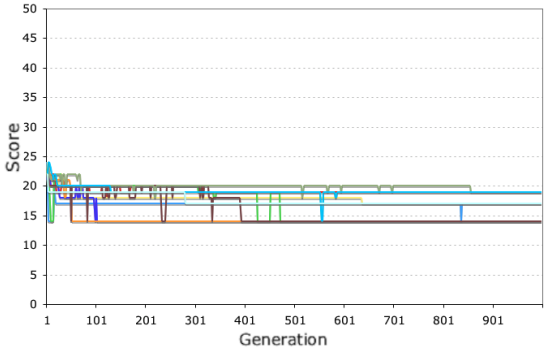

(a) n=3

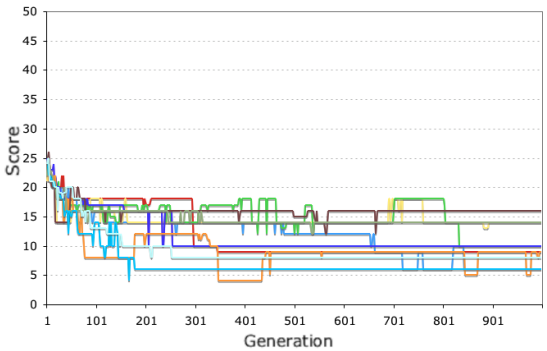

(b) n=11

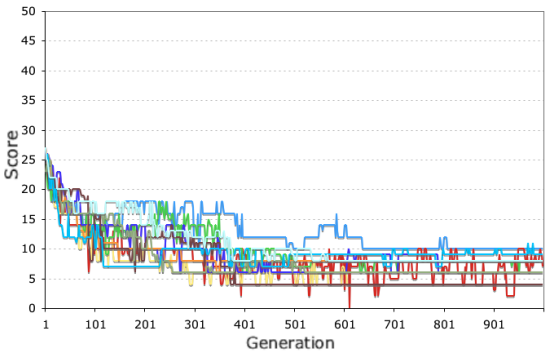

(c) n=23

Figure 5.2: Champion score at each generation for all 10 evolutionary runs (shown in different colours) at target pattern P1. Shown for each genome size.

5.2.2 Average fitness scores

The average scores obtained for each of the genome sizes is shown in Figure 5.3. Average scores are given for the champion individuals at the first and last generations. Overall the larger genomes show slightly less fit (higher) scores at the start of the evolutionary runs, thus indicating that a random population is less likely to match the target patterns. After evolution the n=11 and n=23 genomes achieve very similar average scores, both significantly fitter than for the n=3 case. The evolved differences are therefore correspondingly higher in the larger genome cases.

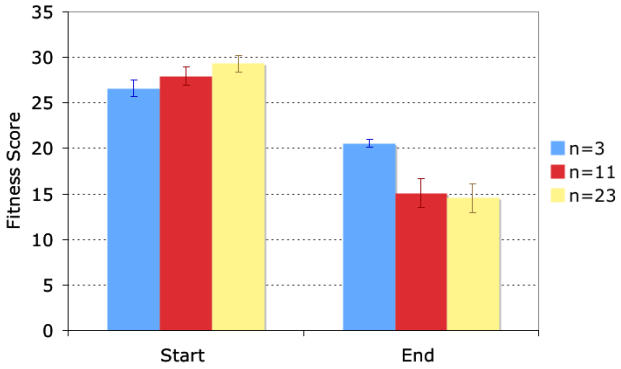

Figure 5.3: The average champion scores attained by each genome size. The data compares the lowest fitness scores from the first generation (labelled 'Start') and the last generation (labelled 'End'), averaged over all target patterns for all 10 evolutionary runs. Error bars show the 95 percent confidence intervals for the mean values.

5.2.3 Comparison with random search

In order to further qualify the relative evolvability at each genome size the fitness scores obtained by evolution were compared with those of a randomly generated population of 500,000. This is the equivalent number of individuals that are searched by the genetic algortithm evolving a fixed population of 500 individuals over 1000 generations. Figure 5.4 shows the champion score at the end of the evolutionary runs (generation 1000 for P1-P8 or generation 5000 in the case of P1+) and compares this with the champion score in a single randomly generated population of 500,000. The n=3 evolved solutions never out-perform the random search solutions. In contrast, for the n=11 and n=23 genomes all of the evolved solutions have a lower mean score (fitter solutions) than for the random search, and only in pattern P4 is this not shown to be significant.

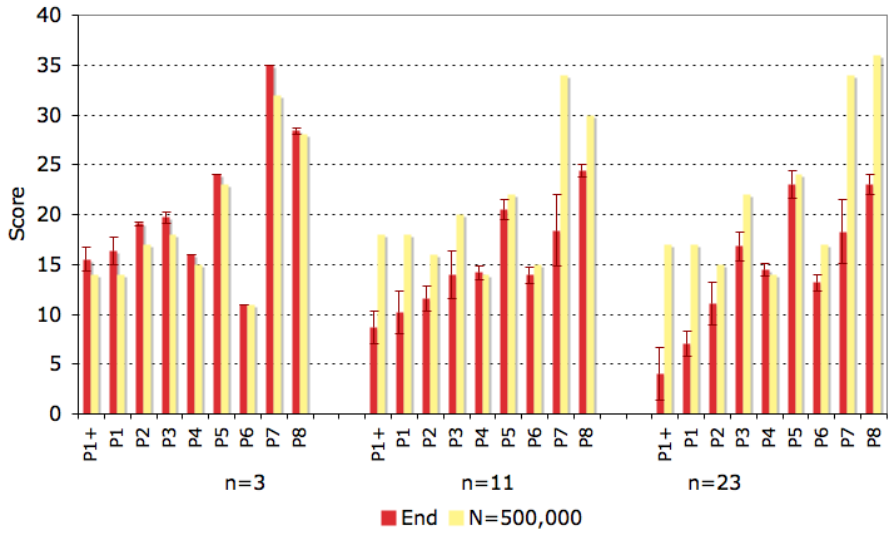

Figure 5.4: Comparing champion scores at the end of the evolutionary process, with the champion score from a single generation of 500,000 individuals. Error bars show 95 percent confidence in the mean value after 10 evolutionary runs.

5.2.4 Fitness scores at each target pattern

There were identifiable differences between fitness scores achieved at each of the target patterns (red bars in Figure 5.4). The n=11 and n=23 genomes consistently outperformed the n=3 genome except

in the case of one target pattern, P6. In general for the two larger genome sizes the regularly spaced target patterns P1, P2 and P7 achieve the fittest relative scores. Where more complex arrangements of cells were encountered these systems did less well in matching the end-state patterns.

5.3 Robustness to developmental cell perturbation

The experiment sought to determine if robustness was an emergent property of evolution in a developmental system and, in addition, whether there was a link between developmental robustness and genome complexity. To analyse the effects of genome size on developmental robustness in this system cell perturbations were made to both evolved and unevolved individuals (see method for details). Figure 5.5 shows a plot of this data. Here, the average percentage damage score has been plotted against the size of the end-state patterns. For the random genomes each individual data point is plotted together with a trend line indicating the population mean and associated confidence intervals for this value. For the evolved solutions, data points are plotted showing the mean value obtained over the 10 evolutionary runs with associated confidence intervals.

5.3.1 Comparing evolved solutions with randomly generated genomes

The evolved solutions for the n=23 genome all sit on the same trend line as for the random genomes and the range of random data in this case is much more constrained than for the n=3 and n=11 genomes. In contrast, for the n=3 and n=11 genomes the distribution of the random data is larger than for n=23. For some target patterns the mean robustness of the evolved solutions patterns is different to the mean random data of equivalent size. The n=3 evolved solutions for target patterns P1, P2, P3, P5 and P6 all have a mean robustness that is significantly lower than for the random data (evolved individuals show higher percentage damage scores within an equivalent pattern size range). For n=11 genomes, the solutions at target patterns P1 and P2 are significantly less robust than the average data. This would suggest that evolution towards these specific target patterns has repeatedly selected for combinations of rules and transition times that are less robust than the average random sample. Part of this loss of robustness may be attributed to the fact that these individuals sometimes show a sustained period without pattern growth that is inherently weak to any perturbation; as can be observed in the examples shown in Figure 5.1 where a single cell is maintained over a number of time-steps before any larger pattern finally develops. A perturbation during this early period without growth will remove the entire pattern. In contrast, the n=23 solutions consistently employ periods of growth and patterning throughout the pattern development. Another factor underlying the loss of robustness of some of the evolved solutions may be a selection for individual rules that are inherently sensitive to perturbations. This will be analysed further in the discussion section.

5.3.2 Pattern size dominates in determining robustness

For all three genome sizes the predominate factor determining robustness is the end-state pattern size itself. To further investigate the effects of end-state pattern size as well as genome size, the mean trend lines from the randomised data are plotted together in Figure 5.6. The curves from each genome size all follow the same trend and there is no significant variation in robustness. Thus, it can be concluded that the use of a greater number of rules does not translate into a change in robustness in this system.

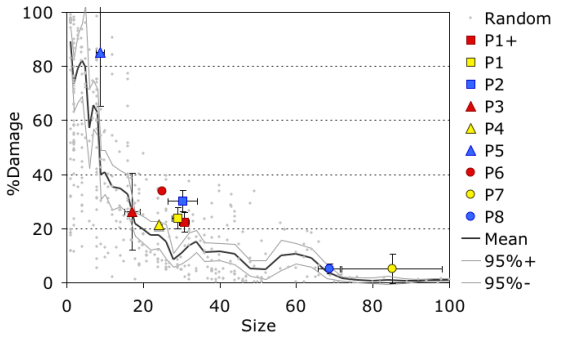

(a) n=3

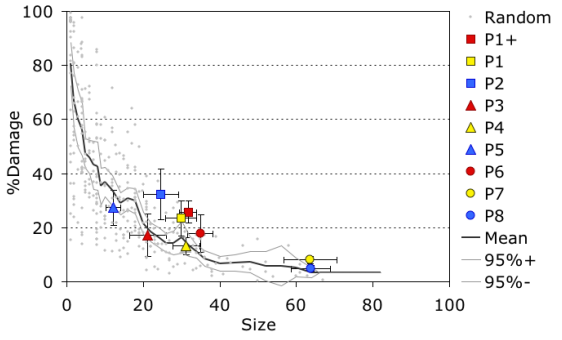

(b) n=11

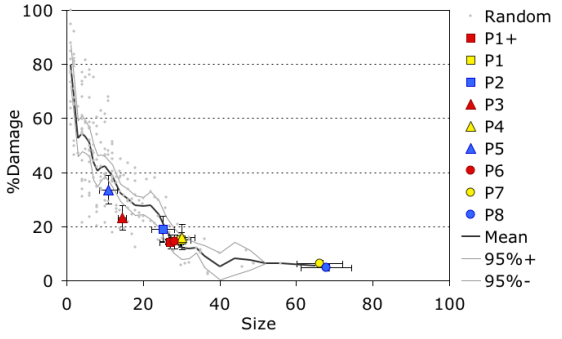

(c) n=23

Figure 5.5: A plot of end-state pattern size against cell perturbation damage expressed as a percentage of size. Data was obtained from 750 randomly generated genomes of each genome size. The trend line shown the mean of this data with associated 95 percent confidence intervals (derived from data bins across ranges of sizes). For the evolved solutions, mean values and confidence intervals derived over 10 evolutionary runs are shown.

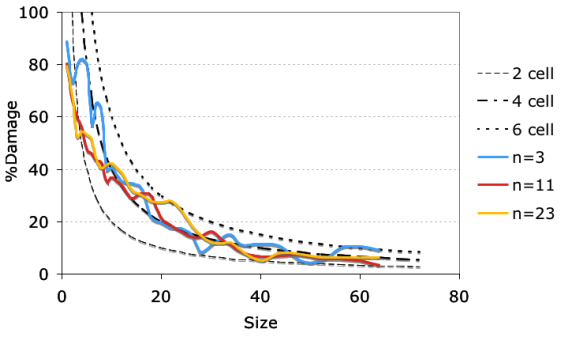

Figure 5.6: The mean trends of end-state pattern size against the average cell perturbation damage expressed as a percentage of the original pattern size. The data was derived from 750 randomly generated genomes of each genome size. This is contrasted with model curves representing a fixed absolute damage, at all pattern sizes, of 2, 4 and 6 cells.

5.3.3 Perturbation damage is independent of pattern size

The real data are contrasted with curves that represent the effects of altering the state of 2, 4 and 6 cells in the end-state pattern; that is, a theoretical plot in which for each cell perturbation the end-state pattern is altered by a fixed amount. The curves obtained from the randomised genomes all follow a trend very similar to that of a fixed 4 cell perturbation. Only for very low pattern sizes, below approximately 10 cells, do the curves align more closely with a fixed absolute damage of 2 cells. This would suggest that regardless of the size of the pattern generated (and thus the average rate of growth of black cells) the average, absolute damage caused by cell state perturbations remains fairly constant over a wide number of randomised genomes. It is important to note that this is an average quantity. The effect of a cell perturbation early in development, where there are fewer cells, causes significantly more absolute damage than one very late in development (where there are likely to be many more cells). What is suggested here is that, averaged over developmental time, the absolute damage caused by a perturbation is largely independent of the ultimate pattern size. The effects of a cell perturbation do not scale in accordance with the rate of pattern growth and end-state pattern size, as might be expected. Hence, the percentage damage caused by a single perturbation rapidly decreases with increasing pattern size as the curves here demonstrate.

5.3.4 Analysing the robustness of individual cellular automaton rules

The results have shown that for all three genome sizes, there is very similar trend between the average robustness of randomly generated cellular automata and their end-state pattern size. However, some evolved solutions show a lower than average robustness than was obtained for cellular automata derived from random genomes of equivalent pattern size. Therefore, it may be inferred that in order to match targets the evolutionary algorithm is repeatedly selecting for particular combinations of rules that degrade overall robustness in these particular cases.

In order to better understand the effects of individual cellular automaton rules on robustness in this system, the rules were categorised and analysed in isolation. Figure 5.7 demonstrates how the individual rules were categorised. The figure shows the behaviour of each rule after input from an arbitrary pattern comprising 11 cells in 9 discrete blocks at time-step one. Each was run for only 40 time-steps to account for the additional 'width' of the input pattern. This 'input' pattern was selected to illustrate the behaviour of the rules at some time into the development of a pattern, as distinct from seeding by a single cell.

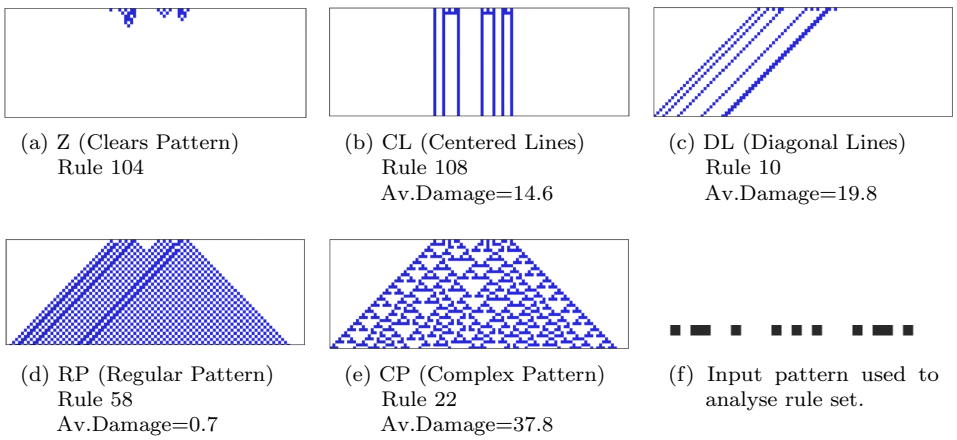

(a) Z (Clears Pattern) Rule 104

(b) CL (Centered Lines) Rule 108 Av.Damage=14.6

(c) DL (Diagonal Lines) Rule 10 Av.Damage=19.8

(d) RP (Regular Pattern) Rule 58 Av.Damage=0.7

(e) CP (Complex Pattern) Rule 22 Av.Damage=37.8

(f) Input pattern used to analyse rule set.

Figure 5.7: Rules classified according the defined criteria. Shown here are examples of each rule 'type'. The rule number is quoted along with average percentage damage score for that particular rule when each cell was systematically perturbed.

A measure of the end-state pattern size and the average percentage damage caused by cell perturbations was made for each individual pattern of each rule type. These are plotted in Figure 5.8.

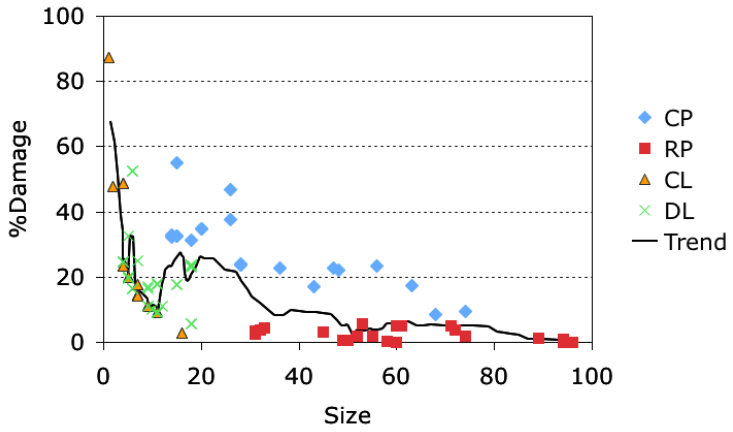

Figure 5.8: The robustness of individual cellular automaton rules of each classification type. The average percentage damage caused by cell perturbations is plotted against the end-state pattern size at time-step 40. The trend line shows a rolling mean average of all the data.

This analysis shows how the regular patterning (RP) rules are significantly more robust to cell perturbation than the complex patterning (CP) rules, regardless of the pattern size. The emergence of a regular pattern of growth from the irregular input pattern indicates that for the RP rules the system has a stable attractor state that is largely insensitive to initial conditions. Thus, perturbing the system later in development has a similarly low effect on the emergent pattern. There is a self organisation inherent in these types of rules. For the complex patterns the system is more sensitive to the initial conditions and forms complex pathways in the development of the pattern, with subsequent interactions when pathways intertwine; this results in the nested triangles characteristic of their developmental profiles. In this case information about previous cell states is transmitted throughout the cellular automata in such a way that cell perturbations have an escalating effect on the emergent patterns at subsequent time-steps. The 'DL' and 'CL' rules that produce substantially less pattern growth show a perturbation response that scales very sharply with pattern size.

The mean trend line gives an indication of the average damage at each size for all the individual rules. It is interesting to note that when contrasted with the curves shown in Figure 5.6 the mean trend among the individual rules closely follows the mean trend for the randomised genomes. This suggests that the average robustness of each of the combinatorial rule systems is essentially the same as the average robustness of the individual rules themselves. This reinforces the finding that the genome size has no intrinsic effect on the average robustness. In addition, it appears that the approximation towards a constant absolute damage (of approximately 4 cells), that was noted previously, can be attributed to a combinatorial effect of the different types of rules. Individually the different types of rules have quite distinct relationships to pattern size and robustness. However, the trend line shows that when aggregated they mimic a system with a fixed average response to perturbations that depends on pattern size.

It should be noted that the classification scheme adopted here is not concrete and there are a few rules that generate pattern that appear to be on the border between these types of classification. There is a correspondence with Wolfram's classification system for this type of cellular automata, such that CL and DL are Class 2, RP Class 1 and 2, and CP Class 3. Rules that fall between between RP and CP are Class 4 systems [Wolfram: 2002]. This system of classification is similar to other definitions relating to the dynamical properties of cellular automata [Wuensche and Lesser:

1992]. The principle distinction made here is that the RP rules are more dynamically stable than the CP rules.

5.3.5 Evolution may select for complex rules that are less robust

To further investigate why the evolved solutions showed differences in their robustness in comparison to the randomised data, an analysis was carried out with regard to the proportion of rules adopted by the evolved genomes. For each of the evolved solutions the ratio of CP rules to RP rules was determined. The increase in this ratio, as compared with the actual rule set was then calculated. This value is plotted in Figure 5.9 against the increase in the average perturbation damage score (or decrease in robustness) obtained by evolved solutions as compared to the mean randomised data of equivalent size (as illustrated in Figure 5.5).

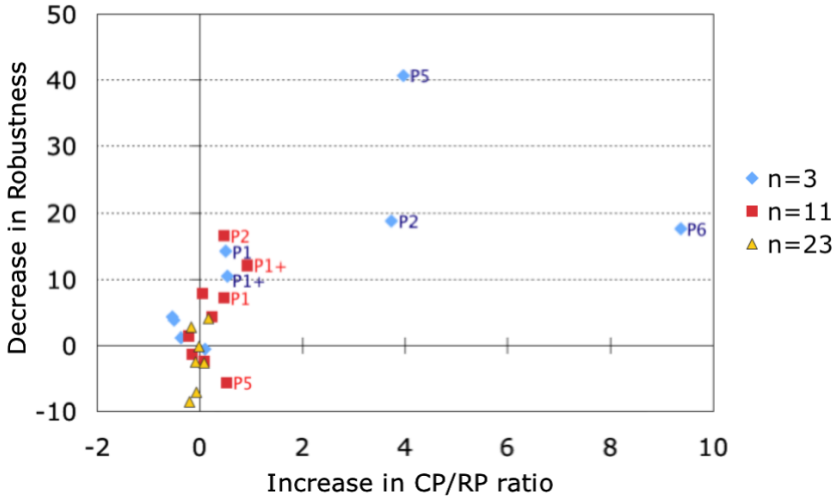

Figure 5.9: The effect of complex patterning rules on the robustness of evolved solutions. The x-axis shows the average difference between the evolved CP/RP ratio with the rule-set ratio. The y-axis shows the average difference between the evolved robustness scores (expressed as an average percentage damage due to cell perturbation) and the mean robustness of random data of equivalent pattern size (from Figure 5.5). Data points located in the upper right quadrant reveal a correlation between complex patterning and a loss of robustness.

This analysis reveals that where CP rules have been used in high proportion, there is, in most cases, an equivalent decrease in robustness (increase in the percentage damage caused by cell perturbations). Therefore, a loss of robustness can be explained by an increased uptake in CP rules, which are required in order to match certain target patterns and are thus selected for by the genetic algorithm. This generalisation is true in all but one example, where for the n=11 genome at target pattern P5 the evolved solutions are seemingly more robust than average whereas the CP/RP ratio is higher than for the rule set itself. This may be attributable to the very small end-state pattern size that was adopted by these solutions, making them more robust than equivalently sized random patterns, even though a significant amount of their development was undertaken by complex growth rules.

5.4 Summary

In this model system, simple 1D cellular automata rules were implemented sequentially so that target patterns could be evolved. The model demonstrated that by changing the rules and their associated transition times complex target patterns could be achieved that were unattainable by

single rules. As one might expect the larger, more complex genome was generally more able to explore the phenotypic landscape; however, for one of the target patterns a smaller genome was better suited as a certain individual rule was particularly well matched to the target pattern.

When the system was tested for robustness to perturbations this exposed how some rules were less robust. Individual rules with different emergent properties had very different responses to perturbations that were closely related to their dynamical properties. Rules that generated patterns with complex divergent patterns were more likely to amplify the effect of a perturbation. Rules that generated more simple regular, repeating patterns were more likely to either rapidly replace a perturbed cell or locally contain the perturbation.

This analysis has demonstrated that there is no intrinsic emergent robustness as a result of increasing the number of sequential 'rules' in a cellular automaton system but there is a potential loss of robustness associated with evolved rule biases in smaller genomes. On average the two larger genomes were shown to evolve better (more fit) solutions than the smaller genome. The evolvability of the larger genome sizes is related to the size of the parameter space that they may select from. The greater complexity of the genome provides the means for complex adjustments in the patterning of cells that is not present in the individual rules themselves. Thus, the n=3 genomes and to some extent the n=11 genome were more reliant on the use of specific rules for the generation of particular patterns and it was shown that when complex rules were used their robustness was degraded. Though the n=23 solutions were not inherently more robust to cell perturbations than the n=3 or n=11 genomes, they did not deviate from a random distribution in their selection of rules.

For randomised genomes of each genome size individual cell perturbations, on average, produced approximately the same amount of absolute damage to the emergent patterns. This was shown to be equivalent to approximately 4 cells. Robustness, here, was explicitly defined as a percentage change in the phenotypic patterns. Hence, there was a strong correlation between robustness and pattern size. In biological systems there may be a corresponding relationship between organism size and robustness, such that larger organisms, containing a greater number of cells, may show less phenotypic response to both developmental and genetic perturbation. Research into the evolutionary adaption of size highlights the physiological or environmental constraints acting on an organism [LaBarbera: 1989]. It may be that there is also an underlying selective pressure to increase organism size for developmental robustness.

There was no evidence for emergent robustness as a product of the genetic algorithm itself. Adding stochasticity or noise to the cellular automata development, by introducing random cell death, may cause the system to evolve more robust solutions. In this scenario it may be that 'fit' solutions that can withstand developmental noise are more likely to be repeatedly selected for during evolution.

The particular cellular automata used here contain update rules that operate at every site. These can be interpreted in different ways as a physical model for development. For example the system could be regarded as a 1D line of cells, signalling to one another and altering their cell state at each time step. For this model to hold, all cells must update their gene expression in perfect synchronicity. Many of the emergent properties of the patterning process relate to this perfect synchronisation of the cell updates. In particular, the complex patterning rules which form nested triangle patterns in their development, rely on the repeated interaction of divergent developmental pathways and without the synchronous cell updates cannot form these stereotypical patterns. Therefore, this system perhaps makes for a potentially poor model of a patterning process of this kind, where it is unlikely that signalling cells could update there gene expression states with perfect synchronicity. As an alternative model it could be regarded as a 2D growth system in which a new line develops at each discrete time step. The rules would then represent a cell growing (or

adhering) based on the state of the preceding line of cells. As long as each line of cells is added before any subsequent line then this 2D system would behave like a synchronous 1D system.

A further potential problem with this model system is in finding a physical basis for the rule transitions. These were made to occur at specific times according to the genome. As a model of a real biological system, this would infer the existence of some kind of genetic clock that triggered different systems on and off at very specific times. However, it is more likely that in a real biological patterning system there must be some kind of 'completion' of each patterning stage that would be a prerequisite for entering a subsequent stage. This may be simply because a patterning system enters a homeostatic phase in which no further patterning occurs or because some kind of feedback signal is activated by a particular checkpoint. This was therefore a fundamental problem with this experiment. It represented a clear departure from reality and an alternative, more complex system for rule transitions would be preferable. However, with this caveat in place, the model did show how using multiple rules different patterns were achievable. The individual cellular automaton rules display a limited set of emergent patterns. It has been demonstrated that even more complex types of cellular automata often show a similar range of pattern types [Wolfram: 2002]. However, nature presents a far wider variety of forms. The experiment here demonstrated how by allowing transitions between different types of patterning rules it became possible to generate patterns that were otherwise unachievable by any single rule. Even though there were large differences between individual rules it was possible to evolve these target patterns using a genetic algorithm in which at each generation rules and transition times could be substituted. The rules themselves were, however, fixed and in a sense were non-evolvable. That is, within each rule there is no continuous variable whose alteration would lead to a continuous change in the emergent pattern. This might therefore represent a true property of biological development where particular stages of patterning may be reliant on a particular type of patterning rule with a limited range of evolvability.

This section has provided an introduction to cellular automata and shown how an artificial system based on simple cellular automata rules could be used to study evolvability and robustness in developmental patterning processes. In the remainder of this thesis a real developmental system is investigated using some of the computational techniques that were developed in this section.

Part II

PATTERNING IN A DEVELOPING EPITHELIAL LAYER

Chapter 6

Developmental patterning and Delta-Notch signalling

This section of the thesis focusses on an empirical study into the patterning of microchaete bristles on the Drosophila notum; a process that is known to rely on cell-to-cell signalling via the Delta-Notch pathway. The following chapter provides an introduction to patterning in animal development and the signalling systems employed by these processes, with a particular emphasis placed on Notch signalling.

6.1 Patterning in biological development

In the introduction to this thesis, developmental patterning was defined as any departure from homogeneity. It was suggested that for patterning to occur, some kind of asymmetrical chemical or physical signal must be generated. Ultimately the process of development is the result of a complex interaction of inter-cellular signalling, cell movement, apoptosis, growth and proliferation but there are subsystems which can be identified in which a particular type of signal or process dominates.

6.1.1 Patterning by chemical diffusion

A common way to set up a pattern in development is to establish a variation in chemical concentrations to which cells (or nuclei in an early embryo) may differentially respond. If a chemical is synthesised at a particular site and allowed to diffuse from that source, a concentration profile is set up to which a cell may differentially respond. A chemical signal of this kind is known as morphogen and this type of process is used by many patterning systems [Wolpert: 2002].

Biological systems are complex and diffusion rarely occurs in a straightforward way. A commonly cited example is in the early Drosophila embryo, where an anteroposterior gradient of the transcriptional regulating protein, Bicoid, controls the differential expression of a succession of further genes and sets out the developing body plan [Reeves et al.: 2006, Lipshitz: 2009]. Whilst it was previously thought that the Bicoid protein was able to freely diffuse from a localised anterior source of maternal mRNA, it has recently been demonstrated that a gradient of *bicoid* mRNA is established in advance, via a novel mechanism involving active transport through a microtubular network [Spirov et al.: 2009]. In the Drosophila wing disc a gradient of the morphogen Dpp is established by a complex combination of processes including extracellular diffusion, ligand-receptor binding and receptor mediated internalisation [Reeves et al.: 2006]. Furthermore, in a dorsoventral patterning system in a vertebrate system, robustly scaling patterns of BMP activation have been

shown to be established via a shuttling process controlled by its inhibitor, Chordin [Barkai and Ben-Zvi: 2009, Ben-Zvi et al.: 2008].

In general, where diffusion is used for patterning, in order to be robust to perturbations and scaling, it often occurs in a complex way involving many cellular processes and control systems. It is therefore not always straightforward to distinguish between long-range signalling and cell-to-cell signalling and patterning systems often employ a combination of both types simultaneously.

Reaction-Diffusion Systems

Although diffusion based patterning systems are repeatedly used throughout development the existence of reaction-diffusion systems is less certain. In chapter 3 a mathematical model was introduced that described the behaviour of reaction-diffusion systems. The model can qualitatively reproduce the type of spots, striping and periodic structures observed in developing organisms ranging from insects, crustaceans, fish and mammals [Maini: 2004, Koch and Meinhardt: 1994, Yamaguchi et al.: 2007, Meinhardt and Klinger: 1987, Murray: 2003, Miura and Maini: 2004] (see figure 3.9). However, the likelihood that this is the correct model to explain biological phenomena is questionable. Although aspects of observable patterning systems are reproduced by the model it has not been conclusively proven in any cases [Othmer et al.: 2009]. The model produces patterning only in a relatively tight parameter regime that can be easily perturbed and therefore lacks the robustness sought after by biological model systems [Plahte: 2001, Britton: 2003]. Patterning is only ever produced when the inhibitor has a much longer diffusion range than the activator. However, molecules dissolved in water tend to have similar diffusion coefficients and so more complex diffusion models are required to substantiate this model. Proposed solutions involve the use of differential adhesion of signalling proteins or including repeated cycles of endocytosis and exocytosis of proteins in and out of cells in order to generate the necessary diffusion rates [Britton: 2003, Reeves et al.: 2006, Teleman et al.: 2001].

6.1.2 Patterning by cell-to-cell signalling

When chemical signalling is restricted to the range of individual cells, this is defined as juxtacrine signalling (as distinct from longer range paracrine, endocrine and autocrine systems) [Gilber: 2009]. Juxtacrine signalling may result in the switching of cell states or it may generate cellular movement via the control of adhesion forces (which are a direct result of membrane bound signalling). Juxtacrine systems include those in which there is communication between cells and a surrounding intercellular matrix; direct communication between cytoplasmic domains through gap junctions; or signalling between membrane bound proteins [Gilber: 2009]. One of the most commonly occurring systems that enables communication between membrane bound proteins is the Notch signalling pathway.

6.2 Notch signalling

This thesis is largely focussed on patterning by Delta-Notch signalling which is used as a model system for studying patterning by cell-to-cell communication. The Notch signalling pathway is an evolutionarily conserved signalling system that is involved in various cell fate decisions in animal development. It functions in various different cellular contexts where it has experimentally been shown to elicit different behaviours and responses [Artavanis-Tsakonas et al.: 1999]. The *Notch* gene encodes a transmembrane receptor, Notch, that is activated by contact with its ligands; Delta and Serrate in Drosophila [Artavanis-Tsakonas et al.: 1999] and their homologues in vertebrates [Lewis: 1998]. Figure 6.1 shows a schematic representation of the Notch pathway in Drosophila.

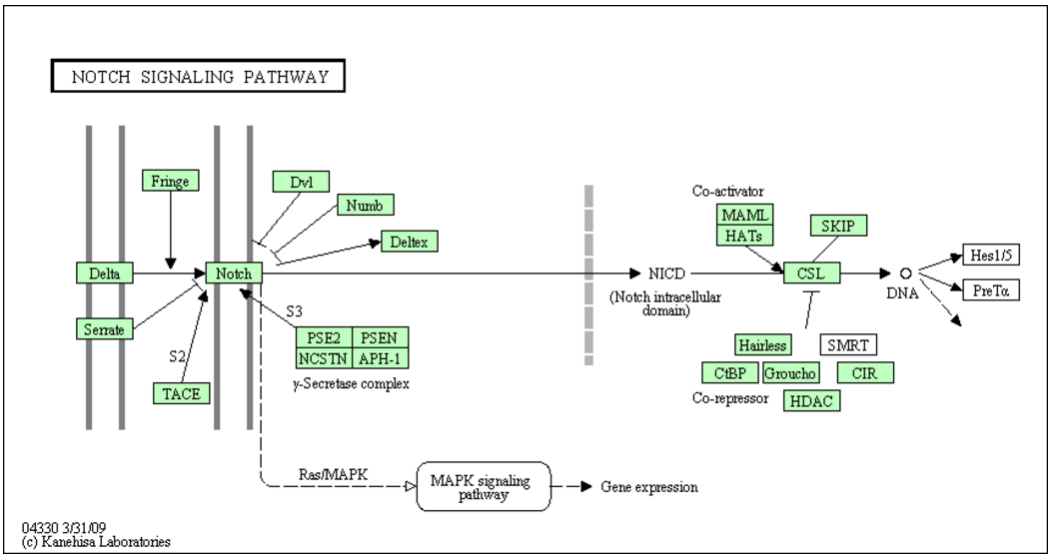

Figure 6.1: The Notch pathway in Drosophila melanogaster. Copied from GenomeNet [*http://www.genome.jp/kegg-bin/showpathway?dme04330*]. The diagram shows the process of activation of Notch by Delta-like proteins on neighbouring cells. This leads to the liberation of the Notch intracellular domain (NICD) from the plasma membrane. The NICD translocates to the nucleus, where it forms a complex with the DNA binding protein CSL, displacing a histone deacetylase (HDAc)-co-repressor (CoR) complex from CSL. Components of an activation complex, such as MAML1 and histone acetyltransferases (HATs), are recruited to the NICD-CSL complex, leading to the transcriptional activation or repression of Notch target genes.

Notch signalling may give rise to patterning directly, when the activation of Notch has an inhibitory effect on the production of its ligand; thereby generating contrasting states of cell differentiation in a process known as lateral inhibtion [Collier et al.: 1996, Simpson: 1990]. Alternatively Notch signalling may induce the same signal in neighbouring cells which can be used to reinforce other patterning processes [Blair: 2003]. Crucially in Notch signalling, direct membrane contact is required for the activation of Notch by its ligands [Artavanis-Tsakonas et al.: 1999, Heitzler and Simpson: 1991]. Indeed, it has been suggested that physical tension is required for Notch cleavage [Ahimou et al.: 2004]. In a recent paper [Agrawal et al.: 2009a] an analysis of the downstream pathways relating to Notch show that the system can exist in a bistable state in which it can either function as a switch or as an oscillator. The precise way in which the different roles for Notch and its ligands are specified during development is as yet unclear but a considerable body of work has provided evidence for a set of identifiable mechanisms.

6.2.1 Lateral inhibition

In lateral inhibition the activation of Notch inside a cell results in the downstream inhibition of the production of Notch ligands within that cell [Artavanis-Tsakonas et al.: 1999, Lewis: 1998, Heitzler and Simpson: 1991]. This resulting feedback loop means that a cell expressing high amounts of a ligand will inhibit neighbouring cells from doing so. This process is known as lateral inhibition. Figure 6.2 shows a schematic of how signalling between Notch and its ligand Delta may lead to a differentiation of cell states in adjacent cells.

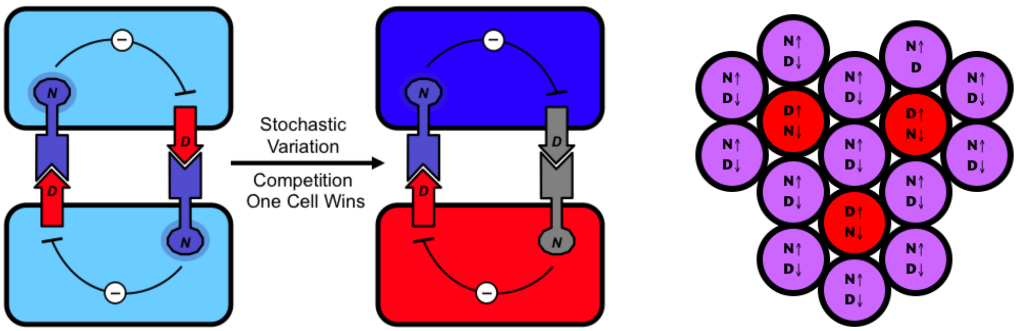

(a) Schematic of Delta-Notch signalling leading to lateral inhibition. Figure derived from [Alberts et al.: 2002]. Delta from contacting cell membranes (D) triggers the Notch (N) receptor which in turn has a downstream inhibiting effect on internal Delta production. Two cells compete until one goes high in Delta and becomes specialized therefore inhibiting the other from doing so.

(b) Stereotypical equilibrium of a 2D layer of hexagonally packed cells undergoing lateral inhibition via Delta-Notch signalling. Cells high in Delta and low in Notch are entirely surrounded by cells low in Delta and high in Notch.

Figure 6.2: Illustration of lateral inhibition via Delta-Notch signalling.

Lateral inhibition is most commonly associated with control of neurogenesis in Drosophila and vertebrates [Lewis: 1998, Cao et al.: 2008, Watt et al.: 2008]. One particularly well studied system of this kind is the patterning of microchaetes, which act as sensory organs, in the epithelial layer of *Drosophila* [Parks and Muskavitch: 1993, Kooh et al.: 1993, Simpson: 1990, 1997, Lai and Rubin: 2001, Lai: 2004]. Here the interaction of Notch with its ligand Delta triggers a chain of intracellular events resulting in the inhibition of the proneural genes *achaete, scute, lethal of scute* and *asense* which give rise to neural development [Lai: 2004, Fiúza and Arias: 2007].

In the neural tube of vertebrates Notch signalling controls the commitment to differentiate as a neuron, between dividing progenitor cells [Lewis: 1998]. Active Notch signalling is typically associated with the inhibition of neural progenitor cell fate though it has also been implicated in promoting the development of glial cell development [Gaiano and Fishell: 2002].

Inhibitory signalling events involving Notch signalling occur in the regulation of many different cell fate choices. Examples include the patterning in the inner ear of vertebrates [Lewis: 1998, Kiernan et al.: 2005], the human endometrium (uterus lining) [Cobellis et al.: 2008], nematode vulva development [Wang and Sternberg: 2001, Braendle and Felix: 2008], differentiation events in the pancreas [Murtaugh et al.: 2003], the regulation of oogenesis [Bender et al.: 1993], Drosophila eye development [Baker et al.: 1996], heart development [High and Epstein: 2008], the regulation of hair cell regeneration in the zebrafish lateral line [Ma et al.: 2008] and the regulation of angeogenesis [Gerhardt et al.: 2003].

Computational models of lateral inhibition by Delta-Notch signalling

Models have been developed in the past to try and analyse Delta-Notch signalling and the generation of patterns of lateral inhibition among different cellular topologies. These vary in the degree to which they make use of analytical mathematical approaches and pure simulation. Mathematical analysis of the system's stable states has previously been applied to single cell, two cell and linear cellular systems; however, only numerical simulations have demonstrated the stable states achievable for a 2D arrays of cells.

In [Collier et al.: 1996] a mathematical stability analysis is applied to a pair of coupled differential equations, where hill function describe the activation and inhibition of Notch and Delta. This is used in conjunction with numerical simulations to interpret the behaviour of the system with 2 cells, a line of cells and 2D arrays with a range of boundary conditions. This model framework

forms the basis for the one adopted later in this thesis

In [Marnellos et al.: 2000] a gene network model is constructed based on the connectionist framework provided by [Mjolsness et al.: 1991]. Their model primarily differs from [Collier et al.: 1996] by combining a 'threshold of activation' in conjunction with a matrix defining the strength of every possible gene interaction; within and between cells. An objective function is used to calibrate the parameters in the model, by aligning the results of numerical simulations, with experimental results obtained from the developing *Xenopus* embryo. The experiment searched for solutions in a 2D array that produced a 1:3 ratio of differentiated to undifferentiated cells and robust solutions with wide ranging parameter sets were found that solved this problem. Notch and Delta injections conducted experimentally were compared with the model results and shown to be in agreement.

In [Ghosh and Tomlin: 2001, 2004, Tiwari and Lincoln: 2002] a hybrid-systems approach is applied to the analysis of the gene network model in [Marnellos et al.: 2000]. In these studies the continuous dynamics of the gene activation processes are modelled as a binary switches which enables a symbolic 'reachability' analysis to be performed on the system. This approach enables an analysis of the two cell system. Conditions are derived for the limiting ratios of the protein production rates and associated switching thresholds at which the system will have a heterogeneous stable state (one specialised and one unspecialised cell).

In all cases it is shown that the positive feedback established between two or more signalling cells will generate patterns of gene expression when the feedback in the system is sufficiently strong.

Cis-regulation of Notch and Delta

In all the aforementioned models, lateral inhibition occurs via the transcriptional regulation of Notch ligands, downstream of Notch activation. In [Miller et al.: 2009] it is suggested that a phenomena known as cis-inhibition might explain the results of a set of genetic mutation experiments performed during the development of photoreceptor precursors in the Drosophila compound eye. About 800 ommatidia form the eye and each is composed of 8 photoreceptor neurons which are recruited by the reiterative use of Notch signalling. In this study they use a mutation to switch off Delta signalling during one of the inhibiting stages. The standard model of transcriptional inhibition of Delta by activated Notch (trans-inhibition) does not entirely explain the resultant data. However, by introducing a new model of cis-inhibition in conjunction with trans-inhibition this result can be explained. In this new model Delta and Notch interact inside the cell cytoplasm in a such a way that Delta molecules attach directly to Notch receptors. In this reaction Delta and Notch will saturate each other so that only when levels of Delta exceed Notch, can Delta signal to neighbouring cells, and similarly only when Notch levels exceed Delta can Notch inhibit Delta production. This is proposed as a general mechanism that co-exists with the trans-inhibition described in the standard lateral inhibition model. In [Smith and Davidson: 2008] it is shown that cis-inhibition of Notch signalling proteins may also play a part in the specification of the endomesoderm in the embryo of sea urchin. In as yet unpublished work [Barad et al.: 2009] it is suggested that the bi-stable property of the cis-interaction can overcome potential problems associated with transcriptional time delays in patterning. The effect of cis-inhibition will be explored further in this thesis.

6.2.2 Lateral induction

Notch activation need not result in the downstream inhibition of the Notch ligand. In some cases the opposite may be true and Notch signalling can induce the production of its ligands. Typically lateral induction is used to ensure homogeneous states among a group of adjacent cells.

Boundary Formation

Notch signalling may be used to when two distinct groups of cells are adjacent to one another, to reinforce a distinct tissue boundary. One example is in the wing imaginal disc in Drosophila where a group of ventral cells expressing Notch and Delta signal to dorsal cells expressing Notch, Serrate and Fringe. Fringe inhibits the ability of Notch to be activated by Serrate, while potentiating the ability of Notch to be activated by Delta [Irvine and Vogt: 1997]. The result is the formation of specialised border cells that organise wing outgrowth. In vertebrates, a similar thing occurs at the apex of the limb buds [Lewis: 1998, Irvine and Vogt: 1997]. Similarly in Drosophila a segmental pattern is formed along the leg by the expression of Notch ligands Delta and Serrate which divide the leg imaginal disc into broad domains which mediate leg segment growth and joint morphogenesis [Greenberg and Hatini: 2009].

Longer range patterning by lateral induction

In [Owen et al.: 2000] and [Wearing et al.: 2000] a distinct type of juxtacrine patterning system is proposed based on lateral induction. In this system the production of free receptors and ligands is induced by the presence of bound receptors and, crucially in this model, is dependent on concentration. They show by analytical methods and simulation that stable patterns of stripes and spots with a range of wavelengths are achievable depending on the particular function invoked. This mechanism has not been further investigated in the context of this thesis and no biological evidence has been identified in support of this model. However, it may represent an example of how longer range patterning could emerge from short range signalling.

6.2.3 Somitogenesis

Somitogenesis is the process by which somites are formed in vertebrates. A molecular oscillator (referred to as the segmentation clock [Giudicelli and Lewis: 2004]) switches on the expression of a set of genes that starts and stops at the formation of each somite; thus converting time and motion into a regular spatial pattern [Giudicelli and Lewis: 2004, Lewis: 2003, Goldbeter and Pourquié: 2008]. The Notch pathway has been shown to be active in somitogenesis where it has been suggested that it regulates both signal generation and synchronisation [Lewis: 2003, Giudicelli et al.: 2007, Rida et al.: 2004]. In a model of this process it is shown that because of the coupling of the Notch pathway with the genes involved in the transcriptional delay circuit, oscillating cells in the system can be synchronised [Lewis: 2003].

6.3 Patterning by physical forces

So far this chapter has focussed on chemical signals that may induce patterning among cells. Alternatively patterns may be generated by movements among cells or tissues brought about by physical forces. Cells can control their short range attractive forces by the use of adhesion molecules. The regulated spatiotemporal modulation of adhesion is often used as a patterning tool in development. This may, for example, give rise to lumen formation in blastula or other types of embryonic compartment formation [Forgács and Newman: 2005, Blair: 2003]. By just changing adhesion properties, cells may move into different compartments. Also changes in surface tensions and internal pressures at a tissue level can lead to further morphogenetic behaviours. Cell growth or cell movement on a tissue scale can generate forces that can result in different types of patterning. Events such as gastrulation and the formation of the neural crest depend on these types of processes [Forgács and Newman: 2005].

The branching of epithelial tissue is another common process in which directed growth or cell movements and shape changes may ultimately govern a patterning process. For example, in models of vasculogenesis the chemotactic movement of endothelial cells in response to an attractant, in combination with a density dependent growth rule can generate fractal type morphologies [Gamba et al.: 2003]. In other types of branching model forces generated at the interface of epithelial and mesenchymal cells can give rise to cleft formation and subsequent branching. [Lubkin and Li: 2002]. Though very different in their detail, in all these examples, underlying physical forces generate motion or deformation which gives rise to patterning.

6.4 Summary

This chapter has provided a brief review of patterning process in developmental systems. It has focussed on the Notch pathway and highlighted the different types of processes that use this cell-to-cell signalling system. Of key importance for this thesis is the process of patterning by lateral inhibition; whereby, one cell expresses high amounts of a Notch ligand and inhibits contacting cells from doing likewise. In the following chapters the behaviour of the microchaete patterning system in Drosophila is extensively analysed using empirical data alongside a computational model.

Chapter 7

Analysis of a biological patterning system

The following chapter provides a summary of data that was generated in order to explore the development of microchaete bristle patterns in Drosophila flies.

The data was accumulated in a collaborative project with Marios Georgiou at the Baum Lab, LMCB, UCL. The biological experiments presented in this chapter were predominantly designed and executed by the project collaborator. The majority of the image analysis and data measurements were performed by the author who also participated in some of the confocal imaging experiments.

7.1 Introduction

The patterning of microchaetes on the notum of Drosophila was selected as a model system to study patterning by cell-to-cell communication. It has previously been shown that the patterning of microchaetes is reliant on communication via the Notch signalling pathway [Simpson et al.: 1999, Heitzler and Simpson: 1991, Parks and Muskavitch: 1993, Kooh et al.: 1993, Artavanis-Tsakonas et al.: 1999]. Furthermore, in this system, the patterning process can be relatively easily imaged live through a window in the pupal case of the fly [Renaud and Simpson: 2002]. Hence, the dynamics can be contrasted with a computational model of the system. Of particular interest in this study was the spacing of the emergent pattern which was used to elucidate details of the underlying signalling system. The signalling is shown to occur through actin based protrusions which can be observed extending from the basal section of epithelial cells. To test this hypothesis genetic perturbations were used to alter the protrusion formation and, as a result, the pattern spacing was correspondingly effected.

7.2 Microchaete patterning in Drosophila

The pattern of mechanosensory bristles (macrochaetes and microchaetes) on the dorsal thorax of the fly has long been used as a system in which to study robust pattern formation [Simpson et al.: 1999, Heitzler and Simpson: 1991]. The larger and more sparse bristles known as macrochaetes are placed relatively precisely on the thorax in response to a complex pre-pattern laid down during earlier stages of development. However, microchaete spacing varies between genetically identical animals. Figure 7.1 shows the arrangement of macrochaetes and microchaetes on the notum of an adult fly. The patterning of microchaetes has been shown to be regulated by Delta and Notch mediated lateral

inhibition [Simpson et al.: 1999, Heitzler and Simpson: 1991, Parks and Muskavitch: 1993, Kooh et al.: 1993, Artavanis-Tsakonas et al.: 1999] and is thought to be self-organising [Wigglesworth: 1940, Simpson et al.: 1999, Heitzler and Simpson: 1991, Artavanis-Tsakonas et al.: 1999]. During the development of this pattern, physical interactions between membrane-bound Delta ligand in the signalling cell and Notch receptors on the surface of the receiving cell trigger an intracellular Notch signal. Because active Notch signalling represses the expression of Delta and proneural gene expression [Tien et al.: 2009], once signalling is initiated, stochastic fluctuations in the levels of surface Notch and Delta in adjacent cells are thought to trigger lateral inhibition (see Figure 6.2 for schematic). This generates a stable pattern of distinct cell types in which each Delta-expressing precursor cell, destined to give rise to a mechanosensory organ, ends up surrounded on all sides by epithelial cells with active Notch signalling [Artavanis-Tsakonas et al.: 1999, Collier et al.: 1996]. Only a few studies, however, have attempted to determine the actual pathway and kinetics of this process in living cells or tissues [Renaud and Simpson: 2002, Masamizu et al.: 2006]

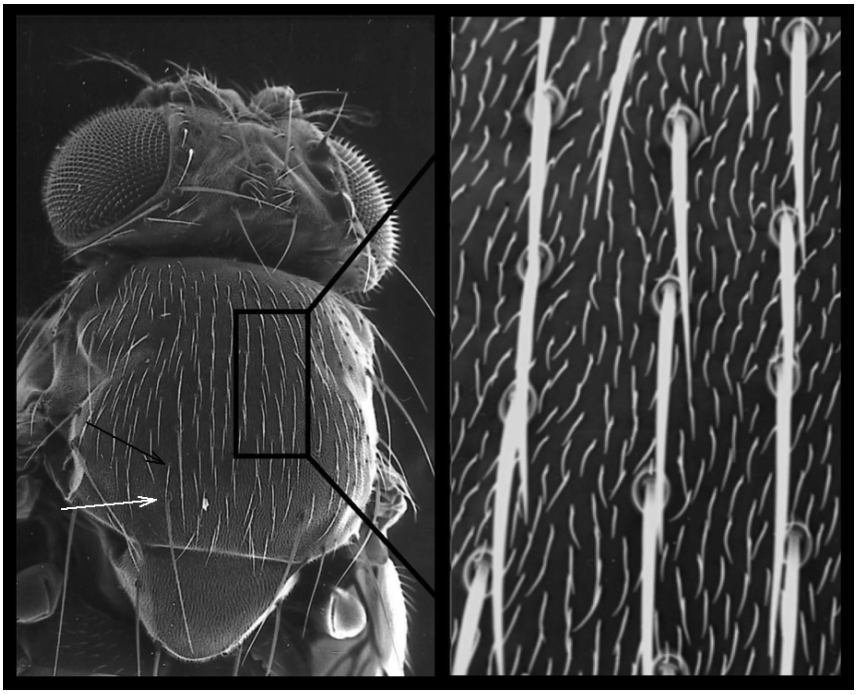

Figure 7.1: The notum of an adult drosophila fly displays precisely located macrochaetes (white arrow) and the more abundant, smaller microchaetes (black arrow) which form in stereotyped rows either side of the fly midline. A few rows of microchaetes are shown in close up on the right. Between each microchaete bristle are 3-5 ordinary epithelial cells each of which display a small hair. [Image adapted from Y. Bellaiche, Institut Curie].

7.2.1 Imaging the emergence of an ordered bristle pattern

By imaging live through a window in the pupal case of the fly the development of a stable pattern could be followed during the period from 12-20 hours after pupa formation (APF) (Figures 7.2, 7.3). Neuralized GAL4;UAS-Moesin-GFP was used to mark proneural gene expression in individual cells as they become committed to a bristle fate [Renaud and Simpson: 2002] (hereafter called Neu-GFP); ubiquitously expressed E-Cadherin-GFP was used to visualize apical cell-cell junctions; and E(spl)mα-RFP was used to visualise active Notch signalling [Castro et al.: 2005].

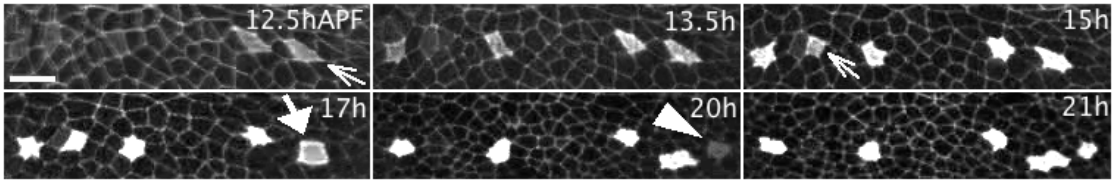

Figure 7.2: A row of Neu-GFP cells emerging and refining over time from an E-Cadherin::GFP labelled epithelium. Small arrows indicate GFP-positive cells that fail to become bristle precursors. Large arrow indicates a Neu-GFP cell switching fate to undergo a symmetrical epithelial division. Arrowhead indicates the initiation of Neu-GFP expression. Scale bar = 10μm. For live imaging, animals expressing the appropriate reporter were prepared by cutting a window in the pupal case, attached to a slide with double-sided sticky tape. A coverslip with a drop of injection oil was then placed over the notum, supported by coverslips at either end to allow imaging from both upright and inverted Leica SP2 or SP5 microscopes.

Although there is an inevitable time-delay between changes in gene expression and the generation of a visible fluorescent signal, it was clear from this analysis that cell movement and division contribute little to the development of a well-ordered pattern during this critical period of development (compare the pattern in Figure 7.3 at 14h APF with the pattern at 26h APF).

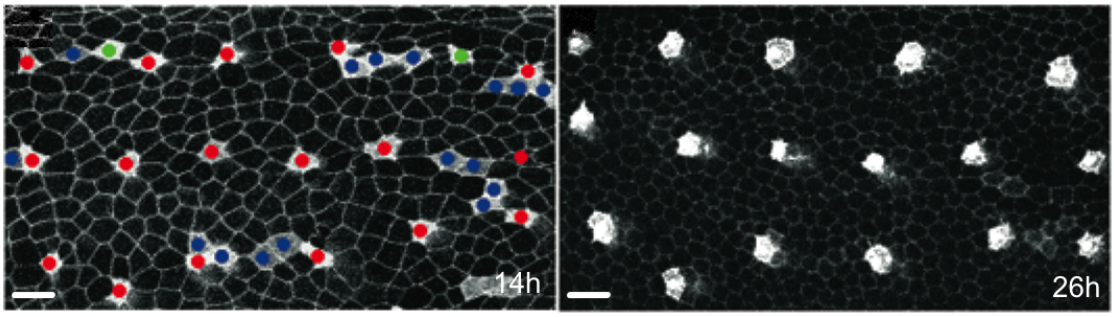

Figure 7.3: Epithelial cells in 3 rows adjacent to the fly midline are labelled prior to pattern refinement. Neu-GFP is used to label microchaete precursor cells. E-Cadherin::GFP labels cell junctions. The Neu-GFP expressing cells are colour coded according to their later development. Red cells develop into bristle precursor cells, blue cells return to an epithelial cell fate, and green cells undergo apoptosis. Note that even though there is a lot of cell division in this system there is very little movement of precursor cells during this time interval. Scale bar = 10μm

7.2.2 Patterns refine dynamically over time

When the fates of individual cells were tracked in individual animals (labelled in Figure 7.3 and quantified for two representative animals in Figure 7.4), a gradual process of pattern refinement was observed (Figures 7.2, 7.3). By 14-16 hours APF the continuing elaboration of this pattern led to an array of potential precursor cells that was overcrowded and poorly organised. A well-ordered pattern then emerged between 16-20 hours APF as 25% of Neu-GFP cells residing in densely packed regions of the notum switched fate and downregulated proneural gene expression (arrows in Figures 7.2, 7.6, 7.7; blue cells in 7.3). This led to a significant increase in bristle spacing and a 2.5-fold reduction in the variance of the spacing (from 2.0 at 16h APF to 0.8 at 26h APF, Figure 7.5). This refinement of the pattern was concomitant with a burst of cell division in the tissue, and Neu-GFP positive cells switching fate invariably underwent a symmetrical epithelial division (large arrow Figure 7.2, weak GFP-labelled epithelial cell doublets in Figures 7.3, 7.6 and 7.7). At the same time, a small number of Neu-GFP cells in crowded areas of the notum delaminated and underwent apoptosis (Figures 7.2, 7.3 and 7.8) and, even at late stages, Neu-GFP expression was

initiated anew in isolated cells in sparsely patterned areas of the tissue (note appearance of a cell expressing GFP at 20h APF Figure 7.2, which takes the place of a cell that switched fate at 17h). Both processes contributed to the development of a well-ordered pattern.

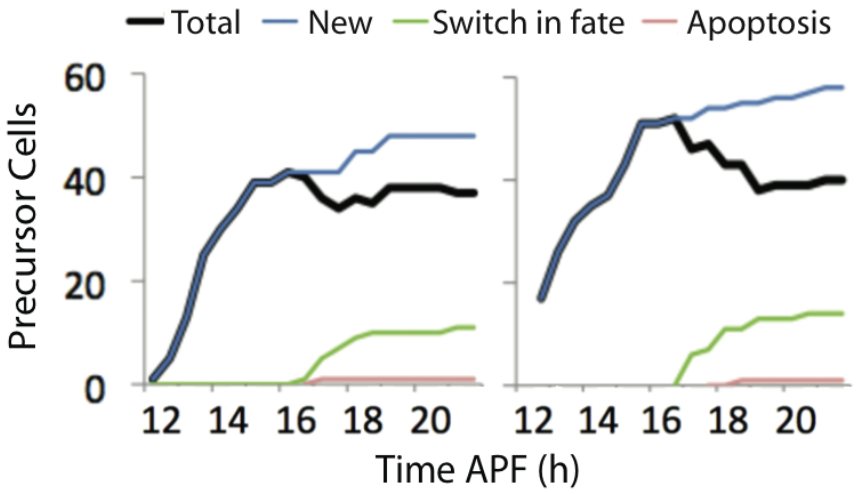

Figure 7.4: Graphs show the total number of Neu-GFP cells (black), cumulative Neu-GFP count (blue), cells that have switched fate (green) or undergone apoptosis (red) for two individual flies. The graphs illustrate the dynamic refinement process as the total number of Neu-GFP expressing cells reduces, predominantly as a result of switches in cell fate.

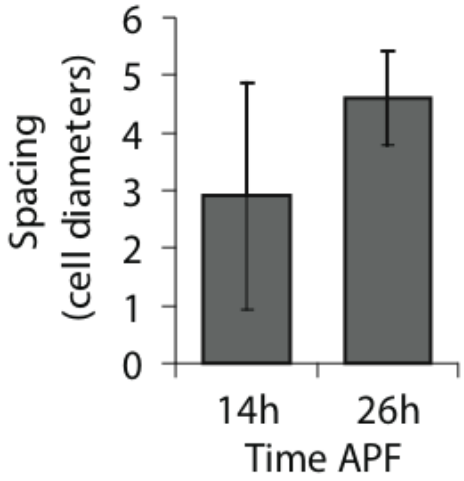

Figure 7.5: Mean and variance in Neu-GFP expressing cell spacing (relative to average cell diameter at 14h APF). Data taken from 3 flies, each with 5 rows, comprising an average of 8 Neu-GFP expressing cells (see Figure 7.11 for details of measurements taken). The variance in spacing is significantly reduced over time whilst the overall spacing is increased. This demonstrates a refinement of the pattern from a relatively disordered arrangement of cells to one in which a larger spacing is well maintained throughout the system.

7.2.3 Neu-GFP and E(spl)mαRFP accurately reflect levels of Notch and Delta in signalling cells

To verify that these visible changes in the Neu-GFP and E(spl)mαRFP signal accurately reflect changes in gene expression status, the tissue was stained with antibodies against Notch and Delta. As expected, surface Notch protein was restored and Delta expression lost in cells that had divided

and begun to down-regulate Neu-GFP (Figures 7.6, 7.7 and 7.8). Moreover, in crowded regions of the notum, cells expressing both Neu-GFP and high levels of the reporter for Notch signalling were seen undergoing characteristically symmetric epithelial cell divisions (arrows in Figure 7.7). These data identify a previously undescribed population of cells that switch their fate during the process of lateral inhibition, as represented by a change in Delta-Notch expression. In addition, they reveal how, by depending on competition with nearby cells in the epithelium, these changes in cell fate contribute to the gradual emergence of a well-ordered pattern of gene expression in the notum.

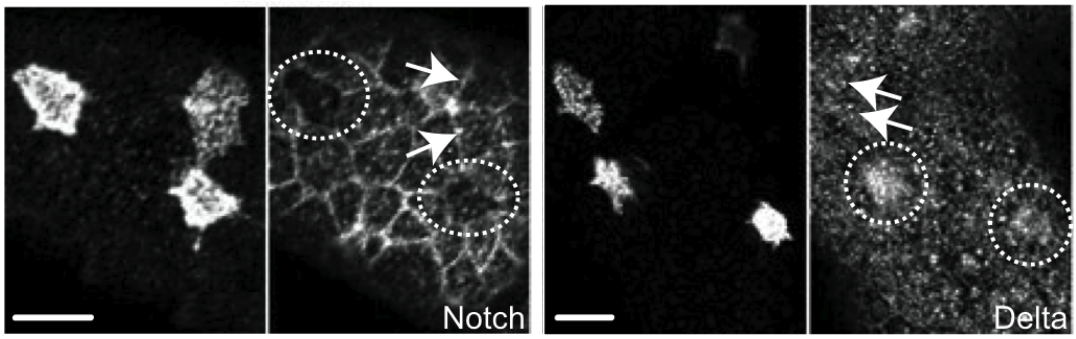

(a) Notch is expressed only in Neu-GFP expressing cells switching cell fate. The cell undergoing division (an indicator) of a switch in cell fate) is identified by lower levels of Neu-GFP (left) and the arrows (right). Notch is expressed on the cell boundaries of this cell but not on the other cells expressing GFP.

(b) Delta is no longer expressed in cells switching fate. The cell undergoing a switch in fate as indicated by low levels of Neu-GFP expression (left) and arrows (right) does not express Delta (right), which is clearly visible in cells that were strongly expressing GFP.

Figure 7.6: Notch and Delta expression is compared in precursor cells and cells undergoing a change of state. Scale bars = 10μm

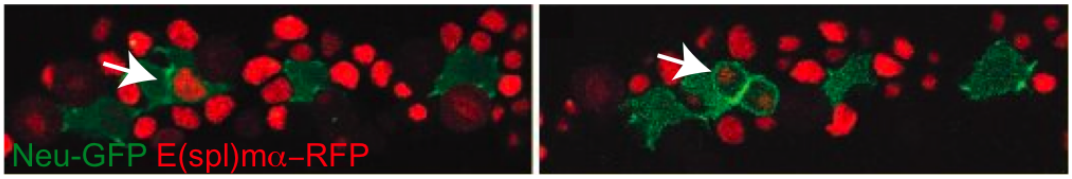

Figure 7.7: E(spl)mα−RFP (red) at 14h APF indicates Notch-signalling among the row of cell. Here in a crowded area of Neu-GFP (green) signalling cells a cell switches fate as indicated by a cell division (arrows).

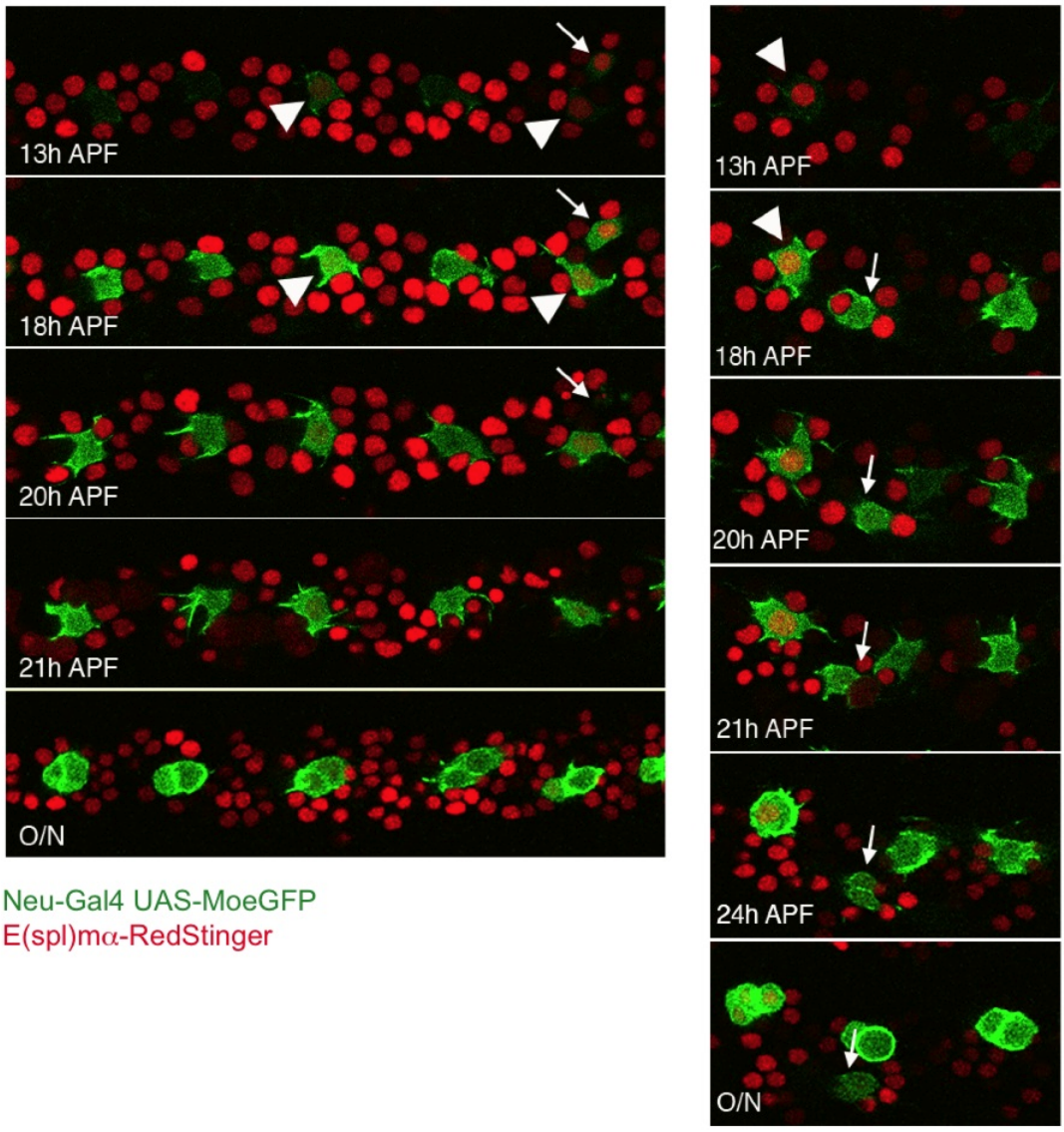

Figure 7.8: Imaging Delta-Notch Signalling in the notum reveals the signalling in rows. These stills show rows of cells expressing Neu-GFP and E(spl)mα-RFP over a period from 12-26h APF during the gradual process of bristle precursor cell patterning. Because of the low temperature, the large-scale divisions began at 20h APF. The small arrow in on the left indicates a Neu-GFP cell that eventually delaminates as a result of being born close to another Neu-GFP positive cell. The small arrow on the right indicates a bright Neu-GFP cell that switches fate and undergoes a symmetrical epithelial cell division, leaving space for a later-born neighbouring Neu-GFP positive cell to take its place. Large arrow heads indicate RFP positive cells that eventually give rise to Neu-GFP positive sensory organs. Note that although there appears to be some shifting of position at very late timepoints, cells do not move much during the patterning process. O/N indicates the last timepoint taken.

7.2.4 Using ablation to demonstrate a self-organising pattern

In order to prove that this emerging bristle pattern is self-organising, as previously suggested [Wigglesworth: 1940, Heitzler and Simpson: 1991, Doe and Goodman: 1985], rather than pre-determined, a series of perturbations were carried out. First, a nitrogen laser was used to ablate an isolated, bright Neu-Gal4 cell within the notum at 14h APF (Figure 7.9). Within 3.5 hours of this procedure, a neighbouring epithelial cell had begun to express Neu-GFP to take the place of the ablated cell; as expected if patterning is self-organising.

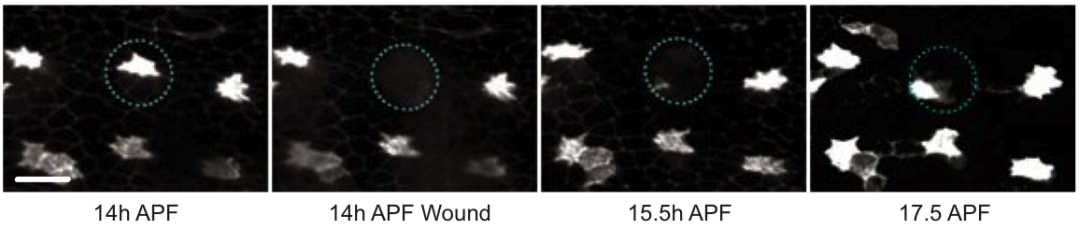

Figure 7.9: Bristle precursor cell ablation results in a neighbouring epithelial cell taking on a precursor fate. Bristle precursor patterning in a fly expressing Neu-GFP prior to a wound (left) and following ablation of a Neu-GFP cell at 14h APF using a nitrogen laser (at site of dotted circle). A neighbouring cell is observed taking on a precursor fate to restore the pattern. Epithelial adherens junctions are labelled with a ubiquitously expressed E-Cadherin-GFP. Scale bar = 10μm.

7.2.5 Using Heat Shock to demonstrate a self-organising pattern

Next, a temperature sensitive Notch allele was used to inhibit Notch signalling in Neu-GFP expressing flies. Heat shock experiments were performed with y1, N1, Nts1, g2, f1 / C(1)DX, y1, w1, f1 flies crossed to Neuralized GAL4:UAS Pon-GFP. Heat shocks were performed at 29^oC for three hours at 10-13h, 12-15h, 15-18h or 18-21h APF. Pupae were dissected and fixed immediately following heat shock. Control experiments were performed using the same Notch temperature-sensitive line without applying a heat shock.

This loss of Notch signalling caused rows of competent epithelial cells to take on a precursor cell fate and to begin expressing Neu-GFP (Figures 7.10). These experiments conclusively demonstrate that Delta-Notch signalling underlies a gradual process of competition-induced cell fate determination that is self-organising, as predicted by classical experiments [Wigglesworth: 1940, Heitzler and Simpson: 1991] and theoretical models of lateral inhibition [Artavanis-Tsakonas et al.: 1999, Lewis: 2003].

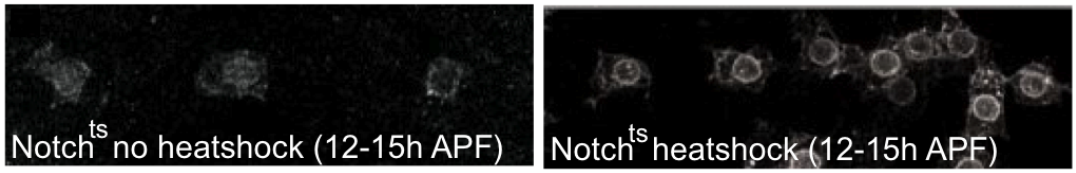

Figure 7.10: Precursor cell spacing is shown in Notch^{ts} Neu-PonGFP flies at 15h APF following a 3h heat-shock (right) or, in parallel, after 3h at room temperature (left). The repression of Notch signalling leads to a significant decrease in the Neu-GFP cell spacing.

7.2.6 Quantifying the spacing of bristle precursor cells

To obtain a consistent and comparable measure of the pattern spacing this was quantified in terms of the average cell diameter prior to the occurrence of any cell division in the system. The apical cell diameters were measured in 2 directions across randomly selected cells (Figure 7.11). For the

mutant flies (described later in this chapter) the wild type cell diameter was assumed. Using the diameter prior to cell division as a unit of spacing meant that it was possible to discount the effect of cell division in contributing to the final spacing. The spacing between precursor cells was measured in the direction of their particular row (Figure 7.11) in flies in which the pattern had refined and the precursors were expected to form into microchaetes. These measurements are summarised in Figure 7.20 where it is shown that the average wild type spacing is 4.6 cell diameters.

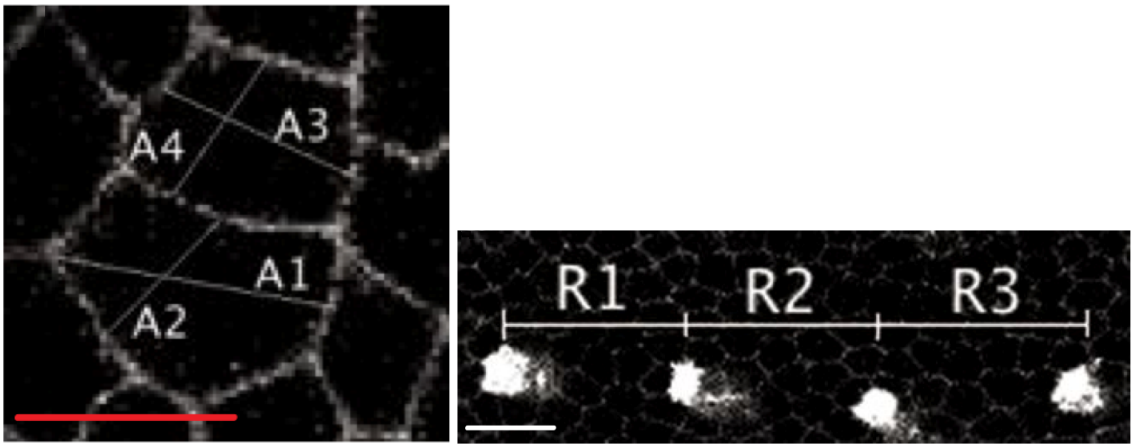

(a) Apical cell diameters (A) were measured in two directions in 60 cells in 3 wild-type flies at 13-15hAPF, prior to any cell division in the system (which occurs at 16h APF). Scale bar = 5μm

(b) The intra-row cell-cell separations (R) were recorded after pattern refinement. For the wild type and Rac mutant these were measured for 3 flies at 23-26h APF, in 5 separate rows close to the fly mid-line, each comprising approximately 8 cells. For the scar mutant, these distances were recorded in 2 flies at 19hAPF carrying large scar mutant clones. Later images of the scar mutants at $> 26h$ APF, in which bristles had begun to develop, were used to confirm the location of precursor cells in the earlier images where the pattern was not yet completely refined. Scale bar = 10μm

Figure 7.11: Extracting apical measurements and precursor spacing from images taken from developing wild type and mutant (detailed later in text) flies. Precursor cells are identified by their expression of Neu-GFP and cell borders by E-Cadherin-GFP.

7.3 Intercellular signalling mediated by filopodia

It is demonstrated in the following chapter that a simple model of cell to cell signalling does not sufficiently describe the spacing of the observed wild type bristle patterns. As was described in the previous chapter lateral inhibition by cell-to-cell signalling gives rise to a mosaic pattern of Delta expression in which cells high in Delta are separated by one or two cells (the following chapter will demonstrate that for most parameters regimes the typical model spacing is 2.3 cell diameters). Previous work has suggested that cell-to-cell contact is required for optimal Delta signalling, since Delta doesnt function when expressed as a diffusible signal in flies [Artavanis-Tsakonas et al.: 1999, Sun and Artavanis-Tsakonas: 1997]; perhaps because optimal Delta-Notch signalling requires physical forces acting on the receptor-ligand pair [Ahimou et al.: 2004]. Therefore, in searching for a mechanism, signalling via cellular extensions was considered as a possible solution to explain the spacing [Renaud and Simpson: 2002, 2001, De Joussineau et al.: 2003, Demontis and Dahmann: 2007].

Lamellipodia and filopodia, were observed forming a lateral web extending across several cell diameters at the basal side of epithelial cells in the developing Drosophila notum (Figure 7.12 and 7.13). These protrusions were found to differ in important ways from those described in [De Joussineau et al.: 2003]. They are exclusively basal, are present throughout the patterning process from 12-20 hours APF at 25C in all cells in the epithelium (Georgiou and Baum unpublished

data), are best seen in unfixed tissue, and are extremely dynamic (Figure 7.13). They extend relatively quickly and then slowly retract with average lifetimes of 537 +/- 54 seconds (Figure 7.15).

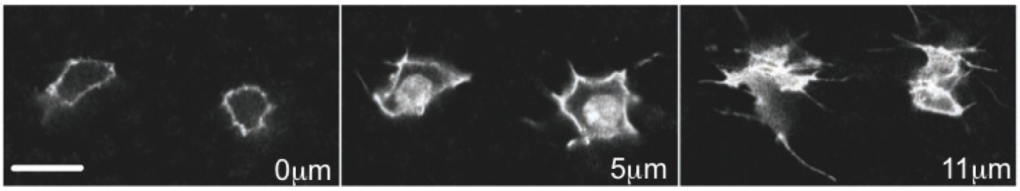

Figure 7.12: An apical-basal scan through the epithelial monolayer (distances from the apex as labelled) reveals basal lamellipodial and filopodial extensions. Here two Neu-GFP expressing cells can be seen, however all cells in the epithelia had similar protrusions. Scale bar = 10μm

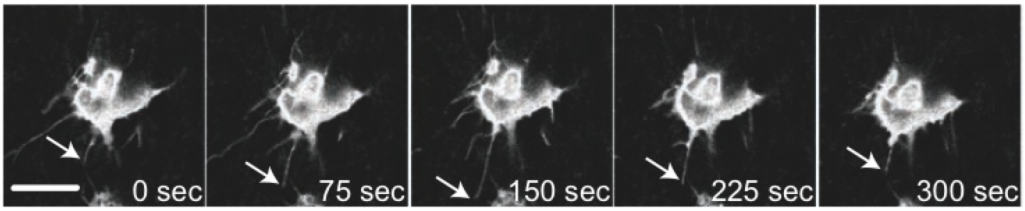

Figure 7.13: Basal filopodia extend and retract, in all directions, from the cell membrane over time. The basal section of a typical Neu-GFP expressing cell is shown. The arrows point to the ends of filopodia that can be observed extending and retracting over the time scale shown. Scale bar = 10μm

7.3.1 Quantifying cellular protrusions

The lamellipodia and filopodia were measured in the way depicted in Figure 7.14. These were recorded in different cells at different times during the patterning process. A summary of the measurements recorded is provided in Figure 7.20. The distribution of lengths during the patterning stage are shown in Figure 7.16 and the mean length over time is shown in Figure 7.17. It was observed that the distribution of lengths between cells was very close to the distribution of lengths obtained for the same cell recorded over time during the patterning stages (12-18h APF). To measure the filopodia dynamics, individual filopodia from 5 cells at 14hAPF were tracked over a 15 minute time course. The lifetime was defined as the time taken to extend to a maximal range and then retract.

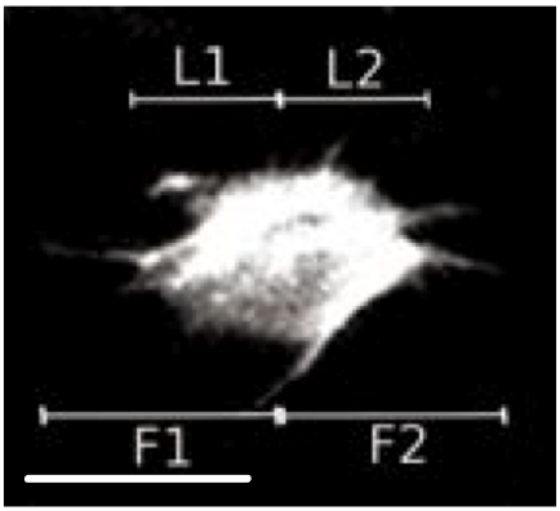

Figure 7.14: Lamellipodial (L) and filopodial (F) extensions were measured from the cell centre in the direction of microchaete rows. For the wild type, these were measured in three flies over 10 cells at two hourly intervals between 12h and 20h APF. For the Rac-N17 expressing flies and scar mutant animals (described subsequently) these were recorded in 10 cells at 18h APF. The image shows the basal section of a precursor cell expressing Neu-GFP. Scale bar = 10μm

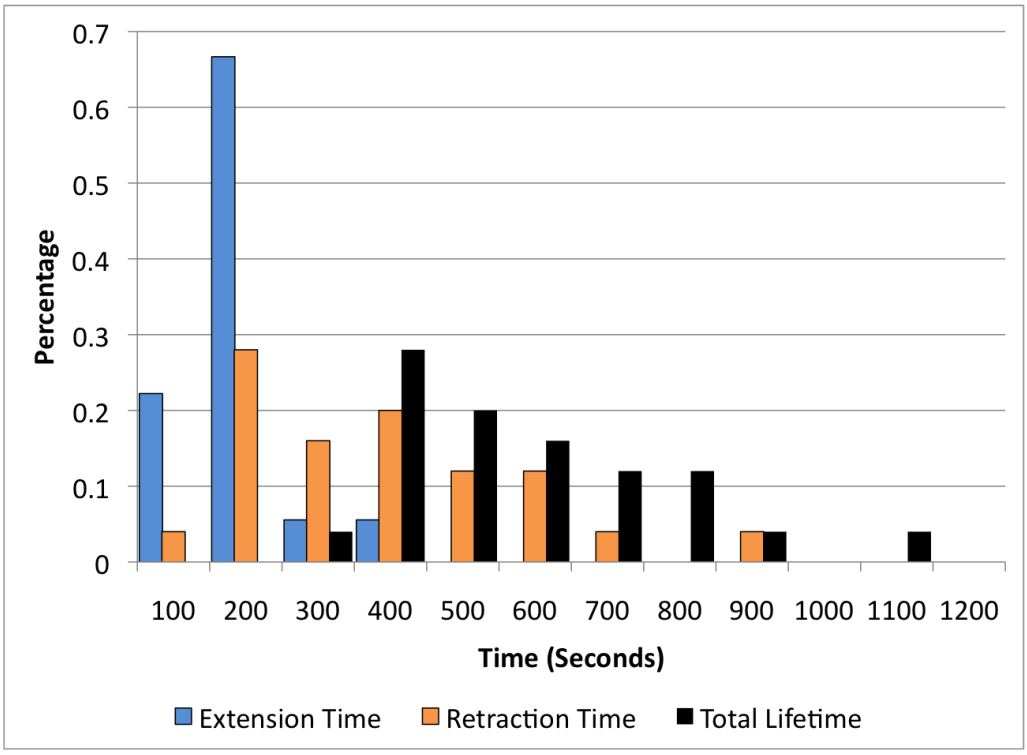

Figure 7.15: The distribution of recorded filopodia lifetimes. The extension time is the time taken to extend from the cell membrane to maximum range, The retraction time is the time from reaching that maximum range to fully retracting back to the cell membrane. The filopodia lifetime is a summation of the extension and retraction times. It is clear from this figure that the filopodia extend relatively quickly and retract more slowly. The average lifetime was 537 +/- 54 seconds (cells number = 5, total filopodia 12)

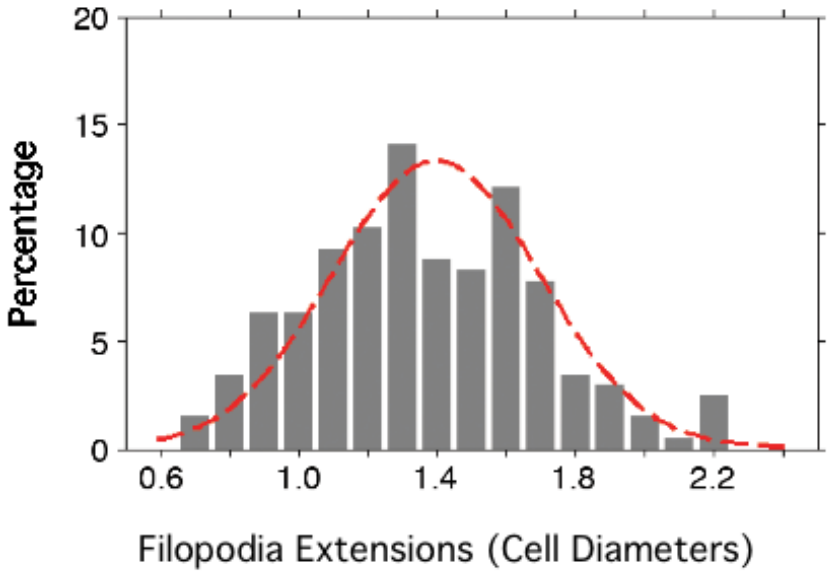

Figure 7.16: Length distributions of filopodia from 3 wildtype animals (recorded from 10 cells each at 16h APF, and expressed in terms of the average cell diameter at 14h APF). The dotted red line shows the Normal distribution, derived from this data (mean 1.4, sd=0.3), used to parameterise model simulations.

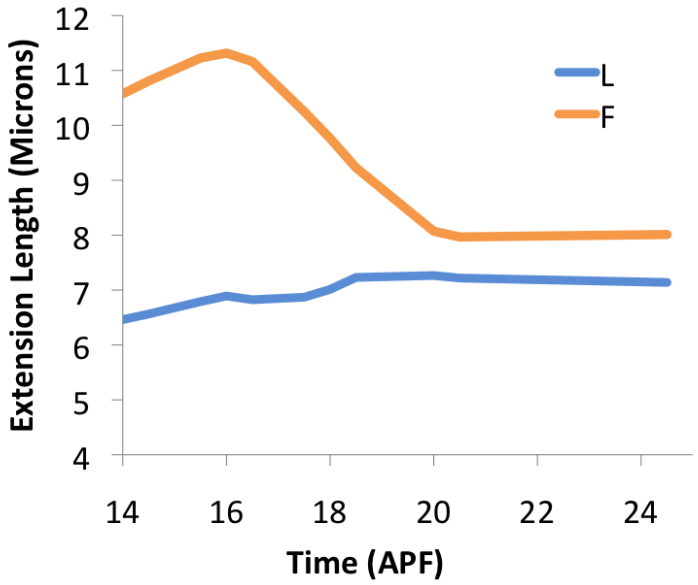

Figure 7.17: Mean length of filopodia recorded over time from 3 animals (10 cells each). Note filopodia are lost between 18h and 20h APF when the patterns becomes fixed.

7.3.2 Filopodia interactions precede switches in cell fate

Significantly, basal protrusions of nearby pairs of Neu-GFP cells were seen engaging in sustained physical interactions in the hours immediately preceding a cell delamination event or a switch in the fate of one of two competing cells (Figure 7.18); implicating these filopodia in the process of lateral inhibition.

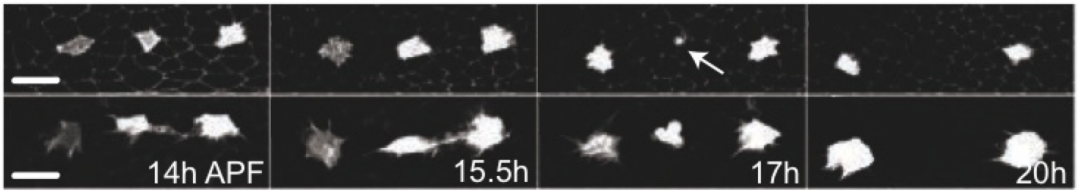

(a) Arrow labels a cell that undergoes apoptosis after a basal interactions

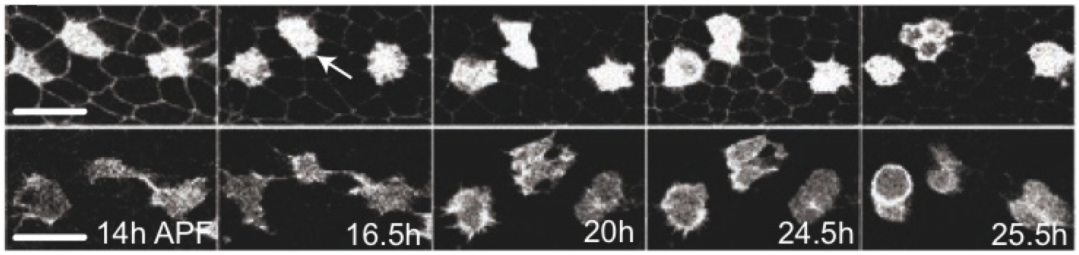

(b) Arrow indicates cell switching fate leading to a symmetrical cell division

Figure 7.18: Filopodia to filopodia touching precedes bristle precursor de-differentiation. Apical (top half: a and b) and basal (bottom half: a and b) confocal slices showing basal interactions between Neu-GFP expressing cells that precede apoptosis (arrow in a) or a switch in cell fate (arrow in b). Scale bars = 10μm

7.3.3 Notch and Delta are detected basally

When the distribution of Notch and Delta molecules was measured it was found that both were detected basally, despite being concentrated within the sub-apical domain of epithelial cells. In line with previousy published estimates [Sasaki et al.: 2007, Fehon et al.: 1991] 22% of Notch (n=59) and 40% Delta (n=50) were found basally in data from > 3 flies). Based on this analysis this population of basal Delta and Notch protein is likely to dominate in the regulation of bristle spacing.

7.3.4 Genetic perturbations to filopodia effect microchaete spacing

Finally, to test the role of protrusion dynamics in the patterning process, actin regulators were searched for, whose function could be perturbed to reduce the length and dynamics of basal protrusions whilst minimizing changes to cell shape, polarity and size, and without compromising junctional endocytosis [Georgiou et al.: 2008] or epithelial organisation [Speck et al.: 2003] (which affects bristle spacing [Renaud and Simpson: 2001]). Having identified SCAR and Rac as key regulators of basal filopodia formation in the notum (Georgiou and Baum, in press), perturbations were carried out in two ways. First, Neu-Gal4 was used to express a dominant negative version of Rac in cells as they take on a bristle precursor fate, in order to test the effects of specifically perturbing filopodia in Neu-Gal4 cells. Second, large epithelial clones of scar mutant tissue were generated using the MARCM technique together with Neu-Gal4 [Georgiou et al.: 2008, Lee and Lou: 2001] to positively label precursor cells within epithelial tissue entirely lacking extensive, dynamic basal protrusions (Figure 7.19).

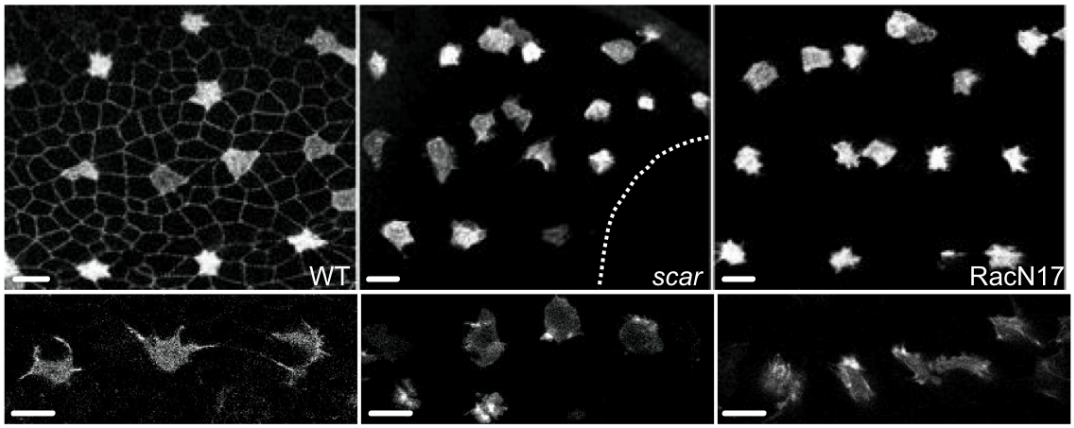

Figure 7.19: Images of the three rows of bristle precursor cells (labelled with Neu-GFP) closest to the midline (located at the bottom of the image) at 14h APF in a wild-type pupa (left) in a positively labelled scar mutant clone (middle) and in a pupa expressing a dominant negative Rac (RacN17) specifically in the bristle precursor cells (right). Reduced apical spacing (top) is evident in the Rac and scar mutants. Basal confocal sections (bottom) illustrate characteristic filopodial extensions in each case. Scale bars = 10μm

The results of these perturbations are summarised in Figure 7.20. In both cases protrusions were inhibited and bristle spacing reduced accordingly. Hence this provided good evidence for filopodia functioning in the lateral inhibition process. In support of this conclusion, two of the other 4 components of the SCAR complex (Hem/Kette and Sip1) were identified as increasing bristle density in a recent genome-wide RNAi screen for regulators of Delta-Notch signalling [Mummery-Widmer et al.: 2009].

	Apical Diameter (A) *Microns*		**Lamellipodial Extension (L)** *Cell Diameters*		**Filopodial Extension (F)** *Cell Diameters*		**Precursor Separation (R)** *Cell Diameters*
Data	**Mean**	**SD**	**Mean**	**SD**	**Mean**	**SD**	**Mean**
Wt	**7.8**	*1.6*	**0.9**	0.1	**1.4**	0.3	**4.6 +/- 0.1**
Rac Mutant	**As per Wt**		**0.8**	0.1	**0.9**	0.1	**3.7 +/- 0.1**
Scar Mutant	**As per Wt**		**0.7**	0.1	**0.7**	0.1	**2.7 +/- 0.1**

Figure 7.20: The mean values and distributions obtained for each of the recorded data sets. L, F and R are quoted in proportions of the average cell diameter of each fly. For the Rac-N17 and scar flies early in the patterning process, the average apical diameter was found to be approximately equal to that of the wildtype in negatively marked clones (data not shown). Therefore the wildtype apical cell diameter was used for calculations in all cases. The standard deviations quoted for L and F in the wild type data were found to be equivalent for different cells and for individual cells over time. Standard errors are quoted for the mean value of R derived across all the data values.

7.4 Summary

This chapter has described how a set of biological experiments were performed in order to analyse the patterning of microchaete bristles in Drosophila. The data indicates that basal protrusions may have a function in this self-organising process. The following chapters describe how a model of Delta-Notch signalling was constructed to analyse these results. The empirical data is used to parameterise this model which provides theoretical support for the hypothesis that dynamic filopodia are required to generate the pattern spacing.

Chapter 8

Modelling Delta-Notch signaling

The following chapter describes a set of 1D and 2D models that were developed to simulate lateral inhibition patterning by Delta-Notch signaling.

8.1 Introduction

The previous chapter revealed that the patterning of microchaetes in Drosophila is a dynamic, self-organising process that relies on the Delta-Notch signalling pathway. It was shown that the pattern spacing in the wild type flies averaged 4.6 cell diameters. In addition the spacing was effected by perturbations to the length (and dynamics) of protrusions present in the basal layer of the epithelium. This chapter seeks to demonstrate that in a simple computational model of the lateral inhibition process the emergent pattern spacing is significantly less than was observed in the wild type animal, irrespective of the model parameters.

8.2 The mathematical model

The mathematical model adopted here is described by equations 8.1. It is derived from a model used in [Collier et al.: 1996]. The model describes the process of gene activation and inhibition by the signalling proteins in contacting cells. Individual cells are represented with dynamically changing levels of Notch and Delta defined by a coupled set of differential equations, each comprising a protein synthesis and degradation term. Hill functions are used to represent the activation and inhibition of protein production induced by inter-cellular interactions. [Alon: 2006].

The model is summarised by the following set of equations which define the protein levels among a group of signalling cells:

$$\frac{dN}{dt} = R_N \frac{{D_{in}}^k}{a + {D_{in}}^k} - \mu N + eN$$

$$\frac{dD}{dt} = R_D \frac{1}{1 + bN^h} - \rho D + eD$$

$$D_{in} = \alpha \sum_{Cells\ in\ contact} D \tag{8.1}$$

N and D refer to the quantity of Notch and Delta in each cell. Synthesis of N and D is controlled by switch functions parameterised by a, b, k, h and the associated production rates, R_N and R_D. The proteins have exponential degradation rates, μ and ρ. The quantity of Delta signal received by each cell, represented by D_{in} is a summation of the level of Delta in all contacting cells, scaled by a factor, α, which represents the proportion of neighbouring Delta signal received by a cell. Finally the term e is used to incorporate an additional stochastic error. This is a randomly generated term obtained from a Gaussian distribution with a standard deviation equal to eN or eD respectively.

8.2.1 Model Units

Arbitrary units of protein concentration (referred to below as $A.U.$) were adopted for the purpose of simulation as the actual protein concentrations in this system were not explicitly quantified experimentally. Similarly simulations were measured in arbitrary units of time (referred to as τ) and the production and decay rates are correspondingly represented.

In summary: N, D are measured in $A.U.$, decay rates, μ and ρ are in τ^{-1}, production rates, R_N and R_D are in $A.U.\tau^{-1}$, a is in $A.U.^{k}$, b is in $A.U.^{-h}$, k, h, α and e are non-dimensional.

In the next chapter, when the model is used to analyse real data, the relationship between these arbitrary units and measurements of real data will be discussed.

In [Collier et al.: 1996] a similar set of equations were cast in a non-dimensional form to facilitate an analytical evaluation of their behaviour. In contrast, here, the equations are parameterised with Notch and Delta production and decay rates, a scaling of the received Delta signal and a random error (or Gaussian noise) term. Using this model each of the relevant parameters could be independently manipulated in simulations to determine their effect on the pattern spacing. This formulation also provided the option to parameterise the model with experimentally derived chemical rates (although this was ultimately not required). The inclusion of a 'noise' term allowed the system to be investigated for its robustness to noise as well as providing an additional level of biological realism in the simulations; in many cases the stochastic patterning process required the inclusion of some kind of noise or asymmetry in the start values. Alternative *connectionist* models of Delta-Notch signalling were described in chapter 6 wherein a transcriptional network is defined by protein threshold levels. However, these types of system directly correspond to a special case of the model used here when parameterised with highly non-linear hill functions (high values of coefficients k and h). The general model adopted here was considered to provide the most appropriate level of description of the underlying system by which to analyse the emergent patterning under different parameter regimes.

8.3 Model analysis

The model was applied to different cell topologies, including; a single cell system, a two cell system a 1D array of cells with a size variance based on real data, a 2D array of uniform hexagonally packed cells and a 2D array that models realistic epithelial cell packing. In each case, cells were allowed to signal to their immediate neighbours (2 in the linear array, and 6 in the hexagonal array, and variable numbers in the epithelial array).

It was demonstrated in [Collier et al.: 1996] that analytical predictions could be derived for the behaviour of a two cell system which could be extended to the linear system; however, for 2D arrays predictive mathematical analysis becomes highly complex as a cells neighbourhood increases in size

and so the number of differential equations that must be solved increases dramatically. Because of the limitations of the analytical approach, in this thesis numerical simulations of the model are used exclusively to analyse the model's behaviour in these larger arrays. Simulations were performed in C++ by numerically solving the differential equations using the Euler method. In a simulation each individual cell was generated with a start level of Notch and Delta (with some specified variance between cells) which was updated at each time step.

8.3.1 Simulation time-step

Numerical simulations used the Euler method to evaluate the differential equations. The effect of varying the size of the integral time-step was investigated. Simulations (of patterning in a 2D hexagonal array) were run with integral time-steps corresponding to $\delta t = 0.001, 0.01, 0.1, 1.0, 10.0\tau$, where the total patterning time was approximately 500τ. In all cases the patterning process was found to be identical (in terms of the pattern spacing and the simulated time taken to reach a stable pattern). The system showed no significant dependency on the size of the integral time-step within the ranges tested. For all the simulations that follow the Euler method was implemented with $\delta t = 1.0\tau$.

8.3.2 The behaviour of single cell system (in vacuo)

The one cell system in vacuo, where there is no D_{in} component, converges to a single stable state with high levels of Delta and zero Notch. Figure 8.1 shows the dynamics of a simulation of the single cell system. Both Notch and Delta levels initially decay with a half life principally dependent on their decay rates (in this case $t_{1/2} \approx 1/0.01 = 100\tau$). As Notch approaches a sufficiently low level, determined by the parameter b, Delta production becomes increasingly significant. Delta levels then rapidly increase, and subsequently slow down as they approach the equilibrium point at which production equates with decay, predicted by equation 8.1: $D = R_D/rho$ (in this example, $1/0.01 = 100A.U.$). The total time to reach the equilibrium point is approximately the sum of the half lives which are determined by the decay rates of Notch and Delta.

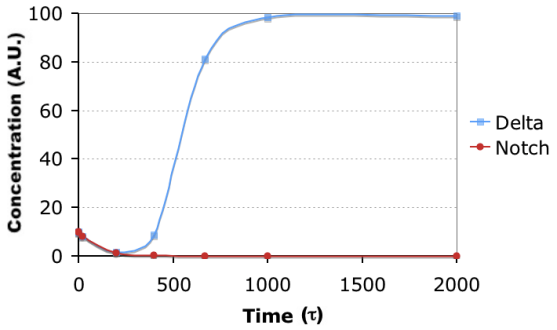

Figure 8.1: The levels of Delta and Notch during a simulation of the single cell system. Start levels of Notch and Delta decay until Notch is sufficiently low for Delta production to begin. The system tends to the predicted stable state in which Delta is high and Notch decays to zero. Simulation parameters: $\mu = \rho = 0.01\tau^{-1}, R_N = R_D = 1A.U.\tau^{-1}, a = 0.01A.U.^{k}, b = 100A.U.^{-h}, k = h = 2, \alpha = 1, e = 0$. Starting conditions: $N = D = 10A.U.$.

8.3.3 Notch Delta signaling in a two cell system

The two cell system has a heterogeneous pair of symmetrically identical stable states and a pair of homogeneous stable states, dependent on the system parameters. In the heterogeneous case one cell exhibits high levels of Delta and low levels of Notch and the adjacent cell exhibits high levels of

Notch and low levels of Delta. In [Collier et al.: 1996] a mathematical analysis of a periodic two cell system is used to show that the strength of the feedback between cells must be sufficiently strong for a pair of stable heterogeneous stable states to exist. Similarly, conditions are derived by [Ghosh and Tomlin: 2001, 2004, Tiwari and Lincoln: 2002] wherein they identify the particular ratios of the decay rates and switch thresholds for which the heterogeneous or homogeneous stable states will incur.

Figures 8.2, 8.3 and 8.4 demonstrate the range of behaviours that can be achieved with the model system. In Figure 8.2 the two cells are initiated with zero variance. As their is no inhomogeneity in the system, both cells follow the same trajectory; with Notch levels initially going high (due to the low value of parameter a which makes Notch active at low levels of Delta). Delta levels then correspondingly decay to zero in the presence of high Notch, and then Notch decays to a stable low level.

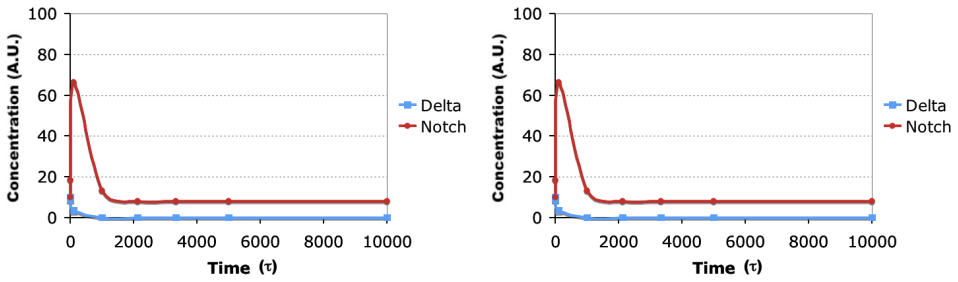

(a) Cell 1 (b) Cell 2

Figure 8.2: A simulation of the two cell system. There was zero variance in the start conditions between cells. Here both cells follow the same trajectory. Simulation parameters: $\mu = \rho = 0.01\tau^{-1}, R_N = R_D = 1A.U.\tau^{-1}, a = 0.01A.U.^{k}, b = 100A.U.^{-h}, k = h = 2, \alpha = 1, e = 0$. Starting conditions: $N = D = 10A.U.$

In Figure 8.3 the same system is initiated with a small variance in the two cells. The initial trajectories are the same as the previous case; however, in this system, after Notch levels have dropped sufficiently, the cells diverge. The cell with initially higher levels of Notch goes high in Notch and low in Delta. The cell with lower start levels of Notch remains low in Notch and end very high in Delta. Any asymmetry in this system will be amplified and lead to a heterogeneous steady state. An equivalent end result could be achieved by including a non-zero noise term (e).

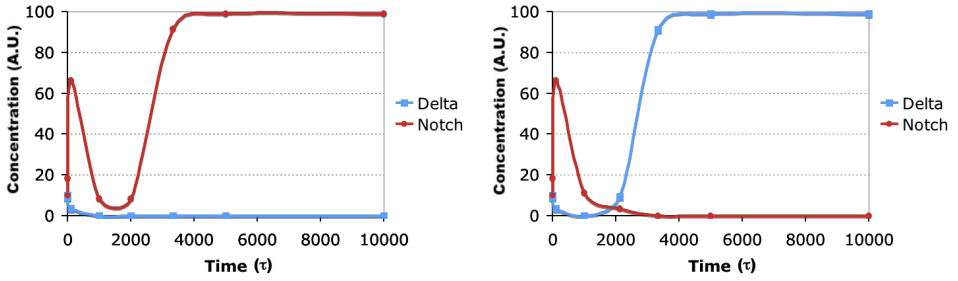

(a) Cell 1 (b) Cell 2

Figure 8.3: A simulation of the two cell system with variance in the initial conditions. Parameters are identical to Figure 8.2; however, start conditions for cell 1 are N=10.1 A.U., D=10.0 A.U., for cell2, N=10 A.U., D=10 A.U.. Here the cells initially follow the same trajectory and then differentiate. Simulation parameters: $\mu = \rho = 0.01\tau^{-1}, R_N = R_D = 1A.U.\tau^{-1}, a = 0.01A.U.^{k}, b = 100A.U.^{-h}, k = h = 2, \alpha = 1, e = 0$.

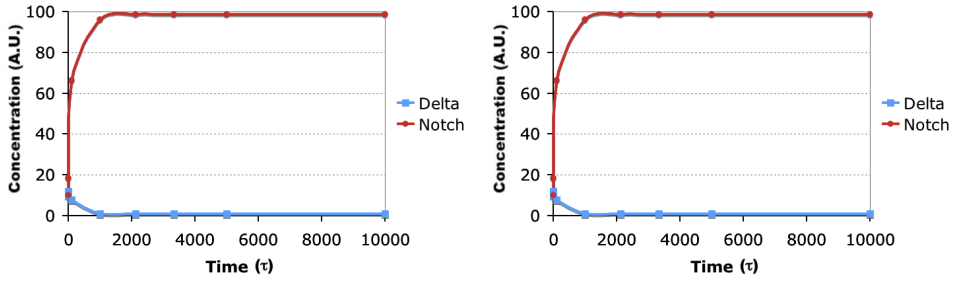

(a) Cell 1 (b) Cell 2

Figure 8.4: A simulation of the two cell system with low feedback. Start conditions for cell 1 are N=10.1 A.U., D=10.0A.U., for cell2, N=10A.U., D=10A.U.. In this case the strength of the system feedback is reduced by making the parameter b very low. The system now has a stable homogeneous state with high Notch and low Delta in both cells. Simulation parameters: $\mu = \rho = 0.01\tau^{-1}, R_N = R_D = 1A.U.\tau^{-1}, a = 0.01A.U.^{k}, b = 0.01A.U.^{-h}, k = h = 2, \alpha = 1, e = 0$.

In Figure 8.4 there is also some variance in the initial conditions but in this case the parameter b has been reduced so that the Delta production in the system is much less sensitive to the Notch levels. Thus, the overall feedback in the system is reduced and the system stabilises in the homogeneous state.

8.3.4 Notch Delta signaling in a linear array of cells

The linear system can be regarded as a periodic version of the two cell system. In [Collier et al.: 1996] it is shown that similar heterogenous and homogenous states exist for this system. Patterns generally emerge from the boundaries early on and then spread inwards. However, if the initial variance in Notch and Delta is sufficiently high then asymmetries in the central field will be amplified and the boundaries have less of an effect on the system. As with the two cell system it is observed that the system may often pass through a nearly homogeneous state before developing significant spatial inhomogeneity (Figure 8.3).

The patterning is driven by stochastic protein levels in the system

In this study the principle aspect of the system that was of interest was the pattern spacing. It was observed here that a perfectly regular patterning (that is every other cell expressing high levels Delta) will occur when there is no initial variance provided there are an odd number of cells in a line. In this case only the boundary conditions provide the initial inhomogeneity and both end cells can satisfy the same condition (for example, zero Delta at the boundary will specify for high Delta cells at the ends of a line). Figure 8.5 demonstrates the relationship between the array dimensions and the patterning. It is shown that even when a perfect pattern may fit into a line of cells, if a variance in initial condition (or transient noise term - data not shown) is included in the simulation the pattern is more likely to demonstrate irregular spacing according to the stochastically driven order in which cells express high levels of Delta.

(a) 21 cells with no variance in the starting values of Notch and Delta ($N = D = 10A.U.$) (and no noise added to the system). The system has a stable state with every other cell high in Delta (coloured in red).

(b) 20 cells with no variance in the starting values ($N = D = 10A.U.$). Here the system still has high Delta cells on the ends but is forced into a stable state with uneven patterning

(c) 21 cells with a small initial variance ($N = D = 10 + / - 0.01$, A.U. NB: $+/-$ refers to the standard deviation). The initial conditions steer the system into a stable state with 2 cells low in Delta appearing twice between cells expressing high Delta levels

Figure 8.5: A set of simulations of the linear system demonstrating the effect of odd or even line lengths and starting variance in a system with zero Delta outside the boundary. All show steady state patterns achieved after 3000 time steps of the simulation. $\mu = \rho = 0.01\tau^{-1}, R_N = R_D = 1A.U.\tau^{-1}, a = 0.01A.U.^{k}, b = 100A.U.^{-h}, k = h = 2, \alpha = 1, e = 0$.

Adjacent cells can sometimes express Delta

As with the two cell system a homogeneous state exists for the linear system when the signal feedback strength is very weak. This can be implemented in the model by setting parameter, a, very high. At an intermediate parameter ranges a pattern can be achieved in which adjacent cells express high levels of Delta (Figure 8.6)

.

(a) A homogenous state, with all cells high in Delta, exists when cells are very insensitive to Delta. $a = 10000A.U.^{k}$

(b) Adjacent cells may express Delta at intermediate values. $a = 1000A.U.^{k}$

Figure 8.6: A simulation of the linear system demonstrating how adjacent cells may express high levels of Delta (red) in the final stable state with sufficiently low Delta signal (α) and high parameter, a. This makes the cells very insensitive to Delta levels in adjacent cells. At extreme levels the system goes into a homogenous state with all cells high in Delta. At intermediate values adjacent cells can express high levels of Delta. $\mu = \rho = 0.01\tau^{-1}, R_N = R_D = 1A.U.\tau^{-1}, b = 100A.U.^{-h}, k = h = 3, \alpha = 0.01, e = 0.01$ Start conditions: $N = D = 10 + / - 0.1A.U.$ Row Size = 20 cells.

The patterning dynamics may depend on the signal sensitivity

Figure 8.6 demonstrated how with extremely low levels of Delta sensitivity adjacent cells can express Delta in a stable pattern. In other less extreme parameter regimes adjacent cells may express Delta earlier in the patterning process before the pattern is refined. Figure 8.7 illustrates this type of patterning dynamic.

Figure 8.8 shows how the patterning dynamic may change at different values of the hill function parameter, a. When cells are very responsive to the Delta signal (low a) the system progresses directly toward the final pattern. In contrast when the cells are very insensitive to the Delta signal at intermediate stages many cells will express Delta and this is later refined in the final pattern.

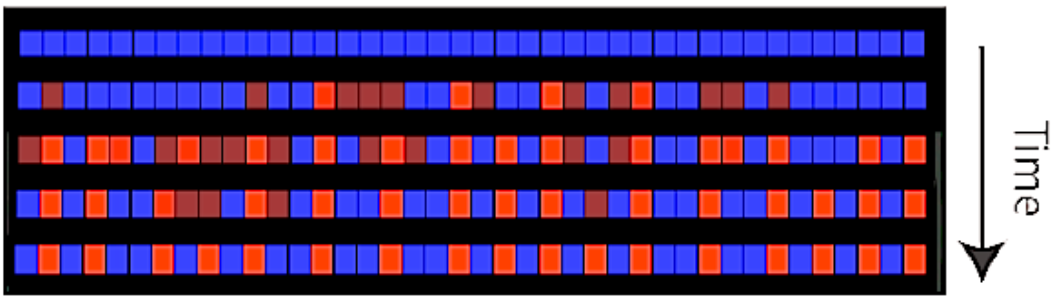

Figure 8.7: Simulations of pattern formation with moderately high a. Here the Delta level is indicated by red intensity. The transition from blue to red occurs at a value of $D > 1A.U.$. Simulation parameters: $\mu = \rho = 0.002\tau^{-1}, R_N = R_D = 0.1A.U.\tau^{-1}, a = 50A.U.^{k}, b = 100A.U.^{-h}, k = h = 3, \alpha = 0.1, e = 0$. Start conditions: $N = D = 0.1 + / - 1$ A.U. Row size = 20 cells

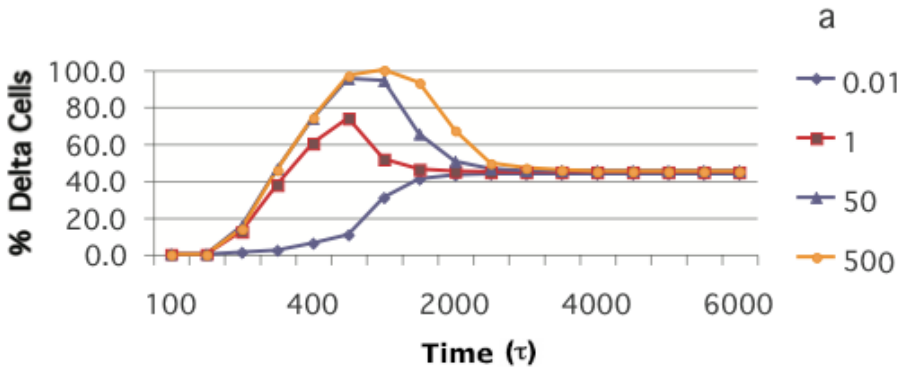

Figure 8.8: Graphs show the percentage of cells expressing Delta (above a value of D=1 A.U.; the average stable cell high in Delta has D=50 A.U. in this model) in simulations of Delta-Notch signalling among a row of 100 cells. Graphs display mean data over the time course of 30 model simulations. Altering the variable a (equation 8.1), changes the level of Delta that triggers a response in neighbouring cells, yielding different dynamics - with the same end state. With high values of the parameter, a, large numbers of cells express high levels of Delta before these are refined and a stable pattern emerges gradually. Simulation parameters: $\mu = \rho = 0.002\tau^{-1}, R_N = R_D = 0.1A.U.\tau^{-1}, b = 100A.U.^{-h}, k = h = 3, \alpha = 1, e = 0.01$. Start conditions: $N = D = 0.1 + / - 0.01$ A.U.

Sensitivity analysis reveals model parameters strongly effect pattern dynamics but not spacing

To test the model sensitivity to each of the parameters and start conditions a set of simulations were run in which each variable was altered independently. For each parameter set simulations were run until a stable pattern was obtained. This was defined as one in which less than 1% of cells high in Delta ($> 1A.U.$) changed state over the course of 1000τ. The pattern spacing and the time taken to reach a stable pattern was determined. In this analysis, cells high in Delta typically had a mean Delta value of 50 A.U., and low Delta cells (high in Notch) had a mean Delta value of $< 0.02A.U.$. The pattern spacing was defined as the distance between successive cells within a row of 100 cells (the default size) that were high in Delta. All simulations were repeated 30 times to obtain mean and standard errors. Parameters were varied within a maximal range for which a stable pattern could be achieved within $100{,}000\tau$. Pairs of related model parameters that had a similar effect on the pattern dynamics were varied together. Initial conditions were also varied to test the effects of; the number of cells in an array or row, the variance in cell size and the starting variance of N and D in each cell.

Figure 8.9 shows the results of this analysis. Where stable patterns were achievable within the range tested, it was found the pattern spacing in the model was highly insensitive to order of magnitude changes in all parameters. However, in contrast the time taken to achieve a stable pattern was sensitive to many of the model parameters.

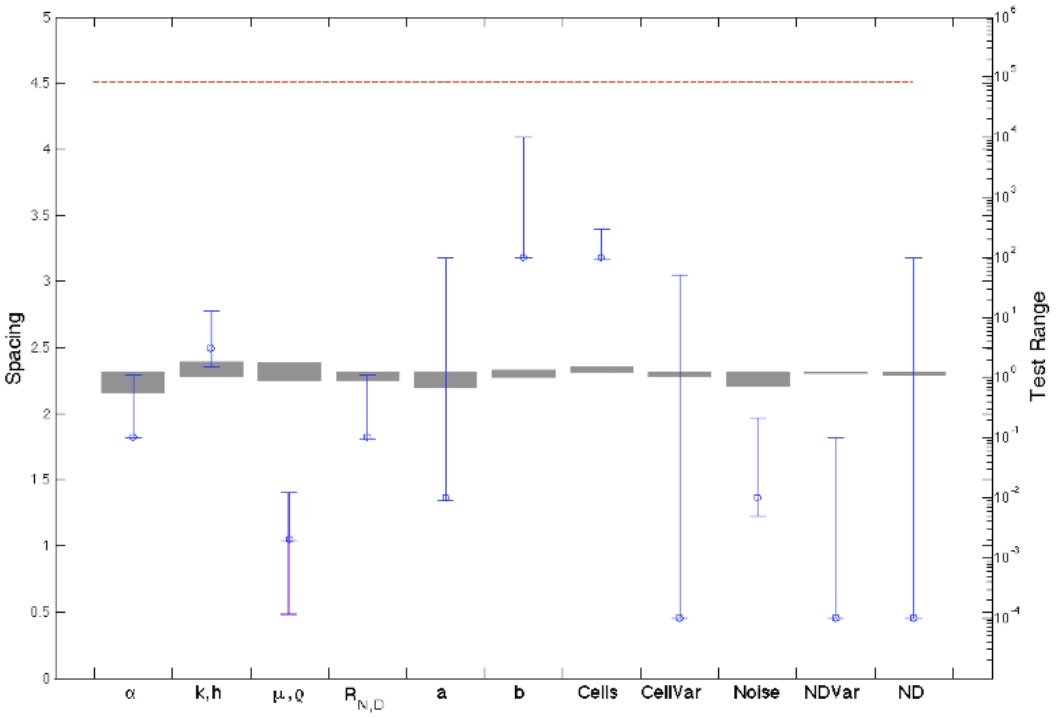

(a) The solid grey bars show the range of spacing obtained in the 1D model for each parameter change (measured in terms of the average cell diameters). (NB: The real values for microchaete spacing obtained in the previous chapter are indicated by red dotted lines.)

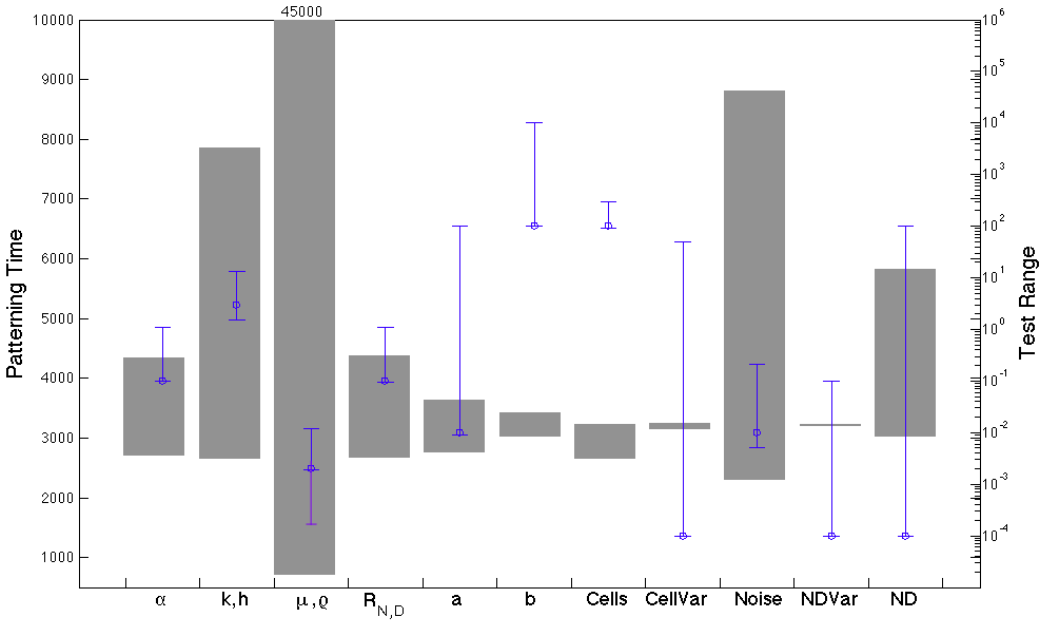

(b) The solid grey bars show the range of times over which a stable pattern was generated in the 1D model

Figure 8.9: The effect of parameter changes on the 1D model. Model parameters and initial conditions have a relatively small effect on the spacing in stable patterns and a large effect on the time to achieve a stable pattern. For each of the models, parameters are shown on the x-axis, the blue bars indicate the range of values (given by the logarithmic scale on the y-axis on the right) for which a stable pattern was achievable. The blue circles show the default parameter values that were used in the simulations. For each model, simulations were repeated 30 times for each test parameter and the average spacing was recorded. The first 6 parameter sets are as defined in equation 8.1. *Cells* refers the number of cells in the row. *CellVar* refers to the variation in cell size as a percentage of the average size. *Noise* refers to the level of a random error term added to N and D at each time step of the simulation. *NDVar* is the start variance of N and D among all cells in the simulation expressed as a fraction of the start levels. *ND* are the start levels of N and D in the simulation. Default parameters were: $\mu = \rho = 0.002\tau^{-1}, R_N = R_D = 0.1A.U.\tau^{-1}, a = 0.01A.U.^{k}, b = 100A.U.^{-h}, k = h = 3, \alpha = 0.1, e = 0.01, N = 0.0001A.U., D = 0.0001A.U., NDVar = 0.0001A.U.$, Cells (Array Size) = 100.

Sampling the full parameter space

The sensitivity analysis previously described was carried out by varying individual parameters, whilst holding others constant. To verify that the results were independent of the particular default set that was chosen for this analysis, a wider sample of the model's parameter space was taken using the latin hypercube sampling method [Iman et al.: 1981]. In this routine a maximal range was defined for each of the model's 9 key parameters. A set of 100 model runs were carried out with parameters selected from a stratified sample within these ranges. For each parameter, its maximal range was divided into 100 discrete regions based on a logarithmic scale. The latin hypercube sampling method ensures that samples from each of these regions are contained within the full set, thus maximising the scope of the parameter space that is investigated by a finite number of random samples. The model was run for a maximum of 200,000τ and if a stable pattern was achieved (as defined previously) the pattern spacing was recorded. The results are shown in Figure 8.10. They further demonstrate that in this model, where stable patterns are achievable, there is very little variation in the pattern spacing. Among the 100 parameter sets, 35 gave a stable pattern with a mean spacing of 2.26 +/- 0.02 cell diameters. The remaining 65 randomly selected parameters sets did not produce a stable pattern.

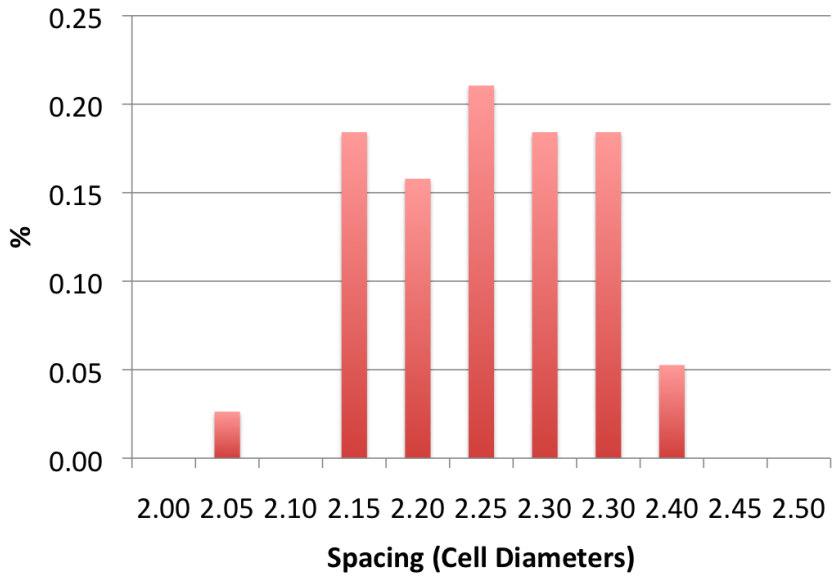

Figure 8.10: Multi-parameter analysis of the 1D system. The distribution of spacing obtained from random sampling of the model parameter space. From model runs carried out with 100 different parameter sets 35 stable patterns were obtained. The distribution of the stable pattern spacing is plotted here. The mean spacing was 2.26 cell diameters with a standard error of 0.02. Parameter sets were derived from a latin hypercube sampling within the ranges: $0.1 < \alpha < 1, 1 < k < 10, 1 < h < 10, 0.001 < \mu(\tau^{-1}) < 0.9, 0.001 < \rho(\tau^{-1}) < 0.9, 0.001 < R_N(A.U.\tau^{-1}) < 100, 0.001 < R_D(A.U.\tau^{-1}) < 100, 0.001 < a(A.U^k) < 10000, 0.001 < b(A.U.^{-h}) < 10000$. Start conditions: $N = D = 0.1 + / - 0.01$ A.U. For this analysis the line of cells was fixed at 100 cells and a noise term, $e = 0.01$ was implemented.

8.3.5 Notch Delta signaling in a 2D hexagonal array of cells

In [Collier et al.: 1996] the behaviour of a 2D array is shown to be similar to the linear system in that typically where a heterogeneous steady state is stable, the cells self-organise such that cells that are high in Delta are entirely surrounded by cells, that are low in Delta. However, as with the linear system, there are certain parameter sets for which this condition may be violated and cells high in Delta are found adjacent to one another.

Patterning dynamics in 2D

The dynamics of the 2D model are also largely similar to the 1D system. Cells typically first express Delta near the boundaries where the largest asymmetries persist (Figure 8.11)

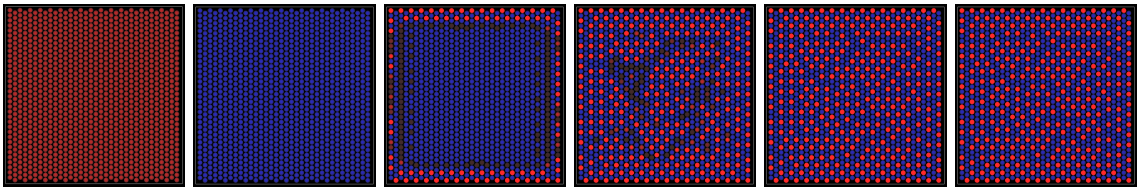

(a) T=200τ (b) T=400τ (c) T=800τ (d) T=1200τ (e) T=1600τ (f) T=2000τ

Figure 8.11: The patterning dynamics in 2D. The pattern typically emerges from the boundaries where the Delta level is set to zero and so the inhibition is lowest. Simulation parameters: $\mu = \rho = 0.01\tau^{-1}, R_N = R_D = 1A.U.\tau^{-1}, a = 0.01A.U.^{k}, b = 100A.U.^{-h}, k = h = 3, \alpha = 0.01, e = 0.01$ Start conditions: $N = D = 10 + / - 0.1$ A.U. Array size = 34x34 cells.

In the 2D system there are more permissible ways for the pattern to pack the array. Figure 8.12 demonstrates the three principle ways in which a steady state periodic pattern of cells expressing high Delta levels may be arranged. In each case cells high in delta are entirely surrounded by cells high in Notch. The ratio of cells high in Delta to those low in Delta is quoted in each case. Typically in a large field patterns may form stochastically and will tend to exhibit a mixture of these three periodic packing types; however, smaller fields may bias the patterning towards one of these regular types.

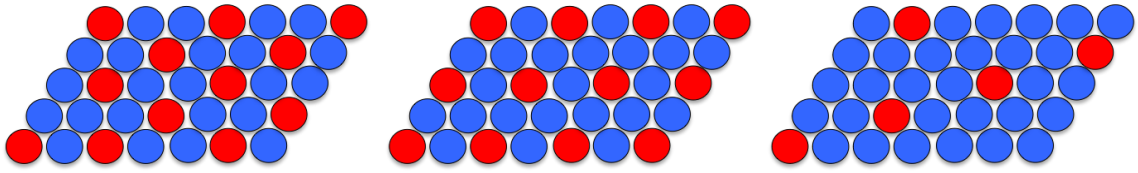

(a) D:N Ratio = 1:2 (b) D:N Ratio = 1:3 (c) D:N Ratio = 1:6

Figure 8.12: Examples of periodic steady-state patterns of cells that can potentially form in a hexagonal grid. Reproduction based on [Collier et al.: 1996]. Cells high in delta are coloured in red. Quoted for each case, is the ratio of cells high in Delta to those that are high in Notch.

Low hill function power terms give a more ordered pattern

Figure 8.13 demonstrates how in a large lattice a combination of the three packing types is observed. The ratio of packing types shows a dependency on the value of the hill function power term. (In contrast, the 1D system demonstrated much less dependence on the system parameters). In the 2D system, the more non-linear the hill functions, the more the patterning arises rapidly due to stochastic variation across the field. When the hill function power terms are lower the system patterns more slowly and in an ordered way.

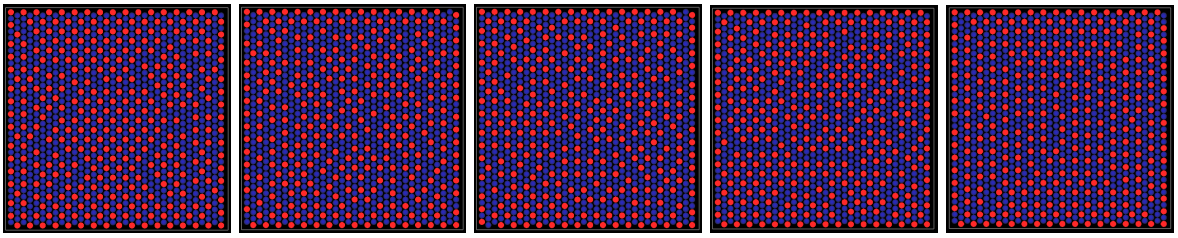

(a) k=h=2 e=0.01
D cells = 31%
CV = 0.16
P-Time = 1700τ

(b) k=h=3 e=0.01
D cells = 28%
CV = 0.19
P-Time = 500τ

(c) k=h=6 e=0.01
D cells = 27%
CV = 0.20
P-Time = 400τ

(d) k=h=2 e=0.1
D cells = 28%
CV = 0.19
P-Time = 1700τ

(e) k=h=6 e=0.0
D cells = 29%
CV = 0.17
P-Time = 400τ

Figure 8.13: At very low values of k and h, the hill function power terms, the pattern is slower to emerge (compare total stable patterning time, P-Time) but is more ordered as reflected by the higher density of Delta cells (in red) and the coefficient of variance (CV) in the spacing between each Delta expressing cell and its 6 nearest neighbours. However, with no noise or variation between cells even non-linear systems become more ordered. Correspondingly for the more linear system with higher noise and hence variance between cells the pattern is less ordered. Simulation parameters:$\mu = \rho = 0.02\tau^{-1}, R_N = R_D = 1A.U.\tau^{-1}, a = 0.01A.U.^{k}, b = 100A.U.^{-h}, \alpha = 1$ Start conditions: $N = D = 10$ A.U.. Array size = 34x34 cells.

Sensitivity analysis in 2D

For 2D models, a similar sensitivity analysis was carried out in an identical way to the 1D model. Here, the pattern density was defined as the percentage of total cells expressing high levels of Delta in a stable pattern. The results are shown in Figure 8.14. Similar to the 1D model analysis, it was shown that the model parameters have relatively little effect on the pattern density; however they significantly alter the time to achieve a stable pattern. In contrast to the 1D system, there are very small but significant changes to the pattern density using different parameters.

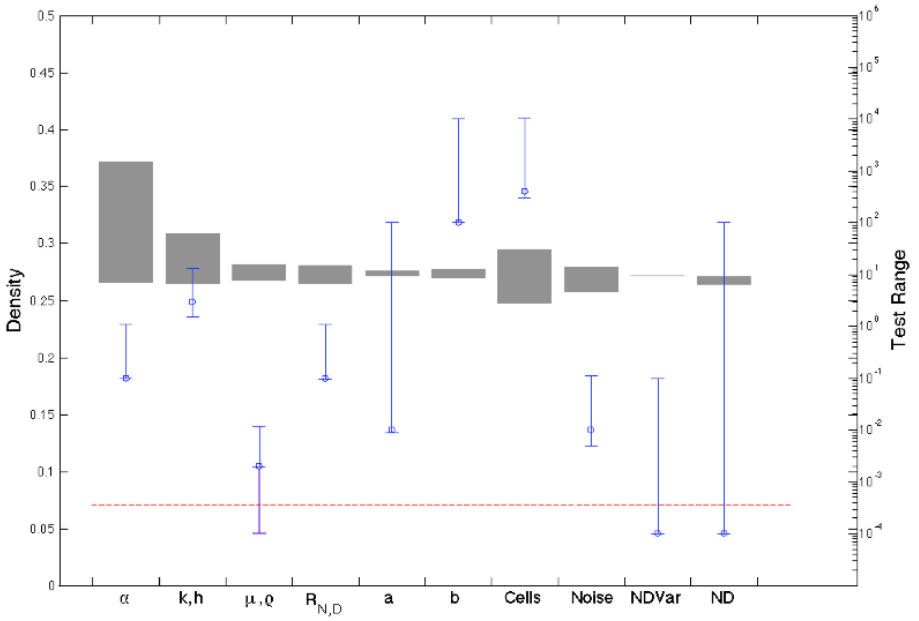

(a) The solid grey bars indicate the density of Delta cells.

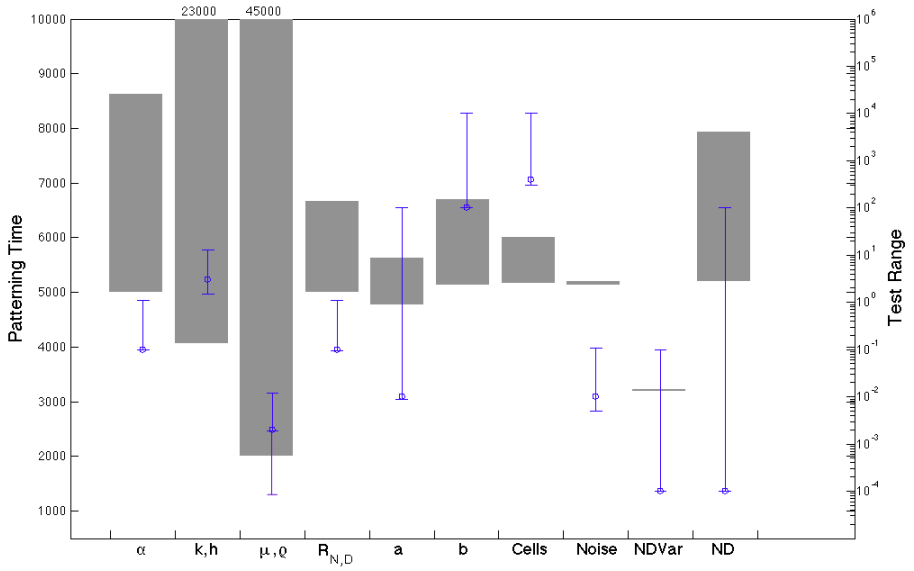

(b) The solid grey bars show the range of times over which a stable pattern was generated in the 2D model

Figure 8.14: The effect of parameter changes on pattern spacing the 2D model. Model parameters and initial conditions have a relatively small effect on the stable pattern density - although there is a small but noticeable effect from the signal strength, α, the hill function power terms, k and h, and the array size. However most parameters have a far greater effect on the time for a stable pattern to form. For each of the models, parameters are shown on the x-axis, the blue bars indicate the range of values (given by the logarithmic scale on the y-axis on the right) for which a stable pattern was achievable. The blue circles show the default parameter values that were used in the simulations. (The real values for microchaete density are indicated by red dotted lines). Simulations were repeated 30 times for each test parameter and the average density was recorded. The first 6 parameter sets are as defined in equation 8.1. *Cells* refers the number of cells in the 2D array. *CellVar* refers to the variation in cell size as a percentage of the average size. *Noise* refers to the level of a random error term added to N and D at each time step of the simulation. *NDVar* is the start variance of N and D among all cells in the simulation expressed as a fraction of the start levels. *ND* are the start levels of N and D in the simulation. Default parameters were: $\mu = \rho = 0.002\tau^{-1}, R_N = R_D = 0.1A.U.\tau^{-1}, a = 0.01A.U.^{k}, b = 100A.U.^{-h}, k = h = 3, \alpha = 0.1, e = 0.01, N = 0.0001A.U., D = 0.0001A.U., NDVar = 0.0001A.U.$, Cells (Array Size) = 34x34.

8.3.6 Real cell model

To test the outcome of signaling in a more realistic 2D topological arrangement of cells a virtual representation of a the apical cellular arrangement from in-vivo data was constructed. In modelling a realistic epithelium, a 200x200 2D cellular array was created based on representative E-Cadherin::GFP labelled tissue (Figure 8.15). Virtual cells were delimited by elements in the array and cells contacting across a boundary element were allowed to signal to one another according to the mathematical model previously described. As in the regular hexagonal 2D array for typical heterogeneous patterning regimes, cells expressing Delta were surrounded entirely by cells with low Delta and high Notch.

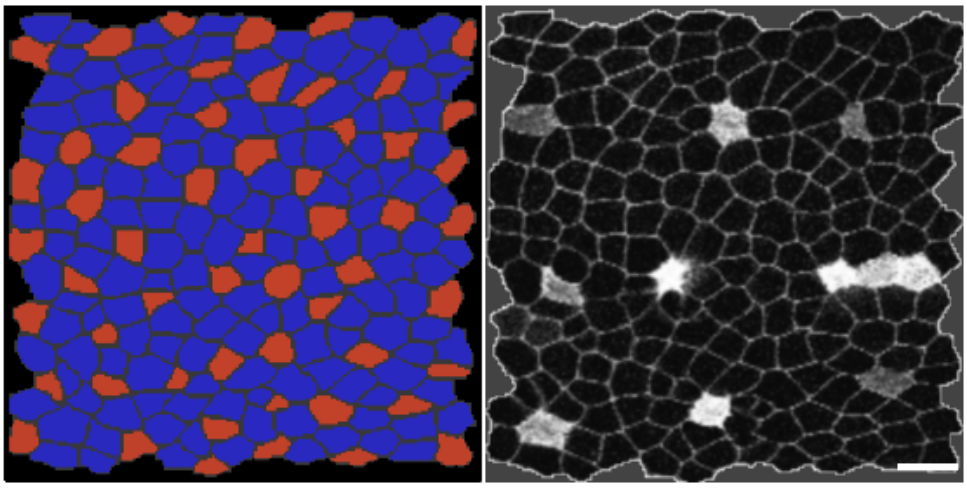

Figure 8.15: A simulation of Delta-Notch signalling was carried out between virtual cells (left) constructed in a finite element array based on an image taken from real data (right). The density of cells high in Delta (red) is 26% compared to 7% coverage by the pattern on the right which shows gene expression in nota labelled with Neu-GFP and E-Cadherin::GFP. Scale bars = 10μm. Left: The simulation parameters used were: $\mu = \rho = 0.01\tau^{-1}, R_N = R_D = 1A.U.\tau^{-1}, a = 0.01A.U.^{k}, b = 100A.U.^{-h}, k = h = 3, \alpha = 0.01, e = 0.01$ Start conditions: $N = D = 10 + / - 0.1$A.U. The pattern is shown after 2000τ.

8.4 Modelling cis-inhibition

Recent studies have demonstrated that in some Notch signalling systems cis-inhibition may take place [Miller et al.: 2009]. To model this process it is assumed that activated Notch will saturate with surrounding Delta molecules in preference to nuclear transcription, and likewise Delta will saturate with Notch before any signalling takes place towards neighbouring cells. Therefore, the following adaptations were made to equation 8.1.

$$if(N > D)\ \{N_{free} = N - D,\ \ D_{free} = 0\}$$

$$if(D > N)\ \{D_{free} = D - N,\ \ N_{free} = 0\}$$

$$\frac{dN}{dt} = R_N \frac{{D_{in}}^k}{a + {D_{in}}^k} - \mu N + eN$$

$$\frac{dD}{dt} = R_D \frac{1}{1 + b{N_{free}}^h} - \rho D + eD$$

$$D_{in} = \alpha \sum_{Cells\ in\ contact} D_{free} \tag{8.2}$$

Here, N_{free} represents the amount of activated Notch that is free to inhibit Delta production through transcriptional regulation, and D_{free} is the amount of Delta that is free to act as a membrane ligand and signal to other cells.

It was found using this formulation that in general the same key behaviours were achievable as for the trans-inhibition model that has thus been used. However for most stable patterning parameter regimes the model behaved much more like the highly non-linear standard model regardless of what hill function power terms were implemented (see Figure 8.16).

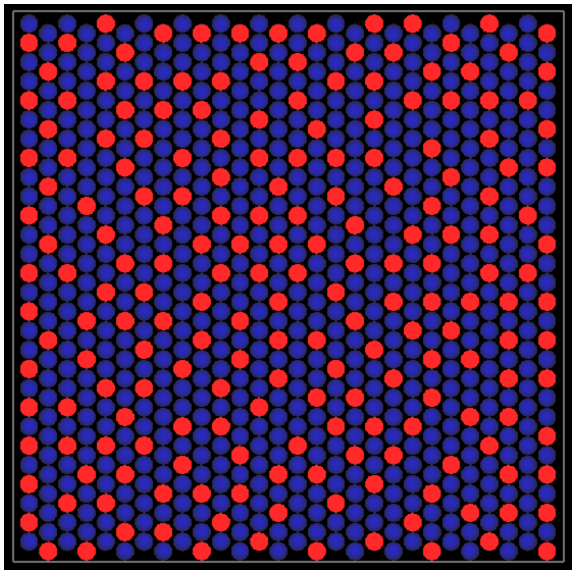

Figure 8.16: The cis-inhibition model produces patterns reminiscent of the standard model with highly non-linear hill functions (compare with Figure 8.13c). Simulation parameters: $\mu = \rho = 0.02\tau^{-1}, R_N = R_D = 1A.U.\tau^{-1}, a = 10A.U.^{k}, b = 1000A.U.^{-h}, k = h = 1, \alpha = 1, e = 0.01$. Start conditions: $N = D = 10 + / - 0.1$ A.U. Array size = 24x24 cells.

The standard trans-inhibition model will be used for most of this thesis; however the cis-inhibition model will be re-examined in a later chapter.

8.5 Summary

In this chapter it has been shown how the Delta-Notch pathway can generate patterns of lateral-inhibition in which a single cell expressing high levels of Delta is surrounded entirely by cells expressing low levels of Delta and high levels of Notch. The mathematical model used here is not the only one that could be describe the signaling system and inherent in it are a number of strong assumptions and simplifications. The real dynamics of this process are far more complex (see Figure 6.1). The downstream interactions that occur in this system undoubtedly have complex effects on the system behaviour and in particular will effect the timing of the inhibition and activation of Notch and Delta in patterning processes. The mathematical model adopted here to describe lateral inhibition therefore represents an aggregate representation of all these downstream interactions. However, it attempts to capture the basic property of Notch activation by cell contact and subsequent inhibition of Delta production and is able to represent a range of possible dynamics relating to this process. The key result that has been demonstrated here is that regardless of the model parameters the system cannot generate patterns with any significant variation in the maximal pattern spacing. When a non-linear signalling system was used, cells expressing Delta were stochastically located according to the lateral-inhibition principle and as such were separated by two or three cell diameters in the 1D system. In very linear systems the spacing was sometimes observed

to emerge in a more regular way such that Delta expressing cells were nearly all separated by two cell diameters. Furthermore for certain parameters sets, cells expressing Delta could be located adjacent to one another. Significantly, however, in no cases were patterns of Delta expressing cells obtained at larger separations. In the next chapter it is shown that when longer range signalling through dynamic filopodia is incorporated into the model it can explain the larger spacing that was observed in the microchaete patterning system presented in the previous chapter.

Chapter 9

Modelling a biological patterning system with intercellular signalling mediated by basal protrusions

The following section uses a model of Delta-Notch signalling to analyse the biological data obtained from the microchaete patterning system in Drosophila. It is shown how a model with filopodial signalling can explain the pattern spacing.

9.1 Cell-to-cell signalling models fail to explain the data

To determine whether or not the microchaete patterning data (chapter 7) in could be explained by the extant model of lateral inhibition through cell-to-cell communication (chapter 8) the spacing of the real patterns was compared with the spacing of patterns generated by the mathematical model in both 1D and 2D simulations.

9.1.1 Comparing simulated pattern density with data

Real cell shape simulations

A comparison was made between real data and a simulation of lateral inhibition among a group of cells constructed using cell shape, coordination, and geometry data obtained from experiment (see Figure 8.15, chapter 8). Here, the Delta signal was transmitted between neighbouring cells with common apical cell-cell junctions. Random noise was used to induce the local differences in Notch and Delta expression needed to seed the pattern formation process. Strikingly, this model of Delta-Notch signalling failed to reproduce the sparse pattern of precursor cells seen in the real data (Delta-expressing precursor cells covered 26% of the model epithelia, as compared to 7% coverage in the wildtype animal).

Hexagonal 2D array

The data was also contrasted with the 2D model in a more methodical way. A parameter sensitivity analysis was conducted with signalling in a regular hexagonal 2D array. In this case the model parameters were varied over order of magnitude ranges (Figure 8.14). The density of Delta expressing cells in stable patterns remained within a range of 25% to 37%; still way in excess of the 7% observed in the wildtype animal.

9.1.2 Modelling in 1D

A 2D model was evidently inadequate to explain the microchaete spacing. However, it was observed in the data that the signalling was restricted to multiple rows of Notch expression either side of the fly mid-line (Figure 7.8). Therefore, a 1D model was used to analyse the intra-row spacing of the pattern. (The use of the 1D model is further justified later in this chapter).

The intra-row pattern spacing in the real data was 4.6 +/- 0.09 cell diameters (Figure 7.11 and Figure 7.20). A parameter sensitivity analysis of the 1D model revealed that regardless of the model parameters the spacing of cells expressing Delta in stable patterns was between 2.2 and 2.3 cell diameters (2.26 +/- 0.02 from 35 patterns obtained from a random sampling of the model parameter space see Figure 8.10). Therefore the 1D model was also unable to account for the pattern spacing.

This suggested that the standard model of Delta-Notch mediated lateral inhibition could not fully account for the pattern of bristles observed in vivo, as has been previously discussed [Renaud and Simpson: 2002, Wigglesworth: 1940, Heitzler and Simpson: 1991, Renaud and Simpson: 2001, De Joussineau et al.: 2003].

9.2 Modelling long range signalling by dynamic protrusions

In chapter 7 it was demonstrated that in the Drosophila notum, lamellipodia and filopodia present in the basal layer of the epithelium may be implicated in Delta-Notch signalling. In order to asses how this would effect the emergent patterning, signalling via these protrusions was introduced into the models.

9.2.1 Basal signalling in the 1D model

Figure 9.1 illustrates how filopodia and/or lamellipodia were implemented in the 1D model. Full details of how the model algorithm was implemented are contained in the methods section (Figure 2.3). Each cell in the array was assigned lamellipodia and filopodia randomly selected from a Normal distribution of lengths (derived from analysis of of in-vivo data - see Figure 7.20). Cells would then signal to all other cells within the maximal range of signalling described by each of the mechanisms in Figure 9.1. The 1D model assumes that a signalling contact is always made between lateral extensions sufficiently large enough to touch or overlap, so that intra-row protrusions directly determine the maximal range of signalling in simulations. For example in type [4] signalling, all cells would communicate with any other cells that either had apical dimensions within the extent of their fillopodia range or had overlapping filopodia or lamellipodia.

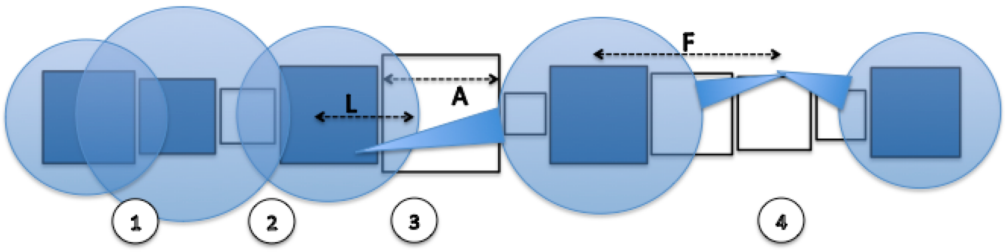

Figure 9.1: Four possible mechanisms of signalling are [1] Apical to apical, [2] lamellipodia to lamellipodia, [3] filopodia to lamellipodia and [4] filopodia to filopodia, modelled in 1D. In each case a different maximum range of signal is achieved dependent on the length distribution of lamellipodia and filopodia applied to each of the cells in the model. Note that for models [2]-[4] all the cells in the system signal through basal protrusions - here only a subset are illustrated for clarity.

In order to simulate protrusion dynamics, filopodia or lamellipodia were reassigned lengths randomly selected from this distribution. It was assumed that the range of extension of a cell's protrusions in each direction (parallel to the line of cells) was independent, and that the distribution of extensions for a single cell over time was the same as the distribution between cells at any instant in time. (This model was applicable as in the real data the variance between cells was the same as for individual cells over time during the patterning phase). A fixed probability of removing an existing filopodia or establishing a new filopodia was applied at each time step. As a result, the filopodia were implemented with an exponential distribution of lifetimes. In simulations of static filopodia, a distribution of protrusion lengths was implemented at the first time step and held fixed throughout the simulation. In all cases apical signalling was assumed to be continuous throughout.

The relation between filopodia lifetimes and model units

The mean filopodia lifetime was set to approximately represent the observed values in the real data (537 seconds). The patterning period in vivo was roughly 8 hours ($\approx$ 50 filopodia lifetimes). In order to establish a realistic framework for the modelling of filopodia, their lifetime in the model was fixed in relation to the total patterning time of a typical simulation. Simulations were run with Notch and Delta decay rates of $\mu = \rho = 0.002\tau^{-1}$. In a row of 100 cells with basal signalling (over a range of lifetimes) the total stable patterning time was 5000τ. Hence, a filopodia lifetime of 100τ was implemented in order to best match the real data.

Given this relationship between total patterning time and filopodial lifetime, it was possible to estimate what the equivalent relative decay times of Notch and Delta would be in the real data. With $\mu = \rho = 0.002\tau^{-1}$, protein half lives are approximately 350τ. Therefore, scaling in the same way as for the filopodia lifetimes gives Notch and Delta half-lives of 1750 seconds (0.5 hours). This is in very close agreement with the limited recorded data on Notch protein lifetimes in other systems [Agrawal et al.: 2009b, Logeat et al.: 1998] and therefore confirms that the relative time scales implemented in the model are sensible in terms of their order of magnitude.

In this study, the relative fluorescence of green or red fluorescent protein tags were used as an indirect indicator of Notch and Delta concentrations and therefore these measurements could conceivably be related to the arbitrary units of concentration (A.U.) employed in the model. However, it was of relatively little importance to explicitly quantify this relationship as the actual steady state concentrations achieved in the model, which are determined by the relative production and decay rates, were shown to have no signifiant effect on the pattern spacing or dynamics.

Modelling wildtype data

The model was applied to a 1D array of cells with a size variance based on real data and the empirically determined filopodial lengths and dynamics were fed into the model (the biological data is summarised in Figure 7.20). Simulations were carried out using a row of 100 cells and repeated 30 times for each model type. A summary of the results for each type of signalling range is shown in Figure 9.2. In all cases a stable pattern was achieved (one for which $< 1\%$ of Delta expressing cells changed their location over 1000τ).

As the signalling range increased in each model the spacing of the pattern increased. When static filopodia were modelled, the mean spacing was 3.8 +/- 0.04 cell diameters, well below the lower limit of spacing observed in wildtype flies, and patterns of cell differentiation were poorly ordered. Significantly, however, when realistic filopodia dynamics were simulated (model type [4]), the model was found to generate a stable pattern very close to that observed in flies (final spacing between Delta expressing cells in the model was 4.5 +/- 0.04 cell diameters, as compared with 4.6 +/- 0.09 cell diameters between precursor cells in the fly). Similar results (not shown) were obtained

Signaling Range	Model Spacing R (cell diameters)	Example Model Output
[1] A to A	**2.3** +/- 0.02	
[2] L to L	**3.1** +/- 0.03	
[3] F to L	**3.7** +/- 0.03	
[4] F to F - Static	**3.8** +/- 0.04	
[4] F to F	**4.5** +/- 0.04	

Figure 9.2: For each model the mean spacing from 30 simulations is shown together with an example model output (displaying a section of a simulated row of 100 cells). In vivo dynamics were simulated, except in case of static filopodia. The models were run until a stable pattern emerged. The mean spacing of the stable patterns increases with the signalling range in each model. Simulation parameters: $\mu = \rho = 0.002\tau^{-1}, R_N = R_D = 0.1A.U.\tau^{-1}, a = 0.01A.U.^{k}, b = 100A.U.^{-h}, k = h = 3, \alpha = 0.1, e = 0.01$. Start conditions: $N = D = 1 + / - 0.01$ A.U. Array size = 100 cells. Filopodia algorithm variables (from Figure 2.3): $A_\mu = 1.0, A_\sigma = 0.2, L_\mu = 0.9, L_\sigma = 0.1, F_\mu = 1.4, F_\sigma = 0.3, F_{rate} = 0.01$.

using other model parameter sets with equivalent ratios between patterning time and filopodia dynamics or with much faster filopodia dynamics (as low as approximately 5 second lifetimes).

Modelling the mutant data

For the RacN17 expression and scar mutant clones, measurements of basal protrusions were also used to parameterise the model (Figure 9.3). In the absence of E-Cadherin-GFP the wildtype apical diameter distributions were used, based upon the fact that Rac and scar were not seen to affect apical area [Georgiou et al.: 2008]. Since Rac and SCAR are required for basal protrusion dynamics, filopodia were modelled as static in both cases. For the scar model, these modifications to basal protrusions were applied to all epithelial cells in each simulation. Because RacN17 was expressed from the Neuralized-Gal4 promoter, in Rac simulations defects in basal protrusions were only implemented for cells expressing intermediate levels of Delta (over a value of 1). All other cells in simulations were allowed to express a wild type distribution of dynamic protrusions. In this model, fluctuations in Delta levels within individual cells are therefore accompanied by changes in the distribution and dynamics of protrusions.

Significantly, these data were in good agreement with the observed spacing for both RacN17 expressing nota (model spacing = 3.6 +/- 0.03 c.f. real spacing = 3.7 +/- 0.2) and scar mutant clones (model spacing = 2.5 +/- 0.02 c.f. real spacing = 2.7 +/- 0.1). In addition, there was a noticeable increase in bristle precursor cell disorder in both types of simulation, as predicted for genes that severely impair protrusion dynamics.

Parameters	Filopodia Extension F (cell diameters)	Real Spacing R (cell diameters)	Model Spacing R (cell diameters)	Example Model Output
Wt	**1.4** SD 0.3	**4.6** +/- 0.1	**4.5** +/- 0.04	
Rac	**0.9** SD 0.1	**3.7** +/- 0.2	**3.6** +/- 0.03	
Scar	**0.7** SD 0.1	**2.7** +/- 0.1	**2.5** +/- 0.02	

Figure 9.3: A comparison of bristle precursor spacing in wild-type, scar mutant or RacN17 expressing tissue with model simulations in which the signalling ranges have been parameterised using distributions obtained from measurements of basal protrusions for each case. Simulation parameters: $\mu = \rho = 0.002\tau^{-1}, R_N = R_D = 0.1A.U.\tau^{-1}, a = 0.01A.U.^{k}, b = 100A.U.^{-h}, k = h = 3, \alpha = 0.1, e = 0.01$. Start conditions: $N = D = 1 + / - 0.01$ A.U.. Array size = 100 cells. Filopodia algorithm variables (from Figure 2.3): Rac (for cells with Delta¿1): $L_\mu = 0.8, L_\sigma = 0.1, F_\mu = 0.9, F_\sigma = 0.1$, static filopodia. Scar (for all cells): $L_\mu = 0.7, L_\sigma = 0.1, F_\mu = 0.7, F_\sigma = 0.1$, static filopodia.

9.2.2 The patterning dynamics with long range signalling

In the real data it was observed that early in the patterning period, relative dense and disordered regions of potential precursor cells would emerge which later refined to leave a regular well spaced pattern (see figures 7.3 and 7.4). A similar process of pattern refinement was achievable in simulations. A typical outcome of a simulation with dynamic fillopodia is shown in Figure 9.4. Here, as with the apical signalling model (Figure 8.7), when the system is parameterised so that cells are relatively insensitive to the Delta signal (high values of parameter a and low α) a pattern initially emerges with adjacent cells high in Delta, which then refines, to leave cells expressing Delta separated at ranges set by the extent of the filopodia. The variation in the patterning dynamics is shown in Figure 9.5.

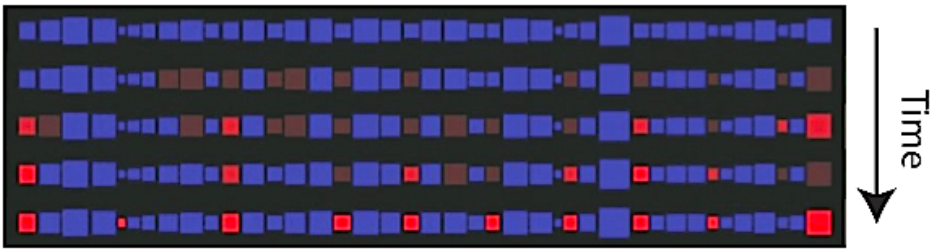

Figure 9.4: Simulations of pattern formation with high a and dynamic filopodia recapitulate gradual patterning dynamics seen in vivo. Here the Delta level is indicated by red intensity. The transition from blue to red occurs at a value of $D > 1A.U.$. Simulation parameters: $\mu = \rho = 0.002\tau^{-1}, R_N = R_D = 0.1A.U.\tau^{-1}, a = 50A.U.^{k}, b = 100A.U.^{-h}, k = h = 3, \alpha = 0.01, e = 0.01$. Start conditions: $N = D = 1 + / - 0.01$ A.U.. Array size = 40 cells. Filopodia algorithm variables (from Figure 2.3): $A_\mu = 1.0, A_\sigma = 0.2, L_\mu = 0.9, L_\sigma = 0.1, F_\mu = 1.4, F_\sigma = 0.3, F_{rate} = 0.01$.

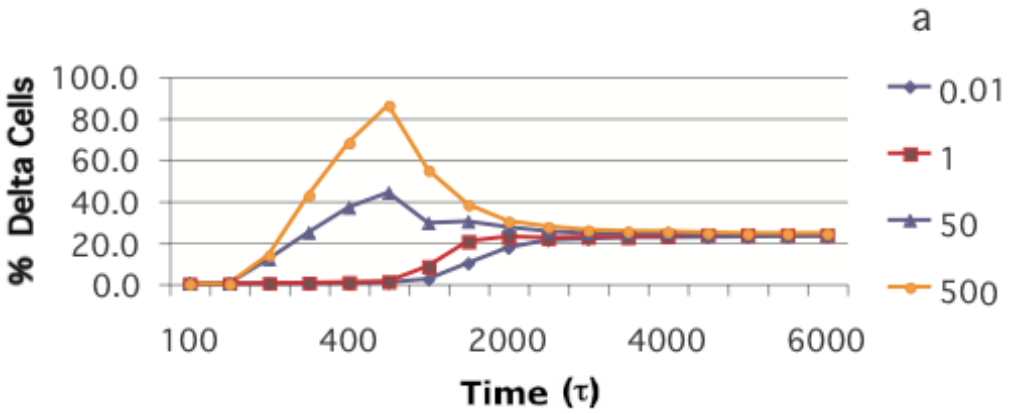

Figure 9.5: Graphs show the percentage of cells expressing Delta (above a value of D=1A.U.; the average stable cell high in Delta has D=50A.U. in this model) in simulations of Delta-Notch signalling among a row of 100 cells. Graphs display mean data over the time course of 30 model simulations. Altering the variable a (equation 1), changes the level of Delta that triggers a response in neighbouring cells, yielding different dynamics. With high values of a large numbers of cells express high levels of Delta before these are refined and a stable pattern emerges gradually. Simulation parameters: $\mu = \rho = 0.002\tau^{-1}, R_N = R_D = 0.1A.U.\tau^{-1}, b = 100A.U.^{-h}, k = h = 3, \alpha = 0.01, e = 0.01$. Start conditions: $N = D = 1 + / - 0.01$ A.U.. Filopodia algorithm variables (from Figure 2.3): $A_\mu = 1.0, A_\sigma = 0.2, L_\mu = 0.9, L_\sigma = 0.1, F_\mu = 1.4, F_\sigma = 0.3, F_{rate} = 0.01$.

The type of pattern refinement identified above was easy to observe in the model when it was parameterised so that cells were slow to respond to Delta signalling. However, even when this

was not the case, another type of dynamic pattern refinement was also occasionally observed in simulations with dynamic filopodial signalling. In these simulations regions of the pattern would form and then subsequently shift position. Figure 9.6 shows an example of this process. This pattern shifting was not common in the 1D system and a single shift was observed in approximately a third of all simulations among a row of 100 cells; however, the ability of the pattern to shift in this way represents a fundamental aspect of filopodial signalling that is investigated further in later chapters of this thesis.

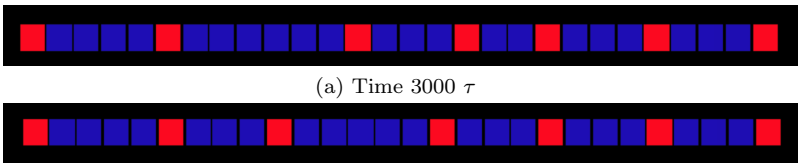

(a) Time 3000 τ

(b) Time 4000 τ

Figure 9.6: Regions of the pattern were sometimes seen to emerge in a semi-stable pattern which would then shift before reaching the condition for stability. Parameters as per Figure 9.5.

9.2.3 The spacing can still be achieved with very low basal signalling

Active Notch production is triggered in the model by a particular level of Delta input from surrounding cells (defined in the hill function). Once triggered the production of active Notch is fixed by the production rate; increasing the amount of Delta signal has no effect on Notch production. Therefore, providing the signal transmitted by the filopodia is sufficient to activate Notch, the pattern spacing will set by the range of the filopodial signal. Figure 9.7 demonstrates how for a particular parameterisation of the model (in this case with relatively high Delta sensitivity) a very low basal signal relative to the apical signal is capable of fixing the pattern spacing at the basal range.

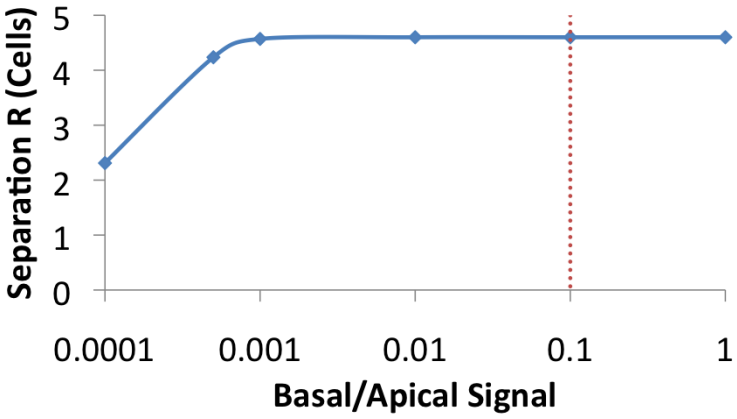

Figure 9.7: When apical and filopodial signalling are combined, robust spacing is achieved even with very low amounts of basal Delta signalling (equivalent to 1/1000 of the apical signal). Dotted red lines indicate apical-basal Delta levels derived from published data [Sasaki et al.: 2007]. Simulation parameters: $\mu = \rho = 0.002\tau^{-1}, R_N = R_D = 0.1A.U.\tau^{-1}, a = 0.001A.U.^{k}, b = 100A.U.^{-h}, k = h = 3, \alpha_{apical} = 0.01, e = 0.01$. Start conditions: $N = D = 1 + / - 0.01$ A.U.. Filopodia algorithm variables (from Figure 2.3): $A_\mu = 1.0, A_\sigma = 0.2, L_\mu = 0.9, L_\sigma = 0.1, F_\mu = 1.4, F_\sigma = 0.3, F_{rate} = 0.0$.

9.2.4 Long range signalling in the 2D hexagonal array

To model long range signalling in the 2D system, filopodial signalling was restricted to communication across an exact number of cell distances in the idealised hexagonal array (as apposed to the continuous

distribution of lengths implemented in 1D). Beyond this range there was no signal and at cell-to-cell range there was a fixed apical signal (see Figure 9.8).

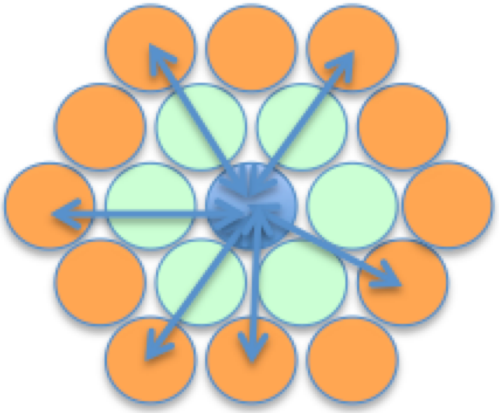

Figure 9.8: Filopodial signalling at a range of 2 cells in the hexagonal array. A single cell and its neighbourhood as described by the model system. Here a cell has n=6 nearest neighbours (green). It has N=12 neighbours at filopodial signalling range of 2 cells (orange). There is a signalling link between 6 out of those 12 possible cells, hence the density of connections = 0.5. Longer ranges of signal were established in exactly the same way using increasingly large hexagonal shells.

With this model filopodial densities and dynamics could be established using the same method as in the 1D model where birth and death probabilities were implemented at each time step of a simulation. The full details of the algorithm implemented are shown in methods section (Figure 2.4). A typical simulation of this model is shown in Figure 9.9.

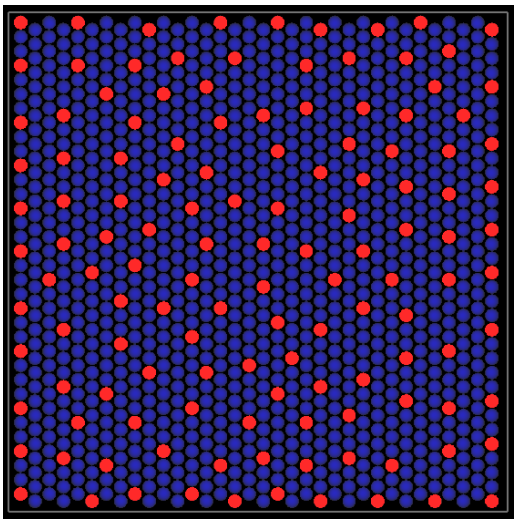

Figure 9.9: A typical example of patterning in the 2D model with filopodial signalling. Delta expressing cells maintain a zone of inhibition of 2 cells wide. Simulation parameters: $\mu = \rho = 0.02\tau^{-1}, R_N = R_D = 0.1 A.U.\tau^{-1}, a = 0.01 A.U.^k, b = 100 A.U.^{-h}, k = h = 3, \alpha = 0.01, e = 0.01$. Start conditions: $N = D = 1 + / - 0.01$ A.U.. Filopodia algorithm variables (from Figure 2.4): F-birthrate = 0.1 , F-deathrate = 0.1. NB: With these parameters filopodia average lifetime = 10 times-steps, average density 50%, total patterning time approximately 1000 time-steps.

Filopodial signalling over multiple rows reduces to a 1D model

In observations of the Drosophila data it was clear that signalling was restricted to a few rows of the epithelial layer (Figure 7.8). In this data it can be seen that Delta expressing cells are generally located in the middle of these regions. However, in all the simulations seen so far it is evident that when the perimeter Delta value is kept low (as one would expect for ordinary epithelial cells) Delta expressing cells will preferentially emerge at the border (for example see Figure 8.5). Using the idealised 2D array a model was constructed with three rows of signalling cells (the approximate width observed in the real data) separated by three rows of non-signalling cells. Filopodial signalling was applied at different maximal ranges of 3 and 4 cells (Figure 9.10). The results of this reveal that with sufficiently long range filopodia the pattern of Delta expressing cells will locate to the middle of the rows.

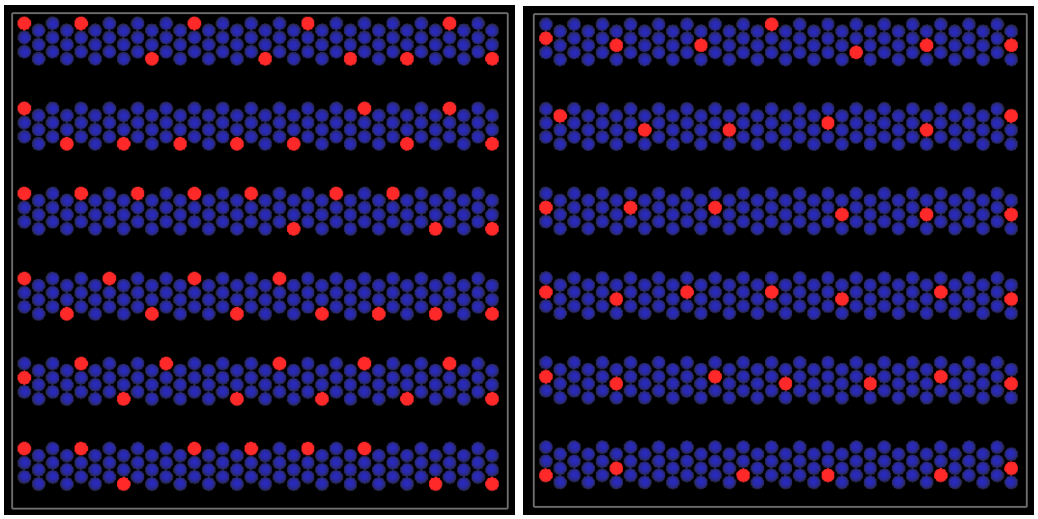

(a) Filopodial signalling range = 3 cell diameters (b) Filopodial signalling range = 4 cell diameters

Figure 9.10: Signalling was restricted to rows of 3 cells, 3 cells apart. When filopodia were sufficiently long, Delta expressing cells are located in the centre of these rows. However when shorter filopodia were used the pattern tends to the edge of the rows where there is the least inhibitory signal. Parameters as per Figure 9.9

The result of these simulations suggest that there may be an interaction between cells in different rows of the epithelial layer. However, with a sufficiently large signal the pattern is restricted to 1D. Based on this simulation one would predict that firstly filopodial signalling must extend across a range greater than the row separation and that when this is not the case the rows should appear less straight and Delta expressing cells would locate at the edges of the signalling region. This is in close agreement with the data (see Figure 7.19) where the mutant flies with shorter filopodial extensions have less well defined rows of microchaete precursors.

9.2.5 Long range signalling in the real cell model

To confirm that filopodial signalling could also give rise to long range spacing without a regular linear or hexagonal array, filopodia were also introduced into the real cell model. The full description of the algorithm are shown in methods section (Figure 2.5). In this case, basal protrusions were implemented as 2D circular areas, extending from the centre of each cell. A distribution of radii was used that was based on the 1D extensions measured from in vivo data. Filopodial dynamics were simulated in the same way as the 1D model by re-sampling from a Gaussian distribution over the simulation time-course. An additional contact probability term was introduced to account for

the angular directions of protrusions that were observed and hence the associated likelihood of two filopodia signalling to each other at different ranges. This was encoded in the model by assigning each cell a randomly selected direction term, r, between 1 and 100. For any two cells (cell1 and cell2) spaced a distance, R, such that their filopodia were of sufficient length to signal, a signal would occur if the condition were met such that: $|r_{Cell1} - r_{Cell2}| < P/R^2$, where, P was a constant variable. Hence the likelihood of a contact being made reduced in proportion to the square of the distance between two cells.

The results of these simulations are shown in Figure 9.11. Here, a high contact probability refers to a value P=1000 (giving a signal probability of approximately 90% at a range of 4 cell diameters) and a low contact probability represents P=100 (giving a signal probability of approximately 15% at a range of 4 cell diameters). Stable 2D patterns could be achieved using basal signalling. Wider spacings were achieved with dynamic filopodia relative to static filopodia regardless of the contact probability. Moreover, when the contact probability was reduced, spacing was better maintained in simulations using dynamic filopodia than for static protrusions. For the dynamic filopodia model there was a 17% increase in pattern density moving from high to low contact probability, compared to a 40% increase in the static model.

This therefore suggests that even with relatively few filopodia emerging from a cell at any one time, actin-based dynamics provide a way to maintain a stable of area of inhibition and thus generate a robust, well-spaced stable pattern. The filopodial signalling model generates well spaced patterns regardless of how the cells are arranged.

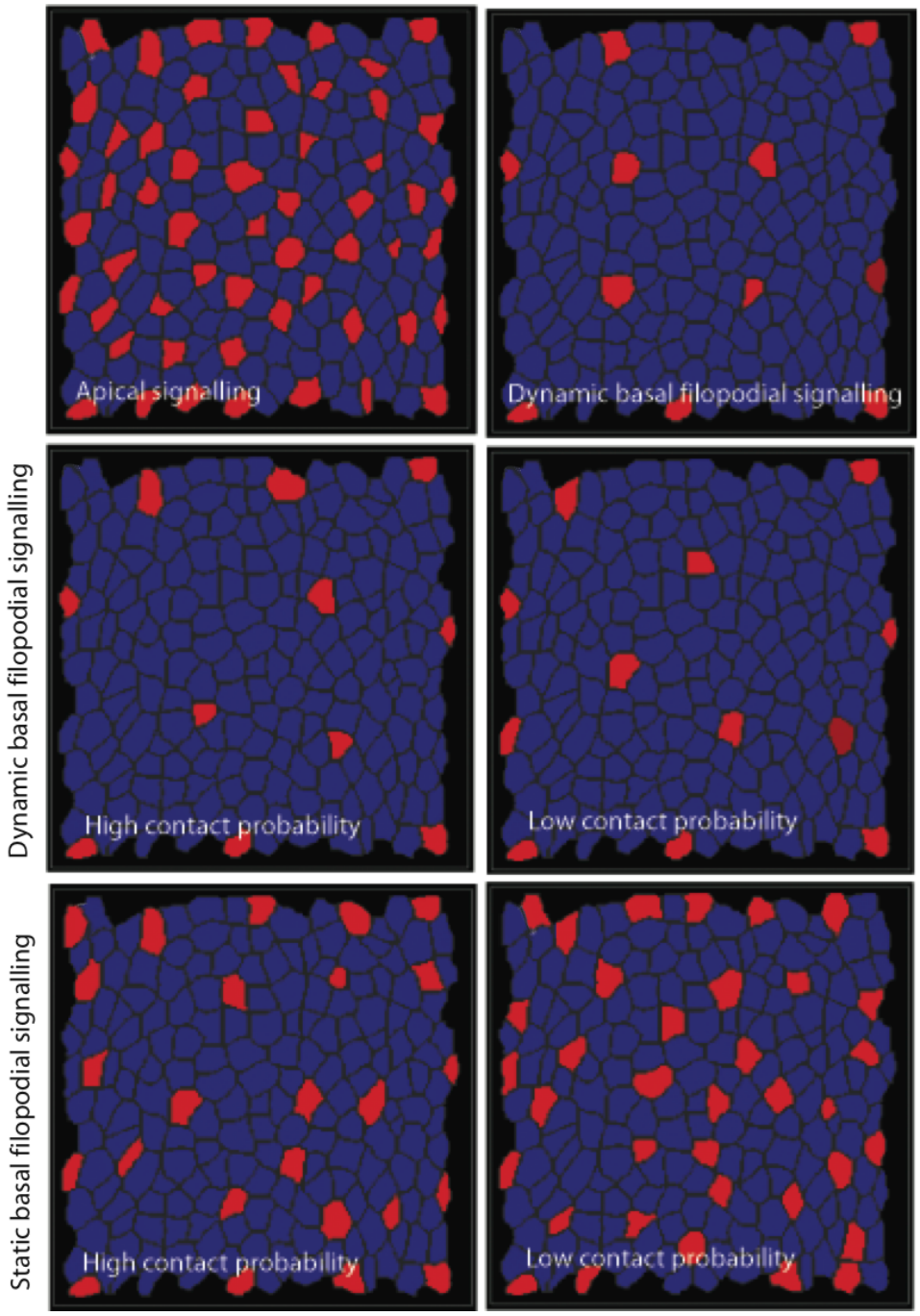

Figure 9.11: Model simulations were carried out using a 2D arrangement of cells derived from the real data (the range of basal signalling in all cases is also based on measurements of real filopodia = 1.7 cell diameters) . All simulations were repeated 10 times to establish density measurement of Delta expressing cells (red). [Top Left]: Signalling across apical cell-cell junctions only (final pattern density = 28.3+/- 1.0%). [Top Right]: Signalling over a fixed area - contact probability = 100 % (final pattern density = 5.9 +/- 1.0%). [Middle Left] : High contact probability (approx. 90% at 4 cell diameters) with dynamic filopodia (final pattern density = 5.9 +/- 1.0%). (Middle Right): Low contact probability (approx. 15% at 4 cell diameters) with dynamic filopodia (final pattern density = 6.9 +/- 2.0%). [Bottom Left]: High contact probability with static filopodia (final pattern density = 13.7 +/- 3.0%). [Bottom Right] : Low contact probability with dynamic filopodia (density = 19.2 +/- 2.0%). Simulation parameters: $\mu = \rho = 0.02\tau^{-1}, R_N = R_D = 1A.U.\tau^{-1}, a = 0.01A.U.^{k}, b = 100A.U.^{-h}, k = h = 6, \alpha = 1, e = 0.01$. Start conditions: $N = D = 1 + / - 0.01$ A.U.. Filopodia algorithm variables (from Figure 2.5): $F_\mu = 1.4, F_\sigma = 0.3, F_{rate} = 0.5$. For high contact probability P=1000, low probability P=100.

9.3 Summary

This analysis has revealed that lateral inhibition in the notum is a gradual process, which occurs by consecutive phases of pattern elaboration and refinement. Importantly, the entire process can be quantitatively reproduced by models of lateral inhibition in which cells are able to exchange Delta and Notch signals via dynamic filopodia over a distance of several cell diameters. This enables cells to compete for the ability to acquire a bristle fate over an extended period of time. Significantly, changes in bristle spacing occur in response to changes in protrusion length, as quantitatively predicted by the model. Moreover, the model suggests that protrusions are likely to determine the spacing of bristle precursors even in instances in which they transmit the minority of the total Delta-Notch signal. Since physical tension has been shown to enhance Notch cleavage and hence Delta-Notch signalling [Ahimou et al.: 2004], it is possible that forces generated through actin-based protrusion dynamics could also enhance basal signalling itself [Rorth: 2003]. Although previous authors have suggested roles for long, stable protrusions in cell-cell signalling events [Demontis and Dahmann: 2007, Rorth: 2003], this analysis shows that the generation of a robust and well-ordered pattern of cell differentiation across an entire tissue requires *dynamic* filopodia. Finally, since a network of filopodia can be quickly established, eliminated and their length and direction regulated in order to define a precise gradient of signalling over a distance of several cell diameters, dynamic filopodial signalling appears to be a credible alternative to morphogen diffusion as a mediator of signalling at a distance [Ashe and Briscoe: 2006, Rorth: 2003].

This section of the thesis has demonstrated how a cellular automata type model could be a applied to a real biological patterning process in order to help develop a quantitative hypothesis regarding the underlying signalling system. The final section explores the limitations of signalling through dynamic protrusions in a more abstract way. It is shown that intermittent signalling can produce a distinct type of patterning dynamic in which the packing of Delta expressing cells is gradually optimised. Furthermore, it shown how the long range signalling brought about by filopodial contact in this model enables the development of patterns of spots and stripes.

Part III

OPTIMISING PATTERNS AND THE GENERATION OF SPOTS AND STRIPES

Chapter 10

Asynchronous cellular automata and optimised patterning rules.

This chapter investigates the behaviour of simple 2-state asynchronous cellular automata in 1D and 2D. These are used to identify a mechanism for the dynamic optimisation of lateral inhibition patterns.

10.1 Patterning by lateral inhibition as a cellular automaton process

The first section of this thesis described an investigation into an evolved cellular automaton system that incorporated logical update rules based on the binary states of nearest-neighbour cells. This revealed that many characteristic complex patterns can emerge from these types of rules. It also demonstrated how certain rules are more robust than others. The second section of the thesis went on to demonstrate how the Delta-Notch signalling pathway can generate patterns of different gene expression among a layer of homogeneous cells. Using a model system to analyse data from Drosophila it was shown that long range signaling may be mediated by basally located dynamic protrusions known as filopodia.

So what, if any, is the link between the two types of model? Lateral inhibition produced by Delta-Notch signaling produces a two state pattern in which cells are either high or low in Delta. Cells high in Delta are surrounded entirely by cells low in Delta. Signaling (without filopodia) is between nearest neighbours only. Therefore, one would expect the behaviour of the lateral inhibition system to be captured by the 1D two state cellular automata rules.

10.1.1 The problem with synchronicity

Based on the logical construction of the cellular automata rules, the lateral inhibition patterning process should be best represented by rule 5. This rule dictates that a black cell can emerge from an empty neighbourhood of black cells or can remain black if both neighbours are white (see Figure 10.1a). However, when this rule is implemented as a synchronous cellular automata the system displays both lateral-inhibition type behaviour and oscillatory behaviour depending on the input pattern used to seed the system. Strikingly this rule does not pattern the whole field with a stable pattern of alternating black and white cells as is required of lateral inhibition (see Figure 10.1c). The oscillatory behaviour is a product of the synchronous update rules whereby each cell in the system is implementing the same rule set at the same time.

So far the cellular automata investigated in this thesis were synchronous. However, these represent a very special case. Cells acting in response to protein levels in developmental systems are not perfectly synchronous. This chapter looks at the behaviour of simple cellular automata rules with no synchronicity. In asynchronous cellular automata the cells are updated at different time steps [Cornforth et al.: 2005]. In this chapter the asynchronous cellular automata are implemented by randomly selecting individual cells which will be updated according to the rule set. By using this type of system any behaviours associated with synchronicity are removed.

In Figure 10.1d rule 5 has been implemented as an asynchronous cellular automaton. Regardless of the input seed pattern the system now establishes a lateral inhibition type pattern in which the whole line of cells is filled with black cells with only white cells as neighbours. The pattern is established fairly rapidly in approximately the time taken for each of the cells in the field to be picked at random. So within 1000 time-steps it is complete and remains in place for all future time steps. In biological terms the pattern could be said to be homeostatic. Note that in these asynchronous cellular automata a finite field size (200 cells) is used and the boundaries are treated as fixed white cells.

(a) Rule 5 - update criteria

(b) Input pattern used to asses cellular automata rule behaviours

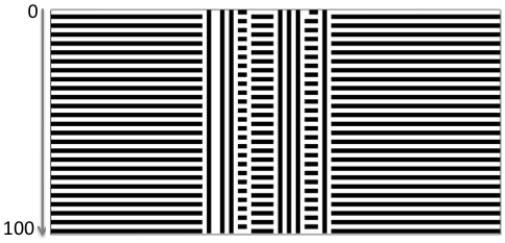

(c) Rule 5 implemented as a synchronous cellular automaton run for 100 time steps. The system shows a degree of lateral inhibition type behaviour but predominantly most cells oscillate between black and white states.

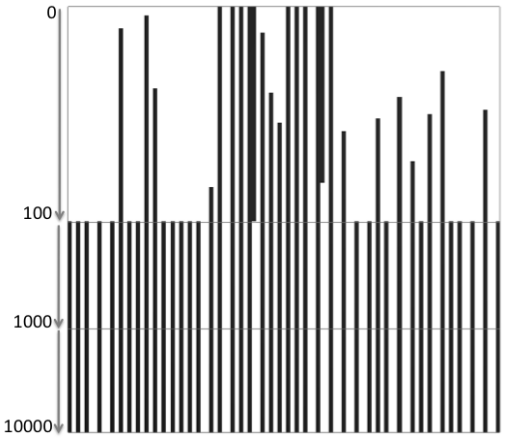

(d) Rule 5 implemented as an asynchronous cellular automaton. The screen shot shows the system over the first 100 time steps and then between 950-1000 and 9950 and 10000 times steps. The system demonstrates lateral inhibition type behaviour whereby a stable pattern rapidly emerges with each black cell separated by one or two white cells.

Figure 10.1: Rule 5 implemented as a synchronous and asynchronous cellular automaton. In the synchronous case many cells oscillate their state. In the asynchronous cellular automaton the system rapidly achieves a stable lateral inhibition type pattern regardless of the input seed pattern used.

10.2 Investigating asynchronous cellular automata

A lateral inhibition type pattern has been shown to be achievable by an asynchronous cellular automaton. Here, the question is posed; what other patterns, if any, are achievable by a 1D two

state asynchronous cellular automaton, and are there other rules that can also achieve a homeostatic lateral inhibition type pattern and therefore provide insights into this biological process.

Figure 10.2 contrasts the behaviour of two cellular automata rules with synchronous and asynchronous cell updates. The complete set of 256 rules were implemented as asynchronous cellular automata. These are shown in appendix Figure A.4. It is immediately striking that much of the complex patterning that characterised the synchronous cellular automata is no longer evident. The fractal-like regular and irregular nested triangular patterns that formed the development profiles of many of the cellular automata patterns can no longer be seen. These patterns were, of course, formed by looking at the single line updating over time. Now that cells update at different time steps these 'structured' developmental patterns are no longer obtained.

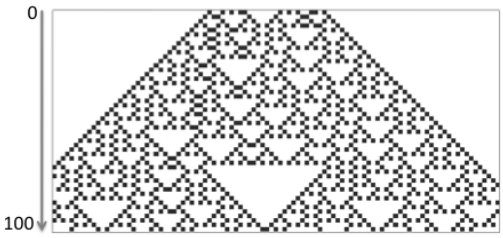

(a) Rule 18 implemented as a synchronous cellular automaton run for 100 time steps. Here nested patterns are formed over the time course of development resulting in regular spaced black cells at discrete time points

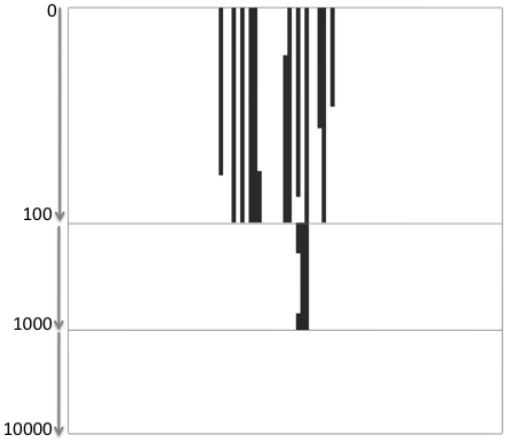

(b) Rule 18 implemented as an asynchronous cellular automaton. The screen shot shows the system over the first 100 time steps and then between 950-1000 and 9950 and 10000 times steps. Now the rule causes the input pattern to be entirely cleared leaving a blank field of white cells.

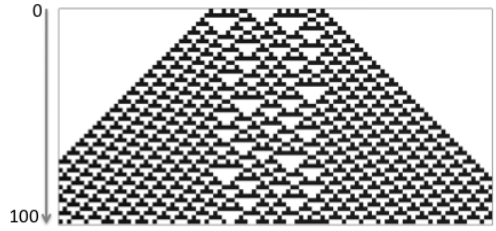

(c) Rule 54 implemented as a synchronous cellular automaton run for 100 time steps. Once again a fairly regular nested pattern is formed over the time course of development resulting in regular spaced black cells at discrete time points

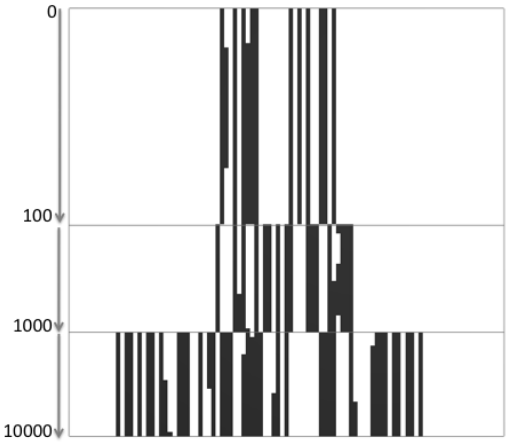

(d) Rule 54 implemented as an asynchronous cellular automaton. Here the CA produces a continually changing seemingly random pattern that never stabilizes - typical of the majority of the asynchronous rules.

Figure 10.2: Contrasting the behaviour of synchronous and asynchronous cellular automata.

In most of the asynchronous cellular automata the line of cells now update in a seemingly random way. These patterns do not stabilise over time and at a single time step appear to be fairly

randomly arranged. In some cases a stable pattern emerges that is completely dependent on the input pattern which is either maintained, or slightly refined and then maintained, over time. The only stable or near-stable patterning that can be observed across the whole field of cells is of a type close to lateral inhibition - that is, where black cells are separated by gaps of one or two white cells.

Of the 256 rules, 18% achieve homeostatic or nearly homeostatic patterning that is very close to perfect lateral inhibition with minor imperfections; 2% achieve a perfect lateral inhibition pattern with the whole field covered in homeostatic black cells surrounded by white. Of the remainder, 40% produced 'noisy' patterns with no obvious indication of homeostasis or any kind of regularity being achieved, 14% clear the input pattern entirely and produce a blank field, 26% achieve homeostatic patterns that fill or partially pattern the field but with an obvious dependence on the input pattern.

In a biological context there is a significant distinction that can be made between symmetrical and non-symmetrical rules; that is, those that differentiate between cells to the left and right. Asymmetric rules effectively require some kind of additional pre-patterning or gradient to be in place, whereas symmetrical rules could be represented be some kind of cellular interaction network based purely on chemical threshold levels. Therefore, this analysis is henceforth restricted to the symmetrical rules that produce some kind of homeostatic patterning in these asynchronous cellular automata.

Of the symmetrical rules, only rule 5 is able to achieve perfect homeostatic lateral inhibition type patterning. A few symmetrical rules that are very similar in form to rule 5 (or its mirror version) also produce similar lateral inhibition type patterns, but with slight variations. These include rules 77, 94, 95, 133 and 205 in which minor errors occur dependent on the input pattern; that is where two stable black cells sometimes remain touching (see Figure 10.3).

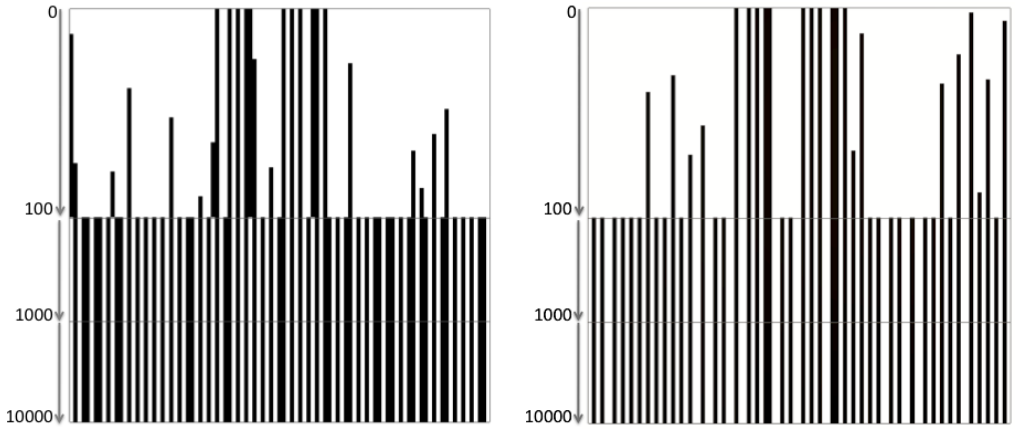

(a) Rule 95 (b) Rule 205

Figure 10.3: Rule 95 and rule 205 are both typical of a those symmetrical rules that almost produce lateral inhibition but allow stable imperfections to persist.

The only remaining symmetrical rule that comes close to a lateral inhibition type pattern is rule 23 which demonstrates a particularly unusual behaviour (Figure 10.4). In the example shown rule 23 never becomes stable but continually updates its pattern, producing regions containing a perfect on-off sequence of black and white cells. In this example a large even numbered array (a line of 200 cells) was used. Figure 10.5 shows the same rule implemented on an odd numbered array (99 cells). The system now self corrects to a stable perfectly packed pattern of black and white cells. Hence, it seems that rule 23 is capable of self-refining with a dependency on the array size and a border interaction. This behaviour can be further explained by a closer examination of the rules.

(a) Rule 23 - update criteria

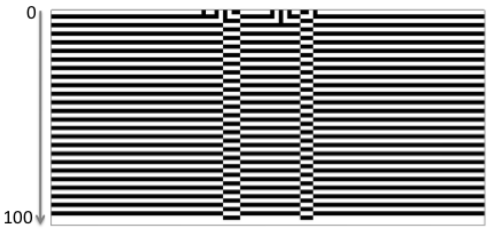

(b) Rule 23 implemented as a synchronous cellular automaton run for 100 time steps. The system predominately oscillates

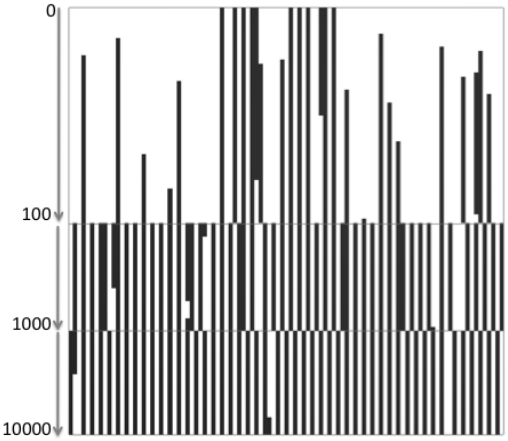

(c) Rule 23 implemented as an asynchronous cellular automaton. The screen shot shows the system over the first 100 time steps and then between 950-1000 and 9950 and 10000 times steps.

Figure 10.4: Rule 23 implemented as a synchronous and asynchronous cellular automaton. In the synchronous case many cells oscillate their state. In the asynchronous cellular automaton the system demonstrates lateral inhibition type behaviour but never stabilises. Instead the pattern seems to constantly attempt to refine towards a state in which a perfect on-off alternating pattern of black and white cells is achieved.

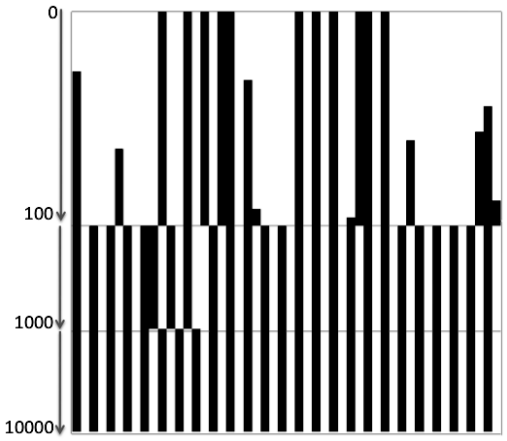

Figure 10.5: Rule 23 implemented over a smaller even numbered field now self corrects to a perfect stable pattern.

10.3 Interpreting the emergent behaviour of the rules

The symmetrical rules can be described in a simplified form. For example, using the notation for a white square; cell = 0, and for a black square; cell = 1, rule 5 can be rewritten in logical notation as:

if (Neighbours < 1 AND cell = 0,1) then (cell = 1)
else if (Neighbours >= 1 AND cell = 0,1) then (cell = 0),

(Adapted rule 5 re-written in a logical form)

where Neighbours is the sum of the states of cells in the neighbourhood. For a line of cells the neighbourhood will simply be two adjacent cells. (NB: Here the notation < 1 and >= 1 rather than 0, 1 or 2 cells is used as this enables the same rule to later be implemented in 2D.)

Rule 23 can similarly be rewritten in logical notation as:

if (Neighbours < 1 AND cell = 0,1) then (cell = 1)
else if (Neighbours = 1 AND cell = 0) then (cell = 1)
else if (Neighbours = 1 AND cell = 1) then (cell = 0)
else if (Neighbours > 1 AND cell = 0, 1) then (cell = 0)

(Adapted rule 23 re-written logical form)

Writing the rule in this format helps to interpret its emergent behaviour. Rule 23 is identical to rule 5 apart from the additional condition that permits a black cell to emerge in a neighbourhood of exactly 1 other black cell. This can be described as an 'unstable' state for a cell to be in, as a black cell with a single black neighbour will reverse its state when it is next selected. Furthermore, because a black cell cannot emerge from a neighbourhood with 2 black cells the system will continually update until the only white cells remaining have 2 black neighbouring cells and correspondingly black cells have only white neighbours. This globally 'stable' scenario corresponds to a perfectly packed pattern of alternating black and white cells (see Figure 10.6 for an illustration of this process). When such a perfectly packed pattern fits into a finite odd sized array the system will stabilise completely. When an even sized array is used the system will continually update as there will always be at least one region remaining in which the rule permits a cell to change state. However, in a large array, such as in Figure 10.4, large regions of perfect patterning emerge separated by an unstable region where cell updates are continually occurring.

Rule 23 behaves in contrast to rule 5, where a stable pattern is formed after each cell updates. With rule 5 the pattern is determined by the order the stochastic cell updates and so gaps of 1 or 2 white cells can remain between each black cell. The key principle that allows patterns generated by rule 23 to shift towards an optimised packing state is that an 'unstable' black cell may emerge. It is unstable because if it selected before there is any change in its local neighbourhood it will return to a white state. The global pattern refines because the probability of obtaining new unstable black cells reduces as the pattern becomes more densely packed as a result more regular. It will be shown that this heuristic principle allows a number of rules similar to rule 23 to also refine in the same way.

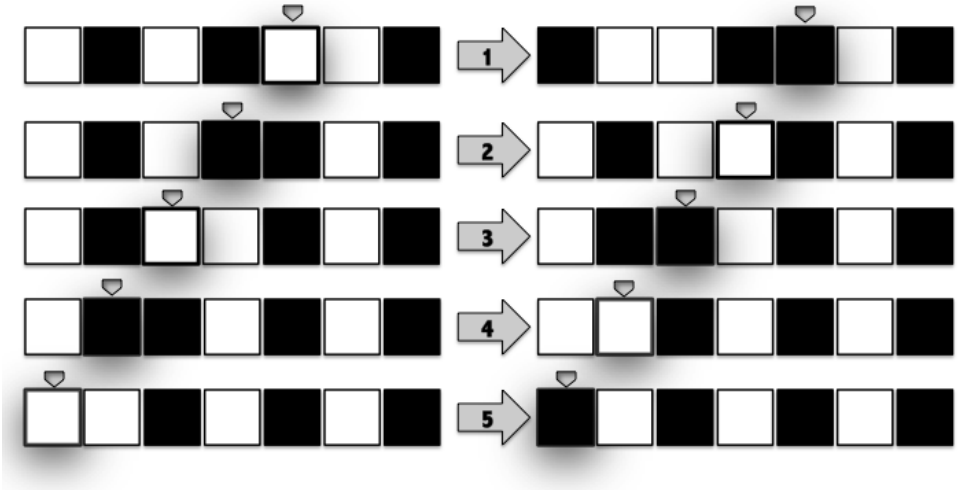

Figure 10.6: The pattern refinement process that occurs as a result of rule 23 type update rules. In stage 1 a white cell is randomly selected. This turns black as it has just one nearest neighbour black cell. In stage 2 a black cell is now randomly selected and turns white as it now has a black neighbour. As a result of this shift in the pattern the process is able to repeat in stages 3, 4 and 5. The final result is a perfectly packed pattern in which no state transitions will occur regardless of which cells are selected.

10.3.1 Applying the rules in higher dimensions

So far this analysis has been restricted to a line of cells, where the cell neighbourhood consists of just two adjacent cells. In a square lattice, the cell neighbourhood increases to 8 cells (including those at a diagonal - known as the Moore neighbourhood in cellular automata terminology). In the above logical representation for the rules the '>,<' notation was deliberately adopted to allow the same heuristic principle to be applied in this larger neighbourhood. The outcome of rule 5 when applied in 2D using this adapted form is shown in Figure 10.7. Here, a pattern is generated much like the 1D case where black cells are surrounded entirely by white cells, and are distributed unevenly according to the order in which cells were randomly selected.

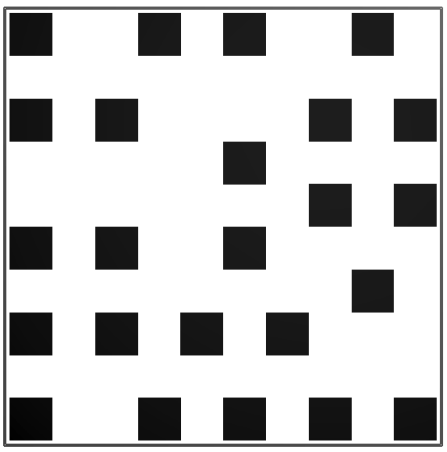

Figure 10.7: A typical stable outcome for the expanded logical form of rule 5 implemented as a 2D rule. Cells are selected at random from the 2D array and updated according to the rule conditions. As for the 1D case a homeostatic pattern is established in the number of time steps it takes to randomly select each cell in the array. In this case approximately 100 time steps. As in the 1D case the pattern does not perfectly pack the field as cells do not reverse their state once they become black and so their initial placement relies on their stochastic selection.

The adapted version of rule 23 can similarly be applied in 2D. Figure 10.8 shows the outcome in a square array with odd dimensions. As in the 1D case a stable perfectly packed pattern is formed over time. When the same rule is applied to an even dimensioned array (Figure 10.9) the result is an unstable pattern. However, in a larger even dimensioned array regions of temporarily stable patterning emerge separated by unstable boundaries (Figure 10.10). Thus, the behaviour of both of these rules is very similar to the 1D case.

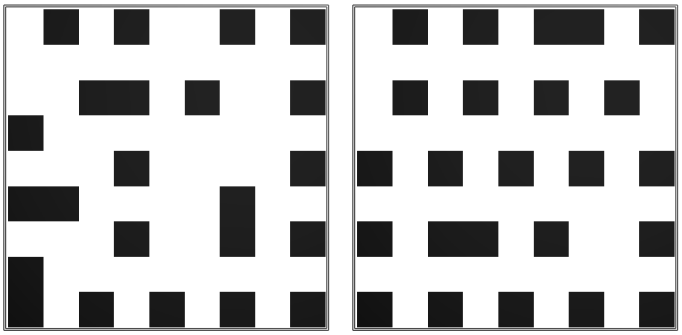

(a) Time-step 500 (b) Time-step 1000

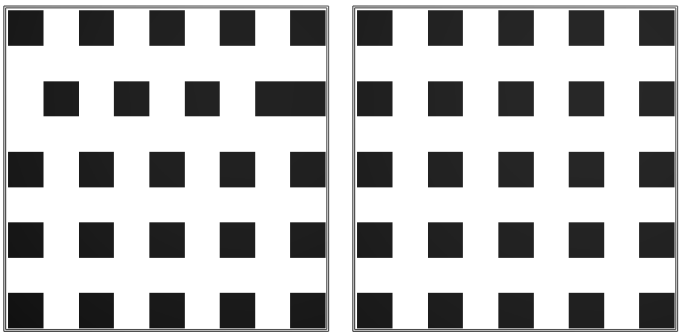

(c) Time-step 1500 (d) Time-step 2000

Figure 10.8: The adapted rule 23 implemented as a 2D cellular automaton in an 11 by 11 array. In this case the odd number dimensions of the array permit a stable outcome after approximately 2000 time steps in which the array is perfectly filled with a black and white pattern.

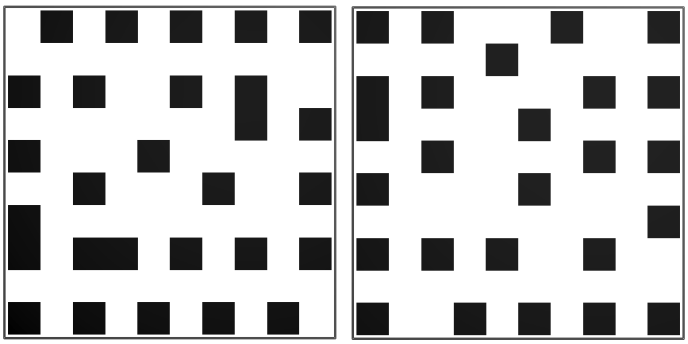

(a) Time-step 1500 (b) Time-step 2000

Figure 10.9: Rule 23 implemented as a 2D cellular automaton in a 10 by 10 array. In this case the even number dimensions of the array never permit a stable outcome. Cells constantly change state as the perfectly packed outcome cannot every be achieved and so the rules permit constant updates to occur.

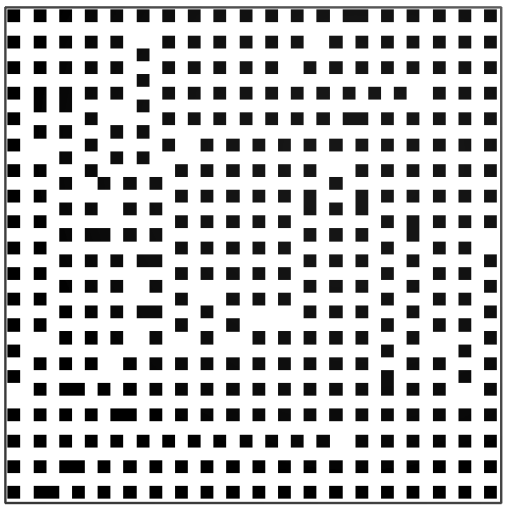

Figure 10.10: Rule 23 implemented in a much larger even sized field (38 x 38 cells) after about 10000 cell updates. The double black cells indicate that the system has not stabilised as these will undergo a state change on their next cell update. Although the system never stabilises in this symmetrical field, temporally stable regions of perfectly packed patterning emerge, separated by the unstable boundaries

10.4 Update conditions based on larger neighbourhoods

In 2D there are many more possible update rules that incorporate conditions based on higher numbers of neighbours. However, it is possible to identify a restricted set of these that share very similar properties to the 1D rules, 5 and 23. The basic property of rule 5 is that a black cell can emerge from a neighbourhood with some minimum number of black cells present (in this case it is zero). Applying this logic of a minimum threshold below which a cell can change state other rules can be derived which generate other types of pattern. (There are potentially many other types of rules that could be constructed in a 2D system based on more complex neighbourhood conditions. Here, it assumed that a simple threshold rule may be easily implemented by a biological system whereas more complex rules involving many thresholds are less realistic and have therefore not been included in this analysis.) One such example is:

if (Neighbours $<$ 5 AND cell = 0,1) then (cell = 1)
else if (Neighbours $>=$ 5 AND cell = 0, 1) then (cell = 0)

(A condition for 2D updates where black cells emerge from a neighbourhood of less than 5 cells)

The outcome of this rule with randomly updated cells is shown in Figure 10.11. This results in a striped pattern with the orientation of stripes randomly arranged.

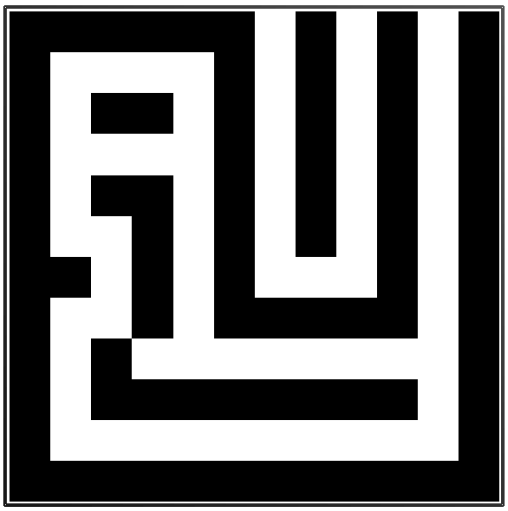

Figure 10.11: A cellular automaton that allows more crowded stable neighbourhoods. Here, a 2D update rule states that a black cell can emerge from a neighbourhood of less than 5 black cells otherwise cells must be white. The result is striping with random orientation.

Adding the extra condition of the type described by rule 23 to this rule gives;

if (Neighbours $<$ 5 AND cell = 0,1) then (cell = 1)
else if (Neighbours = 5 AND cell = 0) then (cell = 1)
else if (Neighbours = 5 AND cell = 1) then (cell = 0)
else if (Neighbours $>=$ 5 AND cell = 0, 1) then (cell = 0)

(An adapted rule in which an 'unstable' black cell can emerge from a neighbourhood of 5 cells.)

The outcome of the rule with this added condition is shown in Figure 10.12

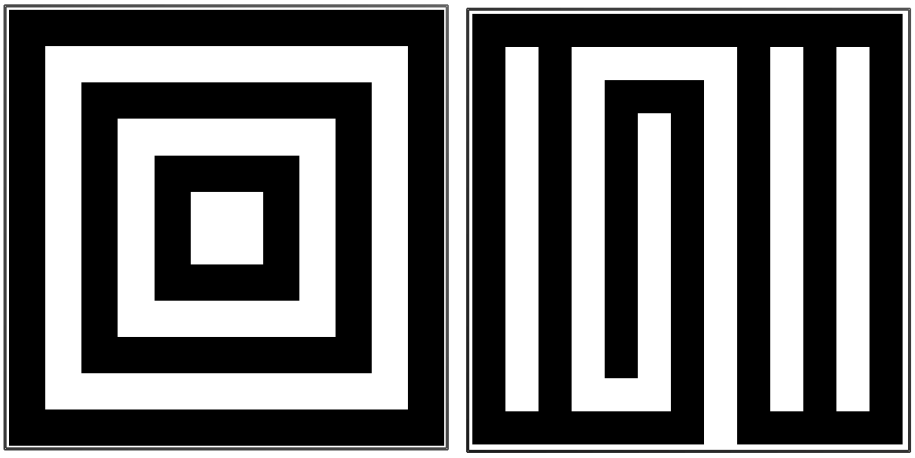

(a) Even sized array - the system stabilizes with a perfect spiral pattern

(b) Odd sized array - the system remains unstable but forms stable parallel lines with unstable junctions

Figure 10.12: Alignment of stripes. The outcome of the rule based on a transition at a neighbourhood of 5 cells with the extra condition that an unstable black cell can emerge from exactly 5 black neighbours. The outcome of simulations with a odd and even sized array is shown.

A similar behaviour emerges from an equivalent rule where the transition occurs at a neighbourhood of 6 cells. Figure 10.13 compares the outcome of this rule with and without the extra condition for the emergence of an 'unstable' black cell.

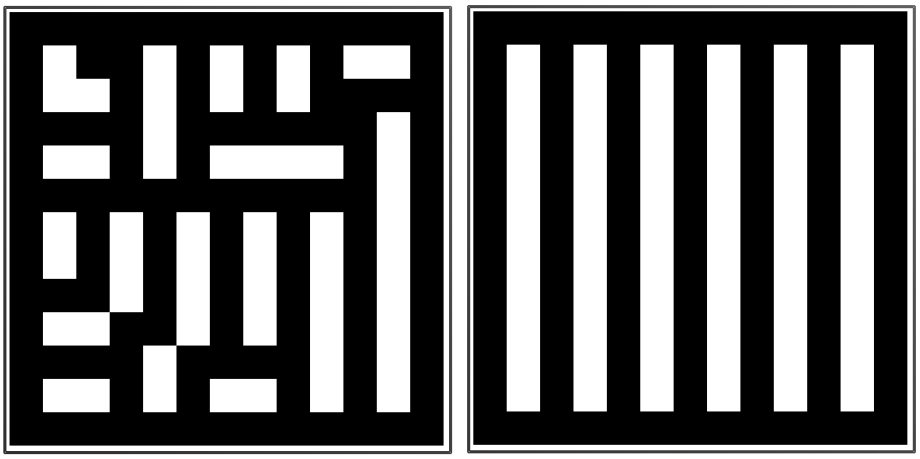

(a) A random stable pattern emerges without the condition in the rule set for an unstable black cell

(b) With the adjusted rule that allows for the emergence of an 'unstable' black cell the odd sized array forms a stable pattern of stripes

Figure 10.13: A rule with the transition for stable black cells at a neighbourhood of 6 black cells forms a stable pattern of perfectly packed stripes when the unstable condition is added.

Evidently there are very similar striped patterns that can be formed by conditions based on a transition at either 5 or 6 cells. In both cases, there are regimes, that are dependent on the boundary conditions, in which the stripes will align themselves with one of the boundaries. The same principle that produces optimisation in the patterns of spots also causes the stripes to align. That is, when the stripes are aligned the probability of seeing a new black cell in an 'unstable' state is at a minimum.

When these rules are adapted so that the transition for stable black cells occurs at even higher numbers of neighbourhood cells, the system begins to pattern in a way that resembles a kind of inverse of the lower neighbourhood condition (see Figure 10.14).

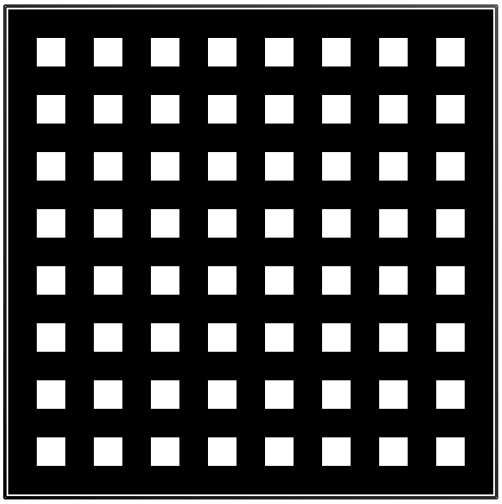

Figure 10.14: A rule with the transition for stable black cells at a neighbourhood of 8 black cells forms a stable pattern.

10.5 Refinement in larger cell neighbourhoods

Until now all of the rules that have been shown in this chapter have used update rules that only consider nearest neighbour cells in 1D or 2D environments. Similar rules can also be applied in larger neighbourhoods - that is where the zone of influence on a single cell reaches further. Figures 10.15 and 10.16 demonstrate how in both a 1D and 2D system, with extended ranges, the systems tend towards an optimised pattern when an adapted version of rule 23 is implemented in each case.

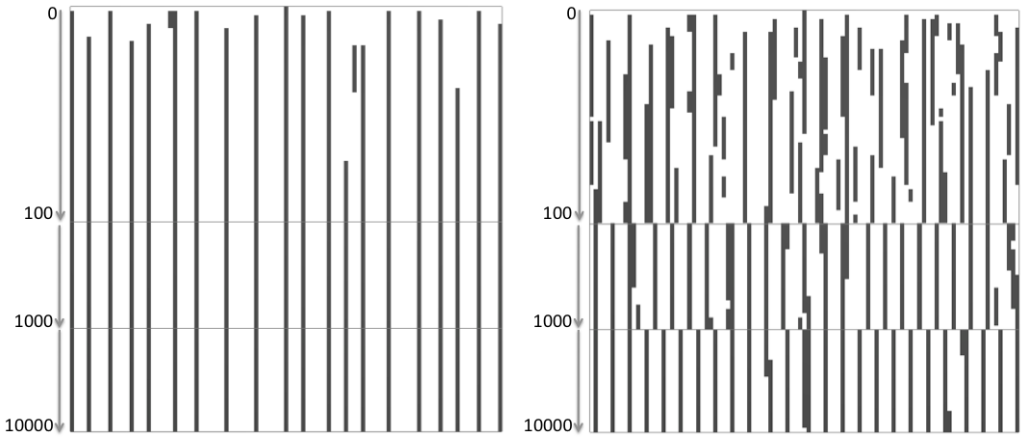

(a) Rule 5 implemented at a range of 3 cells. As for the nearest neighbour situation, the location of each black cell is based on the stochastic timing of cell updates in the system.

(b) Rule 23 implemented at a range of 3 cells. In this case the rule enables the system to continually refine towards the situation where each black cell is separated be exactly 3 white cells.

Figure 10.15: Comparing the behaviour of the adapted versions of rule 5 and rule 23 implemented in 1D asynchronous cellular automata where the total of number of black cells is based on a neighbourhood extending 3 cells to the left and right of each cell. The adapted version of rule 23 in this larger neighbourhood also generates an optimising pattern. In this example the system continually updates as the array size (100 cells) does not fit a perfectly spaced pattern at this range.

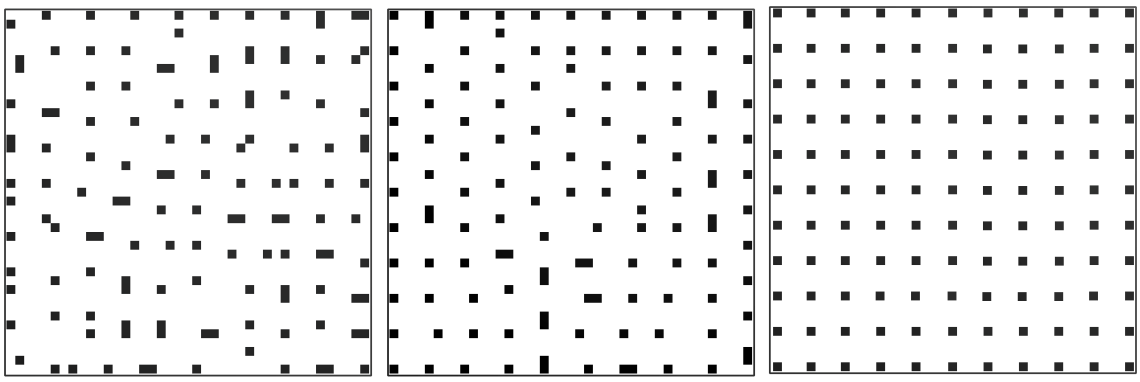

(a) Time-step 3000 (b) Time-step 50000 (c) Time-step 100000

Figure 10.16: Optimising at larger range in a perfectly packed field. The adapted version of rule 23 applied to a 2D array in which each cell has a square neighbourhood extending 3 cells, up, down, left and right. The system is able to refine towards a perfectly packed pattern in this array of size 41 x 41.

10.6 Summary

This investigation of simple cellular automata demonstrates that there are patterning rules, based only on local neighbourhood conditions, that can form patterns of single black cells, and/or stripes, that are able to optimise over time towards a more dense, and as a result regular, packing. This transitional property of rule 23 in the 1D asynchronous system has been previously identified [Grassberger et al.: 1984]. In this chapter it was demonstrated that same heuristic principles were able to explain the optimisation of very different patterns. This included the alignment of stripes which has not been identified in other studies of this kind. In each case the optimising process relied on patterning rules that enable a cell to enter an unstable (black) state which can potentially cause the local pattern to change at subsequent time-steps. Moreover, such transitions are more likely to occur at a low packing densities. Therefore, as the patterns become more densely packed the likelihood of seeing new state transitions reduces and so there is a tendency is for the whole pattern to move towards the more densely packed state and become more stable. The following chapter investigates how in the Delta-Notch cell-to-cell signaling model a similar kind of process can be identified.

Chapter 11

Dynamic optimisation of Delta-Notch patterning

This chapter reveals how Delta-Notch signalling mediated by filopodia can produce patterns that dynamically refine towards a stable state of optimised packing.

11.1 Asynchronous cellular automata rules and refinement heuristics

The previous chapter demonstrated how asynchronous cellular automata can produce lateral inhibition type patterns that refine over time towards a state of optimised packing. The question posed in this chapter is; can a refinement process be identified in the Delta-Notch signalling model that corresponds to the mechanism identified in the asynchronous cellular automata.

In the cellular automata the heuristic process that lead to the refinement of a pattern involved the application of a lateral inhibition type of rule with an added condition that allowed for a locally unstable black cell to emerge in a particular neighbourhood of black cells. The use of the term 'unstable' in this context refers to the fact that if reselected, before there was any other change in the local patterning, that cell would revert to being a white cell. However, the presence of new black cell was equally likely to cause a shift in the surrounding pattern. On a more global scale the likelihood of seeing a new 'unstable cell' transition reduced as the pattern became more dense and as a consequence, more regularly packed. The pattern was described as optimised because it contained the most number of black cells with some minimum spacing which also correlated with a regularity or ordering of the pattern.

In the Delta-Notch system any equivalent optimisation process might therefore require similar features; a temporarily 'unstable' cell expressing Delta in a region in which it would typically be inhibited from doing so; thus, allowing the subsequent inhibition of surrounding Delta expressing cells and, hence, an adjustment of the global pattern; combined with the added property that as the pattern density increases the probability of such an occurrence decreases.

11.2 Filopodia as a refinement mechanism

Previous chapters have already demonstrated the role of basal protrusions in the patterning of microchaetes in the notum of Drosophila flies. These were identified as highly dynamic filopodia. Simulations showed how a stable pattern could be established by intermittent signalling between

filopodia. This provides a mechanism by which the signalling network between cells is constantly broken and re-established over time (see Figure 11.1). Hence, this potentially fulfils the heuristic requirement identified above for optimisation; by breaking filopodial contacts, an inhibitory signal may be lost, allowing a new cell to express Delta and potentially causing a subsequent shifting of the local pattern. Furthermore, as the global pattern becomes more dense the probability of losing inhibitory signals may decrease and thus the pattern may progress towards a more dense, optimally packed state.

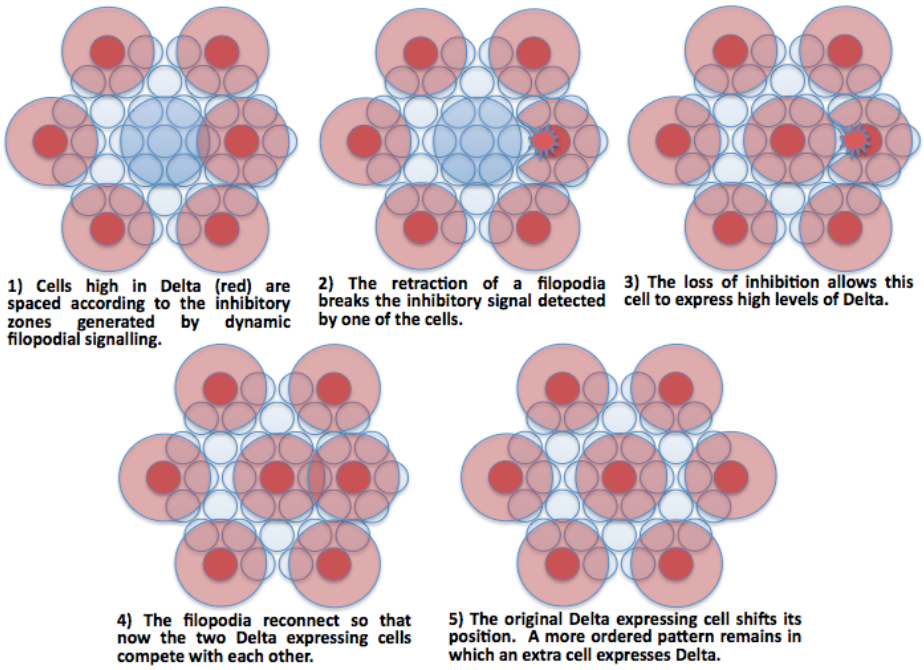

Figure 11.1: A schematic showing how refinement may occur by filopodia signalling.

11.2.1 Simulating filopodial refinement

To investigate the role of dynamic filopodia in the development of an optimal and well-organised pattern across a tissue, an analysis was performed using an idealised hexagonally packed 2D array of 30x30 cells. For this analysis, the cell-to-cell contact probability (equivalent to filopodial coverage) and filopodial dynamics were systematically varied to test how changes in these parameters affect global refinement of the Delta-Notch pattern. All cells in the field were allowed to signal to one another via apical signalling and, where filopodia were present, via filopodial signalling over a range of two cells (see Figure 9.8). Filopodia were implemented by using a 'birth' and 'death' rate at each simulation time step. In this way the average number of connections between cells and the average lifetime of each filopodial signalling connection could be independently varied (refer to chapters 8 and 9 and appendix Figure 2.4 when the algorithm is detailed in full). To determine the pattern 'order' achieved during the course of the simulations, a measure was taken of the distance between each Delta expressing cell in the field (discounting cells within 6 cell diameters from the border) and its 6 nearest neighbours that were also high in Delta. This provided a measure of the average spacing between all cells in the emergent pattern and an associated standard deviation. The ratio of the standard deviation to the average spacing gave the 'coefficient of variation' in this system which was taken to directly represent a measure the global order of the emergent pattern. The hill function coefficients were set at $k = h = 6$ to avoid the ordering obtained in the initial pattern establishment associated with a very linear hill function (refer to Figure 8.13). The simulations were run for 40000 τ to determine the change in the coefficient of variation.

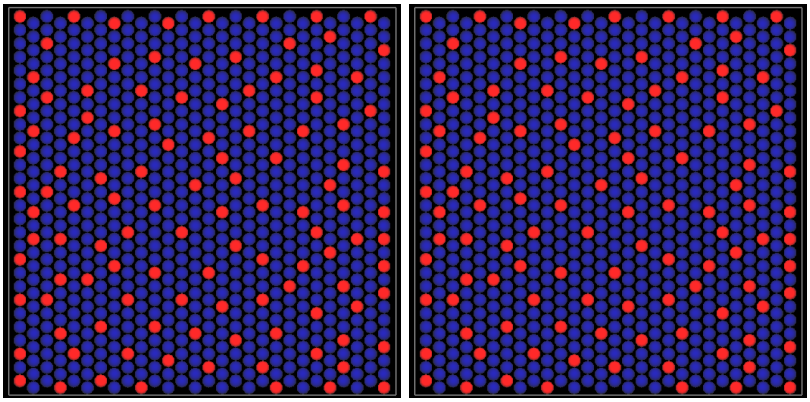

(a) Static filopodia. Time=1000τ. CV=0.22

(b) Static filopodia. Time=40000τ. CV=0.22. No change to the irregularly spaced pattern.

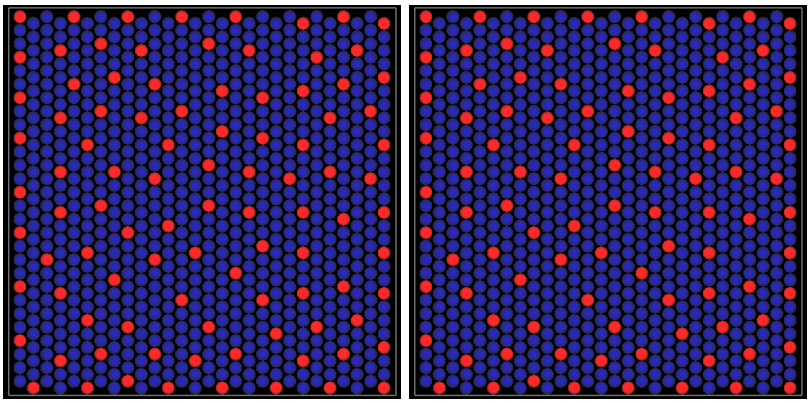

(c) Dense, fast filopodia. (Lifetime = 10τ, Nbrs at R2 = 6). Time=1000τ. CV=0.19. Density = 10.5%

(d) Dense, fast filopodia. Time=40000τ. CV=0.19. No change to well spaced pattern. Final density = 10.5%

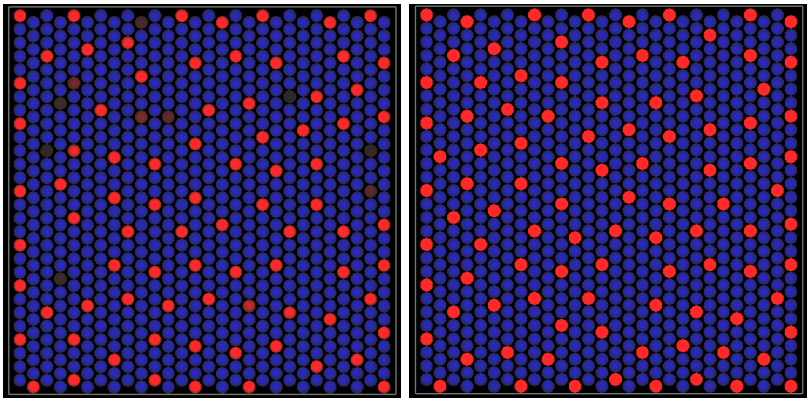

(e) Intermediate filopodia (Lifetime = 100τ, Nbrs at R2 = 6).Time=1000τ. CV=0.19. Density = 10.5%

(f) Intermediate filopodia. Time=40000τ. CV=0.14. Pattern becomes more dense and ordered. Final density = 12.1%.

Figure 11.2: Filopodial signalling can lead to optimising patterns. A set of simulation screen shots demonstrating how filopodia with intermediate lifetimes and densities can generate a pattern that refines over time. Simulation parameters: $\mu = \rho = 0.02\tau^{-1}, R_N = R_D = 1A.U.\tau^{-1}, a = 0.01A.U.^{k}, b = 100A.U.^{-h}, k = h = 6, \alpha = 1, e = 0.01$. Start conditions: $N = D = 10 + / - 0.1A.U.$. Array size = 30x30 cells. Filopodia algorithm variables: (from Figure 2.4) F-birthrate = 0.1 , F-deathrate = 0.1 (for fast dynamics): F-birthrate = 0.01 , F-deathrate = 0.01 (for intermediate dynamics).

The results of the experiment reveal that when dynamic filopodia are used in this system a refinement process may take place (Figure 11.2). When this occurs the system effectively rearranges the whole pattern so that the separation of Delta expressing cells is less varied and more cells can pack into a given field at a given range of separation. This process was described schematically in Figure 11.1.

The refinement process takes place when a balance is achieved between the average density of the filopodia network and their average lifetimes (see Figure 11.3). This allows the pattern to change over time in a way that static or very fast filopodial dynamics do not allow (Figure 11.4). At a filopodial density of 50% (approximately the density observed in the microchaete patterning data) the pattern refines with filopodial lifetimes of around 100τ and the period to reach an stable optimised packing state is approximately 5000τ. This is roughly equivalent to the observed filopodial lifetimes of 500 seconds (over a patterning period of 8 hours). (Equivalent ratios were found for results at other densities i.e at 75% connectivity the optimisation took approximately 40000τ with filopodia lifetimes of 1000τ). Hence, these results indicate that the filopodia dynamics and the seemingly long patterning time in this system may be interpreted by this type of process.

Nbrs at R2	Filpodia Av Lifetime								
	static	2	10	20	100	200	1000	2000	10000
1.2	0.23	0.19	0.18						
3.0	0.22	0.19	0.19	0.16					
6.0	0.22	0.19	0.19	0.20	0.14	0.16			
9.0	0.21	0.19	0.19	0.19	0.18	0.18	0.16		
10.8	0.19	0.19	0.19	0.19	0.19	0.18	0.14	0.17	0.18
12.0	0.19	0.19	0.19	0.19	0.19	0.19	0.19	0.19	0.19

Refined pattern
Stable pattern
Disordered pattern
No stable patterning

Figure 11.3: A table summarising the conditions for filopodia pattern refinement. 2D simulations were run for 40000τ using different combinations of filopodia density (in terms of the number of neighbourhood connections) and the average lifetime of filopodia (in units of τ). The coefficient of variation is shown for each parameter set. The results are colour-coded to distinguish between distinct outcomes. The parameter set used was as per Figure 11.1. The filopodial connectivity and lifetime was varied by changing F-birthrate and F-deathrate as defined by the algorithm in Figure 2.4

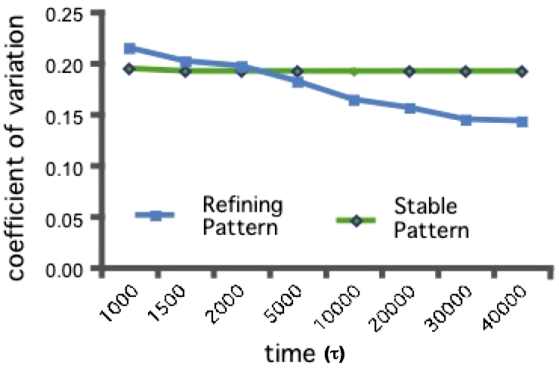

Figure 11.4: Optimisation dynamics. The coefficient of variation in spacing between each Delta expressing cell and its 6 nearest neighbouring Delta expressing cells, plotted over time for filopodia with lifetimes of 10τ (yielding a fixed pattern) and filopodia with lifetimes of 1000τ (refining pattern) at a density of 75% (9 out of 12 filopodial connections). Parameters are as per Figure 11.1

11.3 Probabilistic analysis of the filopodial signalling system

The pattern optimisation has been demonstrated numerically in simulations. To try to better understand the process and qualify the model behaviour, an analytical description of the system was derived. The aim was to establish how the filopodial lifetimes and density would effect the probability an emergent pattern changing over time. Crucially this description has to take into account the possible stable pattern configurations. Only in this way can an accurate description of the likelihood of pattern shifting be derived.

Figure 11.5 shows a single cell in this system, where filopodial signalling is restricted to 2 cell distances in an idealised hexagonal array. The cell has n, nearest neighbours and N neighbours at filopodial signalling range. The density of filopodial signalling connections λ (the proportion of the N possible basal connections made at any instant in time).

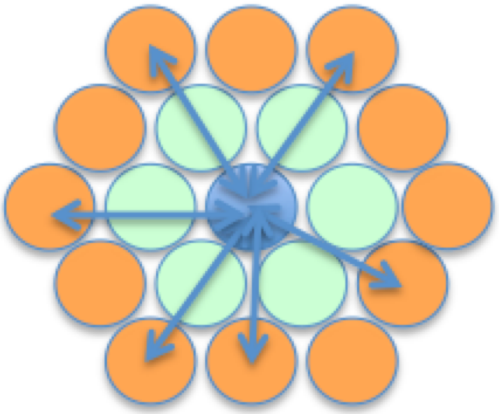

Figure 11.5: Filopodial signalling at a range of 2 cells in the hexagonal array. A single cell and its neighbourhood as described by the model system. Here a cell has n=6 nearest neighbours (green). It has N=12 neighbours at filopodial signalling range of 2 cells (orange). There is a signalling link between 6 out of those 12 possible cells, hence the density of connections, $\lambda = 0.5$.

If through filopodial signalling Delta expressing cells are able to maintain a zone of inhibition exactly 2 cells wide, different pattern configurations can form that satisfy this criteria. Figure 11.6 shows 3 types of potentially stable patterns that could be generated by this signalling system in which each Delta expressing cell is separated by at least 2 cells. In a real stochastic patterning process a mixture of these three types of pattern tessellations will emerge. The figure shows that with different packing types a very different proportion of cells are inhibited by filopodial connections alone. In the most dense packing type all non-Delta expressing cells are inhibited by direct contact with a Delta expressing cell. The term, γ, is used to denote the proportion of cells that are inhibited by filopodial contact only. These are the cells that are potentially able to express Delta due to a temporary loss of inhibition through filopodial dynamics. The term, m, denotes the total number of Delta expressing cells that the γ population of cell connect to via filopodia. Hence these two terms are critical in establishing the likelihood that filopodial inhibition is temporarily broken and hence whether a pattern is ultimately able to reconfigure and optimise its packing.

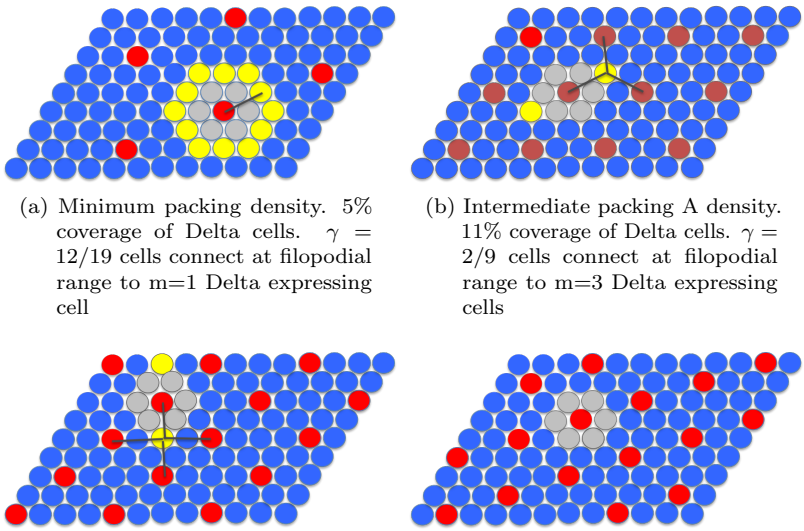

(a) Minimum packing density. 5% coverage of Delta cells. $\gamma = 12/19$ cells connect at filopodial range to m=1 Delta expressing cell

(b) Intermediate packing A density. 11% coverage of Delta cells. $\gamma = 2/9$ cells connect at filopodial range to m=3 Delta expressing cells

(c) Intermediate packing B density. 11% coverage of Delta cells. $\gamma = 2/9$ cells connect at filopodial range to m=4 Delta expressing cells

(d) Maximum packing density. 16% coverage of Delta cells. 0 cells connect at filopodial range

Figure 11.6: Periodic packing types. A schematic showing the different possible packing that can occur in the system where cells signal across a range of 2 cells. When a pattern arrises stochastically a mixture of these types of packing will occur. The red cells are those that are high in Delta. For each tessellating packing formation the different cell signalling types are shown. The grey cells are those that are in direct contact with a Delta expressing cell. The yellow cells are inhibited just at filopodial range. γ describes the percentage of yellow cells in the whole field of cells. In each case the number of Delta expressing cells, m, contacted by cells inhibited at range is shown.

For packing optimisation to occur there must be a finite probability that new Delta cells emerge in low density packing. When this probability is very low a stable pattern will persist and the pattern will not refine. Moreover, this probability must not be too high or there will be too many cell updates and the pattern will be unstable.

To derive approximations of these probabilities the assumption can be made that any signalling connection to a cell that is expressing high levels of Delta will inhibit that cell from doing likewise. This represents the case of a highly non-linear system where there is a very rapid response to a very low Delta signal. Then, for any new Delta expressing cell to appear at any cell site, it must start with no signalling connection and no new signalling connection must be established within the time it takes for a new cell to go high in Delta.

The minimum time taken for a cell to go high in Delta in the absence of an inhibitory signal (expressed here as T) can be derived from the Delta and Notch decay rates specified in equation 8.1. As a close approximation this will be the sum of the time for Notch to fully decay (to very near zero where Delta production may start) and for Delta to reach at least half its maximum concentration in order to inhibit other cells. This gives a value $T \approx \frac{1}{2\rho} + \frac{1}{\mu}$.

The probability for establishing a new cell expressing high Delta within a time step equal to T can be stated as:

$$\begin{aligned} P(New\ Delta\ cell\ in\ time\ T)) \quad = \quad & P(Not\ existing\ Delta\ cell) \\ & \times P(No\ existing\ inhibitory\ Delta\ signal) \\ & \times P(No\ new\ inhibitory\ Delta\ signal\ in\ time\ T) \end{aligned} \tag{11.1}$$

Here, we are assuming that new Delta cells can only arise due to a loss of signalling through dynamic filopodia. Therefore the probability that there is no Delta signal received by a cell in the entire field is equivalent to the probability that there is no filopodial connection to one of the non-Delta expressing cells. The total density of cells that are only inhibited by filopodia, are defined as γ, which varies for the different packing types (Figure 11.6). For any cell there are N cells at filopodial signal range (12 in this system with signalling over 2 cell diameters). For the γ proportion of cells inhibited only by filopodia there are m Delta cells at this range. Therefore the density of Delta expressing cells within filopodial contact range is m/N. The mean number of filopodial connections at any time is $N\lambda$ (as defined in Figure 11.5). Therefore the probability that there is no Delta signal received by a cell in the entire field is equivalent to the probability that any of the $N\lambda$ filopodial connections from the γ fraction of total cells, are linked to the $(1 - \frac{m}{N})$ fraction of cells that are not expressing Delta. This can be stated as:

$$P(No\ existing\ Delta\ signal) = \gamma(1 - \tfrac{m}{N})^{N\lambda} \tag{11.2}$$

If the mean birthrate of a filopodia signalling connection is given by μ, then the expected number of new filopodial connections to N possible locations in time T will simply be $NT\mu$. However, to compare this analysis with the simulations (and experimental data) it is more useful to define this in terms of the filopodial lifetime and density. It is relatively easy to show that in a system with a constant birth rate, μ and death rate, ϵ of filopodia (the algorithm implemented for the simulations), the steady state density, λ, will be given by: $\lambda = \mu/(\mu + \epsilon)$. The mean lifetime of filopodia, given by δ, is approximately equivalent to the inverse of their deathrate ϵ. Therefore the birthrate will be given by: $\mu = \lambda/(\delta(1-\lambda))$, and the expected number of new filopodial connections made by a cell in time T will simply be $NT\lambda/(\delta(1-\lambda))$.

Hence, the probability that in time T no new signalling connection is made with a Delta expressing cell is:

$$P(No\ New\ Delta\ signal\ in\ time\ T)) = (1 - \tfrac{m}{N})^{NT\lambda/(\delta(1-\lambda))} \tag{11.3}$$

Therefore substituting equations 11.2 and 11.4 into equation 11.1 gives:

$$P(New\ Delta\ cell\ in\ time\ T) = \gamma(1 - \tfrac{m}{N})^{N\lambda(1+T/(\delta(1-\lambda)))} \tag{11.4}$$

Where, T is the minimum time taken for a cell to go high in Delta in the absence of an inhibitory signal; γ is the percentage of cells in an emergent pattern that are only inhibited through filopodia connections; m is the number of cells expressing Delta within filopodial range of the γ population of cells; N is the total number of cells connected at filopodial range; λ is the density of filopodia; and δ is the mean lifetime of filopodia.

As expected from this derivation when the density of Delta expressing cells, m/N increases, the probability of a new Delta cell emerging goes down. Figure 11.7 shows the probability of obtaining a new Delta cell at each of the densities associated with the idealised packing scenarios. It is clear from this analysis how very distinct probability transitions occur for different filopodia dynamics at different filopodia densities. When this analysis is contrasted with the simulation data in Figure 11.3 it shows that where in the simulations a refinement process was observed, this is associated with a distinct type of probability transition from around 20% at the minimum packing density down to near zero for higher densities. When the probabilities associated with seeing a new Delta cell are significantly higher across this density transition, this seems to correspond to an unstable pattern in the simulations.

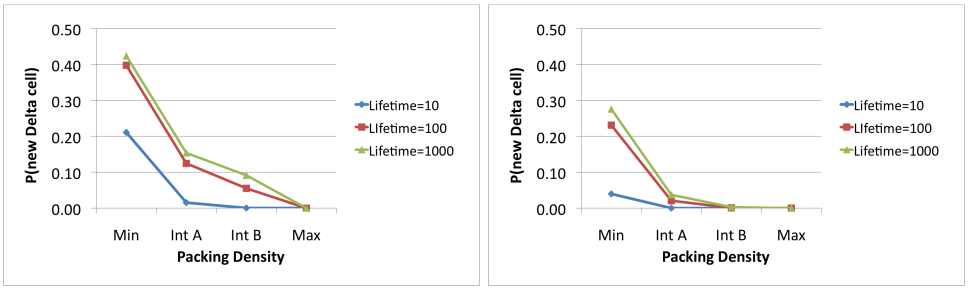

(a) $\lambda = 10\%$. Optimisation in simulations occurred at filopodia lifetimes $\approx 10\tau$.

(b) $\lambda = 50\%$. Optimisation in simulations occurred at filopodia lifetimes $\approx 100\tau$.

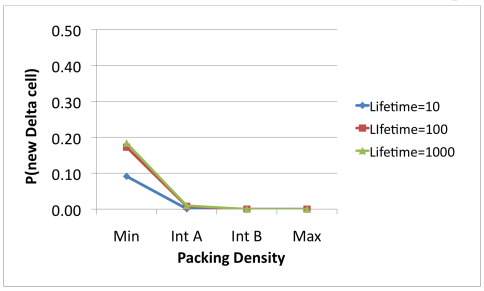

(c) $\lambda = 90\%$. Optimisation in simulations occurred at filopodia lifetimes $\approx 1000\tau$.

Figure 11.7: The probability of observing pattern adjustment. The probability of seeing a new Delta cell (in time τ) is plotted for different filopodia lifetimes (δ) for the four different packing types identified in Figure A.5. Each of the graphs show the result with different levels of filopodia density (λ). All the data is based on a value of $T = 75\tau$ and filopodial signalling across 2 cells in an idealised hexagonal array, as was used for the simulations in Figure 11.3. The figures demonstrate that the optimising patterns observed in simulations correspond to a transition in probability between the minimum packing density (at around 20-25%) and the intermediate packing type (<1%). Higher probabilities seem to correspond to the unstable patterning regimes and lower ones to stable patterning regimes in the simulations.

To confirm that the simulation results were not significantly effected by the relatively small array sizes, simulations were repeated in larger arrays over a longer time span. Figures 11.8 and 11.9 show examples of tests that were carried out using a larger array size for 1 million τ. In neither case was there evidence of significant differences from the analysis in Figure 11.3.

The combined analysis and simulation that has been carried out indicate that there is a maximum density of packing that is reachable by the optimisation process. This density is around 12% and falls short of the maximum possible packing density of 16% (illustrated in Figure A.5). When the probability of seeing a new Delta cell at low densities is very high the pattern remains too unstable to ever make the global transition to a higher density. Therefore, a balance must be achieved between the propensity for the pattern to adjust and its overall stability.

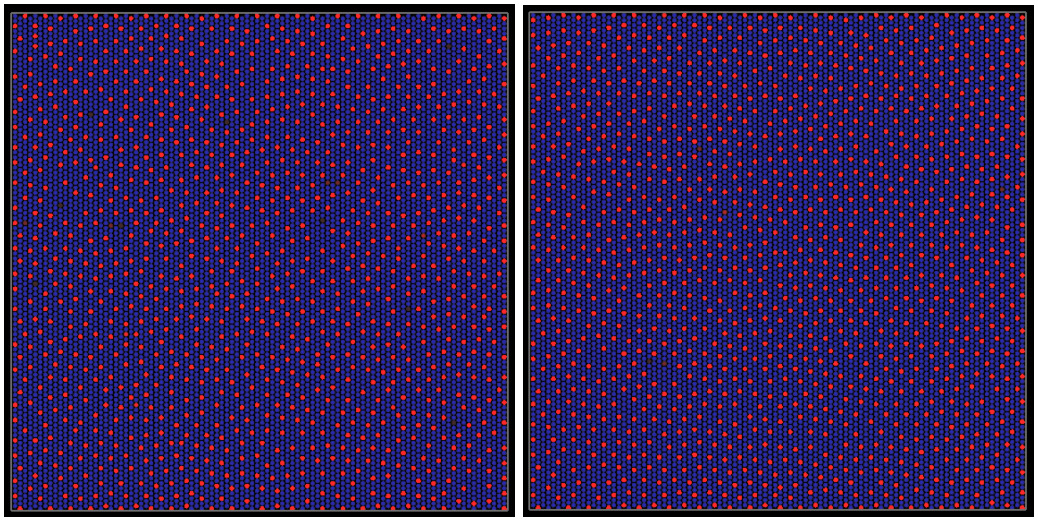

(a) Time-step 2000.CV = 0.19, Density = 10.8%

(b) Time-step 1000000. CV = 0.14, Density = 12.2%

Figure 11.8: The effect of larger field size. Using a larger patterning field over a larger time period yielded similar change in the pattern order and density. 50% filopodial connectivity, Filopodia lifetime=100τ. Model parameters are as per Figure 2.4 with F-deathrate=F-birthrate=0.01.

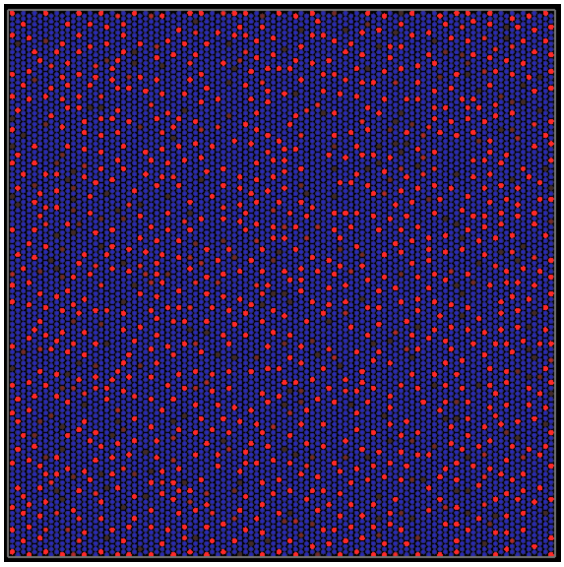

Figure 11.9: The effect of large field in less stable parameter regimes. With filopodial dynamics that give higher cell update probabilities, using a larger field for longer time spans still leads to unstable patterns. Time step shown = 1000000 τ. 50% filopodial connectivity, Filopodia lifetime=1000 τ. Model parameters are as per Figure 2.4 with F-deathrate=F-birthrate=0.001.

11.4 Pattern optimisation by transient signalling

The action of dynamic filopodia imposes a kind of structured noise on an idealised signalling network. In this model signals depend on a stochastically changing distribution of cell-to-cell contacts. An equivalent model could be proposed in which levels of signalling molecules distributed around a cell (either apically or basally) varied with a high degree of stochasticity. The time variance of this type of fluctuation would be equivalent to the filopodia dynamics. Filopodia provide a mechanical basis by which this type of signalling can easily be envisaged. However, one could also imagine alternative models. For example, a fluctuating adhesion force between cells could generate similar dynamics. In each scenario the overall concentration of proteins within a cell can remain fairly constant, while the signalling is made subject to spatial noise.

An alternative model would be to use temporal noise. In such a model a similar process of packing optimisation could conceivably occur by having transient levels of Delta signal across an entire cell. Figure 11.10 shows a schematic illustration of a cell with transient levels of Delta expression. There is a certain probability that a cell's expression of Delta drops below some threshold for a time τ during which it might be possible for a neighbouring cell to begin to express Delta. It is clear that when a greater number of cells are inhibiting a particular cell, the probability that all neighbouring cells go below some threshold at the same time is greatly reduced.

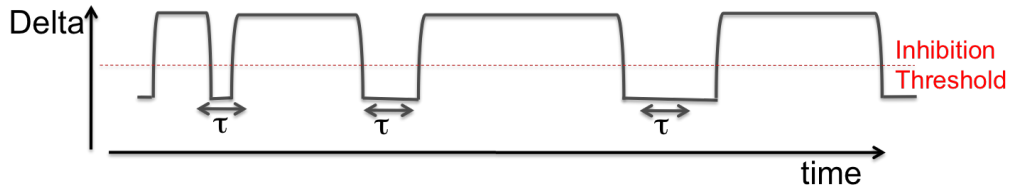

(a) An imaginary Delta signal from a cell fluctuates transiently. There is certain probability that the Delta levels goes low for a time τ - the time for neighbouring inhibited cells to express high levels of Delta.

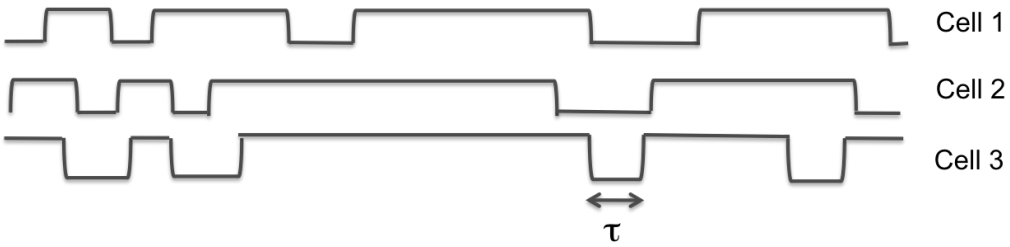

(b) Many cells with similar transient fluctuations have a much lower probability of all signalling low Delta levels for the same time duration τ.

Figure 11.10: A schematic of transient signalling. The probability of many Delta cells showing a transiently low signal at the same time is much lower than for a single cell with a transient signal. Hence, the probability of a cell loosing Delta inhibition reduces with the density of surrounding cells

As a pattern becomes more densely packed the number of Delta expressing cells inhibiting non-Delta expressing cells will increase (see appendix Figures A.5 and A.6 for an illustration of this principle). Hence, with a transient signalling model, it is possible to meet the key requirement for pattern optimisation that was identified above; that a pattern can temporarily express new Delta cells, and that the probability of this occurring reduces as the pattern gets more densely packed (and ordered).

11.4.1 Random noise as a mechanism for transient signalling

The method by which the transient signalling model is implemented will undoubtedly have a strong impact on the ultimate behaviour. The transient signal could be driven by some kind of internal genetic oscillator governing Delta expression; however, it could also relate to a more simple case in which random noise caused temporal fluctuations in a cell's protein expression. In this case there could be some finite probability that random noise would cause a cell's Delta expression to drop low enough to permit neighbouring cells to express Delta. In Figure 11.11 a simulation is shown in which pattern optimisation is achieved with just apical signalling and a random noise term. In this simulation the parameter set was very carefully chosen to permit the refinement to take place. Refinement was only observed in simulations with parameter, a, fixed so that Notch activity occurs in response to a Delta level between 0.6 - 4.0 times the level of a typical Delta expressing cell. At lower values of parameter, a, there is no adjustment of the pattern and at very high values adjacent cells are able to express Delta (see Figure 11.12).

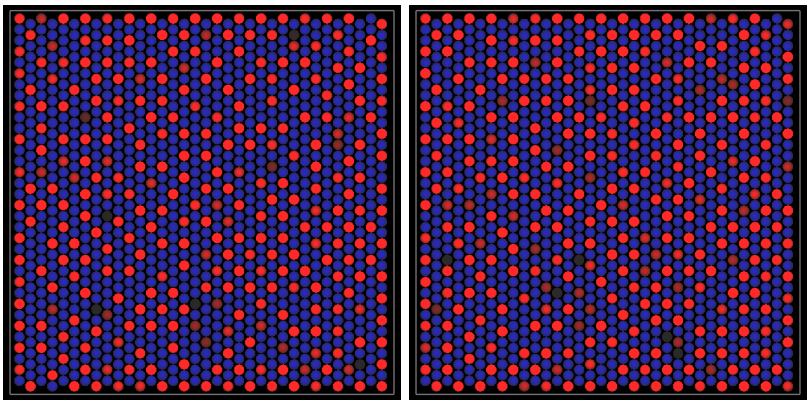

(a) Time=1000τ. Spacing = 2.27. CV = 0.20

(b) Time=10000τ. Spacing = 2.25. CV = 0.19

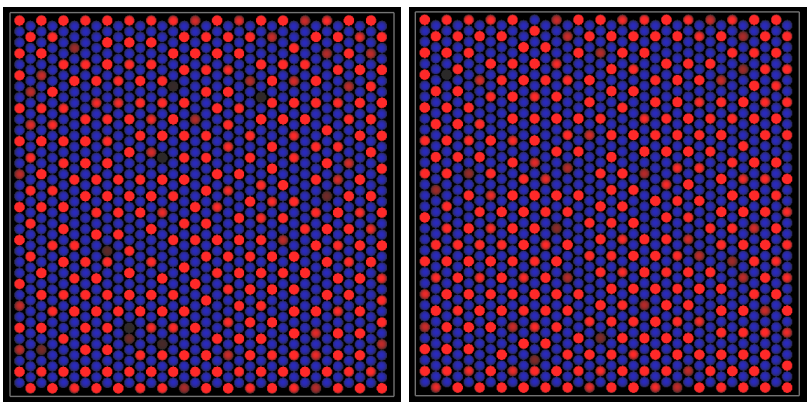

(c) Time=30000τ. Spacing = 2.20. CV = 0.18

(d) Time=60000τ. Spacing = 2.16. CV = 0.17

Figure 11.11: Noise is used to enable the refinement of the pattern. Cells with Delta levels over 25 A.U. are shown in bright red. The dark red cells represent those with Delta levels 0 to 25 A.U., undergoing a transition. Regions of stable perfectly packed Delta cells emerge separated by refining boundaries in which cells continue to switch states. The number of cells switching states reduces over time. The refinement of the pattern is reflected in the reduction in the average spacing between Delta expressing cells and their six nearest neighbours and the coefficient of variation (CV) - a value which reflects the global order in the system - it represents the average ratio of the standard deviation in the spacing and the average spacing. Simulation parameters: $\mu = \rho = 0.02\tau^{-1}, R_N = R_D = 1A.U.\tau^{-1}, a = 50^k A.U.^k, b = 1A.U.^{-h}, k = h = 6, \alpha = 1, e = 0.1$. Start conditions: $N = D = 10 + / - 0.1A.U.$.

Just as critical as the hill function parameters in this model is the noise term, e. This term is implemented in the simulation as a random gaussian fluctuation at each time step, with a standard deviation described as a percentage of the levels of Notch and Delta in each cell. This is a somewhat artificial representation of noise - which is more likely to fluctuate in each cell with some temporal dependency - but it is sufficient to demonstrate the key behaviours of this model. Here a noise term of 10% was used. At higher values, the noise term dominates the system and the patterns are never observed to stabilise. Likewise, for lower levels of noise the model showed no refinement (see Figure 11.12). These simulations demonstrate that using noise in conjunction with the right hill function parameters can lead to pattern refinement. However, this model was also shown to be highly sensitive to parameter changes. In particular, a key requirement was that a cell must show a very specific level of sensitivity to Delta signalling. A similar model in which some kind of transient signal were imposed on the cells might provide a more robust method for pattern optimisation. This model would require further investigation that has not been carried out for this thesis. However, the analysis presented here does provide a case for the adoption of transient signalling in biological patterning systems. Future experimental work could be directed towards searching for this phenomenon.

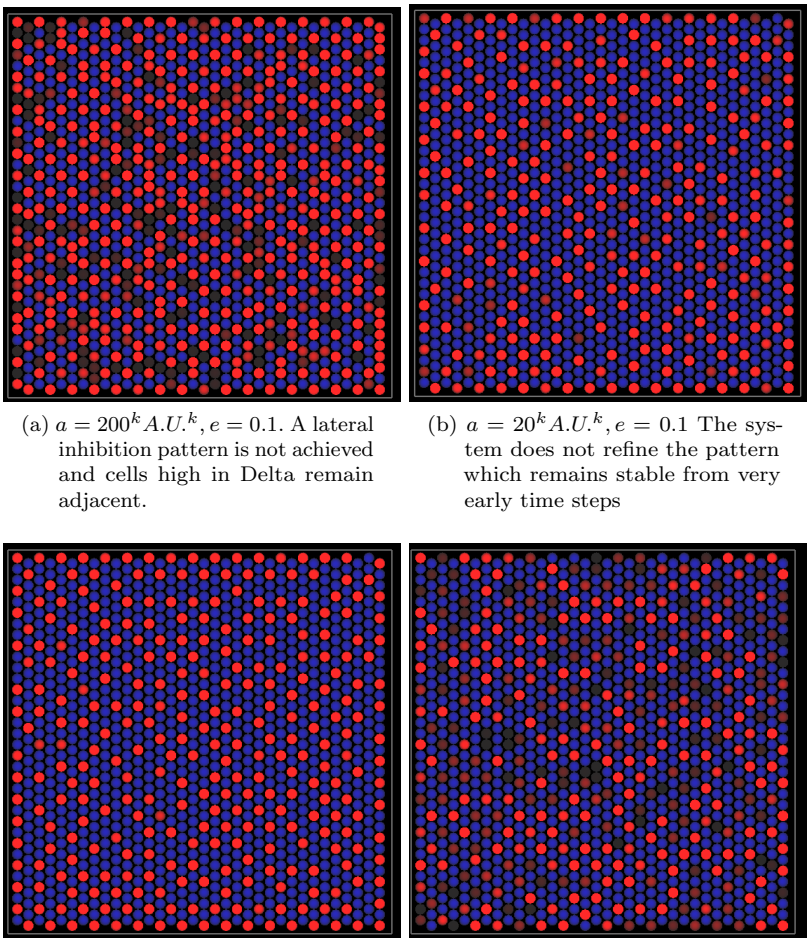

(a) $a = 200^k A.U.^k, e = 0.1$. A lateral inhibition pattern is not achieved and cells high in Delta remain adjacent.

(b) $a = 20^k A.U.^k, e = 0.1$ The system does not refine the pattern which remains stable from very early time steps

(c) $a = 50^k A.U.^k, e = 0.05$ With a 5% noise term at each time step there is no pattern refinement.

(d) $a = 50^k A.U.^k, e = 0.2$ With a 20% noise term at each time step the pattern is unstable.

Figure 11.12: The system is sensitive to parameters when noise is used to optimise packing. A set of simulation screen shots at time step 60000. Using noise as a refinement tool the system is highly sensitive to both cells responsiveness to Delta (as represented by the hill function term, a) and the value of the noise term implemented at each time step. Simulation parameters: $\mu = \rho = 0.02\tau^{-1}, R_N = R_D = 1A.U.\tau^{-1}, b = 1A.U.^{-h}, k = h = 6, \alpha = 1$. Start conditions: $N = D = 10 + / - 0.1A.U.$.

11.5 Summary

This chapter has demonstrated how intermittent signalling can lead to an optimisation of the packing in the Delta-Notch patterning system. This can be achieved with filopodial signalling or using some kind of other transient signal. In chapter 8 it was shown that when a very low hill function coefficient is applied in the Delta-Notch model system, this generates a more regularly packed, optimised pattern than the more non-linear case with higher coefficients. This arrises because at low hill function coefficients all the cells in the field 'compete' for longer to become high in Delta whereas at higher values small random fluctuations are more rapidly amplified by the system. In this chapter optimised patterning has been shown to be achievable even in these more non-linear systems. These potentially have some advantage over the more linear case as they cause a more sharp delineation between neighbouring cells. It is therefore likely that some kind of non-linear process is utilised in the lateral inhibition system (for example cis-inhibition may be included). The filopodia in particular provide a simple mechanism by which, even with a very non-linear patterning system, a pattern can gradually update so that the spacing becomes more regular and the the density increases, whilst maintaining the same minimum spacing.

In [Eglen and Willshaw: 2002] a model is used to investigate Delta-Notch mediated patterning in ganglion cells. Here, they recognise that in this system the patterning is more regular (by a similar measure of pattern order as used here) than the standard model. In order to explain the discrepancy they introduce programmed cell death to the model based on cell area during the signalling phase. This analysis provides an alternative mechanism by which this kind of data could potentially be explained.

The optimisation process in the lateral inhibition system was shown to closely relate to a cellular automaton model. Similar processes are known to be common in physics where variations of the Potts model have applied [Graner and Glazier: 1992]. The general principle derived from such models is that an input of noise (or energy) can be used to disrupt local regions of uniformity to enable the system to reach a global optimum [Cipra: 1987]. Here, the external noise is the intermittent signal which leads to the regular packing of the lateral inhibition pattern. No direct parallel model has been identified in the physics literature. The switching of cell states in a lateral inhibition patterning process is maybe unique to biology although there are obvious similarities with, for example, crystallisation models. In all these types of model it can be shown that there is a balance in the amount of noise that can be imposed to produce order rather than disorder. Cellular automata can be used an a investigative tool to analyse this process.

It was shown in the filopodial system that it was very hard to generate perfectly packed patterns. There seems to be a limitation in the optimisation process due the fact that too much noise disrupts the entire pattern. Future work could adapt the cellular automata identified in chapter 10 to more efficiently analyse how filopodial signalling or transient signals can lead to pattern optimisation in this system. By adding probability terms to describe the likelihood of signalling between neighbouring cells both types of model could be abstractly reproduced by the cellular automata. This could be used to more efficiently determine the limitations of the optimisation process.

Chapter 12

Spots and stripes

The following chapter demonstrates how the Delta-Notch signalling mediated by filopodia may provide a novel mechanism for the generation of spots of stripes observed in a diverse range of biological organisms.

12.1 The condition for spots and stripes

In chapter 10 it was revealed how asynchronous cellular automata can produce patterns of stripes and large clusters of black cells. In some cases these patterns of stripes were also shown to refine over time towards a kind of optimised stable or near stable state consisting of aligned stripes. The cellular automata rules that give rise to striping (or clustering) had cell update conditions in which black cells were permitted in neighbourhoods containing more than one black cell. The question asked in this chapter is whether the Delta-Notch signalling system can produce these kinds of patterns.

As has been previously demonstrated, Delta-Notch signalling typically gives rise to a lateral inhibition pattern in which any cell receiving a Delta signal from a neighbour will eventually be inhibited from doing likewise. To generate patterns of Delta cells in higher numbers, equivalent to the aforementioned cellular automata, lateral inhibition would have to occur among larger neighbourhoods of Delta expressing cells. This can be achieved in the model system by sufficiently reducing the sensitivity of each cell to neighbouring Delta levels. This chapter explores how the model behaves within these parameter regimes.

The maximum steady-state concentration of Delta expressing cells in the model system is determined by the production and decay rates of Delta. For all the examples that will be shown in this chapter the decay rates used will be at $\mu = \rho = 0.02\tau^{-1}$ with associated production rates $R_{Notch} = R_{Delta} = 1A.U.\tau^{-1}$. Hence, the steady state level of Delta in cells expressing Delta is given by $D = 1/0.02 = 50A.U.$. The hill function parameter, a, in conjunction with the coefficient, k, sets a minimum level at which Notch production and subsequent Delta inhibition is triggered among contacting cells. With a highly non-linear system, where k is set high, the value of a can be tuned so that inhibition only occurs at a particular threshold number of neighbouring Delta-expressing cells. In the following examples fixing $a = (50 \times 6)^k A.U.^k$ will mean that approximately 6 Delta expressing cells are required in the local neighbourhood of a single cell before the Notch activation occurs and hence, Delta inhibition. Unless otherwise stated, these model parameters will be used throughout this chapter. The data shown is not intended to represent a comprehensive analysis of the system. Instead it is used to demonstrate some of the more interesting patterning behaviours that were observed which may provided an interesting foundation for future research.

12.2 Striping with apical signalling

Figure 12.1 shows the results of a set of simulations in the 2D hexagonal array with just apical signalling and different values of the parameter, a. It is clear from these simulations that as the value of a increases, equivalent to a decrease in the sensitivity to the Delta signal, Delta expressing cells are able to aggregate in stripes and clusters and eventually at very high values of a all cells can express Delta with no inhibition occurring. Note that similar results were obtained when these simulations were repeated under different parameter regimes providing there was corresponding relationship between the Delta sensitivity and the maximum Delta level as well as sufficiently high values for parameters, k and h.

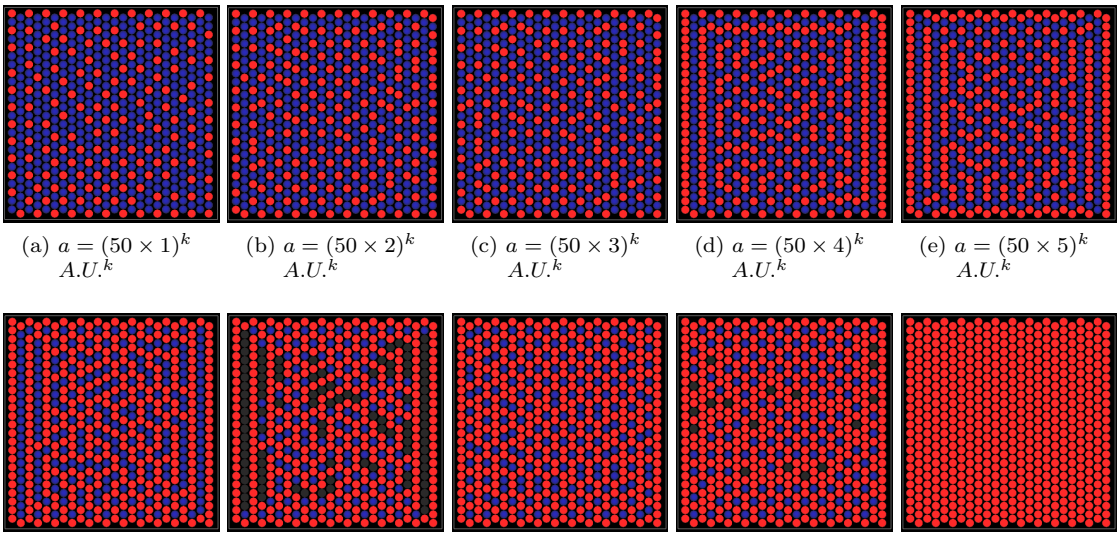

(a) $a = (50 \times 1)^k$ $A.U.^k$ (b) $a = (50 \times 2)^k$ $A.U.^k$ (c) $a = (50 \times 3)^k$ $A.U.^k$ (d) $a = (50 \times 4)^k$ $A.U.^k$ (e) $a = (50 \times 5)^k$ $A.U.^k$

(f) $a = (50 \times 6)^k$ $A.U.^k$ (g) $a = (50 \times 7)^k$ $A.U.^k$ (h) $a = (50 \times 8)^k$ $A.U.^k$ (i) $a = (50 \times 10)^k$ $A.U.^k$ (j) $a = (50 \times 12)^k$ $A.U.^k$

Figure 12.1: With apical signalling there is a transition from single cell patterns of Delta expression to something resembling spots and stripes. Simulation parameters:, $\mu = \rho = 0.02\tau^{-1}, R_N = R_D = 1A.U.\tau^{-1}, b = 1A.U.^{-h}, k = h = 6, \alpha = 1, e = 0.01$. Start conditions: $N = D = 10 + / - 0.1A.U.$. Array size = 24x24.

These simulations generate a set of patterns that are already reminiscent of spots and stripes observed in epithelial patterns [Meinhardt: 2007]. However a striking difference is that the thickness and separation between stripes is restricted to one cell.

12.3 Striping with signalling at filopodial ranges

In Figure 12.2 the signalling is extended to two cell diameters between all cells (equivalent to 100% filopodial connection at this range). Now there is a much more obvious transition from spots through to stripes as the parameter a increases and the patterns are much more reminiscent of those associated with reaction-diffusion systems (see Figure 3.9). Note that the examples shown are highly typical of simulations with a similar relationship between the signalling parameters and illustrate a repeatable model behaviour.

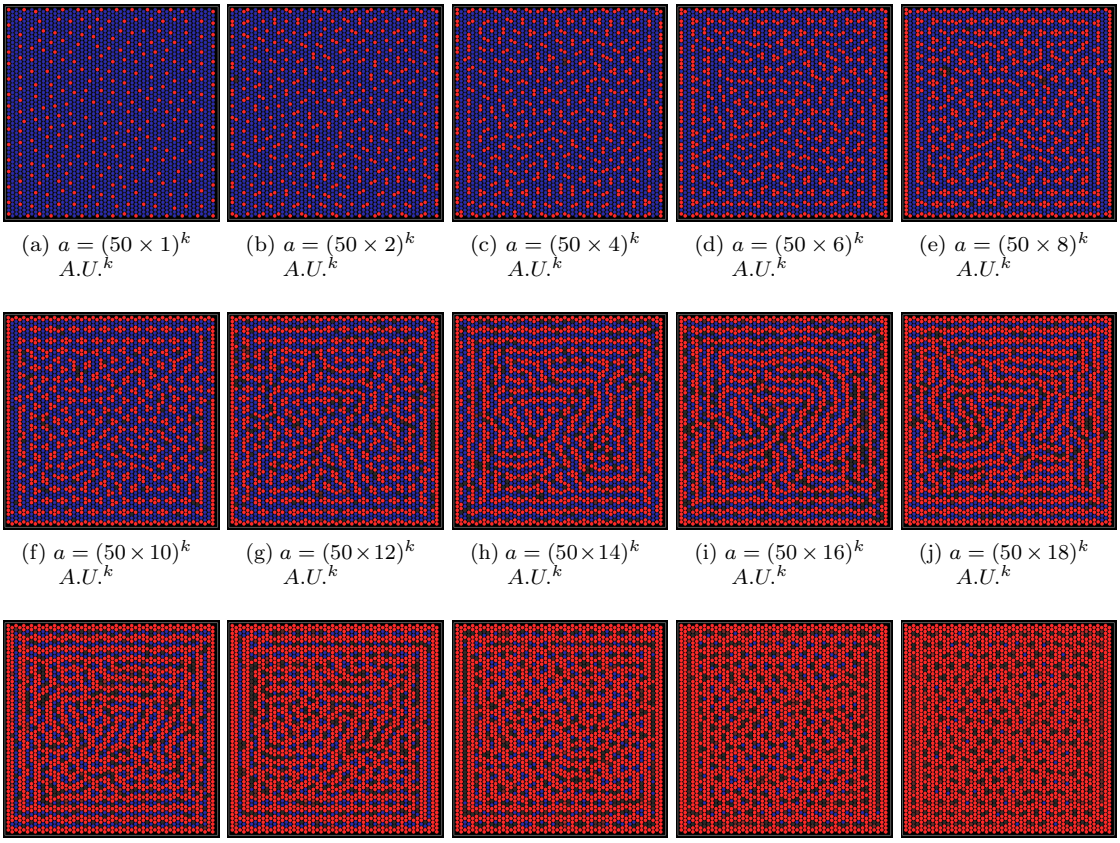

(a) $a = (50 \times 1)^k$ $A.U.^k$ (b) $a = (50 \times 2)^k$ $A.U.^k$ (c) $a = (50 \times 4)^k$ $A.U.^k$ (d) $a = (50 \times 6)^k$ $A.U.^k$ (e) $a = (50 \times 8)^k$ $A.U.^k$

(f) $a = (50 \times 10)^k$ $A.U.^k$ (g) $a = (50 \times 12)^k$ $A.U.^k$ (h) $a = (50 \times 14)^k$ $A.U.^k$ (i) $a = (50 \times 16)^k$ $A.U.^k$ (j) $a = (50 \times 18)^k$ $A.U.^k$

(k) $a = (50 \times 20)^k$ $A.U.^k$ (l) $a = (50 \times 22)^k$ $A.U.^k$ (m) $a = (50 \times 24)^k$ $A.U.^k$ (n) $a = (50 \times 26)^k$ $A.U.^k$ (o) $a = (50 \times 28)^k$ $A.U.^k$

Figure 12.2: Striping with signalling between all cells at a range of 2 cell diameters. The pattern looks much more like the typical examples generated by activator-inhibitor systems. As the sensitivity to Delta decreases the patterns move from spots through to stripes and then to an inverse pattern of spots. Simulation parameters:, $\mu = \rho = 0.02\tau^{-1}, R_N = R_D = 1A.U.\tau^{-1}, b = 1A.U.^{-h}, k = h = 6, \alpha = 1, e = 0.01$. Start conditions: $N = D = 10 + / - 0.1A.U.$. Array size = 50x50.

12.3.1 A highly non-linear system is required for striping

Although it is relatively easy to achieve patterns of stripes with this model by altering Delta sensitivity, there is also a key requirement for a highly non-linear response to the Delta signal. This is controlled in the model by altering parameter, k. In the previous examples a high value was used (k=6). With a more linear system (see Figure 12.3 where k=2) stripes cannot be sustained. This is because with a more linear system there is a less sharp threshold at which the hill function is activated. Hence, even with a very large parameter, a, relatively low levels of Delta will still activate some small production of Notch.

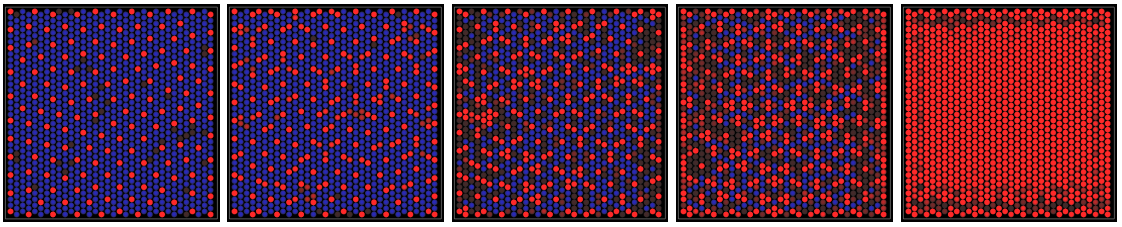

(a) $a = (50 \times 1)^k$ $A.U.^k$ (b) $a = (50 \times 2)^k$ $A.U.^k$ (c) $a = (50 \times 4)^k$ $A.U.^k$ (d) $a = (50 \times 6)^k$ $A.U.^k$ (e) $a = (50 \times 8)^k$ $A.U.^k$

Figure 12.3: Stripes require a non-linear system. With a low hill function coefficient, k, the patterns of stripes are no longer achieved. Simulation parameters:, $\mu = \rho = 0.02\tau^{-1}, R_N = R_D = 1A.U.\tau^{-1}, b = 1A.U.^{-h}, k = h = 2, \alpha = 1, e = 0.01$. Start conditions: $N = D = 10 + / - 0.1A.U.$. Signal range = 2. Array size = 50x50.

12.3.2 Diverse patterns are achievable under different model conditions

Using different shaped arrays, signal ranges and model parameters a versatile range of patterns can be generated by the model. Figure 12.4 illustrates a few examples. The arrangement of the patterns is most sensitive to the shape of the array nearest to the boundaries. Closer to the central field they tend towards a more stochastic arrangement of spots and stripes. The separation of stripes is set by the range of the signal. For any given signalling range there is a small variation in the achievable stripe thickness which increases as the Delta sensitivity decreases.

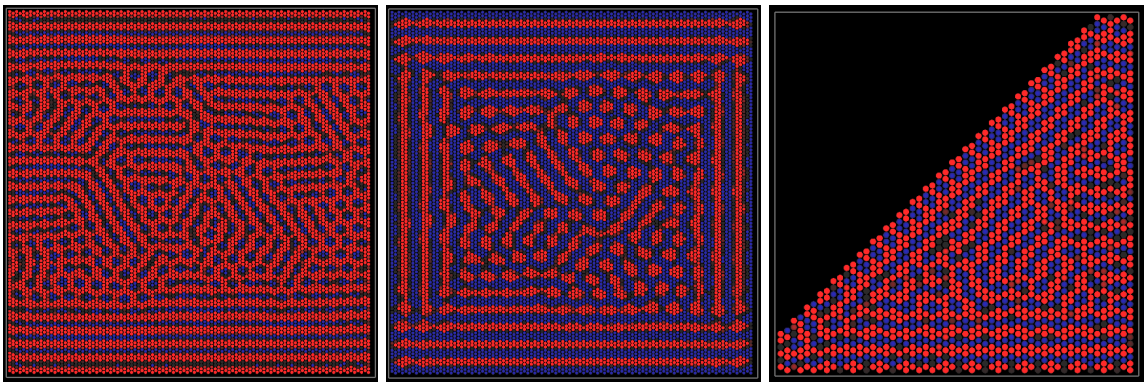

(a) Signal range - 3 cell diameters, $a = (50 \times 40)^k$ $A.U.^k$ (b) Signal range - 4 cell diameters, $a = (50 \times 40)^k$ $A.U.^k$ (c) Signal range - 3 cell diameters, $a = (50 \times 30)^k$ $A.U.^k$

Figure 12.4: A range of spots and stripes patterns can be achieved at different ranges and hill function parameters. Note in these examples the perimeter value of Delta is set higher to demonstrate that patterning need not be fixed to the edge of the array. Also a more irregular shaped array is used to demonstrate that patterns tend to form in a way that is guided by the array boundaries. The black space indicates a vacuum with no Delta signal. Simulation parameters:, $\mu = \rho = 0.02\tau^{-1}, R_N = R_D = 1A.U.\tau^{-1}, b = 1A.U.^{-h}, k = h = 6, \alpha = 1, e = 0.01$. Start conditions: $N = D = 10 + / - 0.1A.U.$. In all cases there is 100% connectivity at each signalling range.

12.4 Optimised patterns of stripes using filopodial signalling

In chapters 10 it was shown how particular cellular automaton rules form patterns of stripes that are able to align. This process works on the principle that a cell can enter a black state with a certain intermediate number of neighbours that would not be possible with a higher number of neighbours. It was shown that in the previous chapter that patterns of spots were able to

optimise by intermittent filopodial signalling with the right parameterisation. A similar process of optimisation can be observed in patterns of stripes. Figures 12.5 and 12.6 demonstrate two cases in which the patterns optimise towards a state of aligned striping using different combinations of filopodial lifetimes and densities. A more thorough analysis would likely demonstrate that for different signalling parameters, as the filopodia density and dynamics are altered there will be a transition from stable patterns of stripes through unstable patterns with an intermediate regime demonstrating pattern refinement.

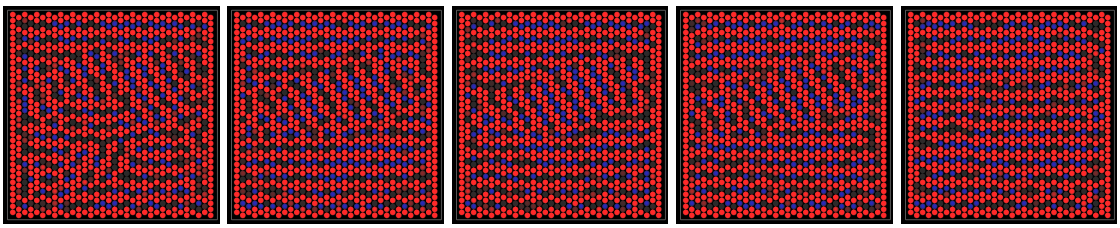

(a) 5000τ (b) 10000τ (c) 20000τ (d) 30000τ (e) 40000τ

Figure 12.5: Stripes can dynamically optimise. With a fairly sparse network of dynamic filopodia the pattern optimises towards and alignment of stripes. Filopodia are simulated with lifetime of 100τ and coverage of an average of 6 out of 12 cells in the neighbourhood at range of 2 cell diameters. Simulations were repeated 3 times to confirm that the alignment of stripes would occur within the same time period. In all simulations the pattern of aligned stripes was found to be stable for subsequent time steps. Simulation parameters:, $\mu = \rho = 0.02\tau^{-1}, R_N = R_D = 1A.U.\tau^{-1}, a = (50{\times}16)^k A.U.^k, b = 1A.U.^{-h}, k = h = 6, \alpha = 1, e = 0.01$. Start conditions: $N = D = 10+/-0.1A.U.$. Filopodial algorithm parameters (from Figure 2.4): F-birthrate=F-deathrate=0.01. Array size = 30x30.

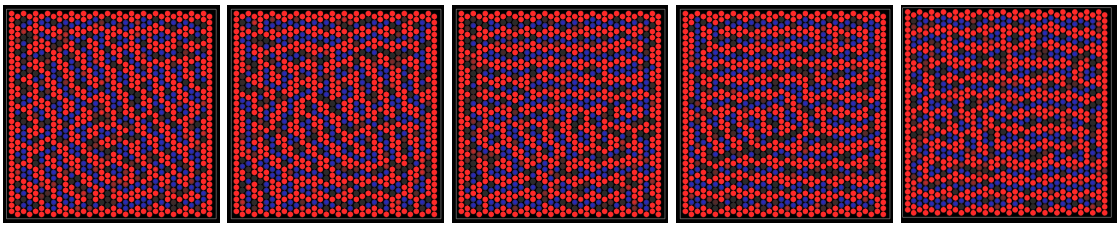

(a) 3000τ (b) 10000τ (c) 20000τ (d) 30000τ (e) 50000τ

Figure 12.6: With a more dense network of filopodia with slower dynamics optimisation still occurs - although the stripes are slightly less stable in this example. Filopodia are simulated with lifetime of 1000 τ and coverage of an average of 10 out of 12 cells in the neighbourhood at range of 2 cell diameters. Simulations were repeated 3 times to confirm that a similar degree of alignment would occur within the same time period. The same degree of alignment would remain in place for all subsequent time steps. Simulation parameters:, $\mu = \rho = 0.02\tau^{-1}, R_N = R_D = 1A.U.\tau^{-1}, a = (50 \times 16)^k A.U.^k, b = 1A.U.^{-h}, k = h = 6, \alpha = 1, e = 0.01$. Start conditions: $N = D = 10 + / - 0.1A.U.$. Filopodial algorithm parameters (from Figure 2.4): F-birthrate=0.005, F-deathrate=0.001. Array size = 30x30.

12.4.1 Stripes align due to interactions with the boundaries

So far, in the examples shown the patterns have all aligned to the sides of the square array (in fact they have aligned with a slight horizontal bias due to the way the hexagonal packing is constructed). There is clearly an interaction with the boundaries that fixed the global patterning. In Figure 12.7 it is shown how with a different shaped patterning array the stripes align in a different manner.

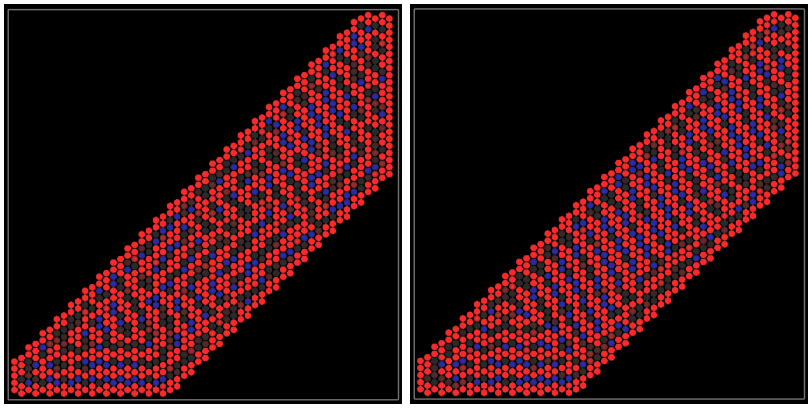

(a) Time= 3000τ (b) Time = 30000τ

Figure 12.7: Striping in irregular arrays. The black region represent a vacuum with zero Delta signal. In this irregular array the pattern refines with an orientation set by the boundary shape. Filopodia are simulated with lifetime of 100τ and coverage of an average of 6 out of 12 cells in the neighbourhood at range of 2 cell diameters. Simulations were carried out 3 times - in each case the alignment was in the same direction and remained stable at later time steps. Simulation parameters:, $\mu = \rho = 0.02\tau^{-1}, R_N = R_D = 1A.U.\tau^{-1}, a = (50 \times 16)^k A.U.^k, b = 1A.U.^{-h}, k = h = 6, \alpha = 1, e = 0.01$. Start conditions: $N = D = 10 + / - 0.1A.U.$. Filopodial algorithm parameters (from Figure 2.4): F-birthrate=0.01, F-deathrate=0.01.

When a very large field is used the boundary effect becomes less significant (see Figure 12.8). In a large field stripes try to align locally in different directions but it becomes harder to establish a dominant orientation.

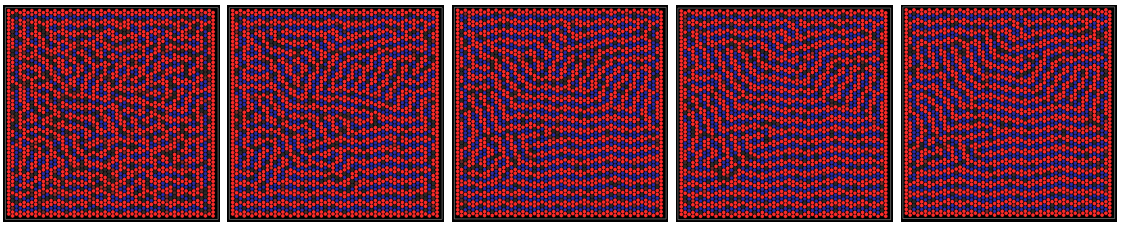

(a) 500τ (b) 2000τ (c) 10000τ (d) 20000τ (e) 40000τ

Figure 12.8: Striping in a larger field. With a large field the stripes are less likely to align in the same direction. A partial alignment of the pattern is possible within 40000 time steps. Filopodia are simulated with lifetimes of 1000 τ and coverage of an average of 10 out of 12 cells in the neighbourhood at range of 2 cell diameters. Simulation parameters:, $\mu = \rho = 0.02\tau^{-1}, R_N = R_D = 1A.U.\tau^{-1}, a = (50 \times 20)^k A.U.^k, b = 1A.U.^{-h}, k = h = 6, \alpha = 1, e = 0.01$. Start conditions: $N = D = 10 + / - 0.1A.U.$. Filopodial algorithm parameters (from Figure 2.4): F-birthrate=0.005, F-deathrate=0.001. Array size=50x50.

12.5 A re-examination of cis-inhibition

In chapter 8 an adapted model of Delta-Notch signalling (equation 8.2) was introduced that included the direct interaction of Notch and Delta proteins in the cytoplasm; a phenomenon referred to as cis-inhibition. It was found using this formulation that, with no filopodial signalling, the model generally produced very similar patterns to the standard trans-inhibition model that has been predominantly used.

To check whether the new phenomena that have been identified relating to basal signalling would still emerge under cis-inhibition, protrusion mediated signalling was added to the model. It was found that with filopodial signalling the cis-inhibition model differed slightly from the standard

trans-inhibition model. When filopodia were implemented with very fast lifetimes relative to the model decay rate very disordered patterns were obtained; in contrast to the standard model where fast filopodia generated a stable zone of inhibition around a cell and thus generated a rapidly emerging stable pattern (Figure 12.9).

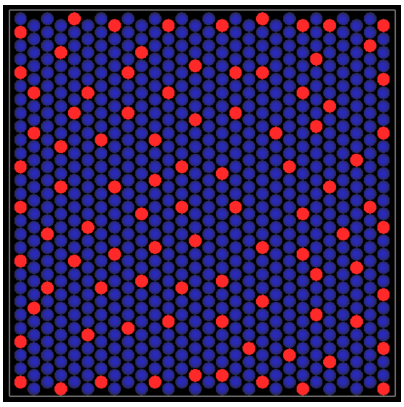

Figure 12.9: Cis-inhibiton produces a disordered pattern with very fast filopodia. Here, some Delta expressing cells are located within the filopodial signalling range. Filopodia lifetime = 10τ. Simulation parameters:, $\mu = \rho = 0.02\tau^{-1}, R_N = R_D = 1A.U.\tau^{-1}, a = 10A.U.^k, b = 1A.U.^{-h}, k = h = 3, \alpha = 1, e = 0.01$. Start conditions: $N = D = 10 + / - 0.1A.U.$. Filopodial algorithm parameters (from Figure 2.4): F-birthrate=0.1, F-deathrate=0.1. Array size = 30x30.

When intermediate filopodia dynamics were used in the cis-inhibtion model, optimising patterns were observed with similar properties as for the trans-inhibition model (Figure 12.10). With this parameter set the patterning time is of the order of 5000-20000τ. Hence a filopodia lifetime of the order of 100τ closely approximates to the real data (filopodial lifetime $\approx$ 550 seconds, patterning time $\approx 8h$). This may therefore imply that there is a minimum lifetime of filopodia for which the model is viable with cis-inhibition which is in close agreement with the observed filopodial dynamics.

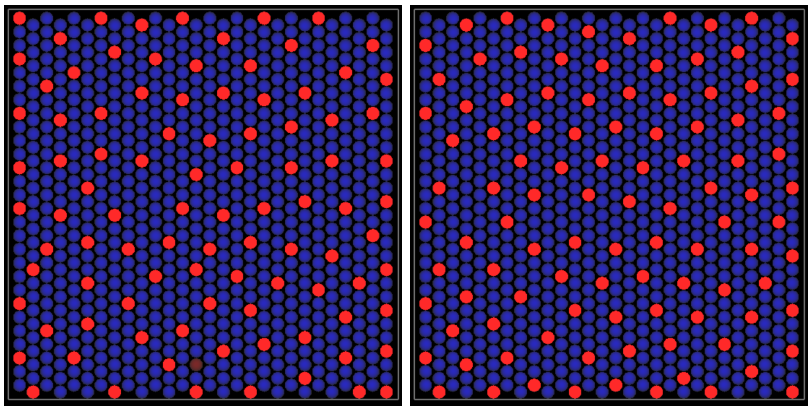

(a) Time = 4000τ (b) Optimised pattern at time = 20000τ

Figure 12.10: With intermediate filopodia cis-inhibition produces optimising patterns similar to the standard model. Filopodia lifetime = 100τ. Simulation parameters:, $\mu = \rho = 0.02\tau^{-1}, R_N = R_D = 1A.U.\tau^{-1}, a = 10A.U.^k, b = 1A.U.^{-h}, k = h = 3, \alpha = 1, e = 0.01$. Start conditions: $N = D = 10 + / - 0.1A.U.$. Filopodial algorithm parameters (from Figure 2.4): F-birthrate=0.01, F-deathrate=0.01. Array size = 30x30.

Patterns of spots and stripes were also achievable in this model; the non-linearity provided by the cis-inhibition meant that for a wide range of parameter space stripes were easily achieved. Similarly

optimisation towards aligned stripes was obtainable, although it was harder to parameterise the model to achieve this and the striped patterns never quite aligned as well with this model. (Figure 12.11).

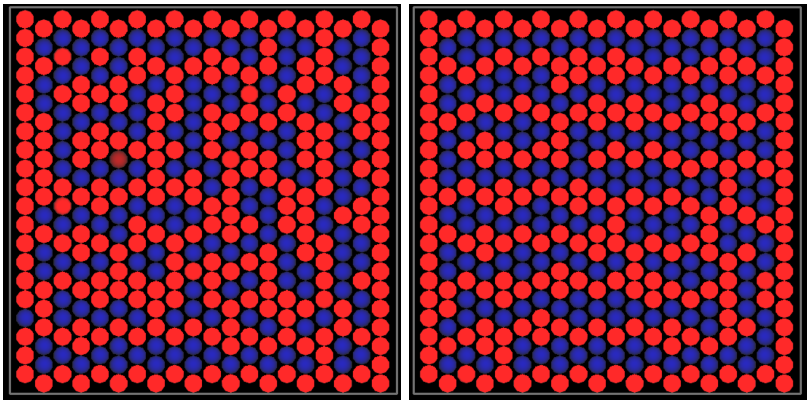

(a) Time = 30000τ (b) Time = 300000τ

Figure 12.11: Optimised patterns of stripes can also be generated with cis-inhibition - though they are harder to achieve than in the standard model. The result shown is typical of 3 simulations performed with this parameter set in which there were consistently vertical 'links' being formed and broken between the horizontal stripes. Simulation parameters:, $\mu = \rho = 0.02\tau^{-1}, R_N = R_D = 1A.U.\tau^{-1}, a = 200A.U.^{k}, b = 1A.U.^{-h}, k = h = 6, \alpha = 1, e = 0.01$. Start conditions: $N = D = 10 + / - 0.1A.U.$. Filopodial algorithm parameters (from Figure 2.4): F-birthrate=0.005, F-deathrate=0.005. Array size = 30x30.

Although the precise dynamics and parameterisation of the models differed under cis-inhibition, in general these simulations demonstrated that the presence of cis-inhibition does not fundamentally preclude any of the key findings that have been identified in this thesis.

12.6 Summary

This chapter has demonstrated that a model of lateral inhibition using cell-to-cell contact mediated by filopodial signalling can generate patterns of spots and stripes. The key requirement for this was that a cell required an inhibitory signal from more than one other cell. With longer range basal signalling the patterns became superficially more like those associated with epithelial patterns (for example zebra stripes); however even with just apical signalling stripes of one cell width were obtainable. The patterns could be gradually changed by altering just one parameter in the model system (the Delta signal sensitivity) and therefore potentially represent a highly evolvable system.

These types of pattern are typically associated with reaction-diffusion models which were introduced in chapters 3 and 6. It was stated that for stable patterns to be generated by this type of system a short range diffusing activator and long range inhibitor must be present. It has previously been suggested that lateral-inhibition by Delta-Notch signalling falls into this category of model and indeed that evidence of the diffusion of Delta proteins [Qi et al.: 1999], might constitute evidence of a possible mechanism for a long range inhibitory signal [Meinhardt and Gierer: 2000]. However, in this model system, neither Notch nor Delta has an obvious role in the context of activator or inhibitor. Neither self-promote their own production and the system works on the fundamental premise that a cell does not inhibit its own expression of Delta, but only effects neighbouring cells. Hence, the Delta-Notch juxtacrine system is fundamentally distinct from a reaction-diffusion system. Only through the membrane bound signalling is this system capable of lateral inhibition and pattern generation. This negates the need for a finely tuned balance between

local self-enhancement and long range inhibition. However there is also clearly a similarity in that in both types of model a self-organised pattern emerges as a result of lateral inhibition from a region producing high amounts of an inhibitory chemical. So it may be that many of the well studied properties of the reaction-diffusion system are reproducible in the Delta-Notch model.

The generation of spots and stripes by cell-to-cell signalling of this type has not previously been specifically identified as a possible mechanism. In particular the alignment of stripes by filopodial signalling is a novel mechanism by which robust patterns arrangements could be specified. Whilst the model is based on a known lateral inhibition system using Notch and Delta, It may be that proteins other than Notch and its ligands could be implicated in a similar process. Future work will hopefully identify if this model is representative of a real system in nature. For examples in [Kondo and Asai: 1995] it is suggested that reaction-diffusion models can be used to explain the dynamics by which a set of stripes become more aligned over time in angelfish. Similarly in [Asai et al.: 1999] the same model is used to explain how a single gene might cause a switch from stripes to spots. In both cases the model suggested here might provide an alternative unexplored mechanism by which such patterns and transitions might be explained without evoking the need for, as yet unidentified, morphogens.

Chapter 13

Discussion

This section provides of summary of the main findings of the thesis and discusses how these results fit into a wider scientific context.

13.1 Summary of key results

The thesis was divided into three distinct sections each of which addressed the fundamental question of how patterning may arise through cell-to-cell communication.

Section I

The first section described an investigation into a system in which cellular automata rules were implemented sequentially so that target patterns could be evolved. The model demonstrated that by changing the rules and their associated transition times complex target patterns could be achieved that were unattainable by single rules. When the system was tested for robustness to perturbations this exposed how certain rules were less robust. Individual rules with different emergent properties had very different responses to perturbations that were closely related to their dynamical properties. Rules that generated patterns with complex divergent patterns were more likely to amplify the effect of a perturbation. Rules that generated more simple regular, repeating patterns did not amplify perturbations or were able to self-repair.

Section II

Section two provided an analysis of microchaete patterning by Delta-Notch signalling. It was shown that the pattern spacing was not sufficiently described by a standard model of cell-to-cell signalling. A model demonstrated the viability of long range signalling through contact mediated by a dynamic network of filopodia. In vivo experiments confirmed that when filopodia lengths were effected by mutations the pattern spacing reduced in accordance with the model.

Section III

In the final section the behaviour of simple asynchronous cellular automata was analysed. A set of rules were identified whose emergent behaviour was similar to a lateral inhibition patterning process. Among these a particular subset were found to produce patterns that optimised their spacing over the course of their development. A re-examination of the Delta-Notch signalling model revealed that a similar type of optimisation could take place with dynamic filopodial signalling or with a transient Delta signal. Under certain parameter regimes the patterns become more densely packed over time whilst maintaining a minimum zone of inhibition around each Delta cell. A probabilistic

analysis of the system helped to further qualify how intermittent signalling lead to a shifting and subsequent optimisation of the packing.

The asynchronous cellular automata also exposed how with adapted rules, conditional upon a greater number of nearest neighbour cells, stripes can be formed and optimised under certain conditions. It was demonstrated that the same principle could be applied in the Delta-Notch model where stripes were reproduced using dynamic filopodial signalling. This was proposed as a novel alternative to the reaction-diffusion mechanism that is commonly used to model the patterning of spots and stripes.

13.2 Analysis of the results

The three approaches all focussed on the same question of patterning via cell-to-cell communication and attempted to explore the limitations of this type of process. Different computational techniques were adopted to approach the problem in different ways. These comprised an entirely abstract cellular automata based model, a more applied simulation of cellular signalling with dynamic filopodia, and a combined approach in which simple asynchronous cellular automata were used to predict further fundamental behaviours under certain parameter regimes in the applied model.

13.2.1 The properties of cellular automata

The thesis sought to understand the subject of self-organisation. Cellular automata rule based models were used in order to capture a wide range of the fundamental properties of self-organising processes. One of the most striking differences that was exposed in this thesis was between synchronous and asynchronous cellular automata and the emergent patterns that they generate. In section one, complex, but highly ordered, developmental patterns of nested triangles characterised many of the cellular automata rules; these were not apparent at all in the the asynchronous case. The more complex nested types of patterns were a direct result of every cell updating at the same time. This allowed the pattern to diverge in time, in a regular, predictable way. The same rules in the asynchronous 1D system would typically generate unpredictable, seemingly random patterning, with no apparent repeatability or ordered spacing. In the asynchronous system the only apparent ordered patterning was of a type similar to lateral inhibition patterns, where cells would alternate black and white in a fairly regular way, with the pattern spacing limited by the extent of the intercellular signal.

In biology the demand for robust patterning is crucial; there must be some kind of predictability in the emergent patterns generated during a particular process. The cellular automata rules that were used here represent the complete set of possible rules that can be constructed in a two state 1D system with nearest neighbour interactions. If the cellular automata are regarded as representing a single of line of cells switching their state in time then it is easy to argue that the asynchronous case is much more realistic; it is hard to conceive of any system in which a set of component parts switch state at the identical moment in time, and this is particularly true of a biological system of cells using chemical signalling. Therefore one could conclude that the asynchronous cellular automata provided a better model for determining the limitations of patterning when restricted to cell-to-cell signalling. However, this does not mean that many of the apparent complex emergent phenomena represented in the synchronous rules have no basis in reality. It may be that a single line of cells could make decisions and update their states over discrete time steps. This would not necessarily imply total synchronicity but is more of a delay based system, where cell based decisions are separated in time from their actions. An alternative model that is maybe more realistic is if

the synchronous cellular automata are regarded as representing growth in 2D. Here, for example a new cell might attach itself beneath an existing line of cells dependent on the local state of cells in the extant line. In this situation the system is still undergoing growth in such a way that is purely dependent on nearest neighbour communication. As long as an entire line of cells is put in place before a subsequent line then the system will behave in the same way as the synchronous CA. There is no longer the conceptual problem presented by a continuous signalling based system. So, for example, developmental branching in lungs or blood vessels may be represented by a 1D nearest neighbour rule being propagated over a 2D (or 3D) system with some degree of synchrony.

13.2.2 Patterning transitions and evolvability

It must be stressed that so far the differences highlighted here between the synchronous and asynchronous rules are associated with individual patterning rules. The limitations are specific to a single rule operating over time. In the synchronous cellular automata system the individual rules were specifically allowed to change over time according to the instructions in an evolved genome. This was intended to simulate real development where one patterning phase builds upon another. One particular problem that was highlighted with this experimental system was establishing a physical basis for the rule transitions. These were made to occur at specific times according to the genome. As a model of a real biological system, this would suggest the existence of some kind of genetic clock that triggered different systems on and off at very specific times. However, it is more likely that in a real biological patterning system there must be some kind of 'completion' of each patterning stage that would be a prerequisite for entering a subsequent stage. This may be simply because a patterning system enters a homeostatic phase in which no further patterning occurs or because some kind of feedback signal is activated by a particular checkpoint. In the case of the Delta-Notch systems that were investigated in sections two and three, the lateral inhibition patterning process achieves what could be described as homeostatic stability after a certain period of time - which varied according to the system parameters and whether or not the pattern went through an optimisation phase. The 'completion' of these patterns could be described as the point at which the field had been filled with Delta expressing cells at the minimum spacing defined by the signalling range.

One of the fundamental features of this thesis is the fact that simple rules can generate characteristic emergent patterns. Therefore it follows that biological development may comprise discrete stages of patterning which are reliant on specific rules and which, therefore, have limited evolvability. For example, in the case of a lateral inhibition pattern it has been shown that (with apical signalling) it is impossible to significantly alter the emergent pattern spacing. This therefore represents a fixed patterning rule. However, there may be a more continuously evolvable aspect to this process via the length (or dynamics) of filopodial protrusions. Establishing the evolvable and non-evolvable mechanisms underlying patterning processes may be a useful way to better understand them.

13.2.3 Determining robustness

Robustness to perturbation was used a method to compare the different evolved developmental programs in section one of this thesis. Here, it was shown that certain rules were more sensitive to perturbations. When these rules were contained in the developmental program this had a significant effect on the robustness of the system as a whole. The complexity of these rules was a direct result of their synchronicity which resulted in diverging, interacting developmental branches. This type of patterning tended to amplify the effect of a single perturbation so that it propagated through the whole system. Looking at the effect of cell perturbations highlights how in different

types of dynamical system there are different levels of intrinsic system stability. This may be a true insight in regard to biological patterning processes which may require different degrees of robustness at different times. For example the location of the lungs relative to other body parts may require a greater degree of robustness or specificity than the exact branching of each bronchiole. Identifying the level of robustness required by a particular patterning event is useful way to analyse its underlying properties.

In Delta-Notch lateral inhibition patterning processes the 'requirement' is to isolate cells of a particular cell state. Thus, in this context any measure of the robustness of this process would have to qualify how well this was achieved under different system perturbations. Added to this may be a further requirement for the pattern to be regularly spaced. An argument could then be made that the robustness of the overall process relates to the regularity of the spacing and that the models that gave rise to packing optimisation in section three of this thesis are therefore more robust.

Although individual patterning rules differed in their robustness to cell perturbations the most significant factor affecting robustness in the combinatorial system was the developed pattern size. It was shown that when a combination of cellular automata rules were used in sequence the overall robustness of the system was an aggregate of each of the individual rules. Cell perturbations produced, on average, a fixed amount of overall damage to a developed pattern. Therefore, pattern size was the predominate factor in determining the system's robustness. This may have implications in evolution where there may be a increase in fitness associated with the size of a developed organism.

13.2.4 Models of filopodial signalling

The second section of this thesis focussed on using a more applied model to help interpret biological data. This was used to demonstrate that filopodial signalling is required to generate the pattern of microchaetes observed in Drosophila. Though filopodial signalling had been previously identified in this system [De Joussineau et al.: 2003] this result was particularly important as it showed that a dynamic network of filopodia could give rise to a stable pattern. Furthermore, when a static network with a fixed distribution of lengths was used the pattern spacing was significantly smaller.

The computational model, therefore, required a sufficient degree of complexity in order to capture the key behaviours of the system. This included a number of key components such as the simulation of protein signalling and transcriptional activation by hill function dynamics. The filopodia dynamics could then be incorporated, with lifetimes that had some physical basis relative to the signalling process. Also required was a realistic representation of space so that filopodial protrusions could be related to the average cell size.

The 'use' of the modelling, in this case, was to provide evidence that filopodia could establish a pattern and, in particular, that intermittent signalling when coupled with transcriptional inhibition dynamics could result in a stable pattern. Similarly, it was not obvious how a distribution of filopodia lengths would relate to a particular spacing of the pattern and in this aspect the model was also required to explain the wild type and mutant results. The model thus served as a tool to substantiate the biological findings and to help direct experiments to address key questions.

The filopodia present a novel mechanism by which a longer range cell-to-cell signal may be established without the need for diffusion. In Delta-Notch signalling they provide a mechanism for establishing a wider spaced pattern. It can be argued that diffusion is not possible in the lateral inhibition system since Delta would inhibit the cell from which it was released. Moreover, experimental data shows that this is unlikely to occur in vivo. Filopodia are, however, ideally suited to carry the signal in the Delta-Notch system as they can maintain the integrity of a cells protein levels and ensure that a cell only inhibits neighbouring cells via cell-to-cell contact.

13.2.5 Deriving optimisation heuristics from cellular automata

In the third section of this thesis the asynchronous cellular automata were used to identify a heuristic mechanism by which a lateral inhibition type of patterning process could optimise over time and ensure the maximum packing density was achieved at a certain minimum separation. By using the cellular automata to identify this mechanism an argument could be formed as to how, in the filopodial signalling system, a similar dynamic might emerge. This meant that simulations could be designed to test this assumption. Here, a simple model was used to identify a possible behaviour in the more complex model and thus directed simulations in an otherwise parameter rich search space. Moreover, the cellular automata were also used to demonstrate how patterns of stripes could be generated and similarly refined. Future work will hopefully expand upon both these model demonstrations by suggesting experiments to identify packing optimisation and striping. Overall this process has identified the importance of simplification of a model in order to identify key attributes of its behaviour.

In the most simple optimising system where filopodia signalled across a range of two cells an analytical interpretation of the system demonstrated how different pattern packing types and filopodial dynamics affect the probability of the pattern shifting. However, for more complex systems with different filopodial ranges, or for the striping system, an analytical interpretation would be much harder to achieve. In these cases the cellular automata provide an alternative reasoning tool by which to explain the behaviour of this complex system.

Similar cellular automata based models have been adopted in physics. Here they are often associated with the Ising model or similar derived models. In these types of system it is typically shown how local energy minima are overcome by the addition of some external energy (or noise) in order to generate more global order. There is no direct parallel with the lateral inhibition model as there is no energy associated with the packing, only a change in probability of seeing a change in the pattern. However, the key result that a certain amount of external energy added to the system leads to more global ordering is common to many types of system.

Here, it was shown that not only filopodia but any kind of transient protein signal can lead to packing optimisation. The filopodia provide an appealing mechanism as they provide a very mechanical basis for establishing the required type of noisy signal. However other systems may achieve the same end result. In further work it might be revealing to contrast the possible differences between these two types of model.

Conclusion

This thesis has addressed the question of how patterning may arise through cell-to-cell communication and has demonstrated how cellular automata can be used to gain insight into these processes. It was shown that synchronous cellular automata rules can generate complex emergent patterns that the more physically realistic, asynchronous cellular automata were unable to reproduce. Where coherent patterns were achievable in the asynchronous system they were found to be very similar to the lateral inhibition patterns established by Delta-Notch signalling. Indeed, this may represent a fundamental limit to the type of patterns that can be generated by a simple cell-to-cell signalling system. However, this thesis has identified novel ways in which these types of pattern may be evolvable. By changing the lengths of filopodia the spacing of lateral inhibition patterns were affected. Similarly, by altering filopodia dynamics it was shown that these patterns can optimise over time towards a more densely packed and ordered state. Furthermore, it was demonstrated that by changing the sensitivity of cells to the inhibitory signals that they receive, a wide range of patterns of spots and stripes can be achieved. It is hoped that in future work these new theoretical models can be applied to the study of other biological patterning systems.

Appendix A

Supplementary material

A.0.6 Configuring genetic algorithm parameters

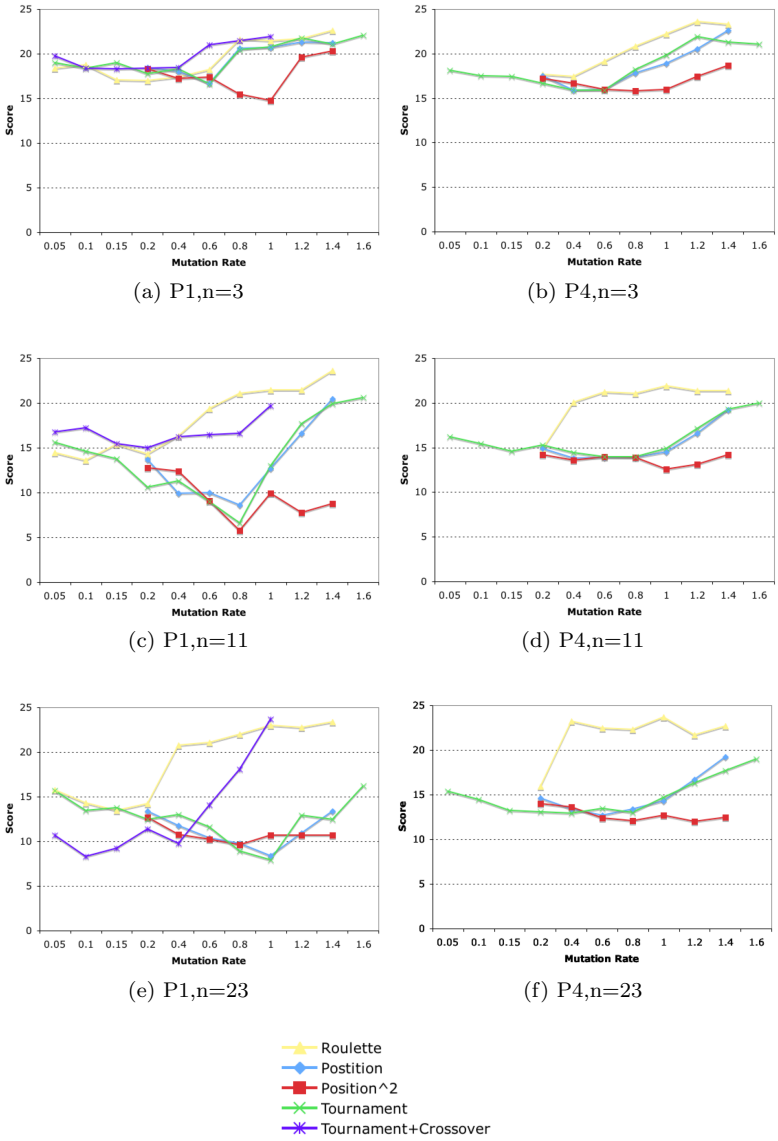

(a) P1,n=3 (b) P4,n=3

(c) P1,n=11 (d) P4,n=11

(e) P1,n=23 (f) P4,n=23

Figure A.1: The effect of varying mutation rate under different selection methods. Champion scores at each generation are shown for each of the selection types used under different mutation rates (the numbers here refer to the chance of a single mutation per individual genome) at n=3,11,23 for patterns P1 and P4. The effect of including crossover was considered for tournament selection for pattern P1 only.

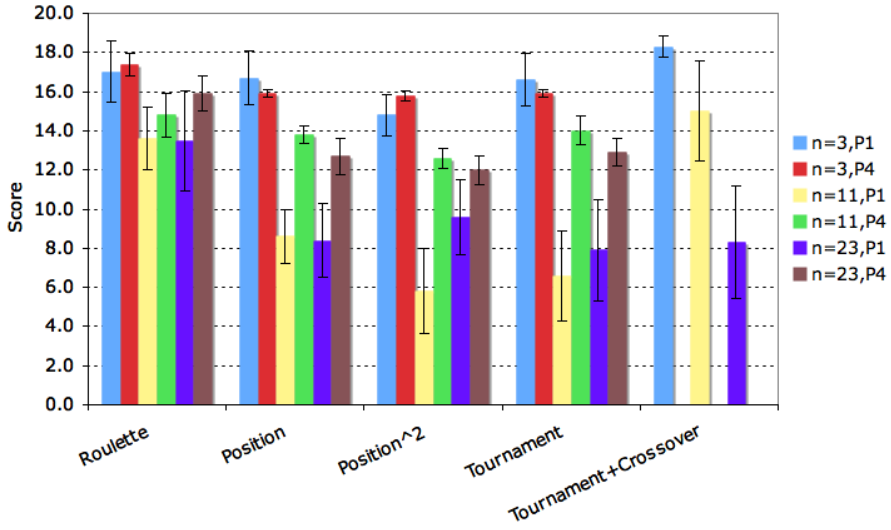

Figure A.2: Summary of the average evolved fitness scores obtained after varying mutation rate for each selection type. Bars indicate 95% confidence in the mean of the 10 evolutionary runs.

A.0.7 Testing Individual cellular automata rules

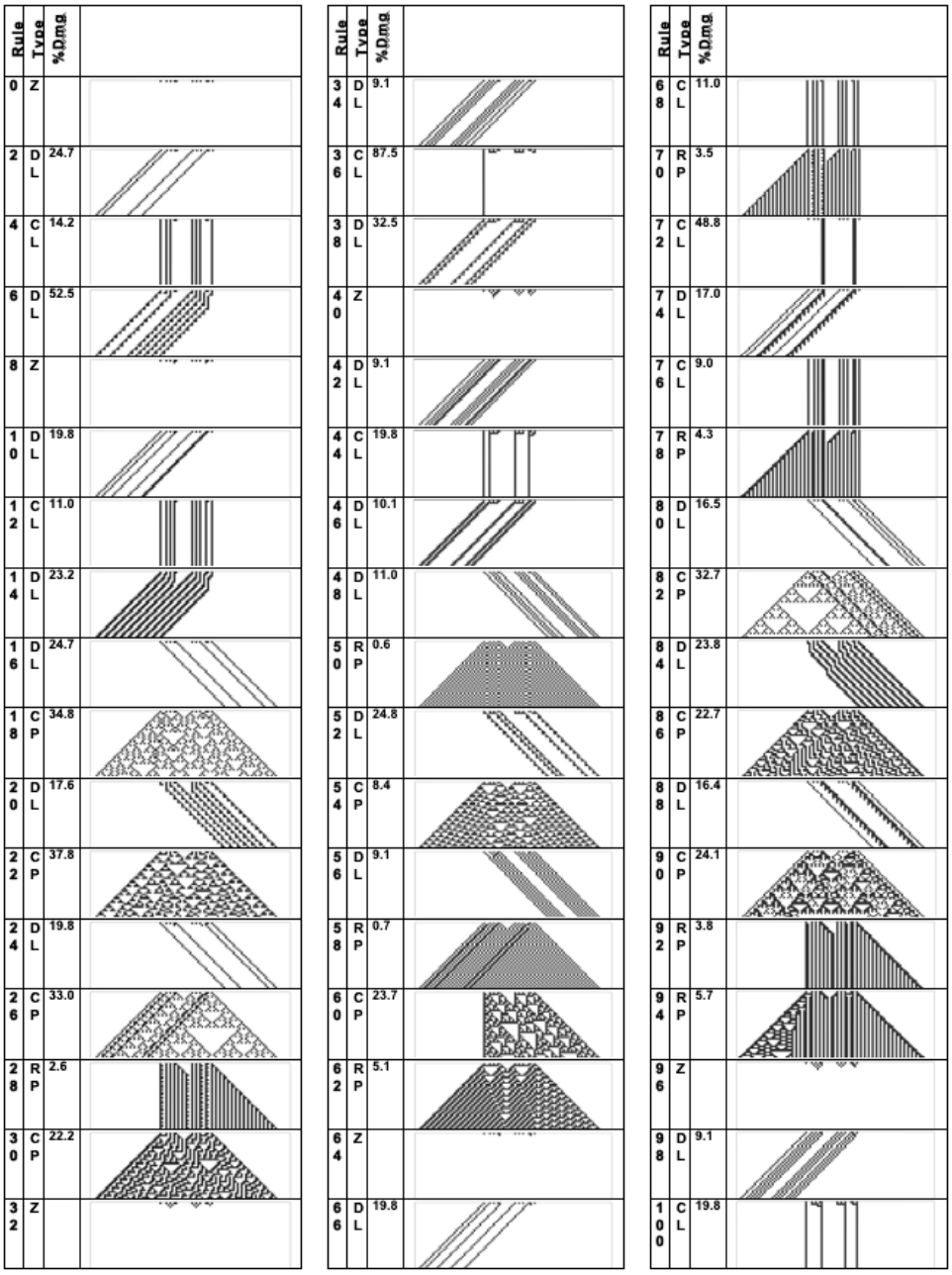

(a) (b) (c)

Figure A.3: The behaviour of the cellular automata rules after input by a pseudo random pattern, classified according to the defined principles

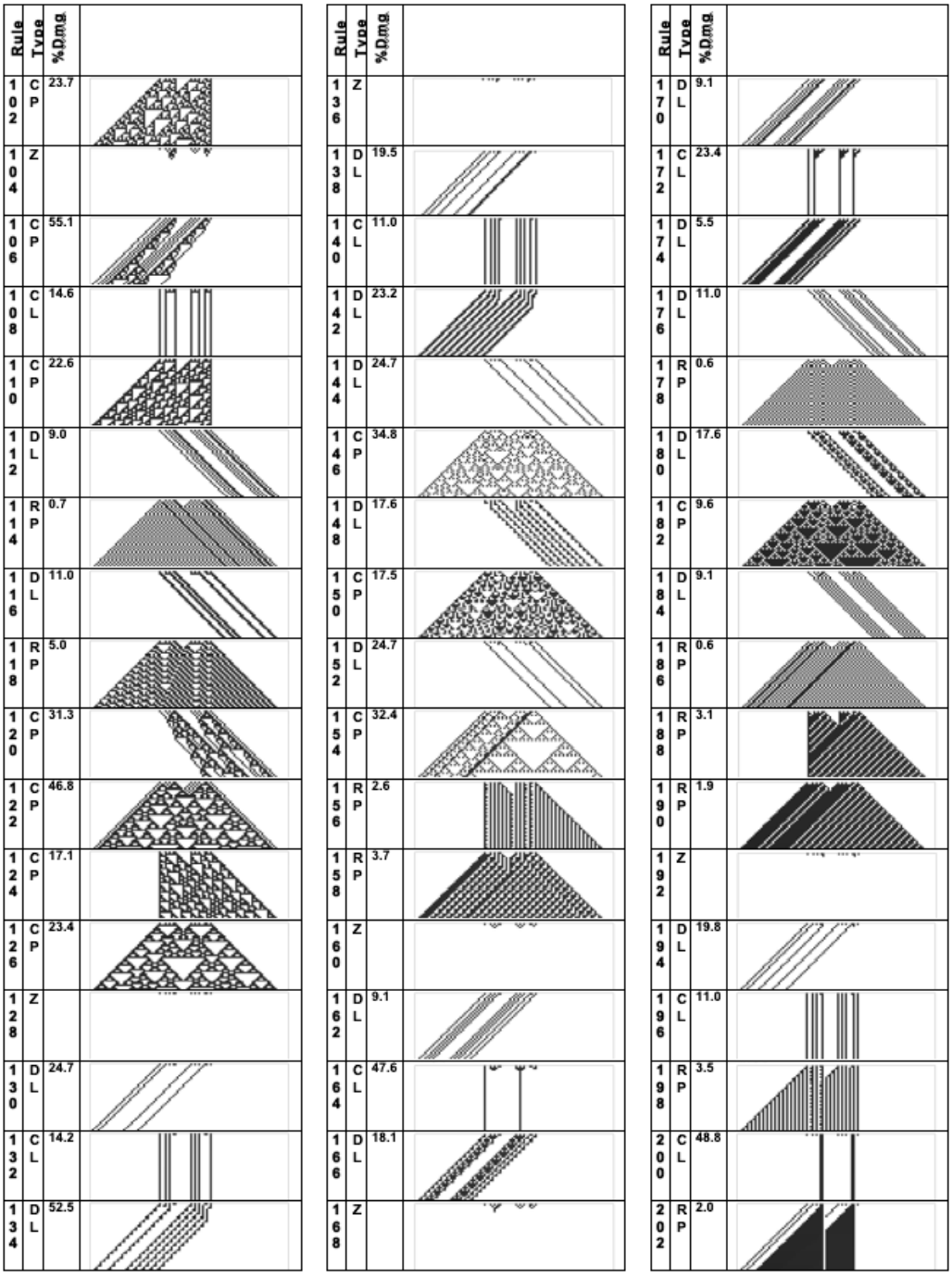

(d) (e) (f)

Figure A.3: The behaviour of the cellular automata rules after input by a pseudo random pattern, classified according to the defined principles

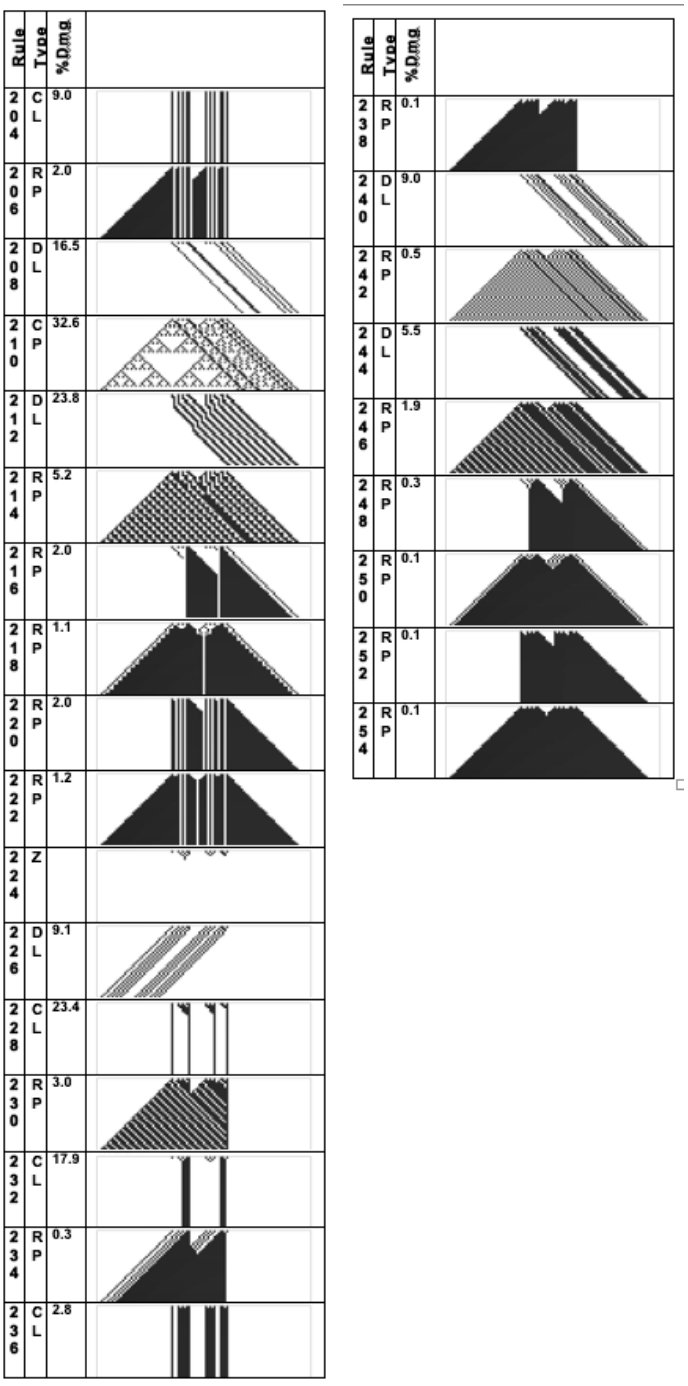

(g) (h)

Figure A.3: The behaviour of the cellular automata rules after input by a pseudo random pattern, classified according to the defined principles

A.0.8 Asynchronous cellular automata

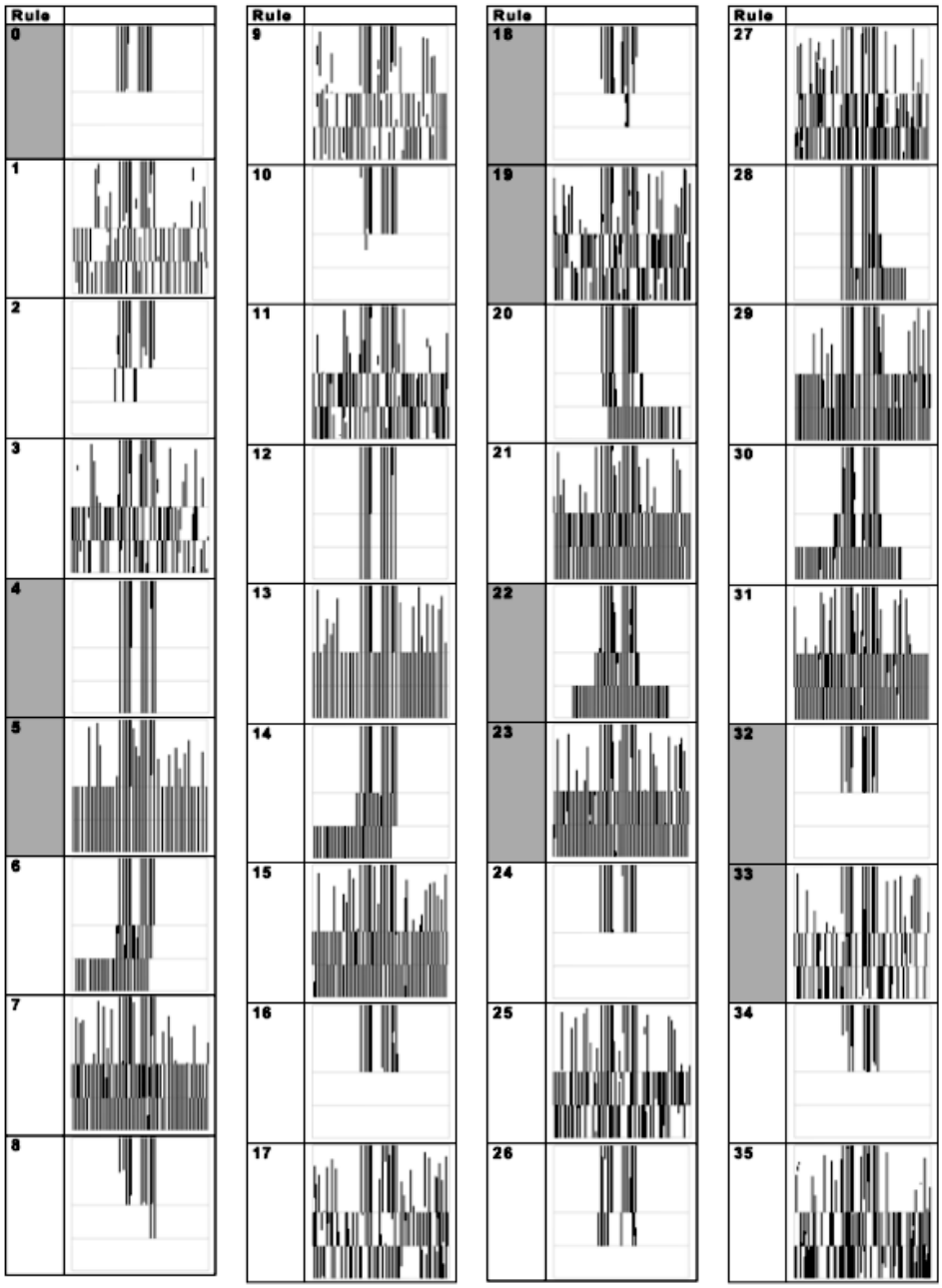

(a)

Figure A.4: The behaviour of the asynchronous rules after pseudo random input. The image shows three sections of the cellular automata run from 1-100, 950-1000, and 9950-10000 times steps. Symmetrical rules highlighted in grey.

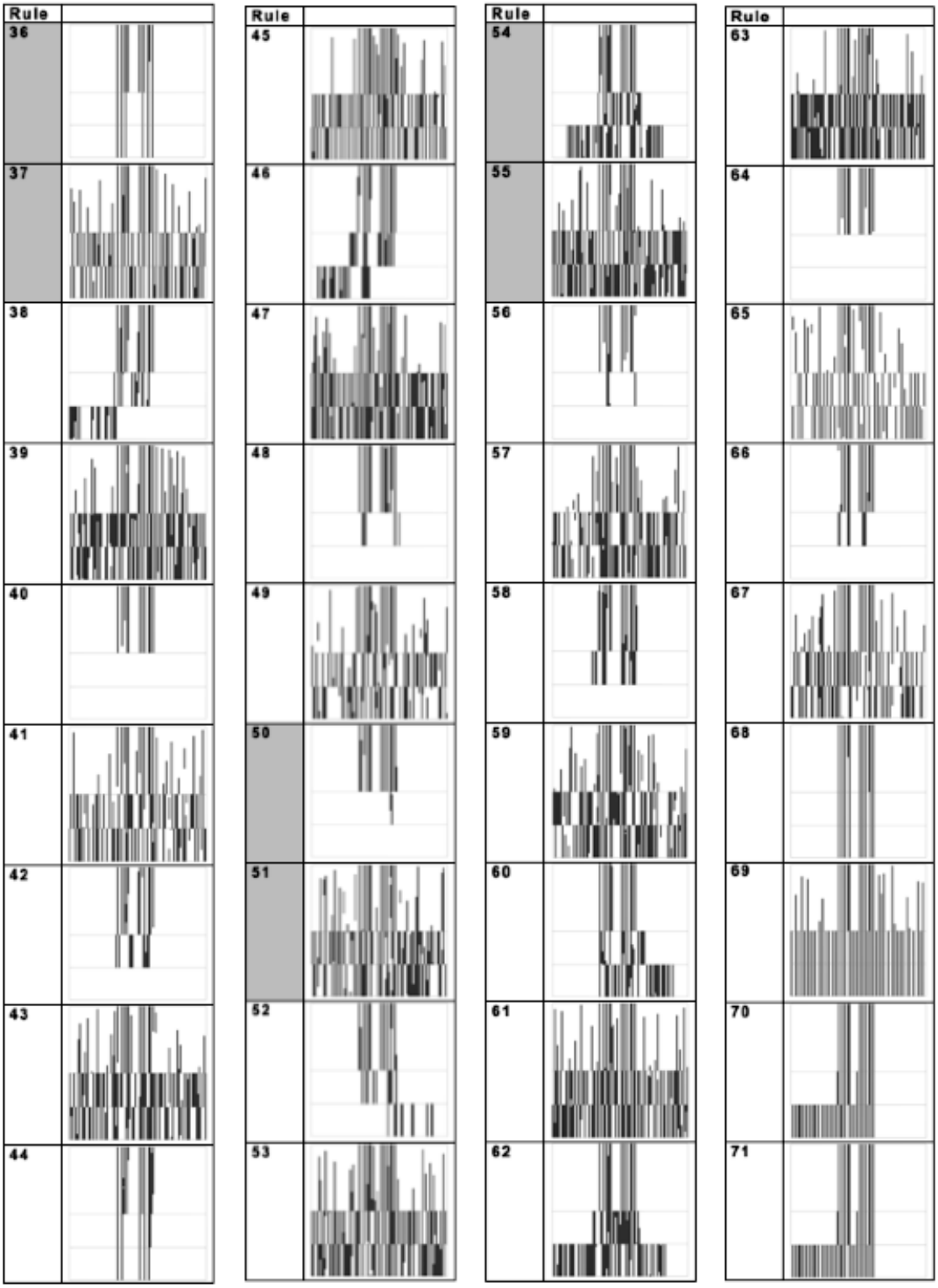

(b)

Figure A.4: The behaviour of the asynchronous rules after pseudo random input. The image shows three sections of the cellular automata run from 1-100, 950-1000, and 9950-10000 times steps.Symmetrical rules highlighted in grey.

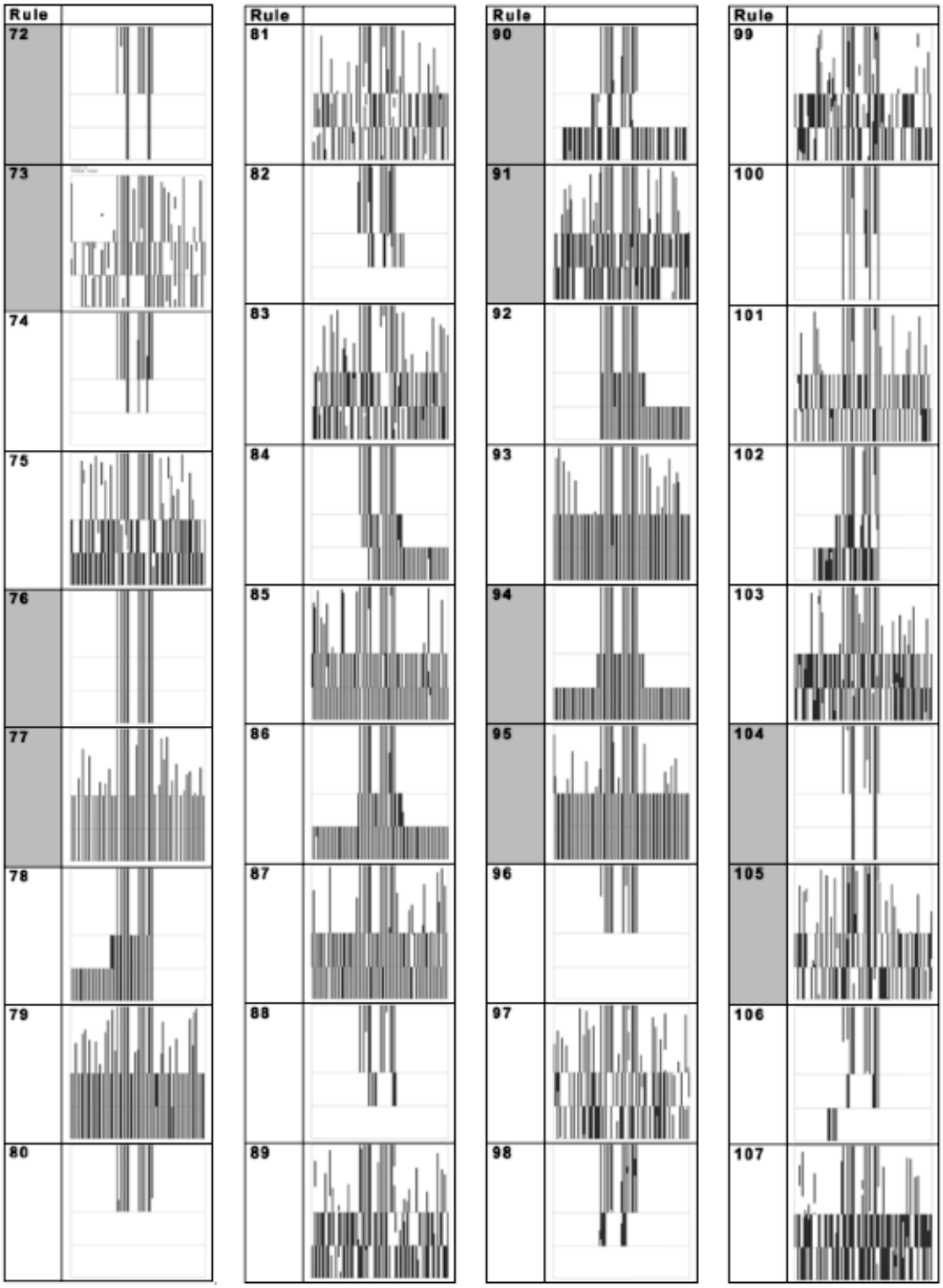

(c)

Figure A.4: The behaviour of the asynchronous rules after pseudo random input. The image shows three sections of the cellular automata run from 1-100, 950-1000, and 9950-10000 times steps. Symmetrical rules highlighted in grey. .

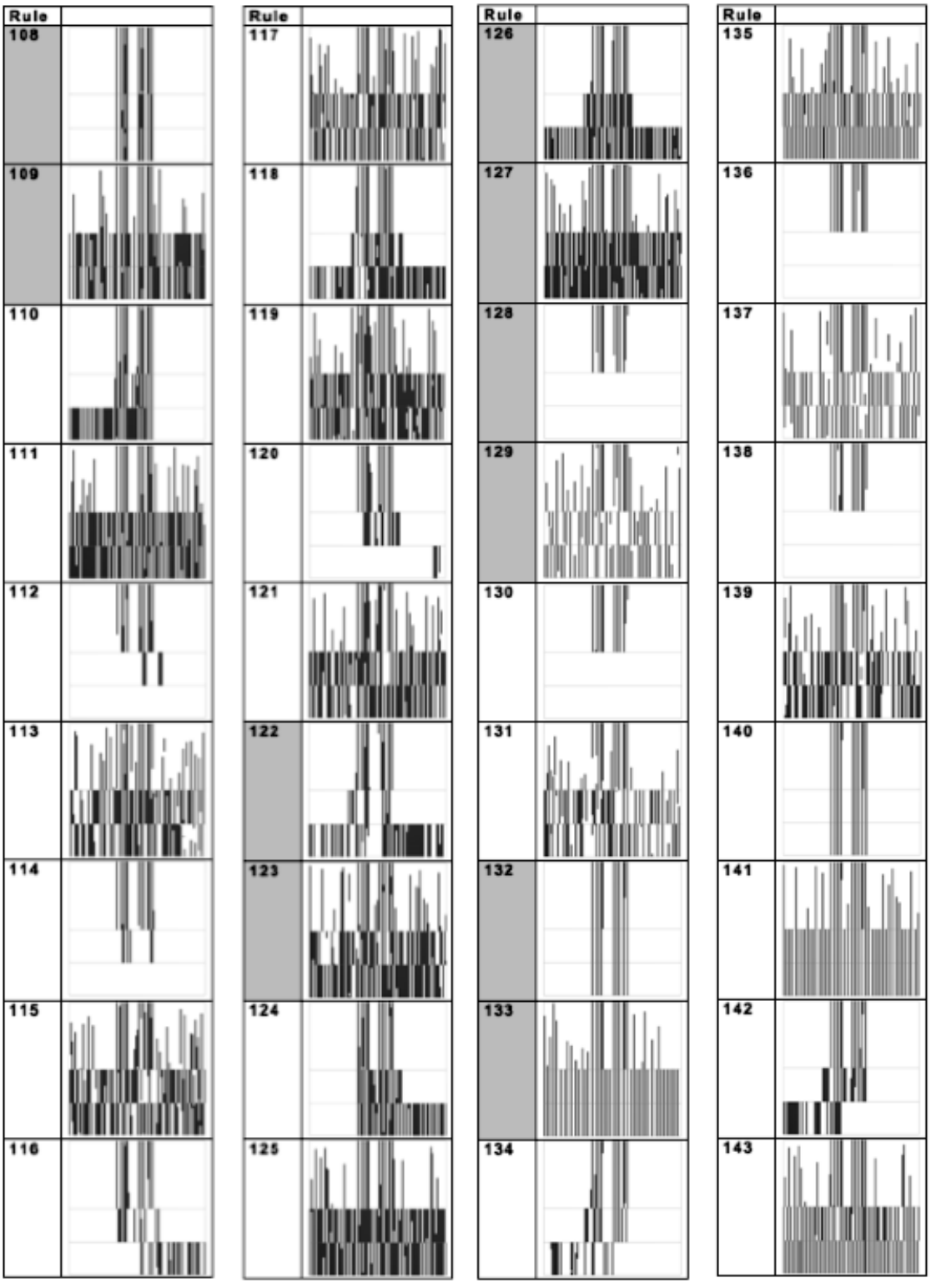

(d)

Figure A.4: The behaviour of the asynchronous rules after pseudo random input. The image shows three sections of the cellular automata run from 1-100, 950-1000, and 9950-10000 times steps.Symmetrical rules highlighted in grey.

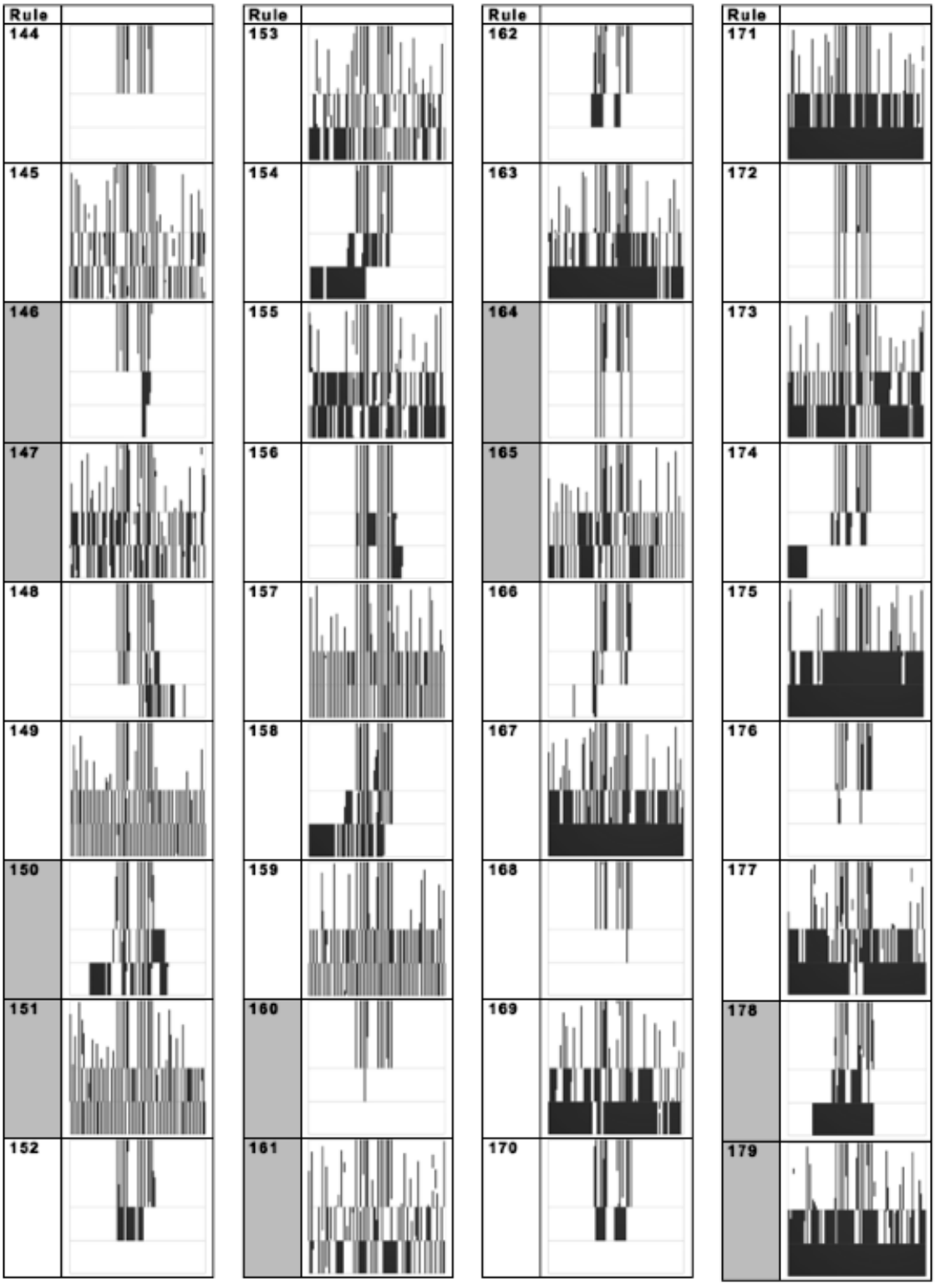

(e)

Figure A.4: The behaviour of the asynchronous rules after pseudo random input. The image shows three sections of the cellular automata run from 1-100, 950-1000, and 9950-10000 times steps.Symmetrical rules highlighted in grey.

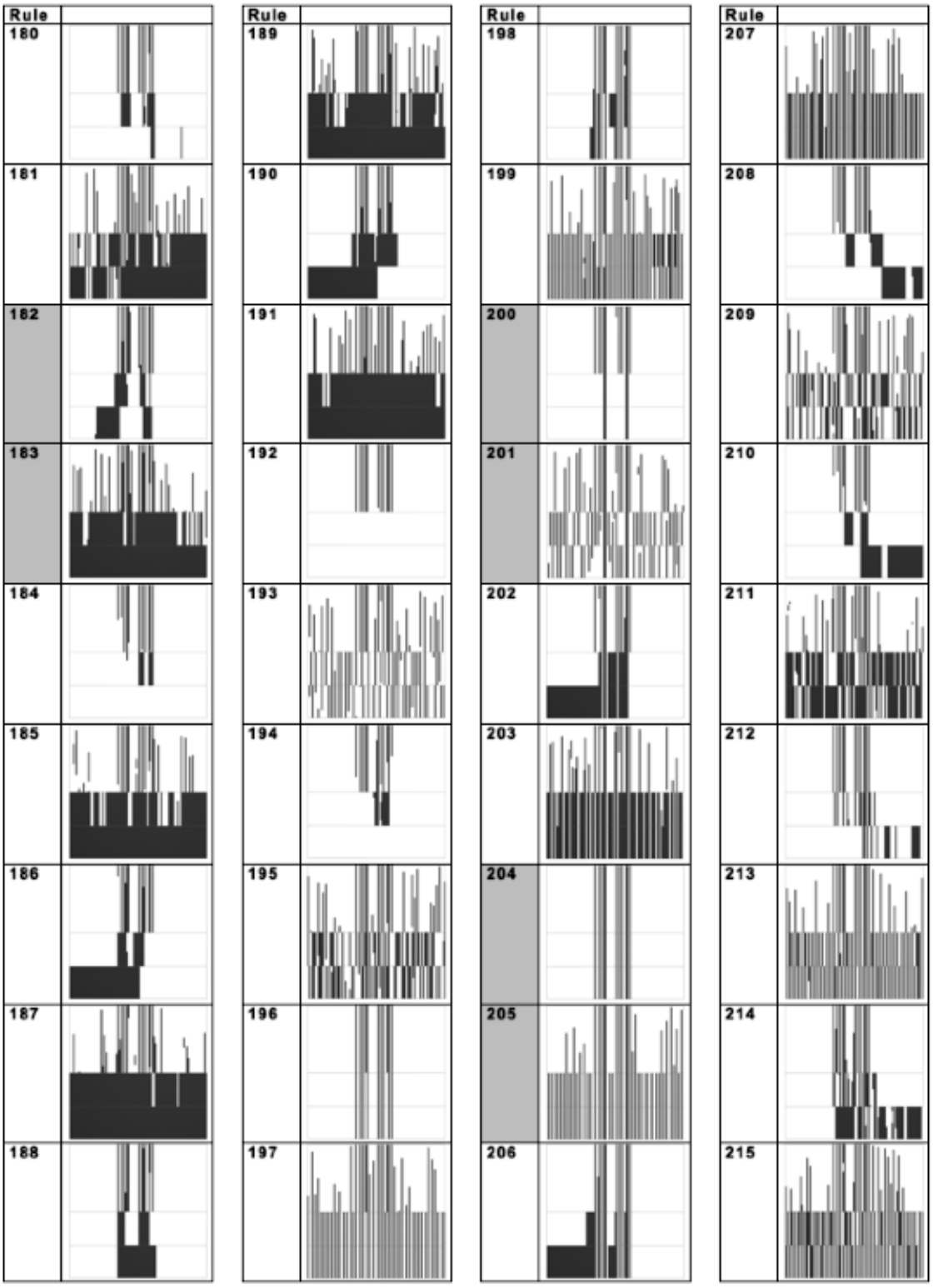

(f)

Figure A.4: The behaviour of the asynchronous rules after pseudo random input. The image shows three sections of the cellular automata run from 1-100, 950-1000, and 9950-10000 times steps.Symmetrical rules highlighted in grey.

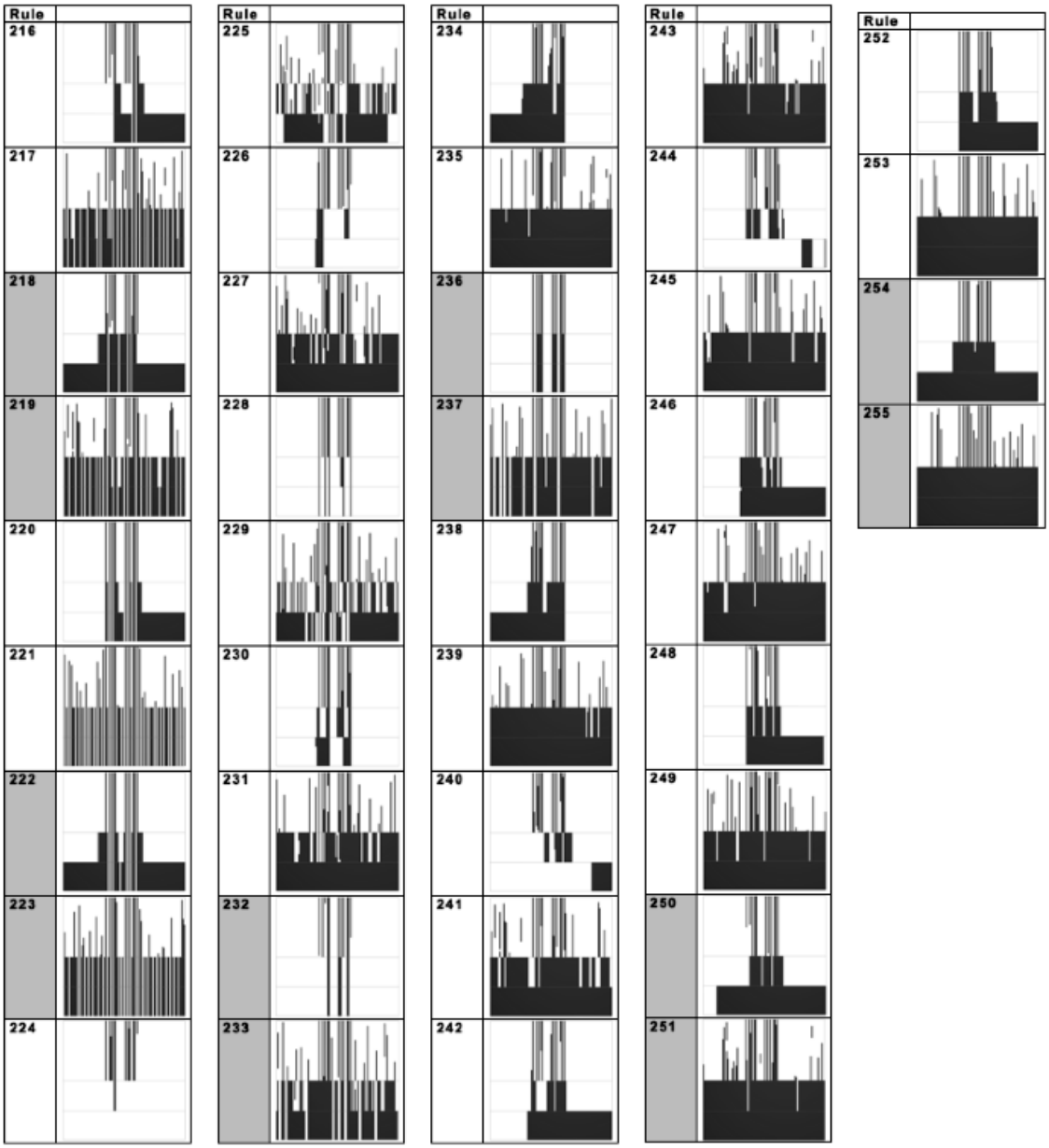

(g)

Figure A.4: The behaviour of the asynchronous rules after pseudo random input. The image shows three sections of the cellular automata run from 1-100, 950-1000, and 9950-10000 times steps.Symmetrical rules highlighted in grey.

A.0.9 Delta inhibition increases with packing density

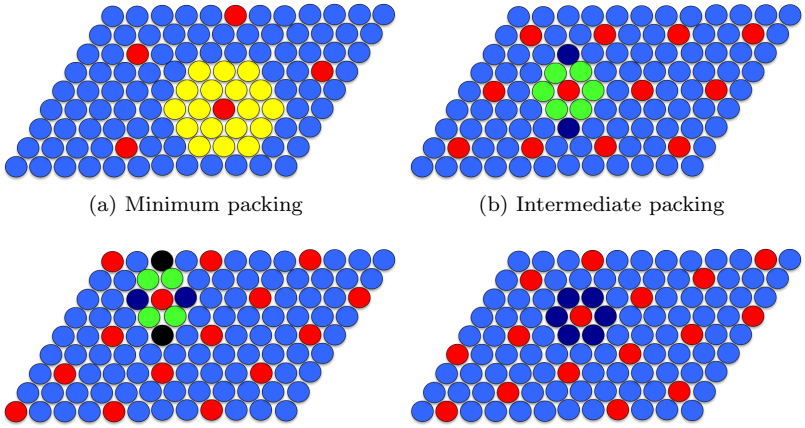

(a) Minimum packing (b) Intermediate packing

(c) Intermediate packing (d) Maximum packing

Figure A.5: Inhibitory contacts with periodic packing at basal signalling ranges. A schematic showing how for each for the packing types previously identified, assuming perfect connectivity at range of 2 cells, the number of cells causing inhibition varies. In each case cells inhibited by a maximum of just 1 Delta expressing cells are labelled yellow, for 2 Delta cells - green, for 3 DeltaCells - Purple and for 4 Delta cells black. As the packing density increases non-Delta expressing cells are inhibited by a greater number of Delta expressing cells.

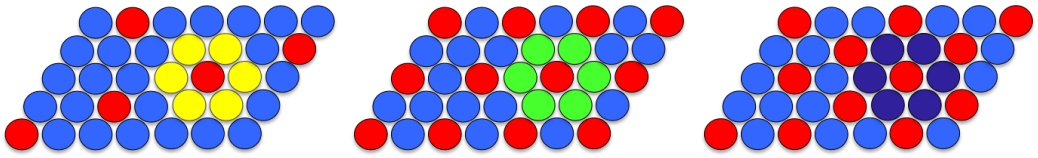

(a) Minimum packing (b) Intermediate packing (c) Maximum packing

Figure A.6: Inhibitory contacts with periodic packing at apical ranges. With just apical signalling, the number of cells causing inhibition varies. In each case cells inhibited by a maximum of just 1 Delta expressing cells are labelled yellow, for 2 Delta cells - green and for 3 Delta Cells - Purple. As the packing density increases non-Delta expressing cells are inhibited by a greater number of Delta expressing cells.

References

D. L. Abel and J. T. Trevors, "Self-organization vs. self-ordering events in life-origin models," *Physics of Life Review*, vol. 3, pp. 211–228, 2006.

S. Agrawal, C. Archer, and D. V. Schaffer, "Computational models of the Notch network elucidate mechanisms of context-dependent signaling." *PLoS Comput Biol*, vol. 5, no. 5, p. e1000390, May 2009.

——, "Computational models of the notch network elucidate mechanisms of context-dependent signaling," *PLoS Comput Biol*, vol. 5, no. 5, p. e1000390, May 2009.

F. Ahimou, L.-P. Mok, B. Bardot, and C. Wesley, "The adhesion force of Notch with Delta and the rate of Notch signaling." *J Cell Biol*, vol. 167, no. 6, pp. 1217–1229, Dec 2004.

M. Alber, M. Kiskowski, J. Glazier, and Y. Jiang, "On cellular automaton approaches to modeling biological cells," *Mathematical systems theory in biology, communication, and finance*, 2002.

B. Alberts, A. Johnson, J. Lewis, M. Raff, K. Roberts, and P. Walter, *Molecular Biology of the Cell - 4th Edition*. Garland Publishing, 2002.

U. Alon, *An introduction to system biology: design principles of biological circuits*. CRC Press, 2006, no. 1584886420.

T. Andersen, R. Newman, and T. Otter, "Development of virtual embryos with emergent self-repair," in *American Association for Artificial Intelligence - Symposium on developmental systems*, Fall 2006, pp. 16–23.

A. R. A. Anderson, M. A. J. Chaplain, and K. A. Rejniak, *Single-cell-based models in biology and medicine*. Basel: Birkhäuser, 2007.

S. Artavanis-Tsakonas, M. D. Rand, and R. J. Lake, "Notch signaling: cell fate control and signal integration in development," *Science*, vol. 284, no. 5415, pp. 770–6, 1999.

R. Asai, E. Taguchi, Y. Kume, M. Saito, and S. Kondo, "Zebrafish leopard gene as a component of the putative reaction-diffusion system," *Mech Dev*, vol. 89, no. 1-2, pp. 87–92, Dec 1999.

H. L. Ashe and J. Briscoe, "The interpretation of morphogen gradients," *Development*, vol. 133, no. 3, pp. 385–94, 2006.

E. Baake and H. Wagner, "Mutation-selection models solved exactly with methods of statistical mechanics," *Genet Res*, vol. 78, no. 1, pp. 93–117, Aug 2001.

N. E. Baker, S. Yu, and D. Han, "Evolution of proneural atonal expression during distinct regulatory phases in the developing Drosophila eye," *Curr Biol*, vol. 6, no. 10, pp. 1290–301, Oct 1996.

O. Barad, D. Rosin, E. Hornstein, and N. Barkai, "Error minimization in the Notch-Delta lateral inhibition system," June 2009.

N. Barkai and D. Ben-Zvi, "'Big frog, small frog'–maintaining proportions in embryonic development," *FEBS J*, vol. 276, no. 5, pp. 1196–207, Mar 2009.

D. Basanta, M. Miodownik, and B. Baum, "The evolution of robust development and homeostasis in artificial organisms," *PLoS Comput Biol*, vol. 4, no. 3, March 2008.

D. Ben-Zvi, B.-Z. Shilo, A. Fainsod, and N. Barkai, "Scaling of the BMP activation gradient in Xenopus embryos," *Nature*, vol. 453, no. 7199, pp. 1205–11, Jun 2008.

L. B. Bender, P. J. Kooh, and M. A. Muskavitch, "Complex function and expression of Delta during drosophila oogenesis." *Genetics*, vol. 133, no. 4, pp. 967–978, Apr 1993.

H. Bersini and V. Detours, "Asynchrony induces stablility in cellular automata based models," *Proceedings of the IVth Conference on Artificial Life*, vol. 204, pp. 382–387, 1994.

S. S. Blair, "Developmental biology: boundary lines," *Nature*, vol. 424, no. 6947, pp. 379–81, Jul 2003.

C. Braendle and M.-A. Felix, "Plasticity and errors of a robust developmental system in different environments." *Dev Cell*, vol. 15, no. 5, pp. 714–724, Nov 2008.

N. F. Britton, *Essential Mathematical Biology.* Springer-Verlag, 2003.

S. G. Brush, "History of the Lenz-Ising model," *Rev. Mod. Phys.*, vol. 39, no. 4, pp. 883–893, Oct 1967.

Q. Cao, J. Lu, C. Kaur, V. Sivakumar, F. Li, P. S. Cheah, S. T. Dheen, and E.-A. Ling, "Expression of Notch-1 receptor and its ligands Jagged-1 and Delta-1 in amoeboid microglia in postnatal rat brain and murine bv-2 cells." *Glia*, vol. 56, no. 11, pp. 1224–1237, Aug 2008.

W. V. Cardoso, "Transcrption factors and pattern-formation in the developing lung," *American Journal of Physiology-Lung Cellular and Molecular Physiology*, vol. 269, no. 4, pp. 429–442, Oct. 1995.

S. B. Carroll, *Endless Forms so Beautiful.* W. W. Norton and Co, 2005.

B. Castro, S. Barolo, A. M. Bailey, and J. W. Posakony, "Lateral inhibition in proneural clusters: cis-regulatory logic and default repression by suppressor of hairless," *Development*, vol. 132, no. 15, pp. 3333–44, 2005.

N. Chen, J. A. Glazier, J. A. Izaguirre, and M. S. Alber, "A parallel implementation of the Cellular Potts Model for simulation of cell-based morphogenesis," *Computer Physics Communication*, vol. 176, pp. 670 – 681, 2007.

B. A. Cipra, "An introduction to the Ising model," *Am. Math. Monthly*, vol. 94, no. 10, pp. 937–959, 1987.

L. Cobellis, F. Caprio, E. Trabucco, A. Mastrogiacomo, G. Coppola, L. Manente, N. Colacurci, M. De Falco, and A. De Luca, "The pattern of expression of Notch protein members in normal and pathological endometrium." *J Anat*, vol. 213, no. 4, pp. 464–472, Oct 2008.

J. R. Collier, N. A. Monk, P. K. Maini, and J. H. Lewis, "Pattern formation by lateral inhibition with feedback: a mathematical model of delta-notch intercellular signalling," *J Theor Biol*, vol. 183, no. 4, pp. 429–46, 1996.

P. A. Coming, "The re-emergence of "emergence": A venverable concept in search of a theory." *Complexity*, vol. 7, pp. 18–30, 2002.

V. Conte, J. J. Muñoz, and M. Miodownik, "A 3d finite element model of ventral furrow invagination in the Drosophila melanogaster embryo," *Journal of the Mechanical Behavior of Biomedical Materials*, vol. 1, no. 2, pp. 188 – 198, 2008.

D. Cornforth, D. G. Green, and D. Newth, "Ordered asynchronous processes in multi-agent systems," *Physica D*, vol. 204, no. 1-2, pp. 70–82, 2005.

P. J. Crutchfield, "The calculi of emergence: computation, dynamics, and induction," *Proc of the Oji Int Seminar: Complex Systems - from Complex Dynamics to Artificial Reality*, 1994.

L. Davis, Ed., *Handbook of Genetic Algorithms*. Van Nostrand Reinhold, 1991.

R. Dawkins, *The Selfish Gene (30th Annviersary Ed.)*. Oxford University Press, 2006.

C. De Joussineau, J. Soule, M. Martin, C. Anguille, P. Montcourrier, and D. Alexandre, "Delta-promoted filopodia mediate long-range lateral inhibition in Drosophila," *Nature*, vol. 426, no. 6966, pp. 555–9, 2003.

F. Demontis and C. Dahmann, "Apical and lateral cell protrusions interconnect epithelial cells in live Drosophila wing imaginal discs," *Dev Dyn*, vol. 236, no. 12, pp. 3408–18, 2007.

A. Deutsch and S. Dormann, *Cellular automaton modeling of biological pattern formation: characterization, applications, and analysis*, ser. Modeling and simulation in science, engineering and technology. Boston: Birkhauser, 2005.

A. Devert, N. Bredeche, and M. Schoenauer, "Robust multi-cellular developmental design," in *Genetic and Evolutionary Computation – GECCO-2007, Part I*, 2007, pp. 982–989.

C. Q. Doe and C. S. Goodman, "Early events in insect neurogenesis. ii. the role of cell interactions and cell lineage in the determination of neuronal precursor cells." *Dev Biol*, vol. 111, no. 1, pp. 206–219, Sep 1985.

E. Domany, "Equivalence of cellular automata to Ising models and directed percolation," *Phys Rev Lett*, vol. 53, no. 4, p. 311, 1984.

L. Dupuy, J. Mackenzie, T. Rudge, and J. Haseloff, "A system for modelling cell-cell interactions during plant morphogenesis," *Ann Bot*, vol. 101, no. 8, pp. 1255–65, May 2008.

S. J. Eglen and D. J. Willshaw, "Influence of cell fate mechanisms upon retinal mosiac formation: a modelling study," *Development*, vol. 129, pp. 5399–5408, 2002.

R. Farhadifar, J. C. Roper, B. Aigouy, S. Eaton, and F. Julicher, "The influence of cell mechanics, cell-cell interactions, and proliferation on epithelial packing," *Curr Biol*, vol. 17, no. 24, pp. 2095–104, 2007.

D. Federici and K. Downing, "Evolution and development of a multicellular organism: scalability, resilience, and neutral complexification." *Artif Life*, vol. 12, no. 3, pp. 381–409, 2006.

R. G. Fehon, K. Johansen, I. Rebay, and S. Artavanis-Tsakonas, "Complex cellular and subcellular regulation of notch expression during embryonic and imaginal development of drosophila: implications for notch function," *J Cell Biol*, vol. 113, no. 3, pp. 657–69, 1991.

U.-M. Fiúza and A. M. Arias, "Cell and molecular biology of Notch," *J Endocrinol*, vol. 194, no. 3, pp. 459–74, Sep 2007.

G. Forgács and S. Newman, *Biological physics of the developing embryo.* Cambridge, UK: Cambridge University Press, 2005.

N. Gaiano and G. Fishell, "The role of Notch in promoting glial and neural stem cell fates," *Annu Rev Neurosci*, vol. 25, pp. 471–90, 2002.

A. Gamba, D. Ambrosi, A. Coniglio, A. de Candia, S. Di Talia, E. Giraudo, G. Serini, L. Preziosi, and F. Bussolino, "Percolation, morphogenesis, and burgers dynamics in blood vessels formation," *Phys Rev Lett*, vol. 90, no. 11, p. 118101, Mar 2003.

M. Georgiou, E. Marinari, J. Burden, and B. Baum, "Cdc42, Par6, and aPKC regulate Arp2/3-mediated endocytosis to control local adherens junction stability," *Curr Biol*, vol. 18, no. 21, pp. 1631–8, 2008.

H. Gerhardt, M. Golding, M. Fruttiger, C. Ruhrberg, A. Lundkvist, A. Abramsson, M. Jeltsch, C. Mitchell, K. Alitalo, D. Shima, and C. Betsholtz, "VEGF guides angiogenic sprouting utilizing endothelial tip cell filopodia," *J Cell Biol*, vol. 161, no. 6, pp. 1163–77, Jun 2003.

C. Gershenson and F. Heylighen, "When can we call a system self-organizing?" *Lecture Notes in Computer Science*, vol. 2801, pp. 606–614, 2003.

R. Ghosh and C. Tomlin, "Symbolic reachable set computation of piecewise affine hybrid automata and its application to biological modelling: Delta-Notch protein signalling," *Syst Biol (Stevenage)*, vol. 1, no. 1, pp. 170–83, 2004.

——, "Lateral inhibition through Delta-Notch signaling: A piecewise affine hybrid model," *LNCS*, vol. 2034, no. 232-246, 2001.

A. Gierer and H. Meinhardt, "A theory of biological pattern formation." *Kybernetik*, vol. 12, no. 1, pp. 30–39, Dec 1972.

S. F. Gilber, *Developmental Biology*, 8th ed. Sinauer Associates, 2009.

F. Giudicelli and J. Lewis, "The vertebrate segmentation clock," *Curr Opin Genet Dev*, vol. 14, no. 4, pp. 407–14, Aug 2004.

F. Giudicelli, E. M. Ozbudak, G. J. Wright, and J. Lewis, "Setting the tempo in development: an investigation of the zebrafish somite clock mechanism," *PLoS Biol*, vol. 5, no. 6, p. e150, Jun 2007.

A. Goldbeter and O. Pourquié, "Modeling the segmentation clock as a network of coupled oscillations in the Notch, Wnt and FGF signaling pathways," *J Theor Biol*, vol. 252, no. 3, pp. 574–85, Jun 2008.

A. Grajdeanu and S. Kumar, "A novel developmental system for the study of evolutionary design," in *Developmental Systems; AAAI Fall Symposium*, 2006.

Graner and Glazier, "Simulation of biological cell sorting using a two-dimensional extended Potts model," *Phys Rev Lett*, vol. 69, no. 13, pp. 2013–2016, Sep 1992.

P. Grassberger, P. Krause, and T. von der Twer, "A new type of kinetic critical phenomenon," *J Phys A*, vol. 17, pp. 105–109, 1984.

L. Gray, "A mathematician looks at wolfram's new kind of science," *Notices of the AMS*, vol. 50, no. 2, February 2003.

L. Greenberg and V. Hatini, "Essential roles for lines in mediating leg and antennal proximodistal patterning and generating a stable Notch signaling interface at segment borders." *Dev Biol*, vol. 330, no. 1, pp. 93–104, Jun 2009.

J. D. Halley and D. A. Winkler, "Consistent concepts of self-organization and self-assembly," *Complexity*, vol. 14, no. 2, pp. 10–17, 2008.

P. Hammerstein, E. H. Hagen, A. V. M. Herz, and H. Herzel, "Robustness: A key to evolutionary design," *Biological Theory*, vol. 1, pp. 90–93, 2005.

W. Hamming, Richard, "Error detecting and error correcting codes," *Bell System Technical Journal*, vol. 26(2), pp. 147–160, 1950.

I. Harvey and T. Bossomaier, "Time out of joint: Attractors in asynchronous boolean networks." *Proceeding of the Fourth European Conference on Artificial Life*, pp. 67–73, 1997.

P. Heitzler and P. Simpson, "The choice of cell fate in the epidermis of Drosophila," *Cell*, vol. 64, no. 6, pp. 1083–92, 1991.

H. G. E. Hentschel, T. Glimm, J. A. Glazier, and S. A. Newman, "Dynamical mechanisms for skeletal pattern formation in the vertebrate limb," *Proc Biol Sci*, vol. 271, no. 1549, pp. 1713–22, Aug 2004.

F. A. High and J. A. Epstein, "The multifaceted role of Notch in cardiac development and disease," *Nat Rev Genet*, vol. 9, no. 1, pp. 49–61, Jan 2008.

P. Hogeweg, "Evolving mechanisms of morphogenesis: on the interplay between differential adhesion and cell differentiation," *J Theor Biol*, vol. 203, no. 4, pp. 317–33, Apr 2000.

——, "Computing an organism: on the interface between informatic and dynamic processes," *Biosystems*, vol. 64, no. 1-3, pp. 97–109, Jan 2002.

E. Hornstein and N. Shomron, "Canalization of development by microRNAs," *Nature Genetics*, 2006.

E. Huerta-Sanchez and R. Durrett, "Wagner's canalization model." *Theor Popul Biol*, vol. 71, no. 2, pp. 121–130, 2007.

R. Iman, J. Helton, and J. Campbell, "An approach to sensitivity analysis of computer models, part 1, introduction, input variable selection and preliminary variable assessment." *Journal of Quality Technology*, vol. 13, no. 3, pp. 174–183, 1981.

K. D. Irvine and T. F. Vogt, "Dorsal-ventral signaling in limb development," *Curr Opin Cell Biol*, vol. 9, no. 6, pp. 867–76, Dec 1997.

E. Jen, Ed., *Robust Design: A repertoire of Biological, Ecological and Engineering Case Studies*. Oxford University Press, 2005.

Y. Kanada, "The effects of randomness in asynchronous 1D cellular automata," *Artifical Life 1V*, 1994.

E. Keller, "Developmental robustness," *Annals of the New York Academy of Science*, vol. 981, no. 189-201, 2002.

A. E. Kiernan, R. Cordes, R. Kopan, A. Gossler, and T. Gridley, "The Notch ligands DLL1 and JAG2 act synergistically to regulate hair cell development in the mammalian inner ear," *Development*, vol. 132, no. 19, pp. 4353–62, 2005.

A. J. Koch and H. Meinhardt, "Biological pattern formation: from basic mechanisms to complex structures," *Review of modern physics*, vol. 66, no. 4, p. 1481, 1994.

S. Kondo and R. Asai, "A reaction-diffusion wave on the skin of the marine angelfish pomacanthus," *Nature*, vol. 376, no. 6543, 1995.

P. J. Kooh, R. G. Fehon, and M. A. Muskavitch, "Implications of dynamic patterns of Delta and Notch expression for cellular interactions during drosophila development," *Development*, vol. 117, no. 2, pp. 493–507, 1993.

S. Kumar and P. J. Bentley, Eds., *On Growth, Form and Computers.* Elsevier Academic Press, 2003.

M. LaBarbera, "Analysing body size as a factor in ecology and evolution," *Annual review of ecology and systematics*, vol. 20, no. 97-117, 1989.

E. C. Lai, "Notch signaling: control of cell communication and cell fate," *Development*, vol. 131, no. 5, pp. 965–73, 2004.

E. C. Lai and G. M. Rubin, "Neuralized functions cell-autonomously to regulate a subset of notch-dependent processes during adult Drosophila development," *Dev Biol*, vol. 231, no. 1, pp. 217–33, 2001.

C. G. Langton, "Computation at the edge of chaos: Phase transition and emergent computation," *Physica D*, vol. 42, pp. 12–37, 1990.

T. Lee and L. Lou, "Mosaic analysis with a repressible cell marker (MARCM) for Drosophila neural development," *Trends in Neuroscience*, vol. 24, no. 5, p. 251, 2001.

J. Lenski, R., E. Barrick, J., and C. Ofria, "Balancing robustness and evolvabilty," *PLOS Biology*, vol. 4, no. 12, p. 2190, 2006.

J. Lewis, "Notch signalling and the control of cell fate choices in vertebrates," *Semin Cell Dev Biol*, vol. 9, no. 6, pp. 583–9, 1998.

——, "Autoinhibition with transcriptional delay: a simple mechanism for the zebrafish somitogenesis oscillator." *Curr Biol*, vol. 13, no. 16, pp. 1398–1408, Aug 2003.

A. Lindenmayer, "Developmental systems without cellular interactions, their languages and grammars." *J Theor Biol*, vol. 30, no. 3, pp. 455–484, 1971.

H. D. Lipshitz, "Follow the mRNA: a new model for Bicoid gradient formation." *Nat Rev Mol Cell Biol*, vol. 10, no. 8, pp. 509–512, Aug 2009.

Y. Liu and J. P. Dilger, "Application of the one- and two-dimensional Ising models to studies of cooperativity between ion channels," *Biophys J*, vol. 64, no. 1, pp. 26–35, Jan 1993.

F. Logeat, C. Bessia, C. Brou, O. LeBail, S. Jarriault, N. G. Seidah, and A. Israël, "The notch1 receptor is cleaved constitutively by a furin-like convertase," *Proc Natl Acad Sci U S A*, vol. 95, no. 14, pp. 8108–12, Jul 1998.

S. R. Lubkin and Z. Li, "Force and deformation on branching rudiments: cleaving between hypotheses," *Biomech Model Mechanobiol*, vol. 1, no. 1, pp. 5–16, Jun 2002.

E. Y. Ma, E. W. Rubel, and D. W. Raible, "Notch signaling regulates the extent of hair cell regeneration in the zebrafish lateral line." *J Neurosci*, vol. 28, no. 9, pp. 2261–2273, Feb 2008.

P. K. Maini, "Using mathematical models to help understand biological pattern formation." *C R Biol*, vol. 327, no. 3, pp. 225–234, Mar 2004.

G. Marnellos, G. A. Deblandre, E. Mjolsness, and C. Kintner, "Delta-Notch lateral inhibitory patterning in the emergence of ciliated cells in Xenopus: experimental observations and a gene network model," *Pac Symp Biocomput*, pp. 329–40, 2000.

Y. Masamizu, T. Ohtsuka, Y. Takashima, H. Nagahara, Y. Takenaka, K. Yoshikawa, H. Okamura, and R. Kageyama, "Real-time imaging of the somite segmentation clock: revelation of unstable oscillators in the individual presomitic mesoderm cells," *Proc Natl Acad Sci U S A*, vol. 103, no. 5, pp. 1313–8, 2006.

H. Meinhardt and A. Gierer, "Pattern formation by local self-activation and lateral inhibition." *Bioessays*, vol. 22, no. 8, pp. 753–760, Aug 2000.

H. Meinhardt and M. Klinger, "A model for pattern formation on the shells of molluscs," *Journal of Theoretical Biology*, vol. 126, pp. 63–89, 1987.

H. Meinhardt, "Computational modelling of epithelial patterning." *Curr Opin Genet Dev*, vol. 17, no. 4, pp. 272–280, Aug 2007.

R. J. Merks and J. A. Glazier, "A cell-centered approach to developmental biology," *Physica A*, vol. 352, pp. 113–139, 2005.

A. C. Miller, E. L. Lyons, and T. G. Herman, "Cis-inhibition of Notch by endogenous Delta biases the outcome of lateral inhibition." *Curr Biol*, vol. 19, no. 16, pp. 1378–1383, Aug 2009.

F. Miller, Julian, "Evolving a self-repairing, self-regulating, French flag organism," in *Genetic and Evolutionary Computation – GECCO-2004, Part I*, K. D. et. al., Ed., vol. 3102, 2004, pp. 129–139.

J. Milnor, "On the concept of attractor," *Communications of Mathematical Physics*, vol. 99, pp. 177–195, 1985.

M. Mitchell, *An Introduction to Genetic Algorithms.* Masachusetts Institute of Technology, 1998.

T. Miura and P. K. Maini, "Speed of pattern appearance in reaction-diffusion models: Implication in the pattern formation of limb bud mesenchyme cells," *Bulletin of Mathemtical BIology*, vol. 66, pp. 627–649, 2004.

E. Mjolsness, D. Sharp, and J. Reinitz, "A connectionist model of development," *J Theor Biol*, vol. 152, pp. 429–453, 1991.

J. L. Mummery-Widmer, M. Yamazaki, T. Stoeger, M. Novatchkova, S. Bhalerao, D. Chen, G. Dietzl, B. J. Dickson, and J. A. Knoblich, "Genome-wide analysis of Notch signalling in Drosophila by transgenic RNAi," *Nature*, vol. 458, no. 7241, pp. 987–92, Apr 2009.

J. D. Murray, *Mathematical Biology II: Spatial Models and Biolmedical Applications.* Springer, 2003.

L. C. Murtaugh, B. Z. Stanger, K. M. Kwan, and D. A. Melton, "Notch signaling controls multiple steps of pancreatic differentiation," *Proc Natl Acad Sci U S A*, vol. 100, no. 25, pp. 14 920–5, Dec 2003.

K. Nagel and M. Schreckenberg, "A cellular automaton model for freeway traffic," *Journal de Physique*, vol. 2, p. 2221, December 1992.

C. L. Nehaniv, "Asynchronous automata networks can emulate any synchronous automata network," *International Journal of Algebra and Computation*, vol. 14, pp. 719–739, 2004.

D. Oberoi and B. Rylander, "Determining the best parent selection method for a genetic algorithm through varying problem sizes and complexities," in *2004 Genetic and Evolutionary Computation Conference*, M. Keijzer, Ed., Seattle, Washington, USA, Jul. 2004.

H. Othmer, K. Painter, D. Umulis, and C. Xue, "The intersection of theory and application in elucidating pattern formation in developmental biology," *Math. Model. Nat. Phenom.*, vol. 4, no. 4, p. 1, 2009.

M. R. Owen, J. A. Sherratt, and H. J. Wearing, "Lateral induction by juxtacrine signaling is a new mechanism for pattern formation." *Dev Biol*, vol. 217, no. 1, pp. 54–61, Jan 2000.

A. L. Parks and M. A. Muskavitch, "Delta function is required for bristle organ determination and morphogenesis in Drosophila," *Dev Biol*, vol. 157, no. 2, pp. 484–96, 1993.

E. Plahte, "Pattern formation in discrete cell lattices." *J Math Biol*, vol. 43, no. 5, pp. 411–445, Nov 2001.

R. B. Potts, "Some generalized order-disorder transformations," *Proceeding of the Cambridge Philosophical Society*, vol. 48, pp. 106–109, 1952.

I. Prigogine, "Time, structure, and fluctuations," *Science*, vol. 201, no. 4358, pp. 777–785, Sep 1978.

P. Prusinkiewicz, R. Karwowski, and B. Lane, "The L+C plant-modelling language," in *Functional Structural Modelling in Crop Production*, J. e. a. Vos, Ed. Springer, 2007.

H. Qi, M. D. Rand, X. Wu, N. Sestan, W. Wang, P. Rakic, T. Xu, and S. Artavanis-Tsakonas, "Processing of the Notch ligand Delta by the metalloprotease Kuzbanian." *Science*, vol. 283, no. 5398, pp. 91–94, Jan 1999.

G. T. Reeves, C. B. Muratov, T. Schupbach, and S. Y. Shvartsman, "Quantitative models of developmental pattern formation." *Dev Cell*, vol. 11, no. 3, pp. 289–300, Sep 2006.

O. Renaud and P. Simpson, "Scabrous modifies epithelial cell adhesion and extends the range of lateral signalling during development of the spaced bristle pattern in Drosophila." *Dev Biol*, vol. 240, no. 2, pp. 361–376, Dec 2001.

——, "Movement of bristle precursors contributes to the spacing pattern in Drosophila," *Mech Dev*, vol. 119, no. 2, pp. 201–11, 2002.

P. C. G. Rida, N. Le Minh, and Y. J. Jiang, "A Notch feeling of somite segmentation and beyond," *Dev Biol*, vol. 265, no. 1, pp. 2–22, Jan 2004.

P. Rorth, "Communication by touch: role of cellular extensions in complex animals," *Cell*, vol. 112, no. 5, pp. 595–8, 2003, rorth, Pernille Review United States Cell Cell. 2003 Mar 7;112(5):595-8.

T. Rudge and J. Haseloff, "A computational model of cellular morphogenesis in plants," in *Advances in Artificial Life*, 2005, pp. 78–87.

P. Sarkar, "A brief history of cellular automata," *ACM Comput. Surv.*, vol. 32, no. 1, pp. 80–107, 2000.

N. Sasaki, T. Sasamura, H. O. Ishikawa, M. Kanai, R. Ueda, K. Saigo, and K. Matsuno, "Polarized exocytosis and transcytosis of Notch during its apical localization in Drosophila epithelial cells," *Genes Cells*, vol. 12, no. 1, pp. 89–103, 2007.

P. Simpson, "Lateral inhibition and the development of the sensory bristles of the adult peripheral nervous system of Drosophila," *Development*, vol. 109, no. 3, pp. 509–19, 1990.

——, "Notch signalling in development: on equivalence groups and asymmetric developmental potential," *Curr Opin Genet Dev*, vol. 7, no. 4, pp. 537–42, 1997.

P. Simpson, R. Woehl, and K. Usui, "The development and evolution of bristle patterns in Diptera," *Development*, vol. 126, no. 7, pp. 1349–64, 1999.

J. Smith and E. H. Davidson, "Gene regulatory network subcircuit controlling a dynamic spatial pattern of signaling in the sea urchin embryo." *Proc Natl Acad Sci U S A*, vol. 105, no. 51, pp. 20 089–20 094, Dec 2008.

O. Speck, S. C. Hughes, N. K. Noren, R. M. Kulikauskas, and R. G. Fehon, "Moesin functions antagonistically to the Rho pathway to maintain epithelial integrity." *Nature*, vol. 421, no. 6918, pp. 83–87, Jan 2003.

A. Spirov, K. Fahmy, M. Schneider, E. Frei, M. Noll, and S. Baumgartner, "Formation of the bicoid morphogen gradient: an mRNA gradient dictates the protein gradient." *Development*, vol. 136, no. 4, pp. 605–614, Feb 2009.

X. Sun and S. Artavanis-Tsakonas, "Secreted forms of Delta and Serrate define antagonists of Notch signaling in Drosophila." *Development*, vol. 124, no. 17, pp. 3439–3448, Sep 1997.

A. A. Teleman, M. Strigini, and S. M. Cohen, "Shaping morphogen gradients." *Cell*, vol. 105, no. 5, pp. 559–562, Jun 2001.

A. C. Tien, A. Rajan, and H. J. Bellen, "A Notch updated," *J Cell Biol*, vol. 184, no. 5, pp. 621–9, 2009.

A. Tiwari and P. Lincoln, "Automated techniques for stability analysis of Delta-Notch lateral inhibition mechanism," SRI, Standford USA, Technical Report, 2002.

A. Turing, "The chemical basis of morphogenesis," *Philosophical Transactions of the Royal Society of London, Series B, Biological Sciences*, vol. 641, pp. 37–52, 1952.

M. Wang and P. W. Sternberg, "Pattern formation during C. elegans vulval induction." *Curr Top Dev Biol*, vol. 51, pp. 189–220, 2001.

F. M. Watt, S. Estrach, and C. A. Ambler, "Epidermal Notch signalling: differentiation, cancer and adhesion." *Curr Opin Cell Biol*, vol. 20, no. 2, pp. 171–179, Apr 2008.

H. J. Wearing, M. R. Owen, and J. A. Sherratt, "Mathematical modelling of juxtacrine patterning." *Bull Math Biol*, vol. 62, no. 2, pp. 293–320, Mar 2000.

V. B. Wigglesworth, "Local and general factors in the development of 'pattern' in Rhodinius prolixus," *Journal of Experimental Biology*, vol. 17, no. 180, 1940.

S. Wolfram, "Statistical mechanics of cellular automata," *Rev. Mod. Phys.*, vol. 55, no. 3, pp. 601–644, Jul 1983.

——, *A New Kind of Science.* Wolfram Media Inc., 2002.

L. Wolpert, "Positional information and the spatial pattern of cellular differentiation," *J Theor Biol*, vol. 25, no. 1, pp. 1–47, Oct 1969.

——, *Principles of Development (2nd Ed.).* Oxford University Press, 2002.

A. Wuensche and M. Lesser, *The global dynamics of cellular automata.* Addison Wesley publishing company., 1992.

M. Yamaguchi, E. Yoshimoto, and S. Kondo, "Pattern regulation in the stripe of zebrafish suggests an underlying dynamic and autonomous mechanism." *Proc Natl Acad Sci U S A*, vol. 104, no. 12, pp. 4790–4793, Mar 2007.